

SYNTHESIS AND LUMINESCENCE PROPERTIES OF
TETRAPHENYLETHENE-BASED SMALL MOLECULES USED IN
ORGANIC LIGHT EMITTING DIODES

A THESIS SUBMITTED TO
THE GRADUATE SCHOOL OF NATURAL AND APPLIED SCIENCES
OF
MIDDLE EAST TECHNICAL UNIVERSITY

BY
SERHAT ODABAŞ

IN PARTIAL FULFILLMENT OF THE REQUIREMENTS
FOR
THE DEGREE OF DOCTOR OF PHILOSOPHY
IN
CHEMISTRY

JANUARY 2014

Approval of the thesis:

SYNTHESIS AND LUMINESCENCE PROPERTIES OF
TETRAPHENYLETHENE-BASED SMALL MOLECULES USED IN
ORGANIC LIGHT EMITTING DIODES

submitted by **SERHAT ODABAŞ** in partial fulfillment of the requirements for the degree of **Doctor of Philosophy in Chemistry Department, Middle East Technical University** by

Prof. Dr. Canan Özgen

Dean, Graduate School of **Natural and Applied Sciences**

Prof. Dr. İlker Özkan

Head of Department, **Chemistry**

Prof. Dr. Cihangir Tanyeli

Supervisor, **Chemistry Department, METU**

Examining Committee Members

Prof. Dr. Metin BALCI

Chemistry Department, METU

Prof. Dr. Cihangir TANYELİ

Chemistry Department, METU

Prof. Dr. Mustafa GÜLLÜ

Chemistry Department, Ankara University

Prof. Dr. Özdemir DOĞAN

Chemistry Department, METU

Assoc. Prof. Dr. Ali ÇIRPAN

Chemistry Department, METU

Date:

17th January 2014

I hereby declare that all information in this document has been obtained and presented in accordance with academic rules and ethical conduct. I also declare that, as required by these rules and conduct, I have fully cited and referenced all material and results that are not original to this work.

Name, Last name : Serhat ODABAŞ

Signature :

ABSTRACT

SYNTHESIS AND LUMINESCENCE PROPERTIES OF TETRAPHENYLETHENE-BASED SMALL MOLECULES USED IN ORGANIC LIGHT EMITTING DIODES

ODABAŞ, Serhat
Ph.D., Department of Chemistry
Supervisor: Prof. Dr. Cihangir TANYELİ

January 2014, 153 pages

Organic light emitting diodes (OLED) is an exciting new technology that attracted much attention to scientist for emissive technology. The basic OLED structure consists of a stack of fluorescent organic layers sandwiched between a transparent conducting anode and metallic cathode. The important problems in luminescence is that, molecules aggregate in solid state that leads formation of excimers which results in emission quenching so that most of the luminescent materials show weak emissions in their solid forms. In order to overcome these problem studies has been carried out to either suppress the quenching of organic luminophores or to produce significant enhancements in their light emission upon aggregation. Aggregation-induced emission (AIE) materials seem to be promising emitters in the fabrication of electroluminescent devices with high efficiency. In this study, various tetraphenylethylene (TPE) emitters were synthesized and characterized for using in OLED applications. The TPE has been functionalized with various heterocyclic aromatic side groups. Photophysical, electrochemical, thermal and AIE properties of the compounds were studied. In addition, the synthesized molecules were examined for their.

Keywords: OLED, aggregation induced emission, tetraphenylethene, photoluminescence

ÖZ

ORGANİK IŞIK YAYICI DİOTLARDA KULLANMAK İÇİN TETRAFENİLETİLEN BAZLI KÜÇÜK MOLEKÜLLERİN SENTEZİ VE LÜMİNESANS ÖZELLİKLERİNİN ARAŞTIRILMASI

ODABAŞ, Serhat
Doktora, Kimya Bölümü
Tez Yöneticisi: Prof. Dr. Cihangir TANYELİ

Ocak 2014, 153 sayfa

Organik ışık yayıcı diotlar (OLED) ışık yayıcı teknolojiler arasında dikkat çeken heyecan verici bir teknolojidir. Genel olarak, temel OLED yapısı flüoresans bir organik katmanın saydam bir iletken anot ile metalik katot arasında sandviç şeklinde sıkıştırılması ile oluşur. Lüminesansla ilgili önemli problemlerden biri moleküllerin katı haldeyken kümeler oluşturmalarıdır. Bu kümeleşme sonucunda ortaya çıkan ekzimerler, emisyonu sönmümlendirerek malzemelerin katı haldeyken daha düşük lüminesans göstermelerine sebep olurlar. Bu problemi çözmek için ya organik luminoforların sönmümlenmelerinin bastırılması ya da oluşan kümeleşme sonucunda ışık emisyonunun artırılması üzerine çalışmalar yapılmaktadır. Kümeleşme ile uyarılmış emisyon özelliğine sahip moleküller yüksek verimlilikte elektrolüminesans cihazların üretimi için umut verici oldukları tespit edilmiştir. Bu çalışmada, çeşitli tetrafeniletillen tabanlı ışık yayıcı özelliğe sahip malzemeler sentezlenip, karakterize edilmiş ve OLED'lerde kullanılmışlardır. Tetrafeniletillen çekirdek yapısı çeşitli N-heterosiklik aromatik yan gruplar ile fonksiyonlandırılmış ve etkileri incelenmiştir. Sentezlenen malzemelerin fotofiziksel, fotokimyasal termal ve kümeleşme ile uyarılmış emisyon özellikleri incelenmiştir.

Anahtar Kelimeler: OLED, kümeleşme ile uyarılmış emisyon, tetrafeniletillen, fotolüminesans

To my beloved wife, son and family

ACKNOWLEDGMENTS

I am deeply grateful to my supervisor Prof. Dr. Cihangir TANYELİ for his support, guidance, and perseverance that have inspired me and made this thesis possible. His office was always open to discuss and he always took the initiative to help me not only grow as a student but as a young scientist.

I would like to thank Scientific and Technological Research Council of Turkey- Marmara Research Center, Chemistry Institute, for the permission and support to complete my Ph.D. thesis.

I also wish to express my profound thanks to my thesis progress committee members Prof. Dr. Mustafa GÜLLÜ and Assoc. Prof. Dr. Ali ÇIRPAN for their guidance and kind contributions to my thesis.

It was great to have the chance to work with Dr. Figen TÜRKSOY. I would like to thank for her endless help. I acknowledge Dr. Emine TEKİN and Selin PIRVIDALI MUCUR for their endless help in device setup and characterizations. Also, I would like to express my sincere gratitude to each of my friends at TUBITAK MAM for providing a great atmosphere and a wonderful work place. I would like to give my special thanks to my lab mate Gülçin HAYKIR for her warm friendship and help.

I would like to express my special thanks to my family for their support and encouragement. The care and love that they showed was always the relief and motivation for me when I met difficulties.

Words fail to express my gratefulness to my wife Esen ODABAŞ for her patience, understanding, and support throughout my entire Ph.D. thesis work. Without her understandings, I would never have been able to finish my long graduate career. Life is easier with her.

TABLE OF CONTENTS

ABSTRACT	v
ÖZ.....	vi
ACKNOWLEDGMENTS	viii
TABLE OF CONTENTS.....	ix
LIST OF FIGURES	xii
LIST OF TABLES	xix
LIST OF SCHEMES.....	xx
ABBREVIATIONS	xxi
CHAPTERS	1
1. INTRODUCTION.....	1
1.1. General Remarks.....	1
1.2. Photoluminescence and Electroluminescence.....	2
1.2.1. Photoluminescence	2
1.2.2. History of Electroluminescence.....	4
1.3. Organic Electronics.....	5
1.4. Organic Light Emitting Devices	6
1.4.1. Introduction.....	6
1.4.2. OLED light generating mechanism	6
1.4.3. Advantages and Disadvantages	9
1.4.4. Device Structure	12
1.4.4.1. Anode Materials.....	12
1.4.4.2. Cathode Materials	12
1.4.4.3. Hole Transport Materials (HTM).....	13
1.4.4.4. Electron Transport Materials (ETM).....	15
1.5. OLED Fabrication.....	16
1.5.1. Thermal evaporation under high-vacuum.....	16
1.5.2. Spin Coating System.....	16
1.6. Device characterization.....	18

1.7. Aggregation Induced Emission	19
1.7.1. General Remarks	19
1.7.2. Tetraphenylethene	23
1.8. Aim of the Work.....	27
2. RESULTS AND DISCUSSION.....	29
2.1. Synthesis of N-heterocyclic luminogens	29
2.1.1. Synthesis of N-heterocycle attached benzophenone derivatives	31
2.1.2. Synthesis of Tetraphenylethene derivatives.....	32
2.2. Thermal properties.....	32
2.3. Electrochemical properties	39
2.4. Optical Properties	42
2.5. Aggregation Induced Emission Properties	48
2.6. Lifetime Measurements	69
2.7. Application in Organic Light Emitting Devices.....	70
2.7.1. Optimization studies for device layout.....	70
2.7.2. Further OLED applications.....	76
3. EXPERIMENTAL	89
3.1. Materials and Methods	89
3.2. General Procedure for C-N coupling reactions	90
3.2.1. Synthesis of bis(4-(1H-pyrrol-1-yl)phenyl)methanone (33).....	91
3.2.2. Synthesis of bis(4-(1H-pyrazol-1-yl)phenyl)methanone (34).....	91
3.2.3. Synthesis of bis(4-(1H-imidazol-1-yl)phenyl)methanone (35).....	92
3.2.4. Synthesis of bis(4-(1H-indol-1-yl)phenyl)methanone (36).....	92
3.2.5. Synthesis of bis(4-(5-methoxy-1H-indol-1-yl)phenyl)methanone (37)	93
3.2.6. Synthesis of bis(4-(1H-benzo[d]imidazol-1-yl)phenyl)methanone (38).....	93
3.2.7. Synthesis of bis(4-(3,4-dihydro-1H-carbazol-9(2H)-yl)phenyl) methanone (39).....	94
3.2.8. Synthesis of bis(4-(3,6-di-tert-butyl-9H-carbazol-9-yl)phenyl) methanone (40).....	95
3.3. General procedure McMurry coupling reactions.....	95

3.3.1.Synthesis of 1,1,2,2-Tetrakis(4-(1H-pyrrol-1-yl)phenyl) ethane (41).....	96
3.3.2.Synthesis of 1,1,2,2-Tetrakis(4-(1H-pyrazol-1-yl)phenyl)ethane (42).....	96
3.3.3.Synthesis of 1,1,2,2-Tetrakis(4-(1H-imidazol-1-yl)phenyl)ethane (43).....	97
3.3.4.Synthesis of 1,1,2,2-Tetrakis(4-(1H-indol-1-yl)phenyl)ethane (44).....	98
3.3.5. Synthesis of 1,1,2,2-Tetrakis(4-(5-methoxy-1H-indol-1-yl)phenyl) ethane (45).....	99
3.3.6. Synthesis of 1,1,2,2-Tetrakis(4-(1H-benzo[d]imidazol-1-yl)phenyl) ethane (46).....	100
3.3.7. Synthesis of 1,1,2,2-Tetrakis(4-(3,4-dihydro-1H-carbazol-9(2H)-yl) phenyl)ethane (47).....	100
3.3.8. Synthesis of 1,1,2,2-Tetrakis(4-(3,6-di-tert-butyl-9H-carbazol-9-yl) phenyl)ethane (48).....	101
3.4. Preparation of aggregates.....	102
4. CONCLUSION.....	103
REFERENCES.....	104
APPENDIX.....	115
CURRICULUM VITAE.....	152

LIST OF FIGURES

FIGURES

Figure 1. Jablonski Diagram.....	3
Figure 2. Single layer OLED.....	6
Figure 3. Multi layer OLED.....	7
Figure 4. Schematic of charge transport by hopping.....	8
Figure 5. Basic energy band illustration (1) charge carrier injection (2) charge carrier transport (3) exciton formation and (4) radiative decay.....	9
Figure 6. Recombination of charge carriers.....	10
Figure 7. Performance statics of phosphorescent OLEDs ⁵⁸	11
Figure 8. Hole transport materials.....	13
Figure 9. Hole transport materials with high thermal stabilities.....	14
Figure 10. Common electron transport materials.....	15
Figure 11. High vacuum thermal evaporation.....	17
Figure 12. Schematic representation of spin coating system.....	17
Figure 13. Traditional luminogenic system.....	20
Figure 14. (Left) Structure of N,N-dicyclohexyl-1,7-dibromo-3,4,9,10-perylenetetra - carboxylic diimide, (Right) Fluorescence emission of DDPD molecule under different water:THF fractions. ¹⁰⁶	21
Figure 15. Non-traditional luminogenic system.....	22
Figure 16. Various molecules exhibiting aggregation induced emission phenomenon.....	22
Figure 17. Molecular packing pattern of TPE.....	23
Figure 18. Synthesis of TPE.....	24
Figure 19. Synthesis of TPE.....	24
Figure 20. Various tetraphenylethene based OLED devices having full color emission ¹⁴⁰	25
Figure 21. TPE based compounds having hole transport ability.....	26

Figure 22. Research areas related with TPE	26
Figure 23. CV of TDCPE (47) and TTBCPE (48).....	39
Figure 24. CV of TPPE (41) and TPyPE (42).....	39
Figure 25. CV of TIMPE (43) and TBIMPE (46).....	39
Figure 26. CV of TIPE (44)	41
Figure 27. CV of T5MIPE (45).....	41
Figure 28. Emission spectrum of synthesized luminogens	42
Figure 29. UV-Vis spectrum of TPPE, TPyPE and TIMPE	43
Figure 30. UV-Vis spectrum of TIPE, TBIMPE and T5MIPE.....	45
Figure 31. UV-Vis spectrum of TIPE, TDCPE and TTBCPE	45
Figure 32. Absorption behavior of TIPE in different solvents.....	47
Figure 33. Emission behavior of TIPE in different solvents.....	47
Figure 34. (Left) UV-Vis spectrum of TPPE in solution (100% THF) and in aggregate (90% water – THF) (Right) Fluorescence quantum yield increase.....	50
Figure 35. PL spectra of TPPE in THF (10 μ M) with different water fractions. The inset shows the change in the luminescence intensity	51
Figure 36. The emission images of TPPE in THF with different water fractions under UV light (365 nm) illumination at room temperature.....	51
Figure 37. (Left) UV-Vis spectrum of TPyPE in solution (100% THF) and in aggregate (90% water – THF) (Right) Fluorescence quantum yield increase.....	52
Figure 38. PL spectra of TPyPE in THF (10 μ M) with different water fractions. The inset shows the change in the luminescence intensity	52
Figure 39. The emission images of TPyPE in THF with different water fractions under UV light (365 nm) illumination at room temperature.....	53
Figure 40. (Left) UV-Vis spectrum of TIMPE in solution (100% THF) and in aggregate (90% water – THF) (Right) Fluorescence quantum yield increase.....	54
Figure 41. PL spectra of TIMPE in THF (10 μ M) with different water fractions. The inset shows the change in the luminescence intensity	55
Figure 42. The emission images of TIMPE in THF with different water fractions under UV light (365 nm) illumination at room temperature.....	55
Figure 43. (Left) UV-Vis spectrum of TIPE in solution (100% THF) and in aggregate (90% water – THF) (Right) Fluorescence quantum yield increase.....	56

Figure 44. PL spectra of TIPE in THF (10 μ M) with different water fractions. The inset shows the change in the luminescence intensity	56
Figure 45. The emission images of TIPE in THF with different water fractions under UV light (365 nm) illumination at room temperature	57
Figure 46. Particle size analysis of TIPE molecules in 90% water – THF mixtures	58
Figure 47. TEM Images (0.2 μ m scale) of TIPE in different THF/water fractions. A) 60% water B) 90% water	59
Figure 48. (Left) UV-Vis spectrum of T5MIPE in solution (100% THF) and in aggregate (90% water – THF) (Right) Fluorescence quantum yield increase	60
Figure 49. PL spectra of T5MIPE in THF (10 μ M) with different water fractions. The inset shows the change in the luminescence intensity.....	60
Figure 50. The emission images of T5MIPE in THF with different water fractions under UV light (365 nm) illumination at room temperature	61
Figure 51. (Left) UV-Vis spectrum of TBIMPE in solution (100% THF) and in aggregate (90% water – THF) (Right) Fluorescence quantum yield increase	62
Figure 52. PL spectra of TBIMPE in THF (10 μ M) with different water fractions. The inset shows the change in the luminescence intensity.....	62
Figure 53. The emission images of TBIMPE in THF with different water fractions under UV light (365 nm) illumination at room temperature	63
Figure 54. (Left) UV-Vis spectrum of TDCPE in solution (100% THF) and in aggregate (90% water – THF) (Right) Fluorescence quantum yield increase	64
Figure 55. PL spectra of TDCPE in THF (10 μ M) with different water fractions. The inset shows the change in the luminescence intensity.....	64
Figure 56. The emission images of TDCPE in THF with different water fractions under UV light (365 nm) illumination at room temperature	65
Figure 57. (Left) UV-Vis spectrum of TTBCPE in solution (100% THF) and in aggregate (90% water – THF) (Right) Fluorescence quantum yield increase	66
Figure 58. PL spectra of TTBCPE in THF (10 μ M) with different water fractions. The inset shows the change in the luminescence intensity.....	66
Figure 59. The emission images of TTBCPE in THF with different water fractions under UV light (365 nm) illumination at room temperature	67

Figure 60. Device layout 1	70
Figure 61. (Left) Luminance-voltage, (Right) Luminous efficiency, curves of the OLED 1	71
Figure 62. Device Layout 2	72
Figure 63. (Left) Luminance-voltage, (Right) Luminous efficiency, curves of the OLED 2	72
Figure 64. Device Layout 3	73
Figure 65. OLED device using TIPE as an emitter	74
Figure 66. Performance curves of device 3	75
Figure 67. Optimized device architecture	76
Figure 68. (Top-left) Luminance-voltage, (top-right) luminous efficiency, (bottom left) electroluminescence and (bottom right) chromaticity coordinate curves of OLED device 4 using TTBCPE as a light emitting layer	77
Figure 69. (Top-left) Luminous efficiency, (top-right) EQE – current density, (bottom left) Luminance-voltage and (bottom right) electroluminescence curves of OLED device 5 using TDCPE as a light emitting layer.....	78
Figure 70. (Top-left) Luminous efficiency, (top-right) Luminance-voltage, (bottom left) electroluminescence and (bottom right) chromaticity coordinate curves of OLED device 6 using TPPE as a light emitting layer	79
Figure 71. OLED device 6 using TPPE as an emitter	80
Figure 72. (Top-left) Luminance-voltage, (top-right) luminous efficiency, (bottom left) electroluminescence and (bottom right) chromaticity coordinate curves of OLED device 7 using TIMPE as a light emitting layer	80
Figure 73. OLED device using TIMPE as an emitter	81
Figure 74 (Top-left) Luminous efficiency, (top-right) Luminance-voltage, (bottom left) Electroluminescence and (bottom right) Chromaticity coordinate curves of OLED device 8 using TPyPE as a light emitting layer.....	82
Figure 75. (Top-left) Luminous efficiency, (top-right) Luminance-voltage, (bottom left) Electroluminescence and (bottom right) Chromaticity coordinate curves of OLED device 9 using TBIMPE as a light emitting layer.....	83
Figure 76. OLED device using TBIMPE as an emitter.....	83

Figure 77. (Top-left) Luminous efficiency, (top-right) Luminance-voltage, (bottom left) Electroluminescence curves of OLED device 10 using T5MIPE as a light emitting layer	84
Figure 78. (Top-left) Luminous efficiency, (top-right) Luminance-voltage, (bottom) External quantum efficiency results of device 11 using TIPE as a light emitting layer.....	85
Figure 79. Device Layout 4	86
Figure 80. (Top-left) Luminous efficiency, (top-right) Luminance-voltage, (bottom left) External quantum efficiency, (bottom right) Electroluminescence curves of device 12 using T5MIPE as a light emitting layer	87
Figure A 1. ¹ H NMR spectrum of compound 33.....	115
Figure A 2. ¹ H NMR spectrum of compound 34.....	116
Figure A 3. ¹³ C NMR spectrum of compound 34.....	116
Figure A 4. ¹ H NMR spectrum of compound 35.....	117
Figure A 5. ¹³ C NMR spectrum of compound 35.....	117
Figure A 6. ¹ H NMR spectrum of compound 36.....	118
Figure A 7. ¹³ C NMR spectrum of compound 36.....	118
Figure A 8. ¹ H NMR spectrum of compound 37.....	119
Figure A 9. ¹³ C NMR spectrum of compound 37.....	119
Figure A 10. ¹ H NMR spectrum of compound 38.....	120
Figure A 11. ¹³ C NMR spectrum of compound 38.....	120
Figure A 12. ¹ H NMR spectrum of compound 39.....	121
Figure A 13. ¹³ C NMR spectrum of compound 39.....	121
Figure A 14. ¹ H NMR spectrum of compound 40.....	122
Figure A 15. ¹³ C NMR spectrum of compound 40.....	122
Figure A 16. ¹ H NMR spectrum of compound 41.....	123
Figure A 17. ¹³ C NMR spectrum of compound 41.....	123
Figure A 18. ¹ H NMR spectrum of compound 42.....	124
Figure A 19. ¹³ C NMR spectrum of compound 42.....	124
Figure A 20. ¹ H NMR spectrum of compound 43.....	125
Figure A 21. ¹³ C NMR spectrum of compound 43.....	125
Figure A 22. ¹ H NMR spectrum of compound 44.....	126

Figure A 23. ^{13}C NMR spectrum of compound 44	126
Figure A 24. ^1H NMR spectrum of compound 45	127
Figure A 25. ^{13}C NMR spectrum of compound 45	127
Figure A 26. ^1H NMR spectrum of compound 46	128
Figure A 27. ^{13}C NMR spectrum of compound 46	128
Figure A 28. ^1H NMR spectrum of compound 47	129
Figure A 29. ^{13}C NMR spectrum of compound 47	129
Figure A 30. ^1H NMR spectrum of compound 48	130
Figure A 31. ^{13}C NMR spectrum of compound 48	130
Figure A 32. ESI-TOF spectrum of compound 33	131
Figure A 33. ESI-TOF spectrum of compound 34	131
Figure A 34. ESI-TOF spectrum of compound 35	132
Figure A 35. ESI-TOF spectrum of compound 36	132
Figure A 36. ESI-TOF spectrum of compound 37	133
Figure A 37. ESI-TOF spectrum of compound 38	133
Figure A 38. ESI-TOF spectrum of compound 39	134
Figure A 39. ESI-TOF spectrum of compound 40	134
Figure A 40. HRMS spectrum of TPPE (41)	135
Figure A 41. HRMS spectrum of TPyPE (42)	135
Figure A 42. HRMS spectrum of TIMPE (43)	136
Figure A 43. HRMS spectrum of TIPE (44)	136
Figure A 44. HRMS spectrum of T5MIPE (45)	137
Figure A 45. HRMS spectrum of TBIMPE (46)	137
Figure A 46. HRMS spectrum of TDCPE (47)	138
Figure A 47. HRMS spectrum of TTBCPE (48)	138
Figure A 48. Fluorescence decay curve of TPPE (41)	139
Figure A 49. Fluorescence decay curve of TPyPE (42)	139
Figure A 50. Fluorescence decay curve of TIMPE (43)	140
Figure A 51. Fluorescence decay curve of TIPE (44)	140
Figure A 52. Fluorescence decay curve of T5MIPE (45)	141
Figure A 53. Fluorescence decay curve of TBIMPE (46)	141
Figure A 54. Fluorescence decay curve of TDCPE (47)	142

Figure A 55. Fluorescence decay curve of TTBCPE (48).....	142
Figure A 56. FTIR spectrum of TPPE (41)	143
Figure A 57. FTIR spectrum of TPyPE (42)	143
Figure A 58. FTIR spectrum of TIMPE (43).....	144
Figure A 59. FTIR spectrum of TIPE (44)	144
Figure A 60. FTIR spectrum of T5MIPE (45).....	145
Figure A 61. FTIR spectrum of TBIMPE (46).....	145
Figure A 62. FTIR spectrum of TDCPE (47).....	146
Figure A 63. FTIR spectrum of TTBCPE (48).....	146
Figure A 64. DSC Thermogram of TPPE (41).....	147
Figure A 65. DSC Thermogram of TPyPE (42).....	147
Figure A 66. DSC Thermogram of TIMPE (43)	148
Figure A 67. DSC Thermogram of TIPE (44).....	148
Figure A 68. DSC Thermogram of T5MIPE (45)	149
Figure A 69. DSC Thermogram of TBIMPE (46).....	149
Figure A 70. DSC Thermogram of TDCPE (47).....	150
Figure A 71. DSC Thermogram of TTBCPE (48)	150
Figure A 72. TGA thermograms of the synthesized luminogens (41-48).....	151

LIST OF TABLES

TABLES

Table 1. Synthesis of TPE luminogens	33
Table 2. Thermal properties of synthesized compounds	34
Table 3. Electrochemical behavior of synthesized luminogens	40
Table 4. Photophysical Characterization of compounds	43
Table 5. Fluorescence quantum yield values of synthesized compounds in THF with different water fractions	49
Table 6. Particle size analysis results of TIPE with fractions 70-90% in THF	58
Table 7. Fluorescence decay parameters of synthesized compounds in 90% water in THF	69
Table 8. Performance of devices 1-3	73
Table 9. All the OLED device characterization data of the synthesized luminogens	88

LIST OF SCHEMES

SCHEMES

Scheme 1. Synthesis scheme.....	28
Scheme 2. TPE based luminogenic compounds	30

ABBREVIATIONS

CRT	Cathode Ray Tube
PDP	Plasma Panel Display
LCD	Liquid Crystal Display
OLED	Organic Light Emitting Diode/Device
EL	Electroluminescence
PL	Photoluminescence
UV-Vis	Ultraviolet-Visible
PVK	Polyvinylcarbazole
ETL	Electron Transport Layer
HTL	Hole Transport Layer
Lm/W	Lumen/Watt
Cd/A	Candela/Ampere
EQE	External Quantum Efficiency
CIE	Commission Internationale de L'Éclairage
HOMO	Highest Occupied Molecular Orbital
LUMO	Highest Unoccupied Molecular Orbital
DSC	Differential Scanning Calorimetry
TGA	Thermo Gravimetric Analysis
T _g	Glass Transition Temperature
T _m	Melting Temperature
T _c	Cold Crystallization Temperature
T _d	Degradation Temperature
ITO	Indium Tin Oxide
TPD	N,N'-Bis(3-methylphenyl)-N,N'-diphenylbenzidine
NPD	N,N'-Di-[(1-naphthyl)-N,N'-diphenyl]-1,1'-biphenyl)-4,4'-diamine
TCTA	Tris(4-carbazoyl-9-ylphenyl)amine
TPBI	1,3,5-tris(N-phenylbenzimidazol-2-yl)benzene
Alq ₃	Tris-(8-hydroxyquinoline)aluminum

PBD	2-(4-Biphenyl)-5-phenyl-1,3,4-oxadiazole
DDPD	N,N-dicyclohexyl-1,7-dibromo-3,4,9,10-perylenetetracarboxylic diimide
HPS	Hexaphenylsilole
TPE	Tetraphenylethene
AIE	Aggregation Induced Emission
ACQ	Aggregation Caused Quenching
HRMS	High-resolution mass spectrometry
ESI-TOF	Electrospray ionization - Time-of-flight
FTIR	Fourier transform infrared spectroscopy

CHAPTER 1

INTRODUCTION

1.1. General Remarks

In the last decade the dominant lighting and display technologies were tungsten light bulb and cathode ray tube (CRT), respectively.^{1,2} Although these technologies lead the 20th century, the change in the consumer needs together with the increasing trend in energy saving actions, has decreased the popularity of these technologies.

An incandescent bulb is the least efficient lighting source among the other lighting resources. It converts not more than 5% of the energy into visible light, 95% or more is transformed into heat rather than emission as a light.^{3,4} The efficiency of an incandescent bulb is about 15 lm/W and its lifetime is approximately 1000 h.⁵ Inefficient incandescent light bulbs are started to remove from the markets after European Commission adapted a regulation (244/2009).⁶ The development of fluorescent light bulbs was increased the efficiency up to 60 lm/W and improved the operating lifetime about 3-fold comparing with an incandescent bulb. Although they are more effective than incandescent bulbs, the cost, environmental and health concerns are the major drawbacks.⁷

Since the beginning of display technology there have been several types of device technologies starting from cathode ray tubes (CRT), plasma display panels (PDP), and finally the liquid crystal displays (LCD).⁸ Although the cathode ray tube screens have excellent image qualities⁹, the volume of the displays is comparatively high when compared with PDP and LCD. In fact, fabrication of larger sized displays by using CRT technology is extremely expensive.¹⁰ In contrast, PDPs and LCDs are flat panel screens, however, PDPs show screen burn

effects resulted from excessive use of unchanged images.¹¹ Additionally the plasma displays are also very fragile. Furthermore, LCDs function with slower response times, generally in milliseconds and having low viewing angles and require a backlight to function.¹² Organic light emitting devices (OLEDs) have been an advance next generation technology having potential to supplant the outdated technologies in the near future.¹³

1.2. Photoluminescence and Electroluminescence

1.2.1. Photoluminescence

An excited molecule that stimulated to a higher energy level should return to its ground state sooner or later, except participating in a photochemical reaction and consequently losing its uniqueness.¹⁴ Due to an energy loss in the excited state, the wavelength of the emitted light is longer than the absorption wavelength.

Fluorescence and phosphorescence are similar in a way that the excitation is related about photonic absorptions which are located on the spectral range of Ultraviolet-Visible (UV-Vis) region. The two terms can be generalized to more common phenomena called photoluminescence. In contrast to photoluminescence, electroluminescence is stimulated by an injected current or electrical field.¹⁵

Figure 1. represents the energy level diagram of a luminescent molecule. The flat line at the lowest part of the diagram symbolizes the ground state of the molecule represented as S_0 . S_1 and S_2 are the first and second singlet electronic states and T_1 is the first triplet electronic state. There are also many vibrational energy levels belonging to the aforementioned energy levels.

If a molecule is supposed to excited to the higher state from the ground state S_0 , the molecule have many possible mechanistic de-excitation pathways to return into its ground state.

If the molecule is in liquid phase, it can give the excess vibrational energy by colliding with the other molecules. This process is extremely fast with an average lifetime of 10^{-12} s. Moreover, minimizing the excess energy by vibrational relaxation causes an increase in the temperature of the solvent.¹⁶

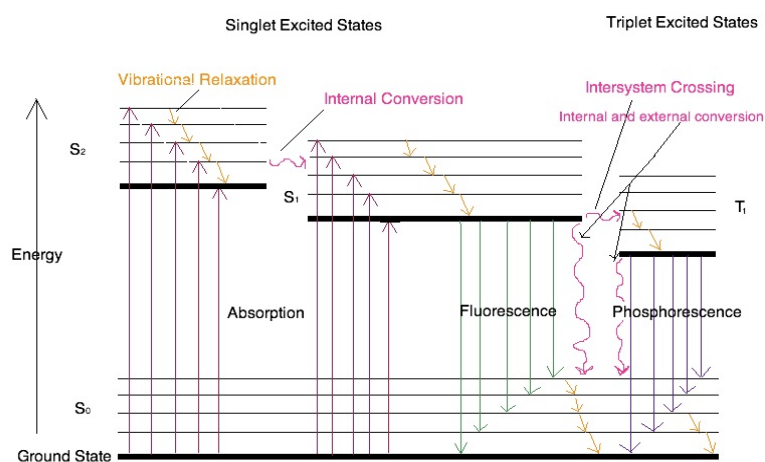


Figure 1. Jablonski Diagram

The electronic energy of the higher energy levels S₂ or S_n was lost to the surroundings and passed to lower energy states without any emission of radiation. This process called internal conversion. The average rate is as same as vibrational relaxations and valued as 10^{-13} to 10^{-12} s. Once the molecule reaches to zero vibrational level of the first excited state S₁, there are two possible pathways for decay processes. The excited molecule could prefer to direct transition from first excited state to the ground state named as fluorescence. The average lifetime of fluorescence is about 10^{-9} to 10^{-7} s. Sometimes the electron can reverse its spin and as a result a multiplicity change could be occurred. This process called intersystem crossing. After intersystem crossing happened to a triplet state, the excited molecule can turn back to its ground state by a relaxation process called phosphorescence. The average lifetime of phosphorescence emission is between 10^{-4} to 10s.¹⁷

1.2.2. History of Electroluminescence

The discovery of electroluminescence (EL) was observed by H. J. Round using a piece of carborundum (SiC) crystal in 1907.¹⁸ After about fifty years later, in 1962, Holonyak and his coworkers commercialized these researches by producing the first inorganic LED.^{19,20} Acridine orange and quinacrine were the first pioneer compounds that an electroluminescence of an organic material was observed by Bernanose in 1950 using high voltage alternating current (AC).^{21,22} After that, Pope et al.²³ chose to apply direct current (DC) rather than AC current and the electroluminescence was shown by using single crystals of anthracene. Still, the device gave an emission only above 400 V and had 10-20 μm thickness.²⁴ Schneider and Helfrich used electron and hole injecting electrodes and produced double injection recombination electroluminescence in single crystal of anthracene and succeeded to lower the turn on voltage to around 60 V for visible emission.²⁵ In 1975, the organic electroluminescence of a polymer, polymer polyvinyl carbazole (PVK), was firstly introduced.²⁶

Until 1980s, all attempts for developing organic electroluminescence had some significant drawbacks, that is, in order to obtain a sizeable light output there had to be applied very high driving voltages higher than 100V.^{27,28} By using the deposition technique of organic materials, in 1982 Vincett et al. used anthracene and had a success to achieve an operating voltage below 30 V, still the external quantum efficiency were quite low with a value of about 0.05%.²⁹

The breaking point of OLED researches was occurred after 1980s. Until this time, the researchers are mainly in academic ground. Tang and his coworkers at Kodak Chemical showed for the first time efficient organic light-emitting devices in multilayer configuration with significant performance improvement.³⁰ This device showed a luminescence greater than 1000 Cd/m^2 , power efficiency about 1.5 lm/W and EQE about 1% with an operating voltage below 10 V.

Together with the progress of organic based EL devices researchers started to concentrate on the new materials having higher and easy processing abilities. In 1990, another significant progress have been occurred in polymer based OLEDs. Friend et al.³¹ exhibited a single layer OLED with poly-p-(phenylenevinylene) (PPV) having highly fluorescent yellow green color.

In order to exceed the boundary of 25% efficiency boundary³², in 1998 Baldo et. al. used phosphorescent dopant material (platinum octaethylporphine) to collect the triplet excitons and 4% EQE was accomplished.. Soon after, Adachi and his coworkers achieved an EQE value of about 22% using a phosphorescent dopant in a high band-gap host³³.

1.3. Organic Electronics

In the last decade conducting a research on organic electronics has become a key concept and the number of studies related in chemistry, physics and material science has grown exponentially.³⁴⁻⁴¹ The organic materials act as an insulator under the low electric field that is below 10^4 V/cm. The importance of organic electronics has been emphasized in 2000 by Nobel Prize awarded by A. Heeger, A. Mac Diarmind and H. Shirakawa⁴²⁻⁴⁵ for their contribution on the discovery and development of semiconducting polymers.

The high demand on the consumer's needs and requirements are giving stimulation for searching efficient materials in order to make electronic components for portable and electronic devices. Many kinds of organic materials have exceptional properties related with photo and electrical conductivity, photo- and electroluminescence and also tune-ability.⁴⁶ As a result of their unique characteristics of special small organic molecules and conjugated polymers they were started to become integral units in the progress of new electronic devices.⁴⁷⁻⁵⁰

1.4. Organic Light Emitting Devices

1.4.1. Introduction

An OLED is a solid state electronic device by depositing a sequence of thin appropriate bias is applied a bright light is emitted.⁵¹ In order to escape the generated light from the device, one of the electrodes must be transparent. In OLEDs the color of the device depends on the emissive material used and the intensity of the device is controlled by amount of current that is applied.

Figure 2 shows the basic architecture of an OLED. OLEDs can be single layered or multi-layered. The single layered OLED could be used for polymeric type emissive materials and multi-layered OLED could be used for emissive layers made from small organic molecules (Figure 3). In order to increase the performance of the device, some other layers apart from emissive layer must be added.⁵²

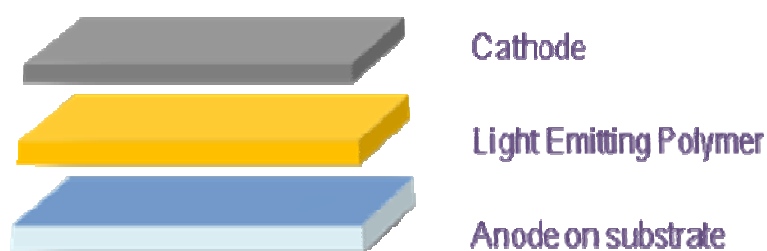


Figure 2. Single layer OLED

1.4.2. OLED light generating mechanism

The light from an OLED was generated with a 3 main step. The first step involves the injection of holes and electrons from anode and cathode, respectively. When a proper voltage is applied between the electrodes, electrons are injected from

cathode into the LUMO of the electron transport layer and holes are injected from the anode into the HOMO of the hole transport layer. In general, there is an energy barrier for injection of electron and holes. This energy barrier is due to the difference in the positions of energy levels between metallic electrodes and organic materials. The relation between the electrode and organic layer determine the probability of the charge injection. The probability could be increased by reducing the energy barriers between the organic layer and the metallic electrode. The work function of the metallic electrodes together with the HOMO and LUMO levels of the organic materials define the energy barrier. To increase the charge injection probability high work function electrode for anode and low work function cathode must be chosen for easy stimulation of holes from cathode and electrons from anode respectively. Furthermore, addition of hole injection or electron injection layers can tune the energy barrier between the electrode and organic layer and an enhancement of charge injection could be achieved.

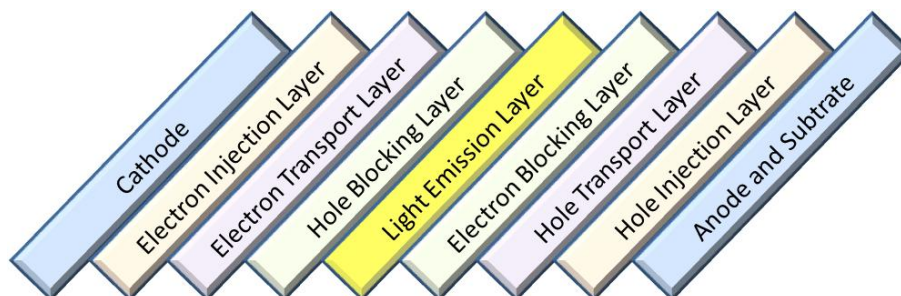


Figure 3. Multi layer OLED

The second step involves the hole and electron movement through the hole and electron transport layers. After the holes and electrons have been injected from the electrodes, they move into HTL and ETL. In these layers electrons and holes form excited states named as radical ions. In fact, the physicist called these ions as polarons. These radical ions migrate into the emissive layer through charge hopping mechanism⁵³⁻⁵⁴ (Figure 4). The definite mechanism for the charge transfer in organic molecules is known as the disorder formalism. It takes place through

localized hopping of charges between ground and excited state of molecules. In fact, the effectiveness of movements of charges is related with morphology and purity of the organic molecules. Impurities may act as detrimental traps both for electrons and holes.⁵⁵

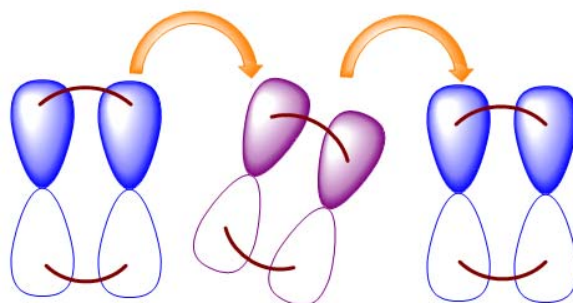


Figure 4. Schematic of charge transport by hopping

The final step involves the recombination of the opposite charges. That is, the opposite charges recombine to form molecular excited state called exciton. According to the behavior of the emissive material (HOMO and LUMO levels), fluorescence or phosphorescence light is emitted. In Figure 5 all the light generating steps of an OLED was summarized.

The holes and electrons are coupled to form four new mutual energy state associated with the spin statistics of general quantum mechanics. There is only one singlet exciton and three triplet excitons (Figure 6). Generally, only singlet excitons can have allowed decay and the triplet excitons show non radiative decay since the triplet states are spin forbidden.

As a general rule, to succeed an effective luminescence, the following subjects must be proceed efficiently:

- (1) good balance between holes and electron currents,
- (2) efficient capture of holes and electrons in the emissive layer,

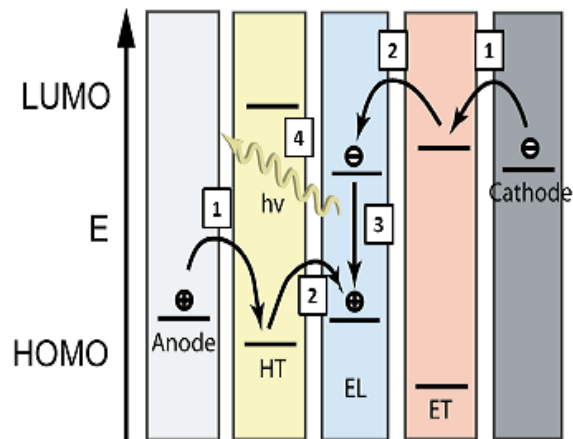


Figure 5. Basic energy band illustration (1) charge carrier injection (2) charge carrier transport (3) exciton formation and (4) radiative decay

- (3) highly radiative transitions for singlet excitons,
- (4) effectual coupling of these excitons to photon states allowed in the device configuration.

1.4.3. Advantages and Disadvantages

Over the period of 100 years, the display technology has grown dramatically starting from Cathode Ray Tube (CRT). The CRT display technology has gradually been changed by the plasma display panel (PDP) and Liquid Crystal Display (LCD). These new technologies came with a big advantage that much smaller volume is required for the same surface area display. Together with LCD displays, OLED's are also a flat panel technology and start to dominate the market starting from millennium and expecting an apex in three to five years. There are several advantages of using OLED as a display or a lighting source.⁵⁶

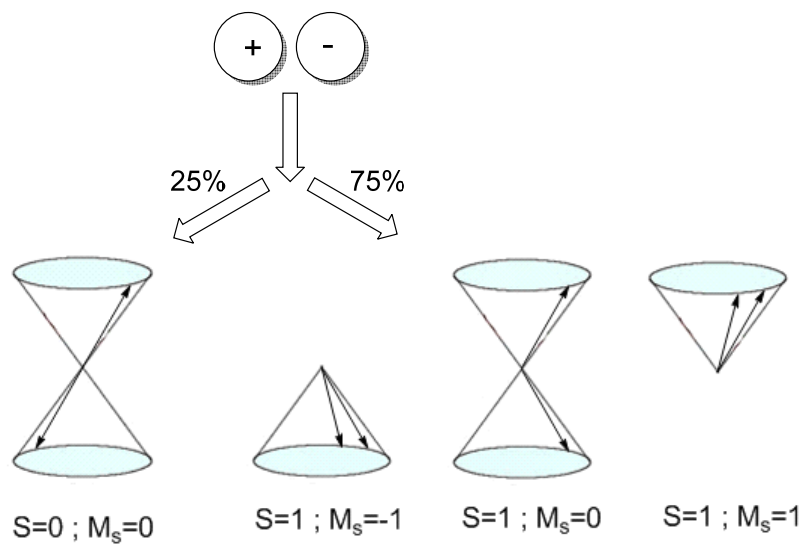


Figure 6. Recombination of charge carriers

- Self Emitting: The luminous efficiency of OLEDs is higher than the other display technologies. OLEDs do not require a backlight, polarizers and diffusers. Therefore much thinner display panels could be made that give OLEDs lightweight ability.⁵⁷
- Easy manufacturing: Apart from inorganic LEDs, OLEDs are producing with cost effective processes such as roll-to-roll, inkjet printing and screen printing
- Flexibility: One of the big advantage of OLEDs is they can be easily manufacture on plastic layers.
- They have large viewing angle (up to 170°) and fast switching times (1000 fold faster than traditional displays)
- They have high resolution, high brightness and high contrast values.
- OLED's require low voltage ($< 5V$) to operate.
- LEDs are made-up from single crystal semiconductors. These inorganic LED's are point light sources like traditional light bulbs; however, OLED's could illuminate much higher area.

PHOLED Performance (at 1000 cd/m ²)	1931 CIE Color Coordinates	Luminous Efficiency (Cd/A)	Operating Lifetime (hrs)	
			LT 95%	LT 50%
DEEP RED	(0.69, 0.31)	17	14000	250000
RED	(0.66, 0.34)	29	23000	600000
RED	(0.64, 0.36)	30	50000	900000
YELLOW	(0.44, 0.54)	81	85000	1450000
GREEN	(0.31, 0.63)	85	18000	400000
LIGHT BLUE	(0.18, 0.42)	50	700	20000

Figure 7. Performance statics of phosphorescent OLEDs⁵⁸

Apart from their exceptional properties, organic LED's have also some drawbacks to be solved. The first important issue is lifetime. Consistent with SID 2012 values the Universal Display Corporation has the phosphorescent OLED materials having lifetime shown in Figure 7.⁵⁸ According to the Figure 8 the lifetime problem was solved for red and green OLEDs, however, the blue OLED has minimum 20 fold less lifetime than the other colors.

Secondly, since they all have organic materials, OLED's are highly sensitive to air and moisture.⁵⁹ Degradation of organic materials determine the lifetime of the device. Therefore encapsulation is a critical issue on OLED technology and must be done properly where a simple encapsulation process with a glass in nitrogen could rise the lifetime of the OLED by the order of two.⁶⁰ Besides, the glass transition temperature (T_g) is another concern as organic molecules with low T_g start to degrade when operating the device.

Thirdly, the OLED technology is currently not a cost effective technology. Although roll to roll processes are relatively inexpensive for large scale productions, vacuum deposition techniques are still expensive. In 2011, the OLED panel cost was \$14000/klm and it will decrease to \$15/klm in the coming 10 years.⁶¹

1.4.4. Device Structure

1.4.4.1. Anode Materials

The anode materials are generally formed on the substrate (plastic or glass) and must have some typical requirements⁶²:

- High conductivity: In order to decrease the contact resistance.
- High work function ($\Phi > 4.1$ eV): To support injection of holes into the organic layers.
- Good film forming and wettability: In order to have good contact with neighboring organic layers.
- High thermal and chemical stability.
- Adequately high transparency: so as the emitted light is able to leave the device effectively.

Indium tin oxide (ITO) is the most used anode for OLED applications.⁶³ It consists of indium oxide and an about 10% amount of tin oxide. It has a high work function varying between 4.5 to 4.8 eV. Because of its high band gap (>4.0 eV), it is transparent in the visible region.

1.4.4.2. Cathode Materials

In most cases, cathode materials are metal alloys or pure metals. The selection of material is due to minimizing the energy barrier between the electrode and the adjacent organic layer. The cathode materials should have some basic properties⁶⁴:

- Must have high conductivity.
- Relatively low work function (Φ): In order to promote injection of electrons into the organic layers.
- Good film forming and wettability: In order to have good contact with neighboring organic layers.

- High thermal and chemical stability.

The metals such as calcium (Ca), magnesium (Mg), aluminum (Al) and their alloys are used as cathode. The problem with low work function metals is, they are very susceptible to air and moisture. Cathode materials degrade by formation and enlargement of non-emissive dark spots. In order to get rid of this unwanted issue, a very thin layer of LiF or CsF can be added.⁶⁵

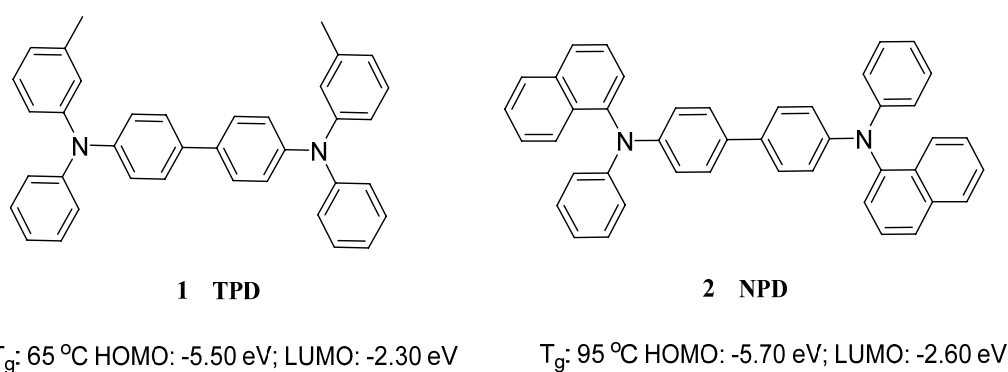


Figure 8. Hole transport materials

1.4.4.3. Hole Transport Materials (HTM)

The hole transport materials are crucial elements for multi-layer small organic OLED devices. The functions of HTMs are to help positive charge carriers drift from anode into the emissive layer by acting as a hole conductive pathway. In contrast, polymers have the ability acting as a hole transport materials by charge hopping, therefore, for polymer based OLEDs usually using HTM are not needed. Generally, HTM must have the following properties⁶⁶:

- Low electron affinity: Helps to prevent negative charge carriers reaching the anode.
- Low ionization potential.
- Easily oxidized.

- Stable in one electron oxidized state.
- Comparably low HOMO level.
- Could act as an electron blocking layer for stopping the electrons not to reach to anode.

The most common hole transport layer compounds are triarylamines because of their electron rich moieties. N,N'-Bis(3-methylphenyl)-N,N'-diphenyl-[1,1'-biphenyl]-4,4'-diamine (TPD), N,N'-Di-[(1-naphthyl)-N,N'-diphenyl]-1,1'-biphenyl-4,4'-diamine (NPD) and 4,4',4''-Tris(N-3-methylphenyl-N-phenylamino)triphenylamine are used frequently as a HTM (Figure 8).⁶⁷⁻⁶⁸

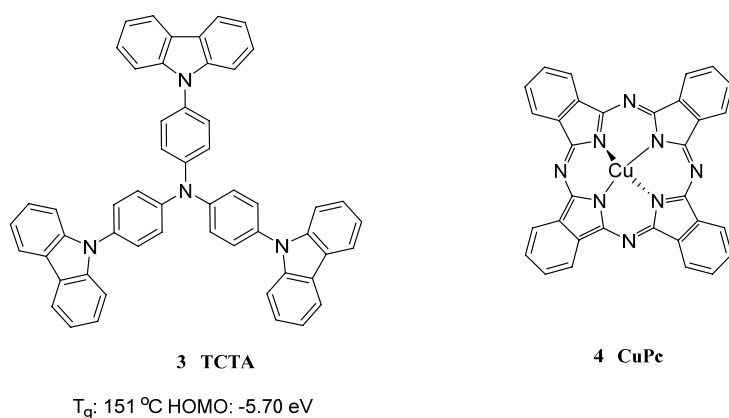


Figure 9. Hole transport materials with high thermal stabilities

For the reason that, TPD and NPD have low glass transition temperatures (lower thermal stability) and inadequate morphological stability (easy crystallization of TPD), compounds with higher thermal stability were synthesized (Figure 9). Furthermore, phthalocyanines (Pc) and their derivatives are also used as HTMs because of their high thermal and chemical stability together with easy oxidation. Copper phthalocyanine (PcCu) is the commonly used derivative as the HTM in OLEDs.⁶⁹

1.4.4.4. Electron Transport Materials (ETM)

Electron transport layer materials are the most extensively studied compounds in OLEDs. The function of ETL layer is to serve as a conducting material and assist electrons moving from cathode to organic layers. ETM must possess the following properties.⁷⁰

- High electron affinity: matching the work function of the cathode and decrease the potential between cathode and the emitter.
- High electron transport mobility.
- Stable in one electron reduce form.
- High thermal stability connected with high T_g .
- Good film forming and wettability: In order to have uniform films for minimizing pin-hole defects.
- Could act as a hole blocking layer (having low lying HOMO) to prevent holes reaching to the cathode by crossing the emitting layer.

Metal chelates and electron deficient heterocycles, like triazoles and oxadiazoles, are the useable ETMs (Figure 10).⁷¹⁻⁷³

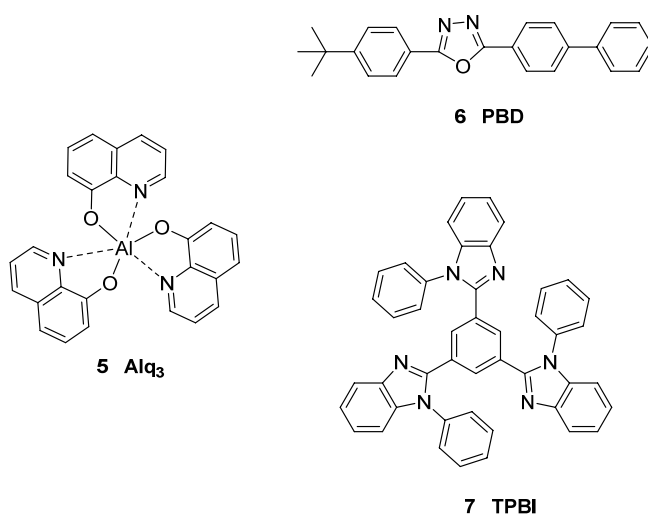


Figure 10. Common electron transport materials

1.5. OLED Fabrication

Since the beginning of the discovery of electroluminescent devices many techniques were used to fabricate these devices.⁷⁴ Generally, organic light emitting devices could be manufactured by means of two main classifications: dry and wet techniques. The dry techniques involve thermal evaporation under high vacuum and wet techniques involve spin coating and ink jet printing.

Low molecular weight small organic molecules could be deposited under high vacuum by thermal evaporation and polymeric type molecules could be deposited by solution processed procedures.

1.5.1. Thermal evaporation under high-vacuum

Thermal vacuum deposition techniques are useful for depositing an extensive range of materials; from inorganics and metals to low molecular weight organic compounds. It is also suitable for fabrication of OLEDs, based on the small organic molecules.⁷⁵ The deposition is generated in a high vacuum chamber ($<10^{-6}$ mbar) contained in an Ar-N₂ filled glove box.⁷⁶ A boat shaped container made of metal like tungsten is used both as a vessel and a resistive heating resource to increase the temperature of the organic sample in the vessel. Using an electron beam for evaporation is less than resistive heating since high energy electrons can harm the OLED device.

Figure 11 shows the simplistic evaporation chamber for thermal evaporation under high vacuum. One of the advantages of thermal evaporation systems is, the thickness of each and all the layers can be controlled when fabricating a multilayer OLED.

1.5.2. Spin Coating System

The wet coating systems are suitable for polymeric type molecules. There are a number of wet coating systems including dip coating, spray coating, ink-jet

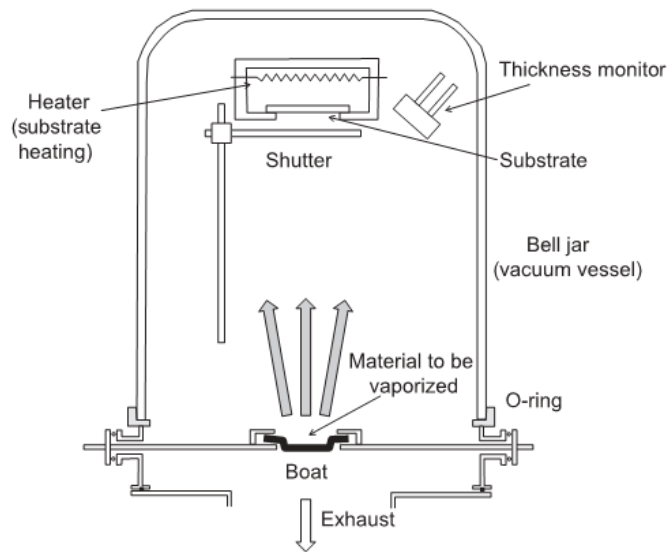


Figure 11. High vacuum thermal evaporation

printing and spin coating etc..⁷⁷ The spin coating technique is more easily applicable among the wet coating systems.⁷⁸ Spin coat systems (Figure 12) do not require high vacuum systems and therefore the coating expenses are reduced. An important criterion for spin coating systems is that the molecule under consideration must dissolve in any kind of solvent. Although solution processed techniques are easy and low-priced, re-dissolving the previously deposited layers are the major drawbacks.⁷⁹ Additionally, the film thicknesses can be controlled by choosing proper solvent concentration but it is hard to get desirable thin films.

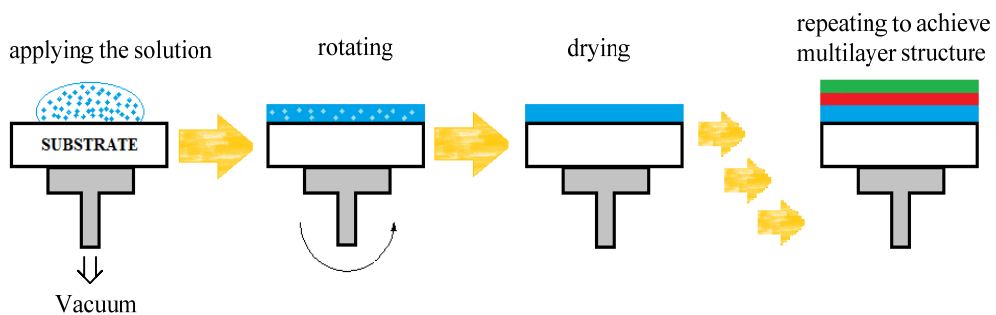


Figure 12. Schematic representation of spin coating system

1.6. Device characterization

The applications of OLEDs are associated with the emission of visible light therefore a number of photometric characterizations must be done to clearly identify the quality of the device that was made.

OLEDs can function only when an electric field, a potential difference, is applied between the two metallic electrodes. The voltage that the OLED is started to emit any detectable color is named as turn on voltage. The energy barriers between the layers are related with the turn on voltage of the device. Lower turn on voltages is better than higher ones since at higher voltages, the organic materials start to degrade eventually.⁸⁰

External quantum efficiency (EQE) is defined as the ratio of the number of photons extracted toward the front to that of electrons flowing through the external driving circuit. The simplest explanation of external quantum efficiency is for each pair of charges that is injected into the device an exciton can be formed and from each exciton a photon can be emitted in the relaxation to the ground state. Ideally the ratios of these events will be 1:1, giving 100% internal quantum efficiency. Unfortunately, this does not translate into 100% external quantum efficiency due to device limitations. The formation of an exciton does not guarantee that a photon can be observed from the device. This is the first of several chance processes that must all occur in order for a photon to be emitted from the device. Indeed, the injection of an electron and hole into the device does not guarantee that an exciton is formed.⁸¹

In fact, as photons penetrate different layers such as ITO, organics and glass before leaving the device they can encounter with a change in the refractive indices. Therefore an important fraction of photons were wave-guided, trapped, or re-absorbed within the device. So these photons could not be able to give a contribution to the forward light emission.⁸²

The current efficiency η_c (in cd/A) is defined as the ratio of the luminous intensity normally in perpendicular direction to the substrate to the current flowing through the OLED and can be identified by ratio of the luminance (cd/m^2) to the current density (A/m^2). It is a frequently used display efficiency unit which is convenient for quantifying the properties of an OLED for display applications. It is proportional with EQE and correlated with the spectral response of the eye.⁸³

Power efficiency (lm/W) also named as luminous power efficiency is like current efficiency and can be defined as the ratio of total output of light in lumens to electrical input power in Watts. Like the current efficiency power efficiency is also a photometric unit and therefore the spectral response of the eyes must be taken into consideration. It is commonly used for solid state lighting applications.⁸⁴

Together with the other terms, luminance is also an important parameter in the device characterization. Luminance can be named as brightness also and the maximum luminance refers to the maximum brightness that can be detected from a device before it breaks down.

The brightness of the device determine the efficiencies and the lifetime of an OLED which are evaluate at 100 cd/m^2 or $1,000 \text{ cd/m}^2$. Today's general small and portable electronic displays function with a brightness value of 100 to 200 cd/m^2 . In contrast, for lighting uses more than thousands brightness is required.⁸⁵

1.7. Aggregation Induced Emission

1.7.1. General Remarks

Solid state technology has been grown extensively starting from the end of the 20th century since it can be applied many important area related with our daily life.⁸⁶⁻⁹³ Molecules with efficient luminogenic properties with excellent solid state emissions have importance for the progress in optoelectronic technology.⁹⁴⁻⁹⁷ Generally the properties of the luminogenic molecules are studying in dilute liquid

phase. Absorption and emission behaviors, lifetime experiments, quantum efficiency studies, etc. all these measurements have been done in very dilute solution conditions⁹⁸⁻¹⁰² because in the solid state or even in concentrated solutions the emissions of the traditional luminogens are starting to weaken or even completely lost. This phenomena first envisioned by Förster and Kasper and they showed that the fluorescence emission of pyrene molecule was decreased when the concentration of pyrene was increased in its solution.¹⁰³ This is common phenomena named as aggregation caused quenching (ACQ) or concentration quenching (Figure 13).¹⁰⁴

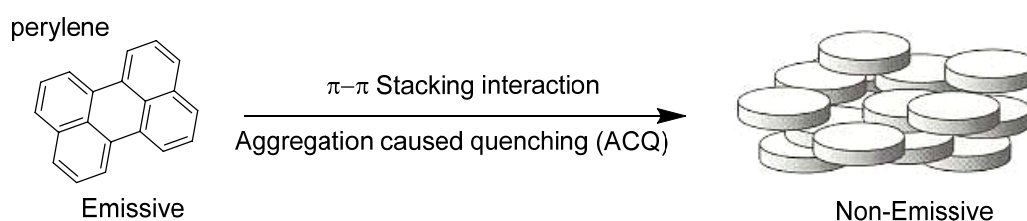


Figure 13. Traditional luminogenic system

In concentrated solution or solid phase, the molecules are very close to each other. In general, luminogenic molecules possess aromatic rings and the aromatic rings experience strong π - π interactions causing to form exciplexes and excimers. Birks et al. explained that, the concentration quenching effect is due to the formation of sandwich shaped excimers and exciplexes assisted by the collisional interactions between the aromatic molecules in the excited and ground states.¹⁰⁵ Moreover, aggregates in the excited states prefer to choose the non-radiative pathways.

N,N-dicyclohexyl-1,7-dibromo-3,4,9,10-perylenetetracarboxylic diimide (DDPD) is a common example that shows ACQ effect. DDPD is extremely luminescent when it completely dissolved in a proper solvent like THF (Figure 14). Adding water to THF solutions, changes the luminescence behavior of DDPD. The fluorescence emission starts to decrease upon increasing the water concentration.

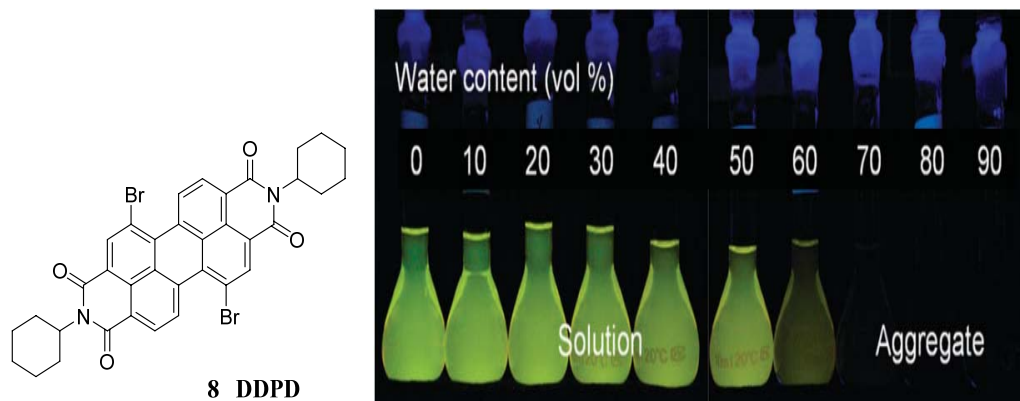


Figure 14. (Left) Structure of N,N-dicyclohexyl-1,7-dibromo-3,4,9,10-perylenetetracarboxylic diimide, (Right) Fluorescence emission of DDPD molecule under different water:THF fractions.¹⁰⁶

When the water concentration exceeded the limit of 60 vol%, the luminescence emission of DDPD quenches completely. Increasing water content decreases the solvating power of THF, so DDPD molecules start to form aggregates. The DDPD molecule consists of disc like perylene unit and this perylene unit plays a fatal role in ACQ effect. When DDPD molecules start to form aggregates while increasing the local luminophore concentration, the disc like perylene units exhibit strong π - π stacking. As a result, the excimer formation leads to ACQ.¹⁰⁶

The researchers tried to find various exits to escape from the ACQ effect. Adding bulky cyclic groups, branched chains and using transparent polymers to dope with the molecules are some of the examples. These approaches have only limited remedy effect on the problem and they ended up with new problems.^{107,108}

In 2001, Tang et. al.¹⁰⁹ reveal an exceptional luminogenic system. In these systems, aggregate formations have constructive effect to enhance the luminogenic behavior of the compounds. Hexaphenylsilole (HPS)¹¹⁰ is the first example of AIE systems demonstrated by Tang et. al. HPS shows no emission when it completely dissolved in a proper solvent like THF or acetonitrile.

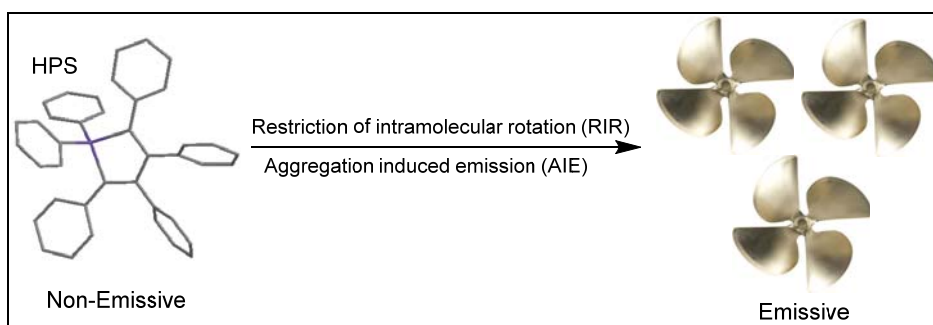


Figure 15. Non-traditional luminogenic system

Increasing the water content of acetonitrile solution of HPS, promote its emission. HPS have six phenyl rings with a non-planar geometry resulting a propeller shaped molecule. In the dilute solutions of HPS, these phenyl rotors perform intramolecular rotations alongside its silole stator via the single bond axes. These rotations act as a relaxation channel for extermination of the excited state non-radiatively. The photonic energy was converted to heat during intramolecular rotation and causes a non radiative deactivation of excited states. When the solution became concentrated and aggregated, the intramolecular rotations became limited and causing to plug the non-radiative decay and unlock the radiative pathway. Since HPS has peripheral phenyls, it does not exhibit and π - π stacking interactions in the aggregate form (Figure 15).

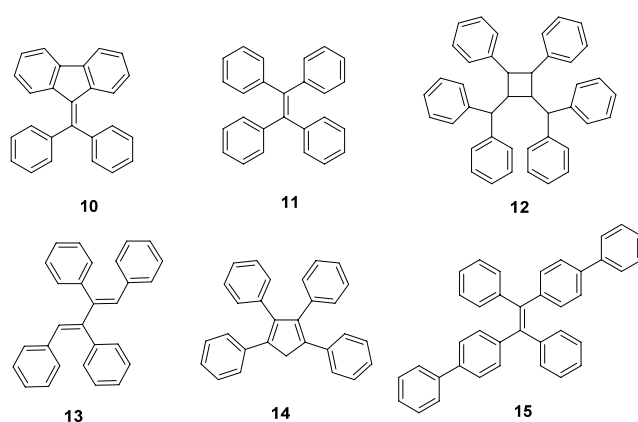


Figure 16. Various molecules exhibiting aggregation induced emission phenomenon.

Since 2001, there has been a rapidly increasing studies related with aggregation induced emission phenomenon.¹¹¹⁻¹¹⁶ Researchers tried to understand and prove the mechanism of this unusual fact.¹¹⁷⁻¹¹⁹ Some of the other molecules apart from HPS were identified as experience aggregation induced emission properties. (Figure 16)

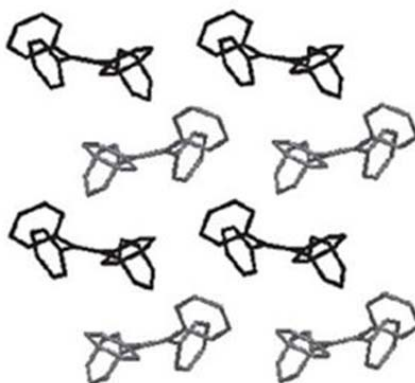


Figure 17. Molecular packing pattern of TPE

1.7.2. Tetraphenylethene

Tetraphenylethene (TPE) or tetraphenylethylene is a polyaromatic compound where an olefin unit is bridged four aromatic hydrocarbon rings. In its solid form, TPE and mostly its derivatives shows propeller-like conformations with the four arene rings roughly perpendicular to the central olefin.¹²⁰ Hong et. al. studied the crystal structure of TPE.¹²¹ Figure 18 shows the molecular packing pattern of TPE. According to the patterns, the four phenyl rings have about 50° twisting angle out of the plane corresponds to central alkene. As a result of this conformation the π - π stacking interactions are prevented.

Tetraphenylethene was synthesized by de Boissieu in 1888. Diphenylmethane was brominated to afford bromodiphenylmethane and dry distillation technique was applied with subsequent recrystallization by benzene to afford TPE between

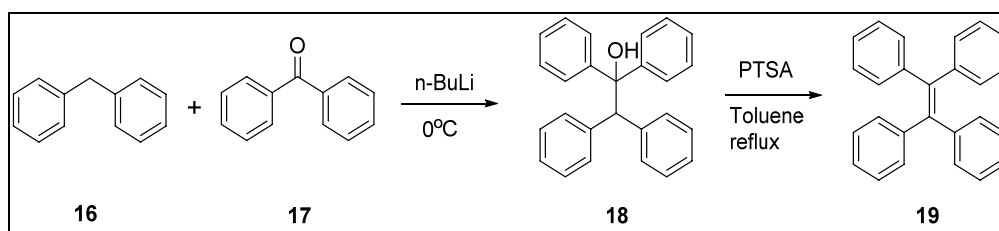


Figure 18. Synthesis of TPE

70-80% yield.¹²² Additionally reactions between diphenylmethane and benzophenone were used to synthesize TPE and its derivatives (Figure 18).¹²³⁻¹²⁵

Okuma et al. used selenobenzophenones and reacted with diphenyldiazomethane using methylene chloride as a solvent (Figure 19).¹²⁶⁻¹²⁸ Both of two syntheses strategy could be broaden for symmetrical and unsymmetrical TPE derivatives.

In fact; the most common way to synthesize TPE derivatives is using the McMurry type coupling reactions.¹²⁹⁻¹³¹ Generally zinc are used to reduce the Ti(III) or Ti(IV) to low valent titanium resulted to benzophenone reduction yielding the tetraphenylethene core. Depending on the starting aldehyde or ketone symmetrical or unsymmetrical substituted TPE derivatives can be synthesized.¹³²

Tetraphenylethene is one of the most studied luminogenic compound¹³³⁻¹³⁵ exhibited AIE property, opposite of aggregation quenching effect. Although TPE has a simple structure it possesses marvelous AIE properties.^{136,137} TPE shows no

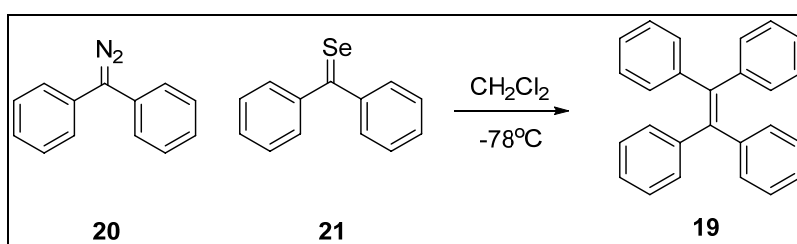


Figure 19. Synthesis of TPE by selenobenzophenones

emission when it is completely soluble in a proper solvent and starts to give emission when it morphs into aggregate form. Decorating TPE with various heterocycles possessing electron donating or electron withdrawing abilities gives TPE excellent luminogenic aptitudes with different colors from blue to red.^{138,139}

Zhao et. al. synthesized various tetraphenylethene based luminogenic compounds (Figure 20) and full color emission was achieved by only inserting benzo-2,1,3-thiadiazole and thiophene units between two tetraphenylethene moiety.¹⁴⁰

Tetraphenylethene could also be used as a hole transport layer by changing the substituents linking the TPE core. Liu et. al. synthesized tetraphenylethene based compounds¹⁴¹ with triphenylamine (TPA) which is used a hole transport material for many applications. In solid state TPA molecule lose its emission property because of aggregation caused quenching. By combining TPE and TPA together, TPE was gained hole transporting ability and TPA was overcome the ACQ effect (Figure 21).

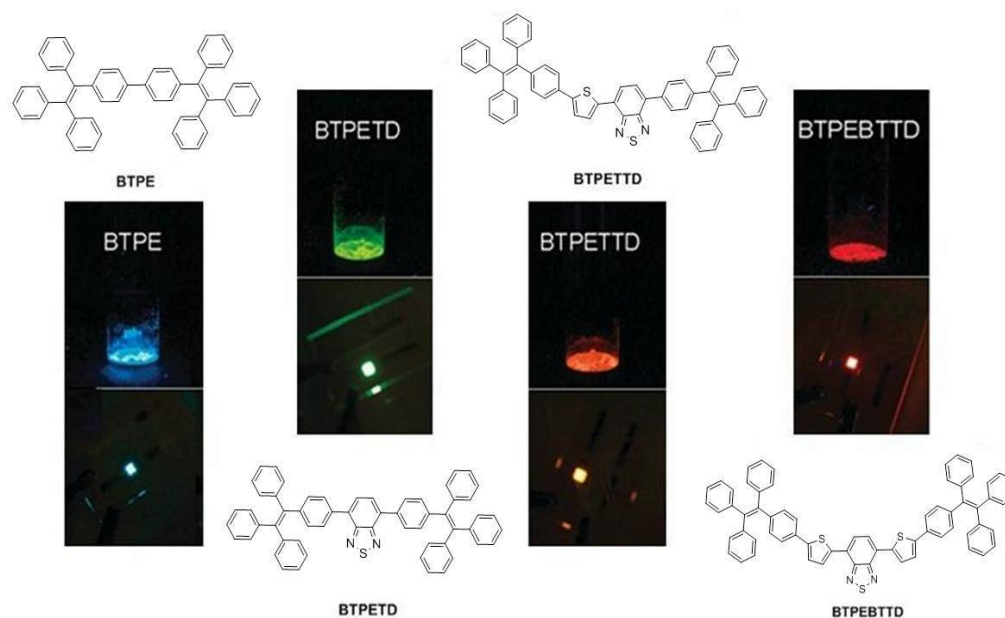


Figure 20. Various tetraphenylethene based OLED devices having full color emission¹⁴⁰

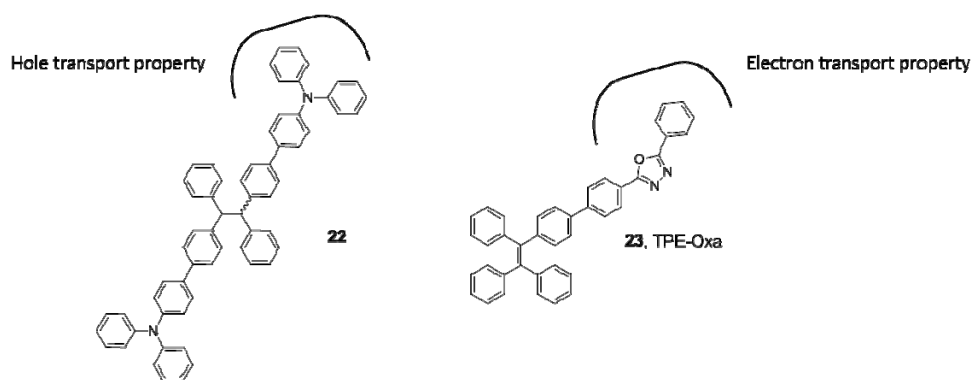


Figure 21. TPE based compounds having hole transport ability

Apart from hole transport ability, TPE could be modified by attaching electron deficient groups like oxadiazoles to gain electron transport ability. Ben Zhong Tang¹⁴² group synthesized oxadiazole attached TPE compounds by simple chemistry and the device made with TPE-Oxa (Figure 21) functioned better without ETL layer.

TPE find place in various applications including electroluminescence devices, fluorescent sensory systems, cell imaging and biomedical applications (Figure 22).¹⁴³⁻¹⁴⁸

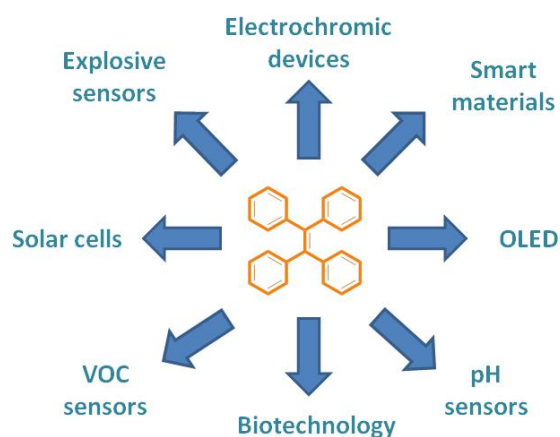


Figure 22. Research areas related with TPE

1.8. Aim of the Work

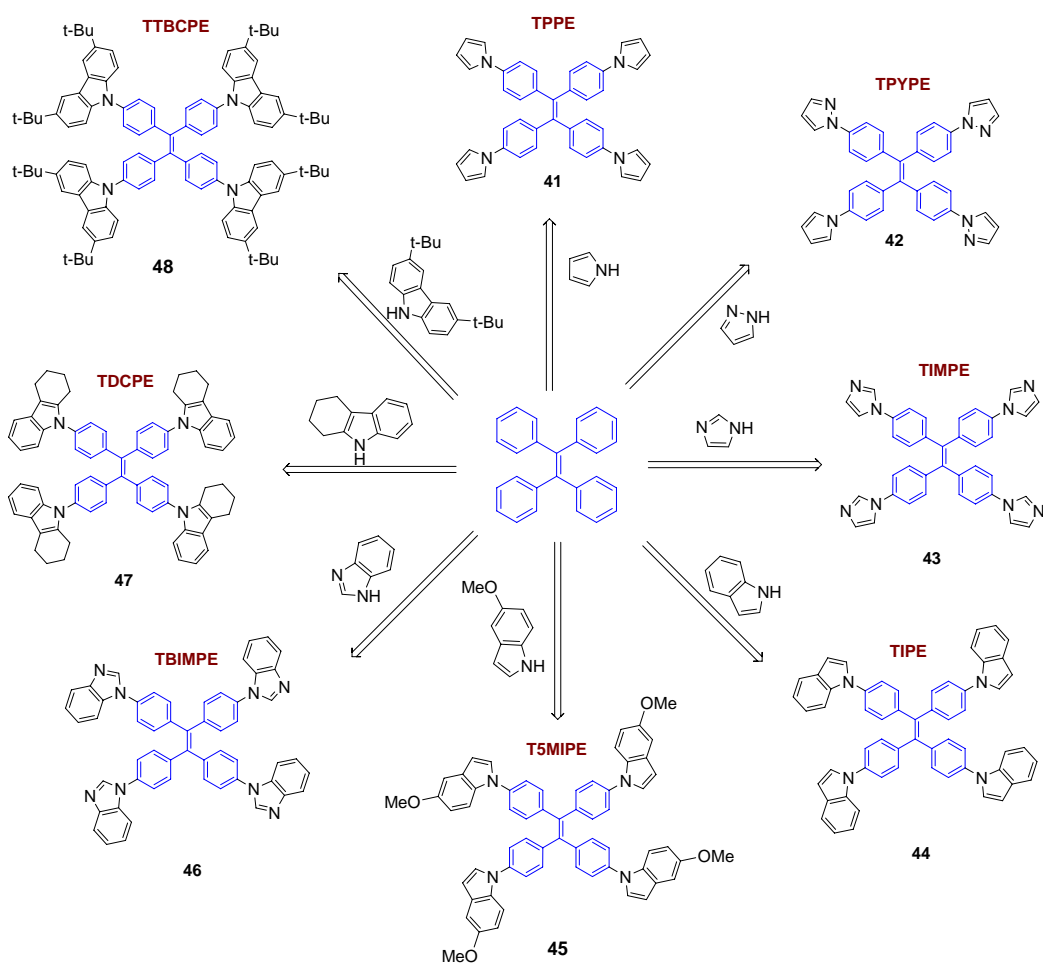
The main purpose of this work is to synthesize new N-heterocyclic tetraphenylethene based small organic molecules having aggregation induced emission properties and additionally the use of these compounds in organic light emitting devices.

In the first part, the syntheses of tetraphenylethene based small organic molecules were planned by using ubiquitous inexpensive chemicals like pyrrole, pyrazole, indole etc.. In general, the synthetic procedures together with the compounds used in OLEDs are expensive comparing with ordinary chemicals. The mainstay of this work is to synthesize luminogenic compounds in an inexpensive way. Scheme 1 shows the synthesis outline of the N-heterocyclic TPE derivatives.

In the second part, the characterizations of the synthesized luminogens were planned. Thermal, including DSC and TGA experiments, photophysical, including absorption and emission behaviors together with lifetime experiments, and electrochemical, including cyclic voltammetry experiments, characterizations were planned to be studied.

In the third part, the synthesized luminogens were planned to test whether they exhibit aggregation induced emission property or not. Therefore aggregate solutions are going to be prepared by dissolving the synthesized compounds in a proper solvent to achieve a complete solubility and then mixing with anti-solvents to promote the aggregate formation.

Finally, in the fourth part, the OLED applications of the synthesized small organic molecules are going to be fabricated. To do this, firstly some pre-device applications were planned for optimizing the device architecture. Moreover, non-doped OLEDs were planned to setup by using the optimized device layout.



Scheme 1. TPE based luminogenic compounds

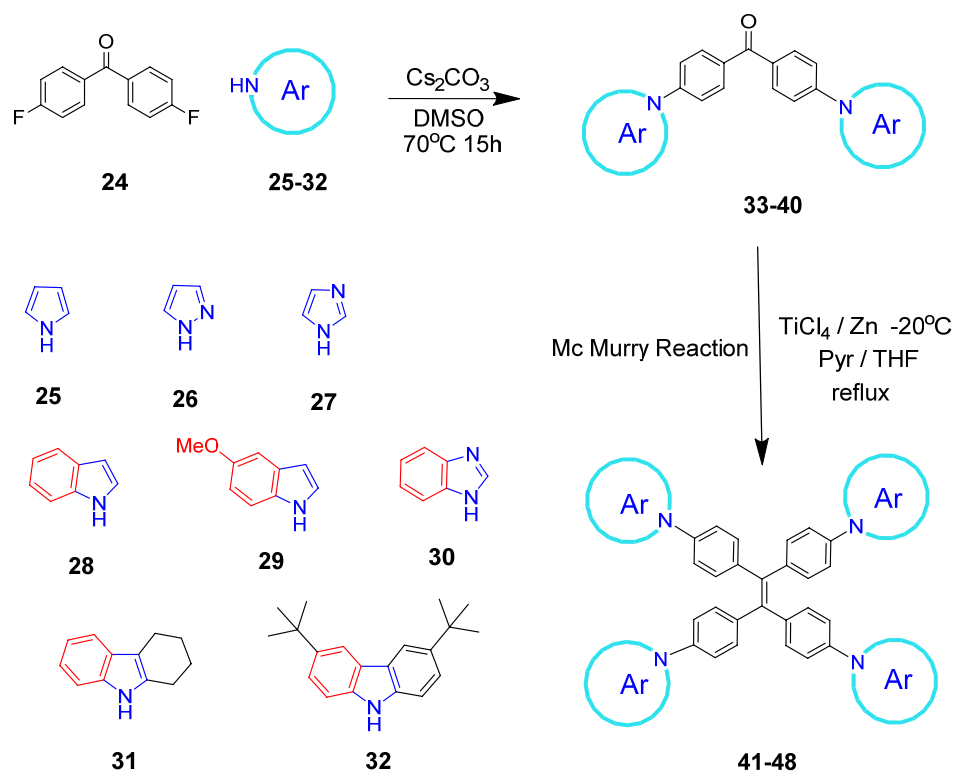
CHAPTER 2

RESULTS AND DISCUSSION

2.1. Synthesis of N-heterocyclic luminogens

The most common way in the synthesis of new conjugated OLED materials is using conventional coupling reactions, such as Suzuki¹⁴⁹ or Sonogashira¹⁵⁰. Although these reactions are so useful to generate conjugated molecules, the cost of the starting reagents and catalysts is the major drawback. Air sensitive Pd metal catalysts and boronic acids are relatively expensive compared with the ordinary chemicals and it is difficult to get rid of the metal catalyst completely from the medium which is a common emission quenching source during operating an OLED device. Even though Pd metal is used in catalytic amounts, quantities varying from hundred to thousand ppm of remaining metal left after workup. Quite the opposite, we used ubiquitous chemicals that can be accessed and supplied easily and comparatively mild reaction conditions. When we compared the price differences, even an ordinary Pd catalyst and boronic acid couple, they are minimum 50 fold expensive than TiCl₄ and our starting materials.¹⁵¹ That gives us an opportunity to overcome aforementioned synthetic drawbacks.

In most of the studies related with TPE either in core or peripheral form, the molecules under consideration were generated by C-C bond formation between the tetraphenylethene and the other reagent.¹⁵²⁻¹⁵⁶ Relatively fewer works were published earlier^{157,158} cover C-N bond formation, showing AIE properties. In addition, apart from OLED applications most of the starting N-heterocyclic compounds are especially significant for biologically important molecules.¹⁵⁹⁻¹⁶⁴



Scheme 2. Synthesis scheme

The target compounds were synthesized according to path illustrated in Scheme 2. 4,4'-Difluorobenzophenone (**24**) was chosen as a precursor material for anchoring hetero aromatic units and subsequent transforming into tetraphenylethene main carbon skeleton. C-N bond formation was conducted via nucleophilic aromatic substitution reaction (S_NAr) using highly ionic cesium salt which mainly favors N-substitution (up to 90% chemical yield).¹⁶⁵ The reactivity of ions in S_NAr reactions depends on how naked the ion in the reaction medium is. Together with an aprotic solvent with a high dielectric constant, like DMSO or DMF, cesium ions are present as naked in the reaction medium.

Subsequently, McMurry type coupling reaction was applied to construct the resultant hetero aromatic anchored tetraphenylethene backbone with the overall chemical yields aroused in 65 - 80%. The synthesized luminogens (Scheme 1) all are soluble in most of the common organic solvents such as chloroform,

tetrahydrofuran, dichloromethane and toluene. The structure elucidations were performed by ^1H NMR, ^{13}C NMR and mass spectroscopy techniques.

2.1.1. Synthesis of N-heterocycle attached benzophenone derivatives

Since our synthetic route depends on the construction of tetraphenylethene derivatives with various N-heterocyclic amines, firstly 4,4-Difluorobenzophenone **24** was functionalized with various N-heterocyclic amines **25-32**. Cesium carbonate was used as a base and DMSO was used as an aprotic solvent. Instead of cesium carbonate and DMSO couple, potassium *tert*-butoxide and DMF could also be used but the chemical yields are lower than Cs_2CO_3 case.

The structure of the synthesized benzophenone derivatives was elucidated on the basis of NMR and MS spectroscopic data. By using ESI-TOF technique, bis(4-(1H-imidazol-1-yl)phenyl)methanone **35** gave monoisotopic peak at 315.12 corresponding to M+H form of the compound. The ^1H NMR spectrum of **35** revealed five sets of proton signals; a triplet centered at 7.99 ppm belongs to two hydrogen located on the fifth position of the imidazole rings. Hydrogens on the benzophenone moiety gave AB system that can easily be recognized by the “roof effect”. A doublet centered at 7.97 ppm belongs to “A part” of the AB system and the “B part” hydrogen also showed a doublet at 7.56 ppm. Another triplet was seen on the spectrum at 7.40 ppm corresponds to two hydrogen on the fourth position of the imidazole rings. Moreover, the last triplet signal was centered at 7.27 ppm belonging to high electron dense protons on the second position of the imidazole moiety. ^{13}C NMR technique was also used to identify the compounds. Bis(4-(1H-imidazol-1-yl)phenyl)methanone **35** afforded eight different signals belonging to nineteen carbon atoms on the compound. The characteristic carbonyl signal appeared at 193.7 ppm. The other carbons gave signals between 140.5 and 117.8.

2.1.2. Synthesis of Tetraphenylethene derivatives

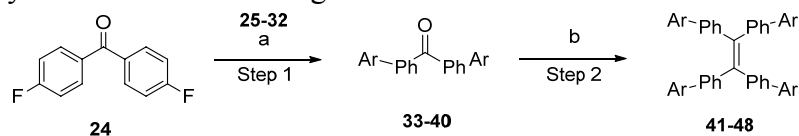
The second part of our synthetic route involves the transforming the synthesized benzophenone derivatives into tetraphenylethene cored compounds. McMurry type coupling reaction was chosen because of its facile synthesis property. Titanium tetrachloride was used and zinc metal was chosen as a reducing agent. In order to decrease the possibility of side reactions the TiCl₄ addition were done at lower temperatures below 0 °C. Furthermore, pyridine was used to decrease the pinacol type reactions.

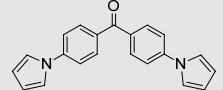
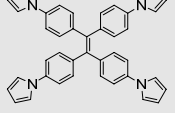
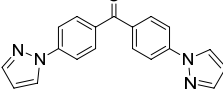
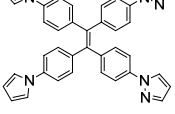
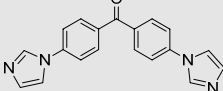
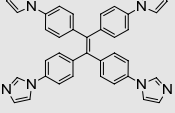
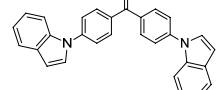
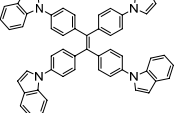
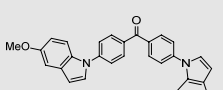
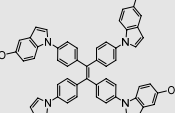
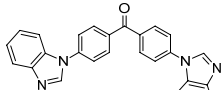
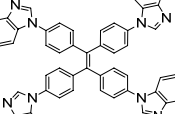
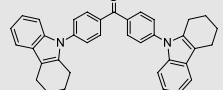
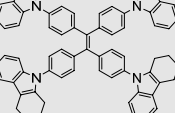
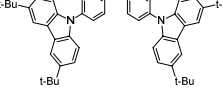
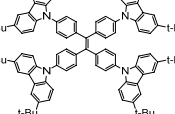
The structure of the synthesized TPE derivatives was elucidated on the basis of NMR and MS spectroscopic data. By using ESI-TOF technique, the HRMS spectrum of the 1,1,2,2-Tetrakis(4-(*1H*-imidazol-1-yl)phenyl)ethane **43**, TIMPE gave monoisotropic peak at 597.2515 corresponding to M+H form of the compound. The obtained result is in good agreement with the theoretical value. The ¹H NMR spectrum of **43** revealed five sets of proton signals; a broad signal centered at 7.85 corresponds to four protons of imidazole moiety. Hydrogens on the tetraphenylethene core gave AB system that can easily recognized by the “roof effect”. A doublet centered at 7.24 ppm belongs to “A part” of the AB system and the “B part” hydrogen also showed a doublet at 7.21 ppm. A triplet signal at 7.26 ppm and another broad singlet at 7.19 ppm were seen on the spectrum. ¹³C NMR technique was also used to identify the compounds. 1,1,2,2-Tetrakis(4-(*1H*-imidazol-1-yl)phenyl)ethane **43**, TIMPE exhibited eight different NMR signal belonging to thirty-eight carbon on the ring system. The characteristic carbonyl signal of the starting compound was disappeared. The carbons gave signals between 141.7 and 117.8.

2.2. Thermal properties

The thermal properties of the synthesized luminogens were studied using differential scanning calorimetry (DSC) and thermogravimetric analysis (TGA),

Table 1. Synthesis of TPE luminogens



Entry	Substrate	Product (Step 1) – Yield (%)	Product (Step 2) – Yield (%)
1	 25	 33 85	 41 75
2	 26	 34 80	 42 75
3	 27	 35 75	 43 65
4	 28	 36 75	 44 80
5	 29	 37 85	 45 85
6	 30	 38 75	 46 65
7	 31	 39 80	 47 65
8	 32	 40 80	 48 65

a) Cs₂CO₃, DMSO, 70°C, 15h; b) TiCl₄, Zn, (-20 °C), pyridine, tetrahydrofuran, reflux.

techniques and the results are summarized in Table 2.

When designing a novel OLED material, durability is one of the most desirable feature associated with a high glass transition temperature and thermal stability. High T_g and T_d values are wanted for any synthesized compounds since these compounds can resist the Joule heating, that is a common degradation source for an OLED device.¹⁶⁶⁻¹⁶⁷ Joule heating plays more crucial role in degradation process at higher current densities and electric fields. It can cause to recrystallize the organic materials, harm the homogeneity of the molecules and diminish the lifetime.

Additionally, DSC analysis can give us information about the morphology of the synthesized luminogens. The morphology of the compound is also important for device efficiencies and lifetime. Amorphous materials are preferred rather than crystalline ones since they have better film forming properties that can diminish the pin hole effect that also affect the OLED performance.¹⁶⁸ Crystallization of

Table 2. Thermal properties of synthesized compounds

Compound	T_g (°C)	T_c (°C)	T_m (°C)	T_d (°C)	
TPPE	41	-	-	292.02	366.09
TPyPE	42	122.59	196.03	239.97	381.26
TIMPE	43	-	-	312.24	461.67
TIPE	44	112.75	158.97	240.37	467.60
T5MIPE	45	109.36	143.26/200.61	275.57	470.09
TBIMPE	46	-	-	305.66	505.06
TDCPE	47	-	267.79	400.13	498.39
TTBCPE	48	-	-	-	515.78

organic materials during operation of the device could decrease the OLED lifetime.

The DSC analyses were done with two subsequent runs and achieved at a scan rate of 10 °C min⁻¹. For the second run, the samples were cooled with 100 °C min⁻¹ after exceeding its melting point together with not reaching the degradation point and then the compound was reheated with a scan rate of 10 °C min⁻¹.

Thermogravimetric analysis also gives us information about the degradation stability of the compound. Compounds having higher degradation temperatures are preferred. The reason is as same as why compounds preferred possessing high T_g values. They have lower risk to degrade during operation of the device compared with compound having low T_d values. Consistent with the literature the decomposition temperatures of the compounds were calculated by finding the temperature at which 5% weight loss occurred during heating under nitrogen atmosphere using TGA. The results of the TGA analysis are given in the appendix.

1,1,2,2-Tetrakis(4-(*1H*-pyrrol-1-yl)phenyl)ethane TPPE, (**41**), pyrrole derivative of TPE, did not show any T_g or cold crystallization peaks and exhibited only a melting point at 292.02 °C in the first run of DSC experiment. In order to find whether TPPE have T_g value or not, a second DSC run was carried out, however, no T_g values was observed. Furthermore, according to TGA analysis, TPPE has a decomposition temperature at 366.09 °C (see appendix Figure A-64 and Figure A.-72).

1,1,2,2-Tetrakis(4-(*1H*-pyrazol-1-yl)phenyl)ethane TPyPE, (**42**), pyrazole derivative of TPE, acted differently than TPPE. In the first DSC run, it showed a melting peak at 239.97 °C but did not show any T_g value. Then in the second DSC run, TPyPE had a T_g value at 122.59 and a cold crystallization at 196.03 and melting point at 239.97 °C. Interestingly, changing one carbon atom on the second position of the pyrrole ring with nitrogen atom changed the thermal properties of mother compounds completely. The nitrogen atom on the second position of the

pyrazole ring presumably makes secondary interactions with the other TPyPE molecules. TPyPE have more amorphous character than TPPE. Additionally, the Tg value of TPPE is quite high comparing with other TPE derivatives and 1-methyl-1,2,3,4,5-pentaphenylsilole (MPPS) and 1,1,2,3,4,5-hexaphenylsilole (HPS) which are the first AIE compounds reported in literature. Moreover, in thermogravimetric analysis of TPyPE gave a decomposition temperature at 381.26 °C (see appendix Figure A-65 and Figure A.-72). The degradation temperature of TPyPE is a bit higher than TPPE so we can conclude that secondary nitrogen unit makes the compound stiffer.

1,1,2,2-Tetrakis(4-(*1H*-imidazol-1-yl)phenyl)ethane TIMPE, (**43**), imidazole derivative of TPE, gave no Tg value in both of the two subsequent DSC experiments. It has a melting temperature at 312.24 °C that is 30% greater than that of TPyPE. The same effect was observed for decomposition of TIMPE. It possessed the highest value among the TPE derivatives having a 5-membered N-heterocycles and appeared at 461.64 °C (see appendix Figure A-66 and Figure A.-72). It is known that imidazole can oligomerize via secondary interactions. The highest degradation temperature and high melting temperature could be possibly due to this fact.

1,1,2,2-Tetrakis(4-(*1H*-indol-1-yl)phenyl)ethane TIPE, (**44**), indole derivative of TPE, has both amorphous and crystalline domains. In the first run, it exhibited an endothermic transition that corresponds to melting temperature with a value of 240.37 °C. In order to find the Tg value of the luminogen, a second heating was performed by cooling and re-heating the sample. In the second run, TIPE gave a Tg value at 112.75 °C. Continuing the DSC experiment after exceeding the Tg value, TIPE gave an exothermic transition appeared at 158.97 °C corresponding to cold crystallization temperature. At this temperature the molecules of TIPE had very ordered arrangements. After Tc value the melting temperature was observed with an onset value of 240.29 °C. The TGA analysis of TIPE gave a Td value 467.60 °C. Adding a fused benzene ring to a pyrrole ring increases the rigidity and

the molecular weight of the system therefore the Td value is higher than that of the 5-membered luminogens (see appendix Figure A-67 and Figure A.-72).

1,1,2,2-Tetrakis(4-(5-methoxy-*1H*-indol-1-yl)phenyl)ethane T5MIPE, (**45**), 5-methoxy indole derivative of TPE, has a structural analogy with TIPE so the methoxy groups on the fifth position determine the difference in thermal stability between the TIPE. In the first DSC run the compound interestingly showed an exothermic transition before the melting temperature with a value of 198.56 °C. The compound also showed a melting temperature at 274.88 °C. The methoxy group on the fifth position has a constructive effect on the melting temperature. To find the Tg temperature of the compound, a second DSC experiment was carried out. In the second run, T5MIPE exhibited a Tg value at 109.36 °C. The methoxy group has a little influence on the flexibility of the compound so there was a small decrease on the Tg value comparing with TIPE. T5MIPE showed also one extra exothermic transition that also corresponds to cold crystallization temperature. The first and second Tc peaks appeared at 143.26 °C and 200.61 °C, respectively. The TGA analysis revealed that there were no such difference between TIPE and T5MIPE with respect to Td values and T5MIPE gave a Td value at 470.09 °C. The small difference could be attributed to increase in molecular weight of the compound (see appendix Figure A-68 and Figure A.-72).

1,1,2,2-Tetrakis(4-(*1H*-benzo[d]imidazol-1-yl)phenyl)ethane TBIMPE, (**46**), benzimidazole derivative of TPE, did not show Tg or Tc values during both of the two runs. It exhibited only a Tm value appeared at 305.66 °C. Interestingly changing one carbon atom on the indole moiety with a nitrogen atom changed the thermal behavior of the compounds completely. When we compared the Tm values of TIPE and TBIMPE, there is almost 30% increase in the melting point. The second nitrogen could make intermolecular interactions that could increase the thermal stability of the compound. Additionally, the degradation temperature was also higher than TIPE and T5MIPE and valued at 505.06 °C (see appendix Figure A-69 and Figure A.-72).

1,1,2,2-Tetrakis(4-(3,4-dihydro-1*H*-carbazol-9(2*H*)-yl)phenyl)ethane TDCPE, (47), tetrahydrocarbazole derivative of TPE, showed a T_m value at 400.13 °C in the first run of the DSC analysis. For the second heating, although we did not find the T_g value, TDCPE gave an exothermic transition appeared at 267.79 °C associated with the cold crystallization temperature. At this temperature the molecule underwent a small amount of crystallization while heating in the DSC. The melting temperature of TDCPE is considerably high for ordinary chemicals. The T_d value is 498.39 °C (see appendix Figure A-70 and Figure A.-72).

1,1,2,2-Tetrakis(4-(3,6-di-*tert*-butyl-9*H*-carbazol-9-yl)phenyl)ethane TTBCPE, (48), tertiary butyl carbazole derivative of TPE, behaved completely different from the others luminogenic compounds. It did not exhibit any transition up to 420 °C related with glass transition or melting temperatures. In order to find any transition, a second DSC run were carried out after cooling the sample but again TTBCPE gave no transition. After first and second heating cycles we run a third heating and cooling cycle but in this case the TTBCPE was removed from the DSC pan after the first heating and immediately dipped into the liquid nitrogen and again a second heating run was carried out. However, no transitions were observed again related with glass transition or melting temperatures. The reason can be presumably due to existence of *t*-butyl side groups which would influence the molecular tight packing in the solid state and forming a highly amorphous structure. It is a common fact that carbazole group have a bulky firm planar molecular structure causing to reduce the rotation effectively resulting with an increase in thermal stability.¹⁶⁹ Herewith, a rigid bulky side groups are significant to influence the thermal stability of the compound (see appendix Figure A-71 and Figure A.-72). In fact, since the TTBCPE did not show any melting temperature we can conclude that TTBCPE has much lower crystallizability than the other synthesized luminogens.

2.3. Electrochemical properties

The red-ox properties together with HOMO and LUMO energy levels are fundamental parameters for the device configuration. The interactions of the

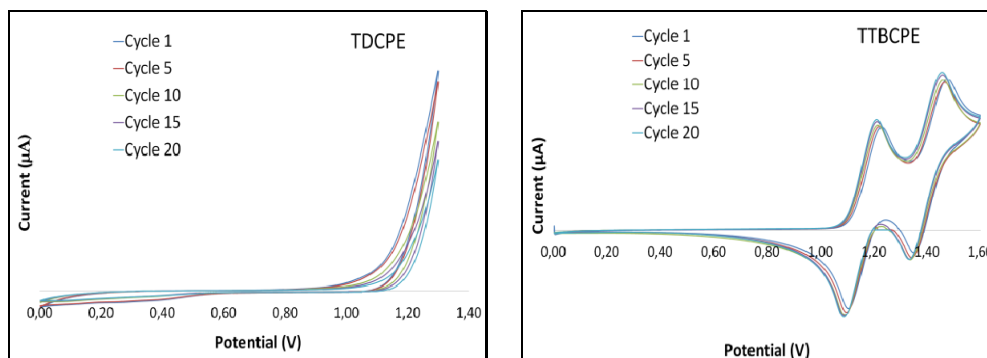


Figure 23. CV of TDCPE (47) and TTBCPE (48)

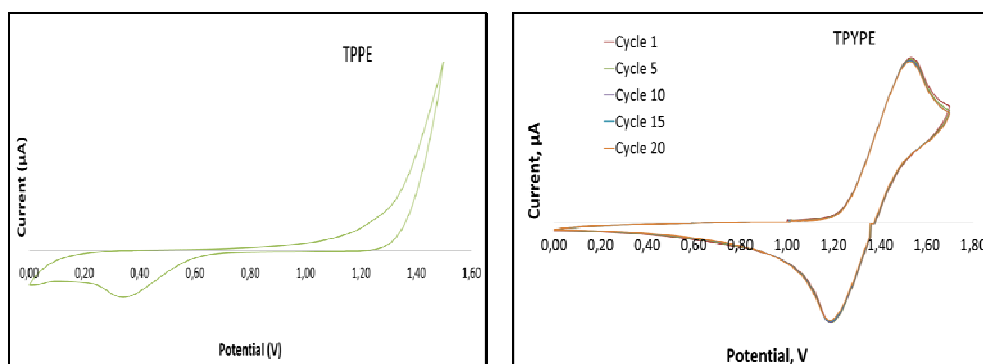


Figure 24. CV of TPPE (41) and TPYPE (42)

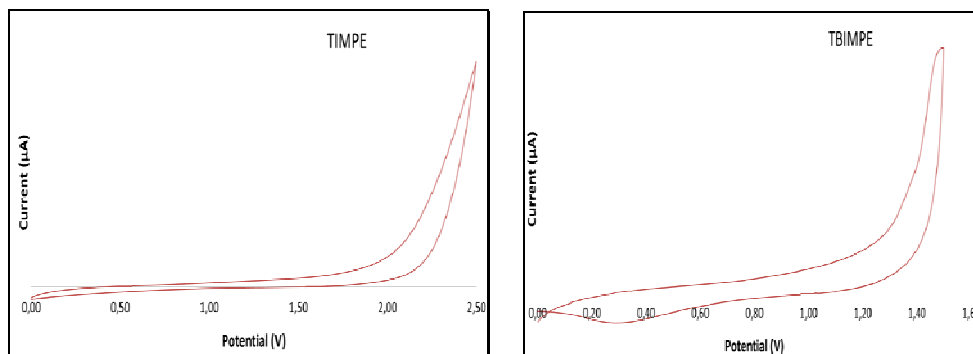


Figure 25. CV of TIMPE (43) and TBIMPE (46)

emitting layer with other layers such as electron/hole transport layers are related with the electrochemical properties of the organic compounds. Thus, cyclic voltammetry (CV) experiments were carried out to explore HOMO and LUMO levels of the synthesized luminogens. In order to perform CV analyses, a three electrode cell system using 0.1 M tetra-n-butylammonium hexafluorophosphate as a supporting electrolyte in CH₂Cl₂ was used. The energy band gaps (E_g) of the compounds were calculated from the onset wavelength of their UV absorption. The HOMO energy levels can be deduced from their onset oxidation potentials measured by cyclic voltammetry based on the value of -4.8 eV for ferrocene as internal standard recommended by IUPAC. The LUMO energy levels were estimated from the HOMO energy levels and the optical band gaps. Figures 23-25 show the cyclic voltammograms of the compounds.

The E_g, HOMO and LUMO levels of the compounds are listed in Table 3. The E_g values were between 3.00 – 3.20 eV. The HOMO values were in the range of 5.40 - 5.70 and the LUMO values located from 2.34 to 2.51. The compounds maintained their electrochemical stabilities up to 20 cycles.

Table 3. Electrochemical behavior of synthesized luminogens

Compound		E _g (eV)	E _{HOMO} (eV)	E _{LUMO} (eV)
TPPE	41	3.08	-5.51	-2.43
TPyPE	42	3.08	-5.59	-2.51
TIMPE	43	3.18	-5.55	-2.37
TIPE	44	3.06	-5.40	-2.34
T5MIPE	45	3.02	-5.41	-2.39
TBIMPE	46	3.20	-5.70	-2.50
TDCPE	47	3.05	-5.40	-2.35
TTBPCE	48	3.00	-5.51	-2.51

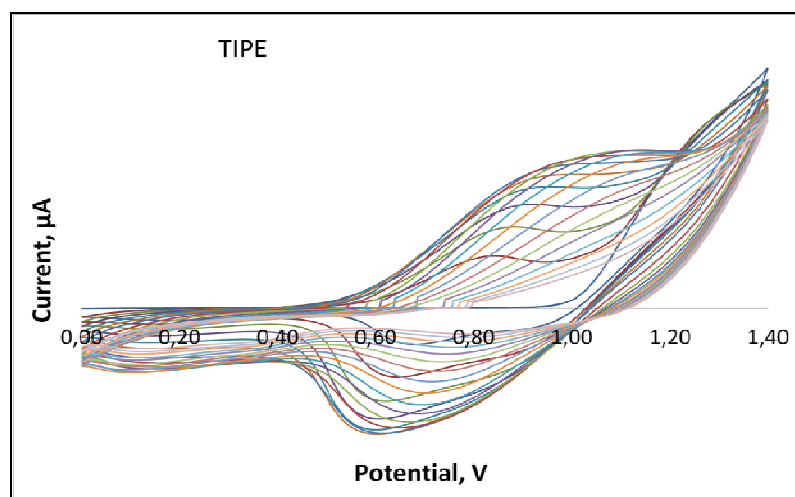


Figure 26. CV of TIPE (44)

Furthermore TIPE and T5MIPE acted differently. They started to polymerize on the Pt working electrode surface after the first anodic cycle and continued up to over 20 cycles without any decomposition (Figure 26 and 27, respectively). The rise in the intensity of anodic peak indicates the electrochemical polymerization of TIPE and T5MIPE. Apart from OLED applications, TIPE and their derivatives could be a good candidate for electrochromic device applications.

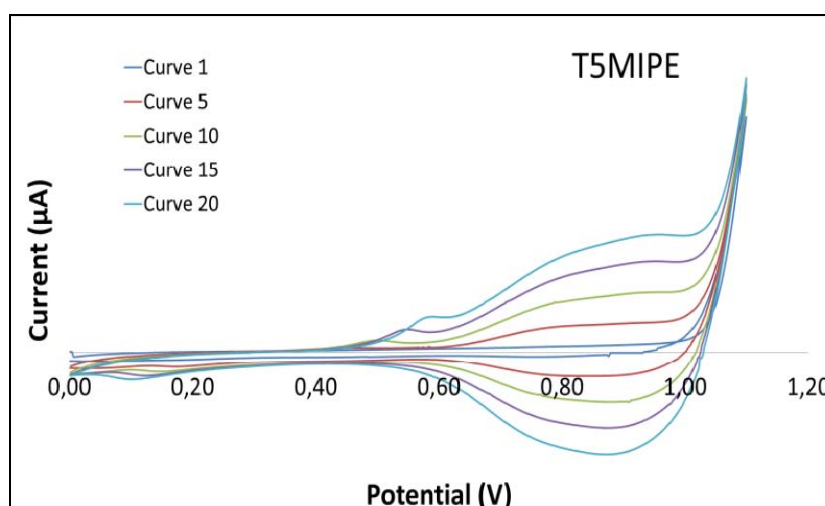


Figure 27. CV of T5MIPE (45)

2.4. Optical Properties

The optical properties of the synthesized luminogens were investigated by UV-Vis and photoluminescence (PL) spectroscopy. The emission behaviors of the synthesized compounds are shown in the PL spectrum in Figure 28. Additionally all the data related with absorption and emission behaviors of the compound are listed in Table 4.

TPPE had a maximum absorption wavelength at ca. 350 nm. and a second absorption at 288 nm corresponds to pyrrole subunits (Figure 29). In literature the central TPE unit has a maximum absorption at a wavelength of 299 nm. The corresponding red shift was the sign of the additional conjugation. Moreover, the PL spectra of TPPE gave a maximum emission at 507 nm (Figure 28).

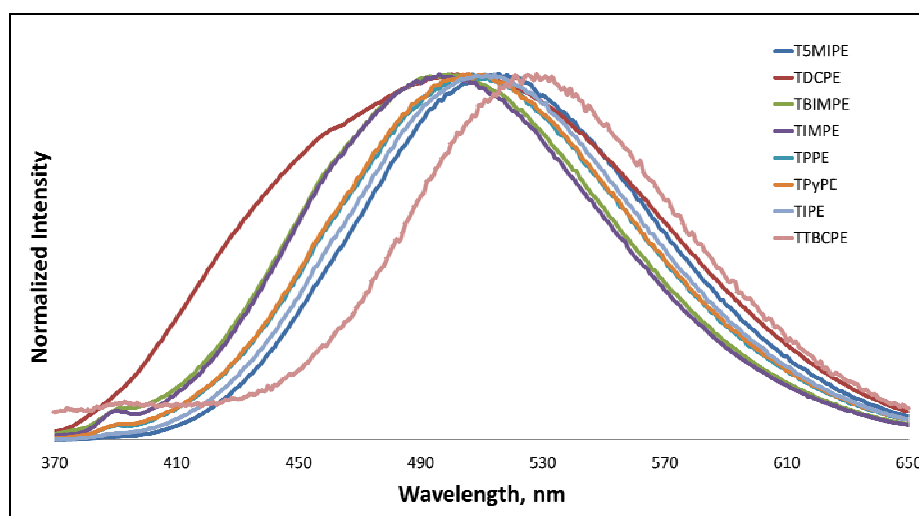


Figure 28. Emission spectrum of synthesized luminogens

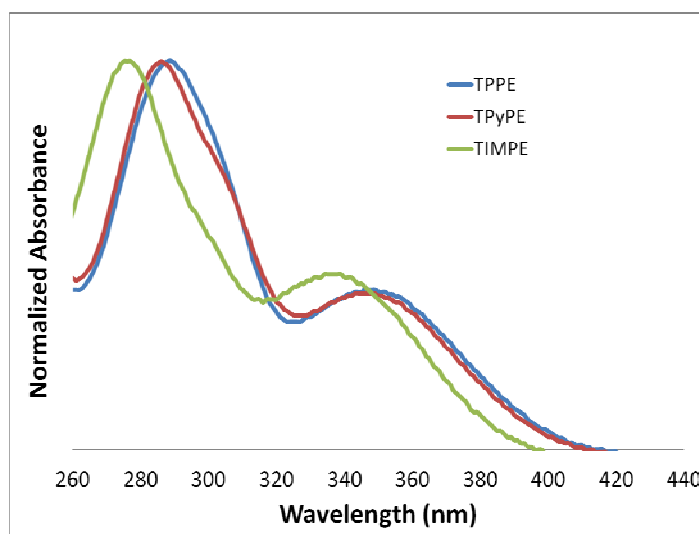
TPyPE showed almost equal absorption behavior as TPPE did. Additional nitrogen atom did not affect the conjugation of the electron, only 3 nm, so compared with TPPE there was no difference in UV-Vis spectra. It gave two absorption peaks ones at ca. 350 nm and another at 288 nm (Figure 29).

Table 4. Photophysical characterization of compounds

Compound		$\lambda_{\text{max, abs}}^{\text{a}}$ (nm)	Stokes Shift (nm)	PL λ_{max} (liq.) ^a (nm)
TPPE	41	347	160	507
TPyPE	42	347	159	506
TIMPE	43	337	159	496
TIPE	44	350	165	510
T5MIPE	45	360	155	515
TBIMPE	46	335	164	499
TDCPE	47	335	167	502
TTBPCE	48	350	175	525

^aMeasured in tetrahydrofuran solution.

The later corresponds to pyrazole subunits. The PL behavior of TPPE is also almost same with TPyPE. Additional nitrogen atom did not affect also the maximum emission of the TPyPE and yielded as 506 nm (Figure 28).

**Figure 29.** UV-Vis spectrum of TPPE, TPyPE and TIMPE

TIMPE showed an absorption maximum at 337 nm that is approximately 10 nm less than TPPE and TPyPE had (Figure 29). The nitrogen atom on the third position of pyrrole ring had a little reducing effect on the conjugation of the whole molecule. TIMPE had another absorption peak at 274 nm that corresponds to imidazole moiety. And comparing imidazole and pyrazole subunits, there were also 14 nm shift between their absorption peaks. TIMPE had a maximum emission peak at 496 nm (Figure 28). Compared with TPPE and TPyPE, the emission spectrum of TIMPE shifted to a shorter wavelength by a hypsochromic shift with a value of 10 nm. Compared with TPPE and TPyPE, TIMPE, imidazole substituted TPE derivative, was electronically less conjugated than the others. The nitrogen on the third position has a reducing effect on the conjugation of the whole molecule.

TIPE had three distinct absorption peaks appeared at 272, 312 and 350 nm (Figure 30). Compared with TPPE, additional benzene ring increases the total conjugation of the π electrons so comparing TPPE and TIPE a red shift was observed. TIPE had a maximum emission wavelength at 510 nm in THF (Figure 28). However, the thin film of TIPE showed a blue shift with the value of 499 nm. The aggregate form of TIPE, measured in THF– water (1:99) solution, gave a maximum emission at 498 nm.

Insertion of -OMe group on the fifth position of indole unit, T5MIPE, exhibited also three absorption peaks at 278, 322 and 360 nm (Figure 30). There was almost 10 nm red shift compared with TIPE. Additional -OMe group has electron donating effect on the ring system so an increase in the electron density of the ring was observed which is the main reason of this 10 nm shift. Moreover, the PL signal of T5MIPE appeared at 515 nm that is 5 nm red shifts compared with TIPE (Figure 28).

TBIMPE had three distinct UV signal as TIPE did. The signals appeared at 268, 295 and 335 nm (Figure 30). Instead of one carbon atom, TBIMPE has one good solvents for TIPE and therefore aggregation may occur in the solution.

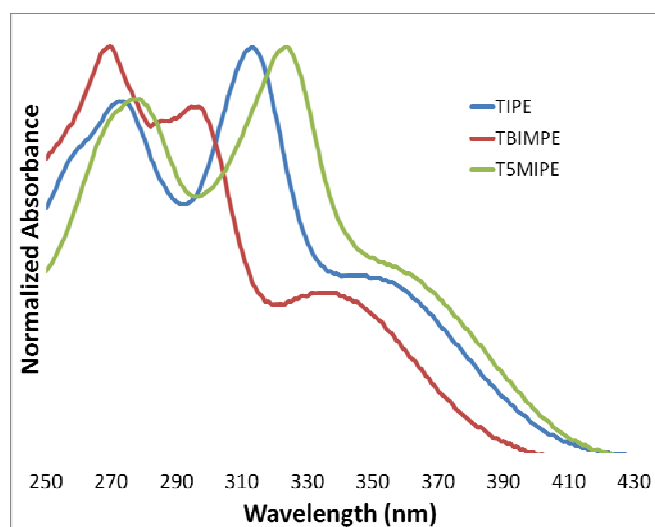


Figure 30. UV-Vis spectrum of TIPE, TBIMPE and T5MIPE

This structural difference reduced the density of the delocalized electrons on the ring and caused about 15 nm blue shift. Like TIMPE, imidazole functionalized TPE, TBIMPE exhibited also blue shift compared with indole or pyrazole functionalized TPE derivatives. The same effect was seen in the emission spectra of TBIMPE. Approximately 8 nm blue shift was observed and TBIMPE exhibited a fluorescence emission at 499 nm.

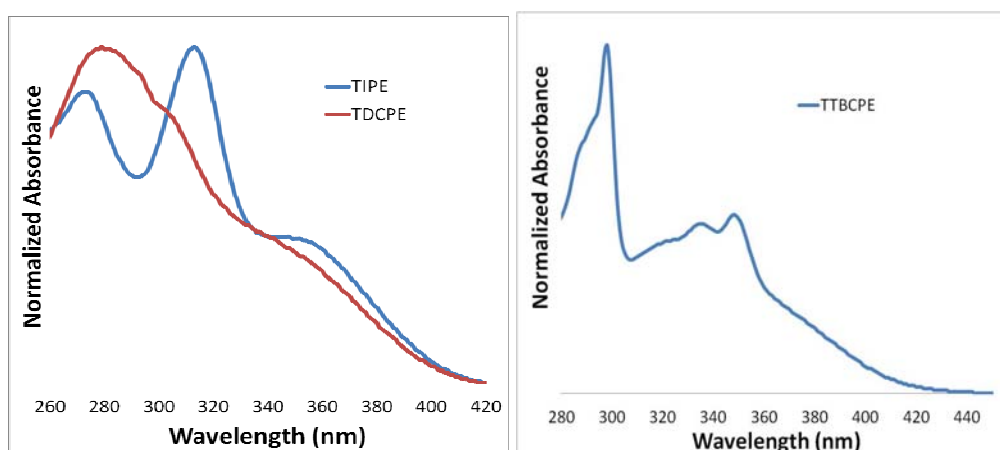


Figure 31. UV-Vis spectrum of TIPE, TDCPE and TTBCPE

Although TDCPE also housing the indole moiety in its molecule; the UV-Vis behavior of TDCPE was different than TIPE. TDCPE had a primary absorption band at 280 nm and a shoulder begins at 335 nm. The primary and secondary bands of TIPE at 272 and 312 nm were merged together to construct the primary band of TDCPE. Since there were no extra π electrons on the cyclohexane units of TDCPE, no further red shift was observed in the luminescence spectrum and appeared at 502 nm. Although TPPE and TDCPE have same π electron density just looking their structures additional cyclohexane moiety somehow harm the electron delocalization on the molecule. Therefore a 13 nm blue shift was observed comparing with the indole functionalized TPE molecule.

For TTBCPE case, it had a maximum absorption around 350 nm. It also had two more absorption bands at 297 and 335 nm correspond to carbazole groups. TTBCPE with additional phenyl ring caused a 10 nm red shift compared with the TIPE. It exhibited a fluorescence emission at around 525 nm.

In general, functionalization of TPE with various N-heterocyclic compounds increased the electron density on the whole molecule. TPE has a maximum absorption at around 300 nm. The synthesized luminogens have maximum absorptions at around 335 - 350 nm, almost 35 to 50 nm red shift compared with TPE molecule itself. The PL spectra of the compounds have a maximum emission in the range of 496 - 525 nm in THF solution. They have colors range from turquoise to light green.

Additionally, the absorption and emission behaviors of TIPE were explored using different solvents with wide range of polarity. According to the results there was no evidence that solvent polarity causes a significant spectral shift in the absorption spectra, however, dissolving TIPE in alcohols demonstrate Mie effect^{170,171} in the long wavelength region. For all the three alcohols a rise in the UV spectrum was seen. The reason for that they formed aggregates in the solution, scattered the light and decreased the transmission. Thus, alcohols are not good solvents for TIPE and therefore aggregation may occur in the solution.

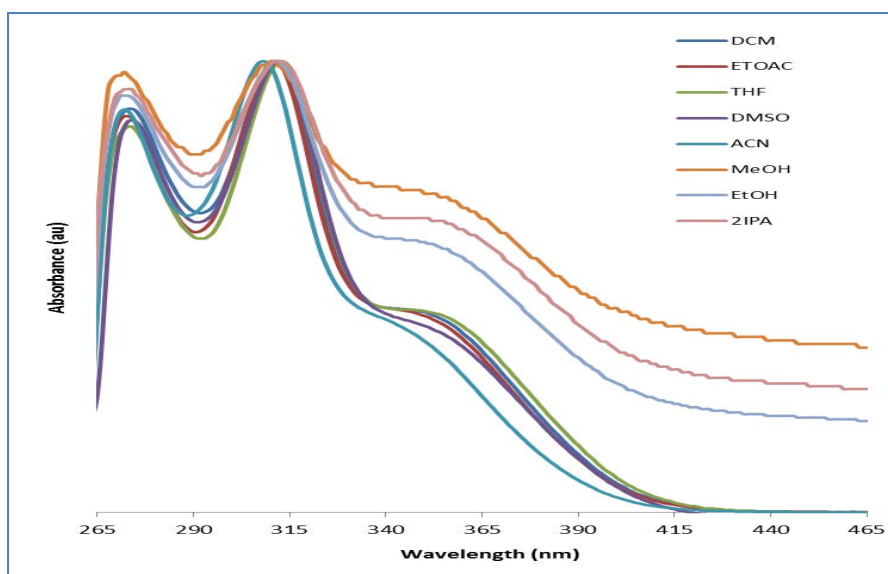


Figure 32. Absorption behavior of TIPE in different solvents

The same effect was observed in the emission spectra. Apart from the alcohols, there are only minor shifts (16 nm) by decreasing the polarity of the solvent. In contrast, there is a 92 nm hypsochromic shift in alcohols compared with the less

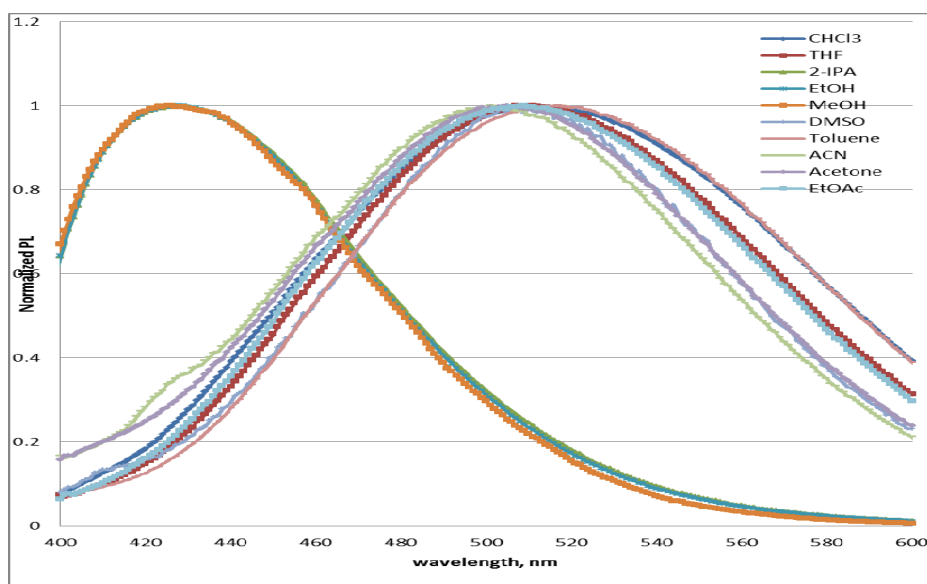


Figure 33. Emission behavior of TIPE in different solvents

polar solvents. Since solvation power of the alcohols is not enough to achieve a complete solution, aggregation occurred in the intermediate. Additionally, H-bond formation between indole and the polar solvent could be presumably the reason of blue emission as well; H-bond formation may disturb the planarity of the molecule and consequently the conjugation.

2.5. Aggregation Induced Emission Properties

The aggregation induced emission properties of the synthesized compounds were examined by studying the fluorescence behavior of their diluted mixtures in water/THF under different water fractions. The aggregates were prepared by adding various fractions of ultra-pure water into the THF solutions. The detailed aggregate sample preparations were explained in the experimental part. Apart from fluorescence spectroscopy, UV-Vis spectroscopy, particle size analysis and Tunneling Electron Microscope techniques helped us to investigate the aggregation induced emission behavior of the luminogens.

TPE is an unusual molecule; it has four phenyl rings having intramolecular rotations that quench its emission, however, when it turns into the aggregate form, the non-radiative decay channels are hindered and TPE becomes active for emission.

All the synthesized compounds have complete solubility in THF and insolubility in water. The molecules started to form aggregates when the water fraction was gradually increased in the solution. The idea behind the procedure is dissolving the compound in a proper solvent to achieve a complete solubility and then by adding an anti-solvent, in most of the case water, gradually decrease the solubility of the compound in its solution and force the compound to become aggregated in the solution.

Table 5. Fluorescence quantum yield values of synthesized compounds in THF with different water fractions

H₂O (%)/ Compound	0	10	20	30	40	50	60	70	80	90
TPPE 41	0.2	0.3	0.3	0.3	0.3	0.3	17.7	48.7	32.5	35.9
TPyPE 42	0.3	0.3	0.3	0.4	0.4	0.5	0.5	0.6	38.8	51.2
TIMPE 43	0.3	0.4	0.6	0.6	0.7	0.8	0.7	0.8	0.7	68.0
TIPE 44	0.6	1.0	1.7	1.4	1.2	1.3	13.7	35.5	67.2	68.3
T5MIPE 45	0.6	0.7	0.8	0.9	1.1	39.6	36.6	27.4	23.4	19.1
TBIMPE 46	0.4	0.6	0.8	0.90	1.0	1.2	1.4	1.3	49.3	51.0
TDCPE 47	1.2	1.3	1.4	17.1	20.8	29.8	46.0	53.1	50.8	59.2
TTBCPE 48	2.4	2.7	2.9	3.5	9.5	15.4	28.8	35.4	39.1	39.8

Solution concentration: 10 μ M

The plot of absorbance versus wavelength explains the UV-Vis behavior of TPPE (Figure 34). Comparing with the solution and aggregate form of TPPE, the spectrum gave a rise in the long wavelength region due to the Mie effect. The aggregates scattered the light and decreased the transmission and increased the absorbance of the sample. The rise in the UV-Vis spectrum was a first indicator for ensuring that the molecules were in an aggregate form in its solution.

The graph of photoluminescence intensity versus wavelength (Figure 35) shows the luminescence behavior of TPPE while changing the water portion from 0% to 99%. Similar to certain AIE molecules, when TPPE was completely soluble in pure THF, it had also almost no luminescence intensity, nearly flat lines. It had

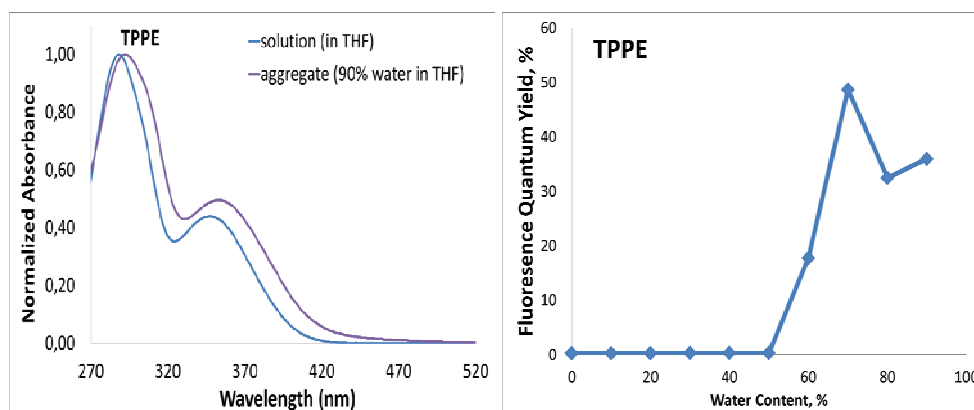


Figure 34. (Left) UV-Vis spectrum of TPPE in solution (100% THF) and in aggregate (90% water – THF) (Right) Fluorescence quantum yield increase

fluorescence quantum yield value of 0.2 (Table 5) and exhibited a greenish color with a wavelength of 507 nm. Adding water to TPPE solution changed the luminescence behavior of the compound. After the limit of 60% water content, a rise in the luminescence intensity together with approximately 50 nm blue shift was observed. This was continued till the end of 80% water content. Between 60 - 80% water fractions, the compound exhibited much crystalline behavior than amorphous one. Therefore a change in the color green to blue was observed.

The dominant wavelength between 60- 80 % water fractions was 456 nm having a good blue color. Adding much water to THF solution turn the morphology of the aggregates to its former state and a red shift was observed. Although TPPE had almost no luminescence in pure THF solution with a Φ_F value of 0.23, the aggregate form of TPPE (90% water – THF) had a Φ_F value of 35.9. There was a 156-fold increase in Φ_F of TPPE between its completely soluble form in THF and its aggregates (Table 5). Figure 36 shows the emission images of TPPE in THF with different water fractions under UV light illumination at room temperature. The color change and intensity rise can clearly be seen in Figure 36.

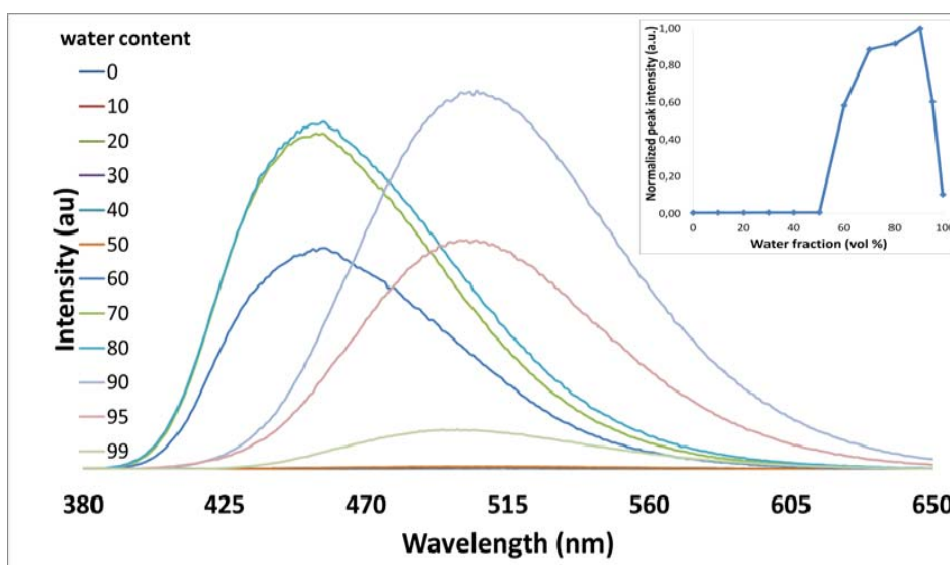


Figure 35. PL spectra of TPPE in THF (10 μM) with different water fractions. The inset shows the change in the luminescence intensity

The structure of TPyPE is similar to TPPE, generating only by changing one carbon atom on the second position with nitrogen atom. Although there is a structural analogy, TPyPE did not behave as TPPE did. According to the absorbance spectrum of TPyPE, it showed also Mie scattering when the molecules morph into aggregate form.

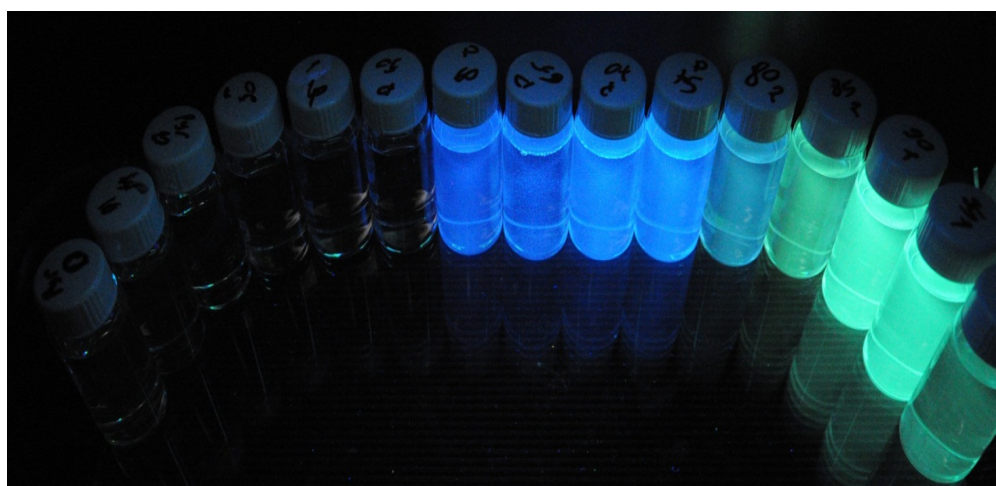


Figure 36. The emission images of TPPE in THF with different water fractions under UV light (365 nm) illumination at room temperature

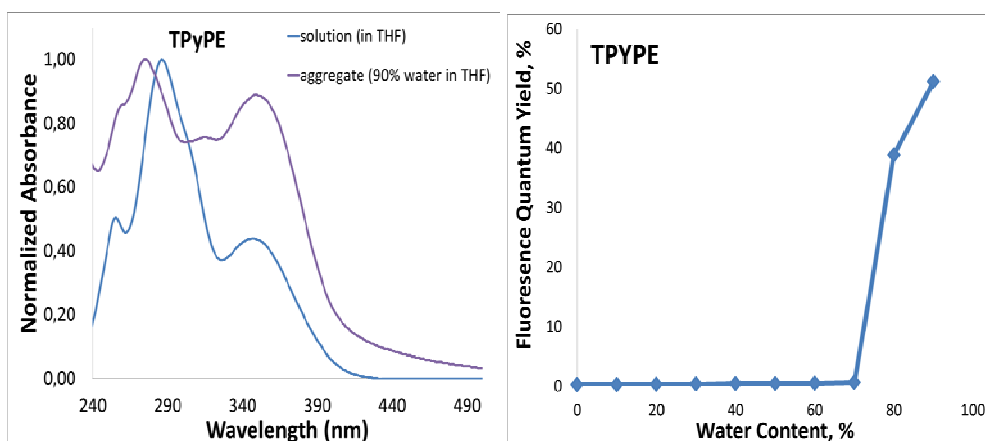


Figure 37. (Left) UV-Vis spectrum of TPyPE in solution (100% THF) and in aggregate (90% water – THF) (Right) Fluorescence quantum yield increase

Interestingly when molecules changed from solution to aggregate form, the absorbance band corresponds to pyrazole group showed a blue shift but the absorbance band corresponds to TPE group showed a red shift (Figure 37).

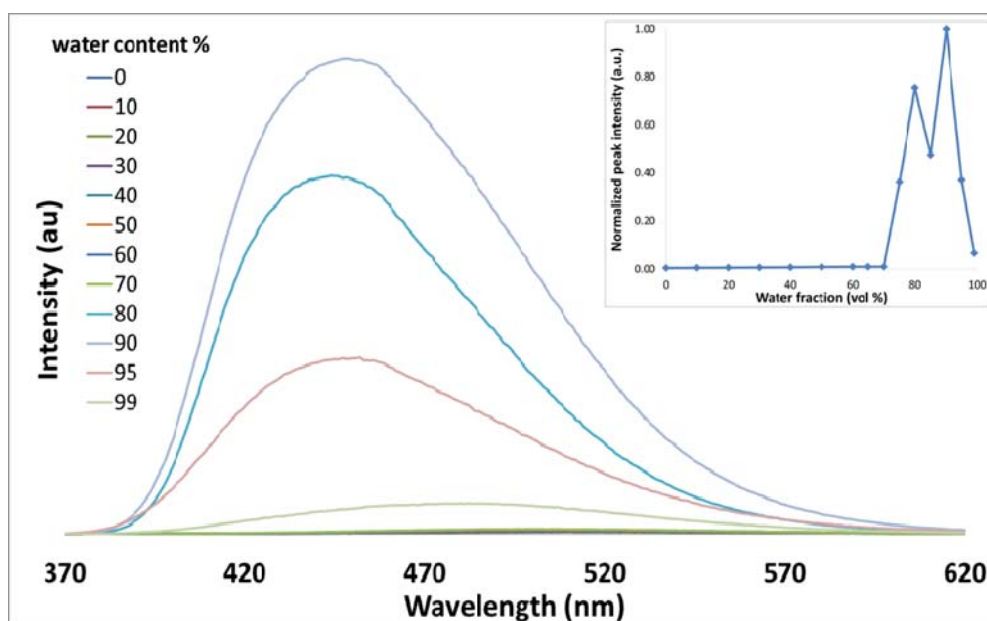


Figure 38. PL spectra of TPyPE in THF (10 μM) with different water fractions. The inset shows the change in the luminescence intensity



Figure 39. The emission images of TPyPE in THF with different water fractions under UV light (365 nm) illumination at room temperature

When TPyPE was completely soluble in THF, it emitted at 506 nm with a Φ_F value of 0.3. Figure 38 shows the fluorescence emission of TPyPE molecules under different water fractions in THF. According to the results, TPyPE molecules did not show any sensible fluorescence emission till the end of 70% water fraction in THF. It started to exhibit an intense blue emission after exceeding 70% water in THF. The leading wavelength was at around 456 nm. It did not demonstrate a color change from green to blue like TPPE did and persisted its blue color with a little change in % 99 water fractions.

Although TPyPE had almost no luminescence in its proper solvent, THF, with a Φ_F value of 0.25, the aggregate form of TPyPE in 90% water had a Φ_F value of 51.2. There was a 205-fold increase in Φ_F of TPyPE between its completely soluble form in THF and its aggregates (Table 5). Figure 39 shows the emission images of TPyPE in THF with different water fractions under UV light (365 nm) illumination at room temperature. The inset of Figure 38 demonstrates the change in the luminescence intensity of the aggregate solutions. In some cases when the water fractions were increased, molecules showed a decrease rather than increase in the luminescence intensity. The detailed explanation will be given at the end of the section.

After the AIE behaviors of TPPE and TPyPE, we wonder what happens when we continue to play the position of the nitrogen atom. TIMPE has also a structural analogy with TPPE and TPyPE, where the carbon on the third position is substituted with a nitrogen atom. Like the other AIE compounds, TIMPE showed a rise in the intensity of its absorbance when it dissolved in 90% water-THF mixture (Figure 40).

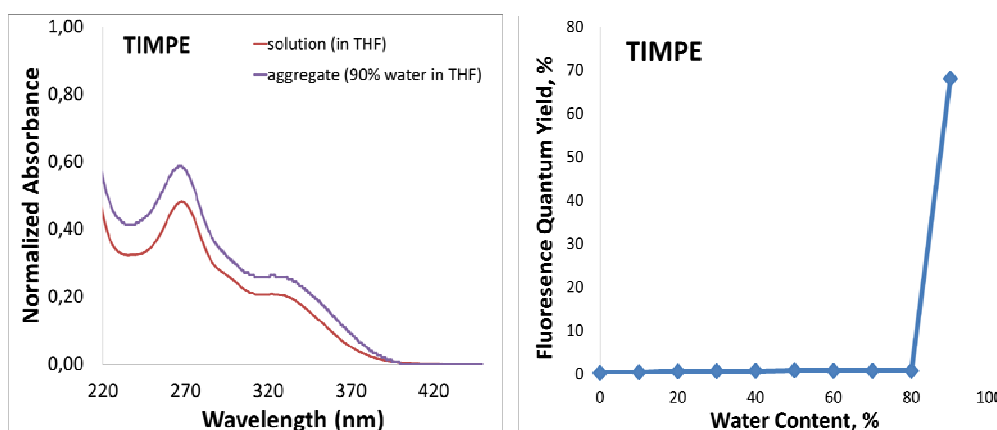


Figure 40. (Left) UV-Vis spectrum of TIMPE in solution (100% THF) and in aggregate (90% water – THF) (Right) Fluorescence quantum yield increase

This fact is one of the proofs that the TIMPE molecules are in aggregate form with 90% water-THF mixture. TIMPE had a fluorescence quantum yield value of 0.3 (Table 5) and exhibited a greenish color with a wavelength of 496 nm.

Like the other two compounds TIMPE did not exhibit any reasonable fluorescence emission when it was completely soluble in a proper solvent (Figure 41). Interestingly adding water to its THF mixture did not induce its fluorescence emission up to 90% water fraction. The relative emission intensity of the compounds did not show any reasonable change. However, when 90% water was added to its THF solution, it started to illuminate a bright blue color but the induction effect was not as high as the TPPE and TPyPE.

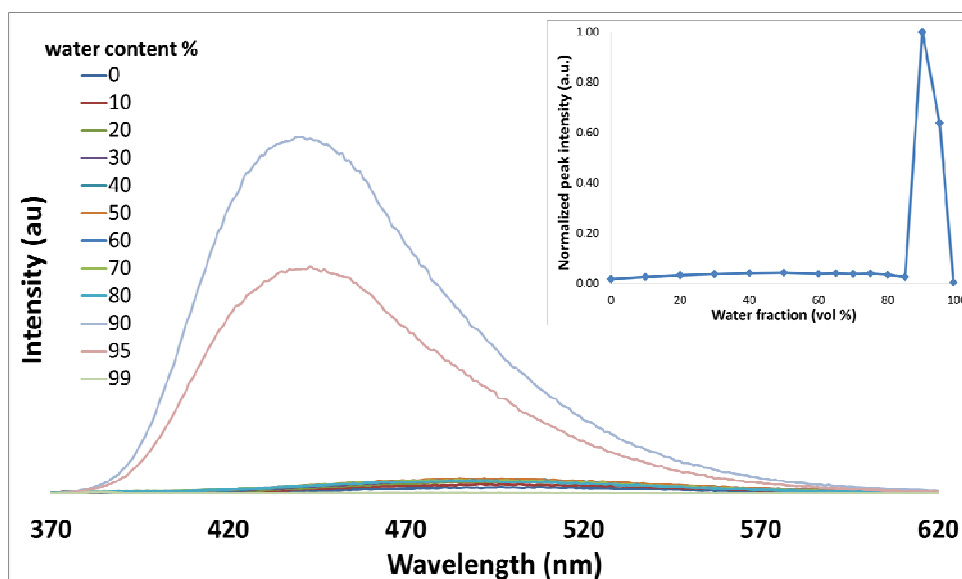


Figure 41. PL spectra of TIMPE in THF (10 μ M) with different water fractions. The inset shows the change in the luminescence intensity

TIMPE showed only a 50-fold increase comparing its molecularly dissolved case with its aggregates. Figure 42 shows the emission images of TIMPE in THF with different water fractions under UV light (365 nm) illumination at room temperature.



Figure 42. The emission images of TIMPE in THF with different water fractions under UV light (365 nm) illumination at room temperature

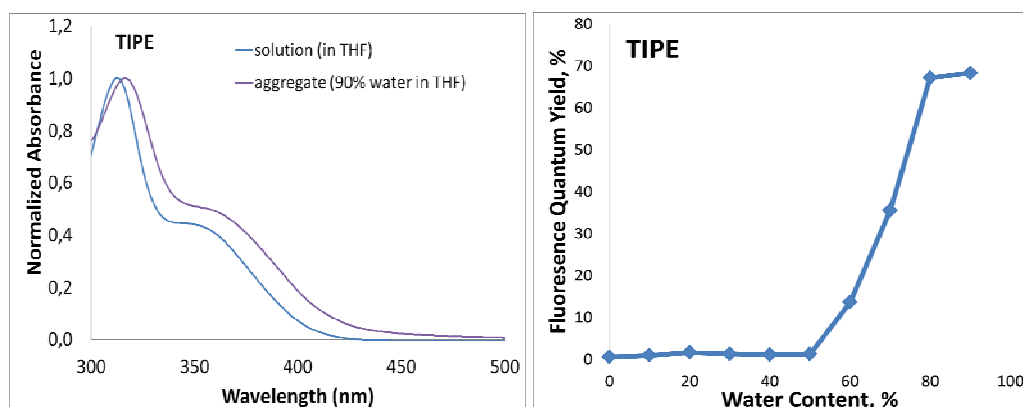


Figure 43. (Left) UV-Vis spectrum of TIPE in solution (100% THF) and in aggregate (90% water – THF) (Right) Fluorescence quantum yield increase

TIPE was insoluble in water and completely soluble in THF. By increasing water content in the mixtures, the molecules started to form aggregates. This fact can be clearly seen by its UV-Vis spectrum (Figure 43). TIPE showed Mie scattering when it morphed in to aggregate form. There was a small red shift between its molecularly dissolve case with its aggregate form. It had a fluorescence quantum

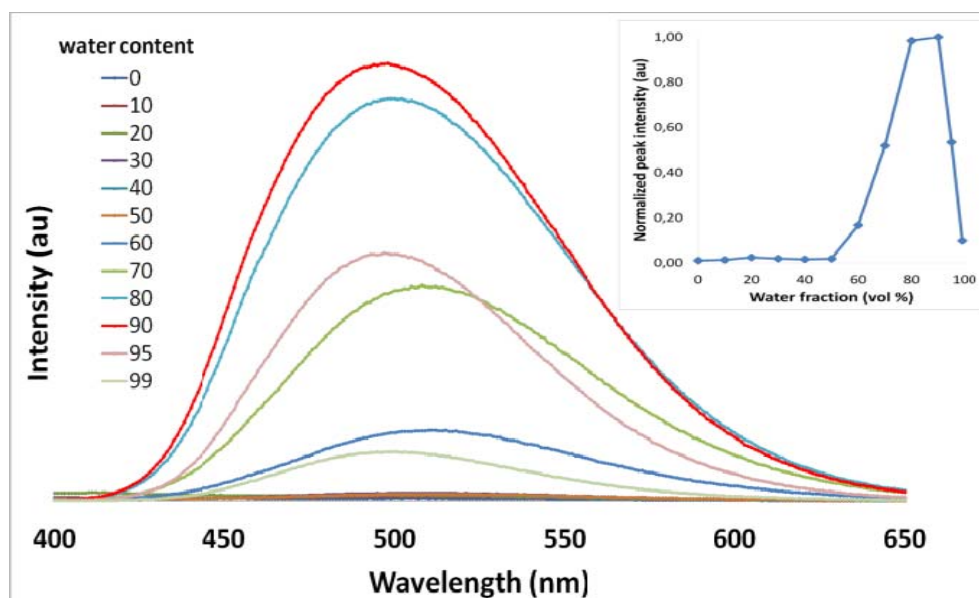


Figure 44. PL spectra of TIPE in THF (10 μM) with different water fractions. The inset shows the change in the luminescence intensity

yield value of 0.6 (Table 5) and exhibited a greenish color with a wavelength of 510 nm. The graph of photoluminescence intensity versus wavelength (Figure 44) shows the luminescence behavior of TIPE while changing the water portion from 0% to 99%.

TIPE had low luminescence intensity, nearly flat lines, when it was completely soluble in THF. It had fluorescence quantum yield 0.6. However, once the water fraction exceeded the limit off 60%, the luminescence intensity started to rise drastically. The fluorescence intensity of TIPE was boosted 175-fold when the water fraction was increased from 0% to 90%. Comparing with the solution and aggregate form of TIPE, Φ_F increased 125-fold. The luminescence intensity started to decrease beyond 90% water content. Adding excess water to THF solution decreased the solubility of molecules dramatically, and reduced also the luminescence intensity. Figure 45 shows the emission images of TPPE in THF with different water fractions under UV light (365 nm) illumination at room temperature. The intensity increase can clearly be seen in Figure 45. Particle size analyses were used to determine the effective diameter (ED) of the aggregates formed in the water:THF mixtures (Figure 46).

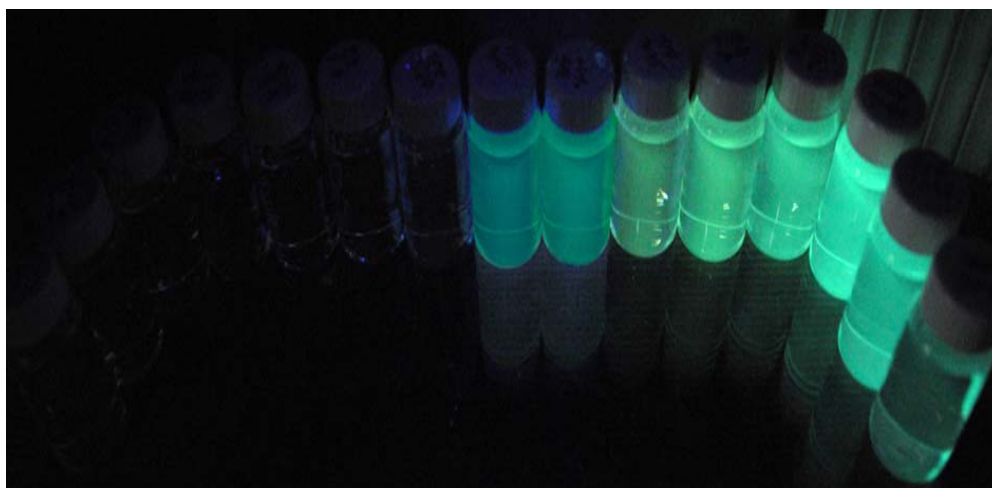


Figure 45. The emission images of TIPE in THF with different water fractions under UV light (365 nm) illumination at room temperature

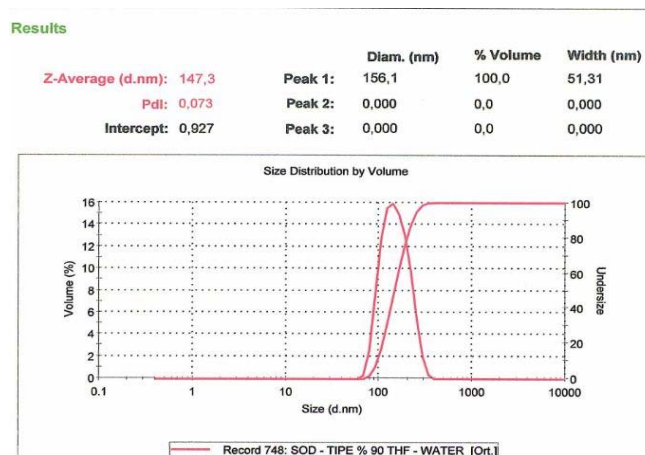


Figure 46. Particle size analysis of TIPE molecules in 90% water – THF mixtures

Table 6. Particle size analysis results of TIPE with fractions 70-90% in THF

Water Fraction (%)	Effective Diameter (nm)
70	342.3
80	169.3
90	147.3

When the water fraction was 60%, the device could not measure any response. This percent is nearby to the ratio that the fluorescence emission sharply improved. At water fraction 70%, the ED was 342 nm and increasing the water fraction to 90%, the ED of the particles decreased to 147 nm. As can be seen, increasing water fraction causes to decrease the ED values (Table 6). This confirmed that TIPE molecules were aggregated as nanoparticles. The TEM images of TIPE point out that the molecules in aggregate form (90% water) consist of submicron particles. TEM images of nanoaggregates of TIPE molecules showed that, in 60% water fraction in THF solution the molecules were apart from each other and adding excess water to THF solution of TIPE brought the molecules together to form aggregates in the molecules. This fact can be clearly seen in the TEM images of TIPE molecule (Figure 47).

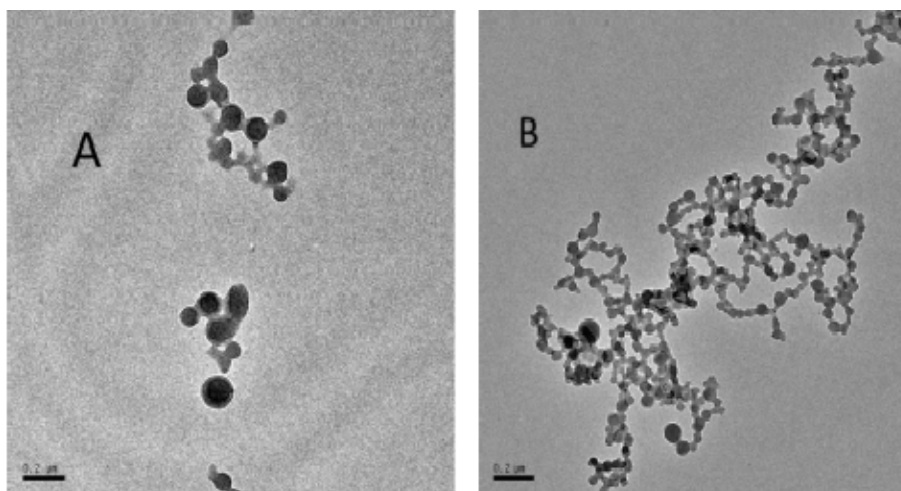


Figure 47. TEM Images (0.2 μm scale) of TIPE in different THF/water fractions.
A) 60% water B) 90% water

T5MIPE is the 5-methoxy derivative of indole substituted TPE therefore it has a structural analogy with TIPE. The left spectrum of Figure 48 shows the absorption behavior of T5MIPE both in molecularly dissolved form in THF and also the aggregate form with 90% water in THF.

Although it showed an increase in its absorption in the aggregate form, the distinction is not so clear as the other luminogenic molecules had. T5MIPE had a fluorescence quantum yield value of 0.6 (Table 5) and exhibited a greenish color with a wavelength of 515 nm expressing a red shift comparing with TIPE molecule.

The graph of photoluminescence intensity versus wavelength (Figure 49) shows the luminescence behavior of T5MIPE while changing the water portion from 0% to 99%. As can be seen from the emission spectrum of T5MIPE, it did not have a reasonable fluorescence emission when it was dissolved in a proper solvent completely. Adding water to solution of T5MIPE started to induce the emission of the compound; however, the induction was not clear up to 50% water fraction. The fluorescence intensity rose by approximately 66 fold reaching a Φ_F value of

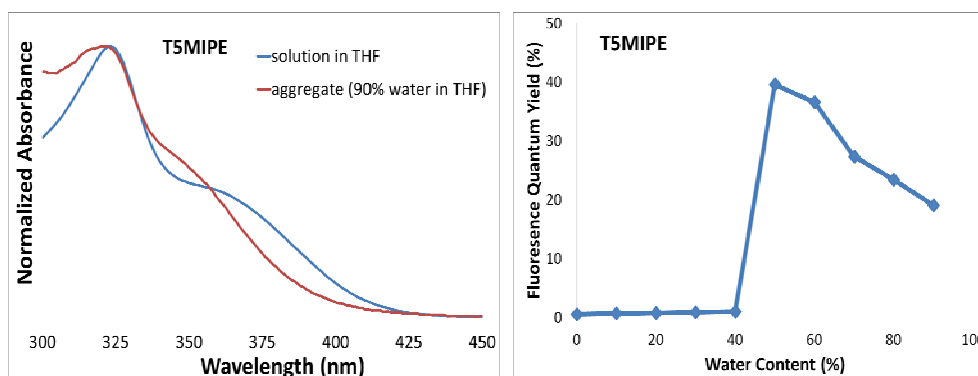


Figure 48. (Left) UV-Vis spectrum of T5MIPE in solution (100% THF) and in aggregate (90% water – THF) (Right) Fluorescence quantum yield increase

39.6. The predominant wavelength was 455 nm having an intense brilliant blue color. The aggregate formation in 50% water fraction caused a blue shift with a value of 60 nm. Continue to adding water after 50% had destructive effect on the fluorescence emission of T5MIPE. It can clearly be seen from in the inset of the Figure 49. Some of the AIE compounds demonstrate such behaviors and the detailed explanation will be given at the end of this section.

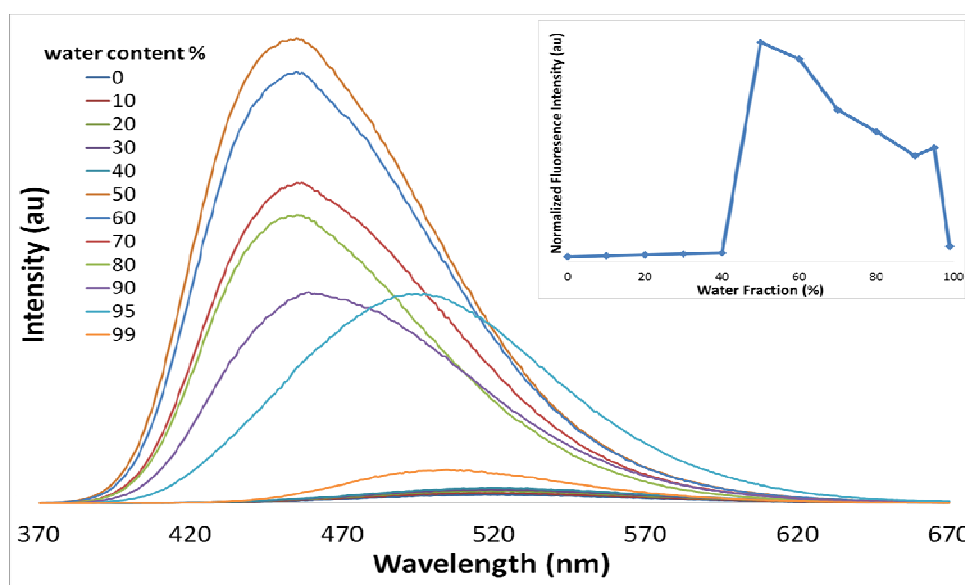


Figure 49. PL spectra of T5MIPE in THF (10 μ M) with different water fractions. The inset shows the change in the luminescence intensity

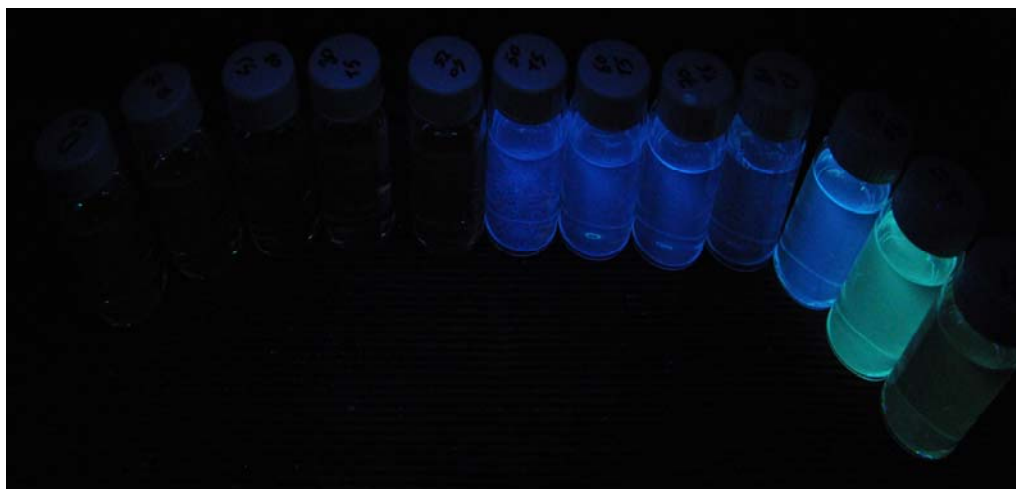


Figure 50. The emission images of T5MIPE in THF with different water fractions under UV light (365 nm) illumination at room temperature

T5MIPE sustained its brilliant blue color up to 90% water fraction and after this percent the molecules started to emit a turquoise color with predominant wavelength 504 nm. Figure 50 shows the emission images of T5MIPE in THF with different water fractions under 365 nm UV light illumination at room temperature. The induction of emission in fluorescence, decreasing the emission strength after 50% water fraction and the red shift from blue to green can be seen clearly in Figure 50.

Furthermore, the AIE behavior of TBIMPE was studied. The given UV-Vis spectrum (Figure 51) showed both its aggregate and solution forms. The aggregation of TBIMPE molecules is so high when it dissolves in 90% water-THF mixture that diminishes the transmittance of the sample by approximately 50%. Therefore a rise in the intensity of absorption of the compound is seen. TBIMPE had a fluorescence quantum yield value of 0.4 (Table 5) in THF and exhibited a greenish blue color with a wavelength of 499 nm expressing a blue shift comparing with TIPE molecule.

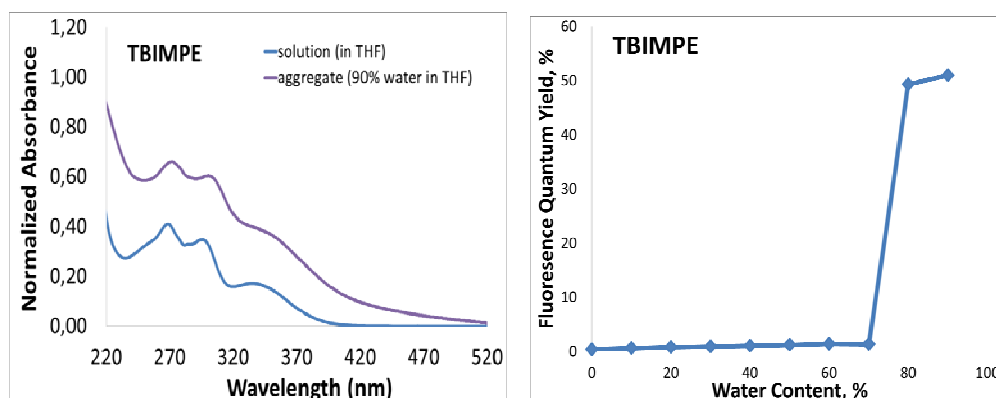


Figure 51. (Left) UV-Vis spectrum of TBIMPE in solution (100% THF) and in aggregate (90% water – THF) (Right) Fluorescence quantum yield increase

Figure 52 shows the photoluminescence behavior of TBIMPE molecules in THF (10 μ M) with different water fractions. When TBIMPE was completely dissolved in THF it gave nearly a flat line emission at around zero. The AIE analysis was continued by adding water to THF mixture of TBIMPE. There was not any reasonable induction of its emission until 75%. At 75% water content, TBIMPE started to exhibit a blue color at 480 nm.

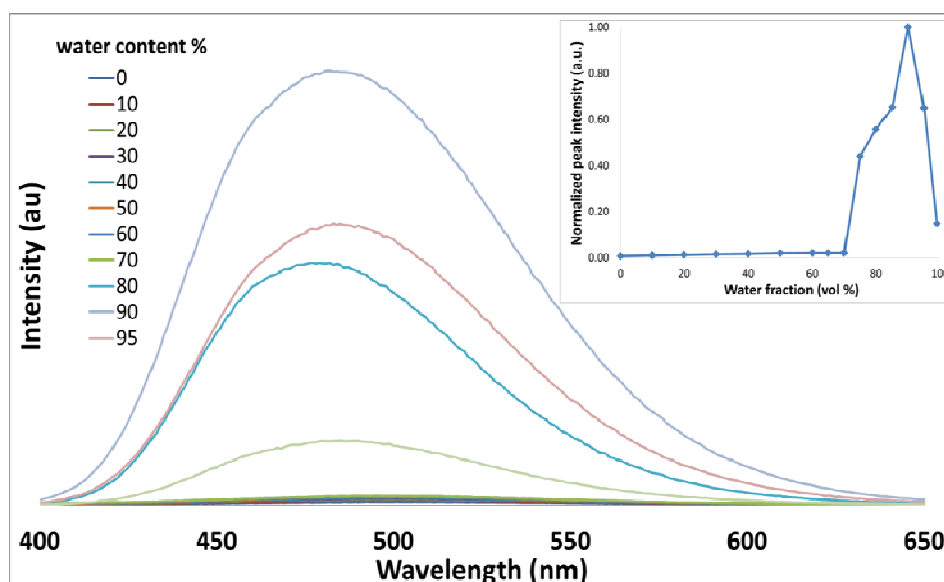


Figure 52. PL spectra of TBIMPE in THF (10 μ M) with different water fractions. The inset shows the change in the luminescence intensity

Changing the carbon atom on the third position of TIPE with a nitrogen atom changed the morphology of the aggregates. The later compound, TBIMPE, became more crystalline than TIPE. As a result of this, TIPE gave green color when it turns into aggregate form; however, TBIMPE gave blue color. There was a 142-fold increase in Φ_F of TBIMPE between its completely soluble form in THF and its aggregates. Figure 53 shows the emission images of TPPE in THF with different water fractions under UV light (365 nm) illumination at room temperature. The color change and intensity increase can clearly be seen in Figure 53.

Figure 54 shows the absorption behavior of TDCPE molecules both in pure solution of THF and its aggregates with 90% water fraction in THF. According to the spectra there is a rise going from solution to aggregate form caused by the Mie effect of the nanoaggregates. In a molecularly dissolved form, TDCPE had a fluorescence quantum yield value of 1.2 (Table 5) in THF and exhibited a greenish blue color with a wavelength of 502 nm expressing a blue shift like TBIMPE comparing with TIPE molecule.

TDCPE showed similar behavior like the other compounds, it had almost no emission in its proper solvent (THF) but it started to gain better emissive



Figure 53. The emission images of TBIMPE in THF with different water fractions under UV light (365 nm) illumination at room temperature

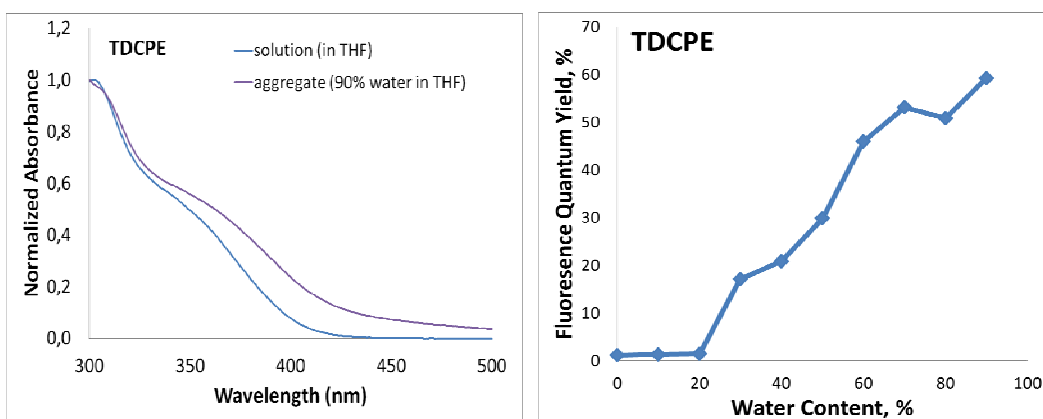


Figure 54. (Left) UV-Vis spectrum of TDCPE in solution (100% THF) and in aggregate (90% water – THF) (Right) Fluorescence quantum yield increase

properties by mixing with high amount of water. Figure 55 shows the photoluminescence behavior of TDCPE molecules in THF (10 μM) with different water fractions and additionally the inset shows the change in the luminescence intensity. When TDCPE was completely dissolved in its proper solvent, it had Φ_F value of 1.2. This is greater than Φ_F value of TIPE. The AIE property of TDCPE can be analyze in three sections.

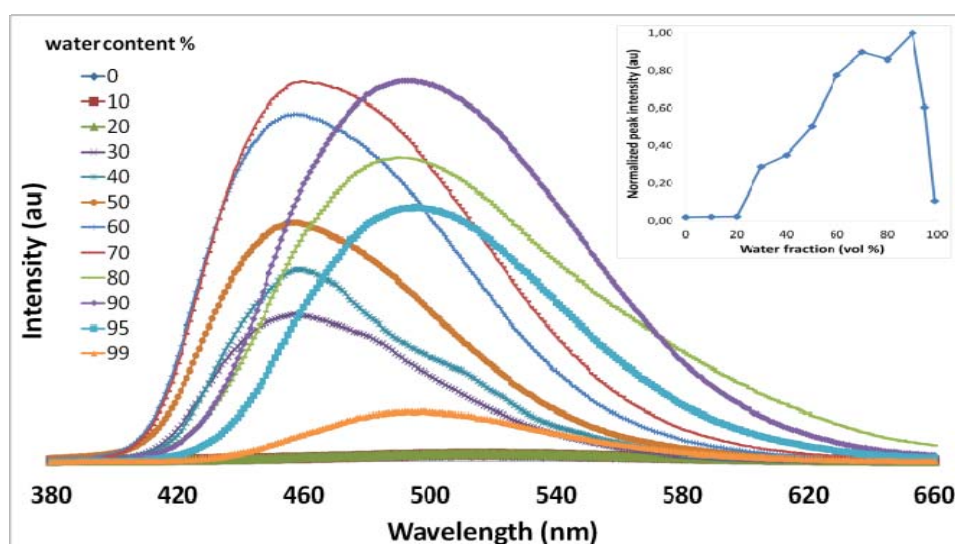


Figure 55. PL spectra of TDCPE in THF (10 μM) with different water fractions. The inset shows the change in the luminescence intensity

Between 0 – 20% water fractions it had green emission with a very low quantum yield. Then it started to emit a blue color with a predominant wavelength of 457 nm and showed a 50 nm blue shift with an increase in its fluorescence intensity. TDCPE maintains this color up to 75% water by having an increase in the Φ_F value by 15 to 45 fold. After passing 75% water fraction TDCPE showed a red shift to turquoise emission with a predominant wavelength of 498 nm. There was a 62 fold increase in its fluorescence emission between 0 to 90%. The color change between blue and green can be explained by morphology of the aggregates. Adding water changed the morphology of the TDCPE aggregates from amorphous state to crystalline state. Therefore, a blue shift was observed up to 75% water fraction. Likewise adding much water and exceeding 75% water fraction, changed the morphology of the TDCPE aggregates from crystalline to amorphous, consequently a red shift to 498 nm was observed. The competition between the crystalline and amorphous states of TDCPE aggregates defines the color of the solution. Figure 56 shows the emission images of TDCPE in THF with different water fractions under UV light illumination at room temperature. The color change and intensity increase can clearly be seen in Figure 56.

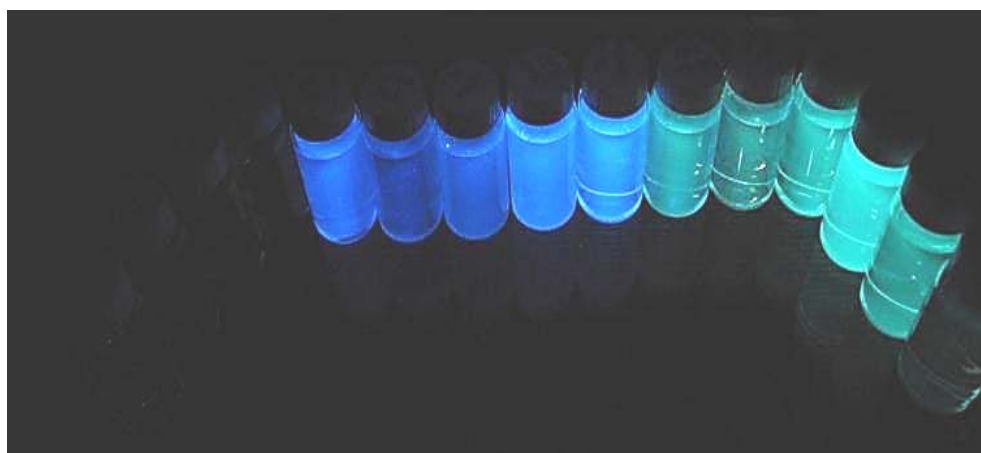


Figure 56. The emission images of TDCPE in THF with different water fractions under UV light (365 nm) illumination at room temperature

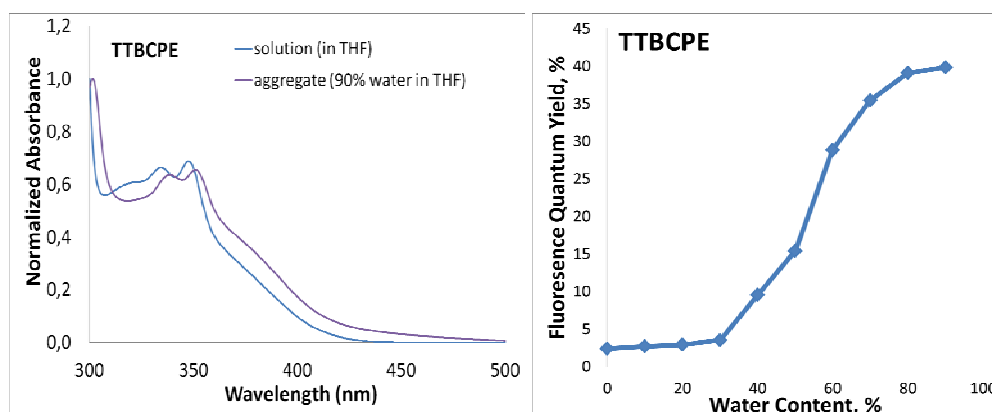


Figure 57. (Left) UV-Vis spectrum of TTBCPE in solution (100% THF) and in aggregate (90% water – THF) (Right) Fluorescence quantum yield increase

Figure 57 shows the UV-Vis spectrum of TTBCPE molecules both in solution and in aggregate forms. Like all the other AIE molecules, TTBCPE showed a rise in the UV-Vis spectrum when it turned into aggregate form from solution. Figure 58 shows the photoluminescence spectra of TTBCPE molecules in THF (10 μ M) with different water fractions starting from 0 up to 99 percent.

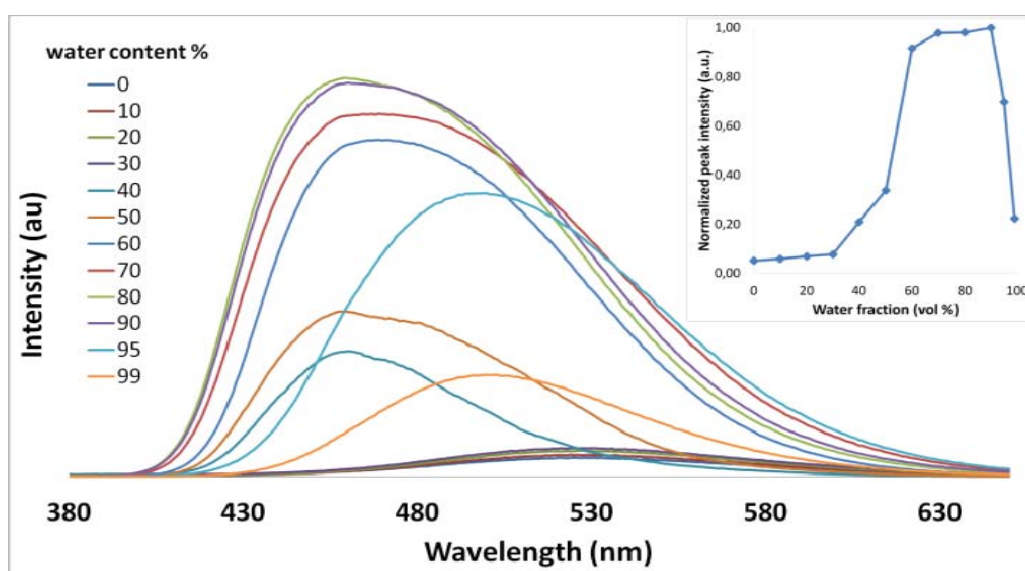


Figure 58. PL spectra of TTBCPE in THF (10 μ M) with different water fractions. The inset shows the change in the luminescence intensity

Moreover, the inset on the Figure 58 shows the change in the luminescence intensity. TTBPCE exhibited a low luminescence when molecularly dissolved in THF ($\Phi_F = 2\%$). Like TDCPE, the AIE property of TTBCPE molecule can be analyzed in three sections. Between 0 to 30% water fraction the predominant wavelength was 528 nm having a low Φ_F value not greater than 3.0. Adding water by passing the 30% water fraction, the aggregates showed a blue shift and the fluorescence emission started to induce the emission. The predominant wavelength was 460 nm and the compounds emitted a bright blue color.

The Φ_F value was boosted between 4 – 16 fold. Between 30 – 90% water:THF mixture the crystalline part of the aggregates dominated the morphology of the compound. Between 95 – 99% water:THF mixture it turned to green again having a predominant wavelength of 500 nm. There was a 21-fold increase in its fluorescence emission between 0 to 90%. The morphology of the aggregates was also changed after exceeding 90% and the molecule become more amorphous. Figure 59 shows the emission images of TTBCPE in THF with different water fractions under UV light (365 nm) illumination at room temperature. The color change and intensity increase can clearly be seen in Figure 59.



Figure 59. The emission images of TTBCPE in THF with different water fractions under UV light (365 nm) illumination at room temperature

TTBCPE molecule had some emission in pure THF solution (i.e. $\Phi_F = 2\%$) and additionally it demonstrated an induction by forming aggregates in the solution. In literature there are also molecules that have an emission in molecularly dissolve form and started to give more induced emission when the molecule turns in to aggregate form. These compounds are classified under the phenomena called aggregation induced emission enhancement (AIEE). Apart from AIE, putting TTBCPE to AIEE category could also be possible.

In general, for some of the compounds having AIE property, increasing the water content could decrease the fluorescence intensity as in TPyPE and T5MIPE aggregates. The reason is unclear. This occurrence was also often detected in some compounds having AIE properties. According to Dong et al.¹⁷² when the aggregation occurred, the light emission was observed only due to the molecules locating on the surface of the nanoparticles and contributed to the fluorescent intensity upon excitation, leading to a decrease in fluorescent intensity. Addition of water increases the size of the aggregates but the number of emissive molecules settling down in the surface of the aggregate decrease. In addition to Dong approach, Yang et al.¹⁷³ handled this fact in a different manner. According to him, when the molecules start to form aggregates by increasing the water content in the solution, the nano aggregates have to form to possible morphological forms. These are crystal nanoparticles and amorphous nanoparticles. The crystal morphology has constructive effect on the fluorescence intensity and the amorphous morphology has destructive effect on the fluorescence intensity. The net outcome of the fluorescence intensity is on account of the competition of these two morphological forms. In fact it's difficult to control the formation of nanoaggregates in solutions. Therefore the measurements do not exhibit any regularity in high water fractions.

2.6. Lifetime Measurements

The photoluminescence decay analyses results are given in Table 7. All the synthesized compounds except T5MIPE exhibit two exponential process with a fitting equation of $F(t) = A + B1 \exp(-t/\tau_1) + B2 \exp(-t/\tau_2)$ and T5MIPE exhibit three exponential process with a fitting equation of $F(t) = A + B1 \exp(-t/\tau_1) + B2 \exp(-t/\tau_2) + B3 \exp(-t/\tau_3)$ (see appendix Figure A-48 - Figure A.-55). B1, B2 and B3 represent the portion of excited luminogen molecules that choose a certain relaxation pathway to decay. Apart from TIMPE and T5MIPE, all the other compounds prefer to decay through the slow relaxation channel ($B1 < B2$). The acceptability of the fits was judged by minimizing the reduced chi squared function χ^2 criteria and visual inspection of the residuals of the fitted function to the data. All χ^2 values were below to 1.2 and close to 1.0. Table 7 shows the fluorescence decay parameters of synthesized compounds in aggregate forms.

Table 7. Fluorescence decay parameters of synthesized compounds in 90% water in THF.

Compound		B ₁	B ₂	B ₃	τ_1	τ_2	τ_3
TPPE	41	21.02	78.98	-	1.89	5.88	-
TPyPE	42	24.46	75.54	-	2.98	6.05	-
TIMPE	43	69.88	30.12	-	2.23	7.22	-
TIPE	44	29.6	70.4	-	3.80	6.85	-
T5MIPE	45	10.40	75.43	15.17	0.86	3.59	8.11
TBIMPE	46	24.32	75.68	-	2.96	6.65	-
TDCPE	47	14.4	85.6	-	2.49	6.45	-
TTBCPE	48	30.5	69.5	-	1.34	4.77	-

Among all the compounds TTBCPE has the shorter relaxation pathway with the estimated lifetimes of 1.34 and 4.77 ns. The fused ring together with tert-butyl groups is responsible for the shorter lifetimes of TTBCPE. Addition of electron donating group to TIPE molecule increased the total relaxation times by slowing down the complete relaxation and a triple exponential function was better to fit the decay process of T5MIPE. To the best of our knowledge, in literature a few compounds with AIE property were exhibiting three decay pathways.^{174,175} Although the first relaxation occurred much faster than indole substituted TPE, the total relaxation time was higher than TIPE with a value of 8.11 ns. In general, multiple lifetimes were due to that decay curves of the synthesized compounds consist of independent emissions coming from the fragments having different π conjugation lengths.

2.7. Application in Organic Light Emitting Devices

2.7.1. Optimization studies for device layout

In order to investigate the electroluminescence characteristics of the synthesized organic molecules, OLEDs were fabricated and characterized. These novel molecules were applied as emitters without any additional dopant molecule. Since they are small organic molecules multilayer OLED layout, additional hole and electron transport layers, were used.

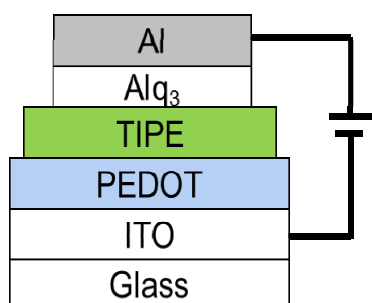


Figure 60. Device layout 1

With the purpose of finding the optimum device layout some pre-device analyses were done. The first device architecture was shown below (Figure 60). TIPE were used as a light emitting layer and prepared in dichloroethane with a 5 mg mL^{-1} concentration. Poly(3,4-ethylenedioxythiophene)poly(styrenesulfonate) (PEDOT: PSS) was chosen as HTL and it was spin-coated at 3000 rpm for 30 seconds, afterwards dried at $110 \text{ }^\circ\text{C}$ for 10 min. Subsequently active layer was spin-coated at 1000 rpm for 40s and cured at $120 \text{ }^\circ\text{C}$ for 10 min. Then the electron transport layer Alq_3 was coated by thermal evaporation at a base pressure of 10^{-6} mbar. Subsequently aluminum was coated as the cathode electrode by thermal evaporation under vacuum.

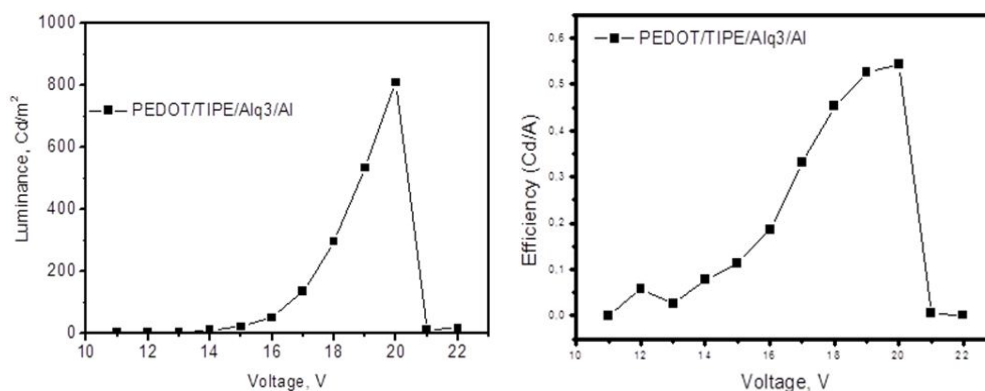


Figure 61. (Left) Luminance-voltage, (Right) Luminous efficiency, curves of the OLED 1.

The OLED performance of the first device was given in Table 8. It had a high turn on voltage with a value of 12 V and had a maximum luminance of 800 cd m^{-2} , maximum luminous efficiency value of 0.6 cd A^{-1} . The first device made by TIPE using as emitting layer gave external quantum efficiencies 0.2 that is quite low (Figure 61). The reason of poor quality device could be misbalance of the hole and electron pairs facing in the emitting layer. Moreover, the thickness could be also another reason for the high turn on voltage of the device 1 since spin coating systems are less effective than vacuum deposition technique for controlling the thickness of the layers.

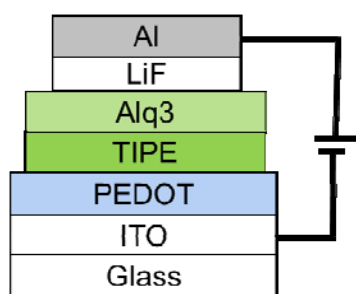


Figure 62. Device Layout 2

After the first device architecture, LiF was used as a cathode interfacial material (CIM). The purpose of LiF is to reduce the work function of the cathode. LiF has also ability to diminish the reactivity of the metal and improve the electron injection.

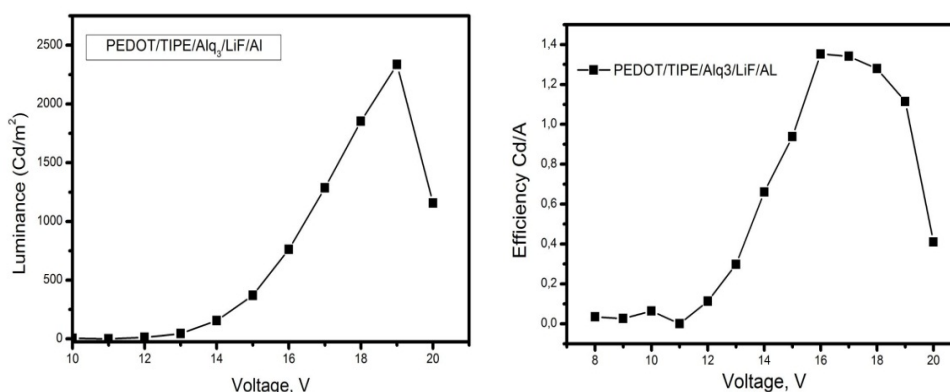


Figure 63. (Left) Luminance-voltage, (Right) Luminous efficiency, curves of the OLED 2

The device architecture was shown in Figure 62. Addition of LiF as cathode interfacial material improved the device performance drastically. The OLED performance of the second device was given in Table 8. The turn on voltage decreased to 11 V. Although LiF addition did not have a big effect on the turn on voltage of the OLED device, the maximum luminance was increased to 2300 cd m⁻²

², and maximum luminous efficiency value increased to 1.4 cd A⁻¹. Furthermore the second device gave external quantum efficiencies 0.5 (Figure 63).

Although using LiF enhanced the device performances, the turn on voltage of the device was higher than our expectations. After the first and second device configuration we decided to change the PEDOT:PSS with N,N'-Di-[(1-naphthyl)-N,N'-diphenyl]-1,1'-biphenyl)-4,4'-diamine using as a hole transport layer. Solution processed OLEDs were operated successfully, but their efficiencies were not satisfactory therefore in device 3 all the organic materials were deposited by thermal evaporation technique (base pressure: 10⁻⁶ mbar). The thickness was controlled by deposition control unit. The third device configuration was shown in Figure 64. In device 3, the thicknesses of the hole transport layer (NPD) were about 50 nm, the active emissive layer were approximately 35 nm, electron transport layer (Alq₃) were 20 nm, LiF layer were 1 nm and finally the cathode layer were 150 nm. The control of thickness of the layers is especially important. Since the thickness of the layers and also the whole device determine the turn on voltage and the device performances. Substituting PEDOT:PSS with NPD caused a dramatic increase in the OLED performance. Figure 66 shows the performance results of the OLED device 3.

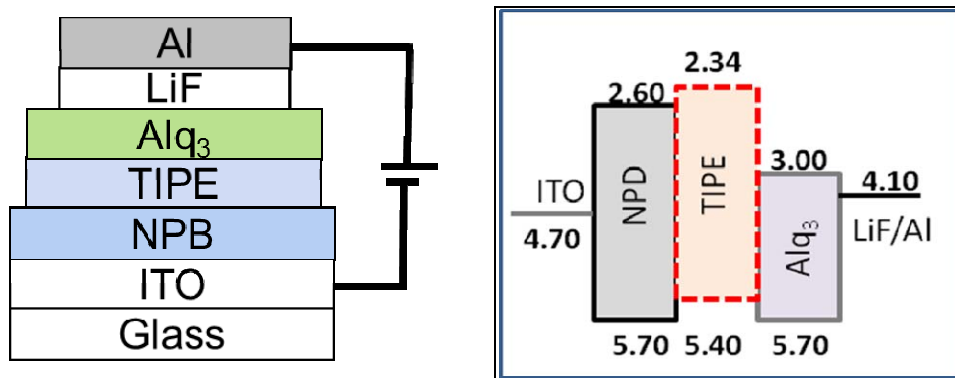


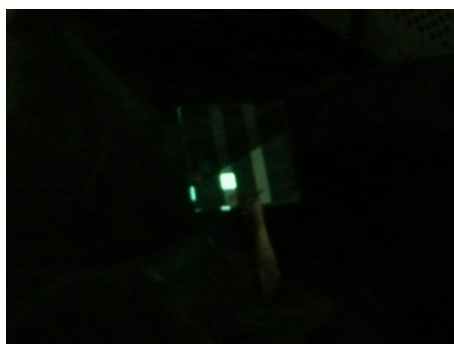
Figure 64. Device Layout 3

Table 8. Performance of devices 1-3

Device No	HTL	ETL	Cathode	V_{ON} (V) ^a	L (cd m ⁻²) ^b	LE (cd A ⁻¹) ^b	EQE (%) ^b
1	PEDOT PSS	Alq ₃	Al	12	800	0.6	0.2
2	PEDOT PSS	Alq ₃	LiF/Al	11	2300	1.4	0.5
3	NPD	Alq ₃	LiF/Al	5	18000	5.2	2.0

a Turn-on voltage at 1 cd/m², b Maximum values.

The turn on voltage decreased to 5.0 V that is a quite a good value. The maximum luminance increased to 18000 cd m⁻², and maximum luminous efficiency value increased to 5.2 cd A⁻¹. Additionally the third device gave external quantum efficiencies 2.0. The Commission Internationale de L'Éclairage (CIE) coordinates at a 1000 cd m⁻² were calculated as 0.20, 0.42 for x and y respectively.

**Figure 65.** OLED device using TIPE as an emitter

When we compare first and third device performances there was 22 fold increase in maximum luminance, 8 fold increase in maximum luminous efficiency and 10 fold increase in external quantum efficiencies. The photo of the OLED device 3,

made by TIPE as a light emitting layer, was shown below. The device emitted a bright turquoise color with a wavelength at 500 nm.

According to the results of the three device configuration the selected device layout for the further studies were shown below. The OLED performance of the remaining luminogenic compounds were tested according to this device architecture (Figure 67).

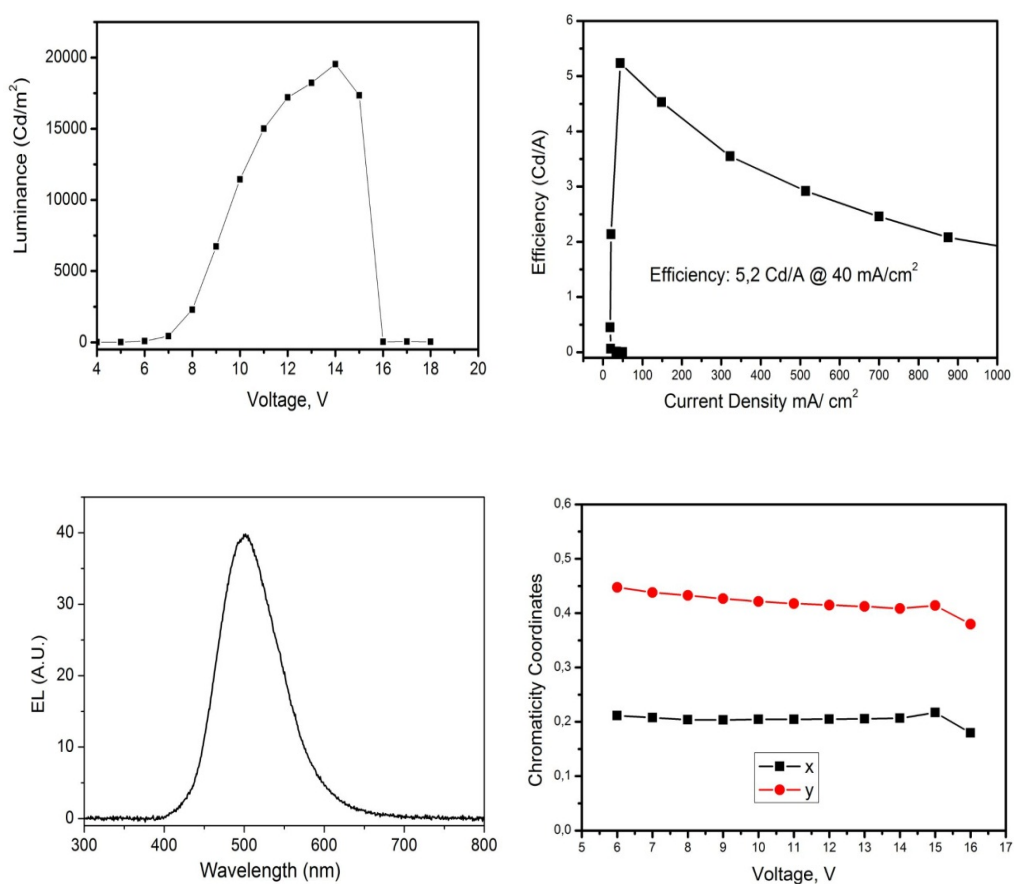


Figure 66. Performance curves of device 3

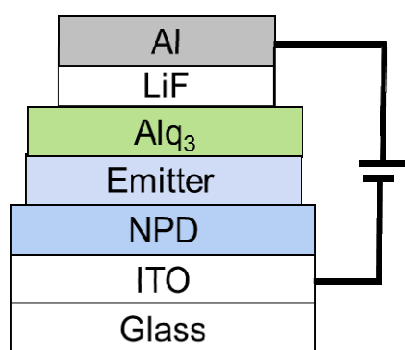


Figure 67. Optimized device architecture

2.7.2. Further OLED applications

The device 4 was fabricated using TTBCPE as a light emitting layer and had an operating voltage at 5.0 V that is a quite a good value. The low lying LUMO level of TTBCPE helps to decrease the operating voltage of the device. The low lying LUMO level induces the electron transfer from the ETL layer to the emissive layer. The maximum luminance value was 1050 cd m^{-2} and the maximum luminous is 1.6 cd A^{-1} . The OLED device 4 gave external quantum efficiency 0.6. The external quantum efficiency was low compared with the Device 3. The CIE coordinates of the device 4 made by TTBPCE as an emitter at a 1000 cd m^{-2} were calculated as 0.24, 0.46 for x and y respectively. The device gave a turquoise color emission appeared at 505 nm. Figure 68 shows the luminance-voltage, luminous efficiency, electroluminescence and chromaticity coordinate curves of OLED device using TTBCPE as a light emitting layer.

The fifth OLED device was made by TDCPE using as an emitting layer. Figure 69 shows the results of OLED device characterizations. Although TDCPE has nearly same HOMO and LUMO levels like TIPE, it did not give good result like TIPE did. The turn on voltage was higher than device 3 with a value of 9.0 V. The maximum luminance value was 1650 cd m^{-2} and the luminance efficiency was 0.8 cd A^{-1} .

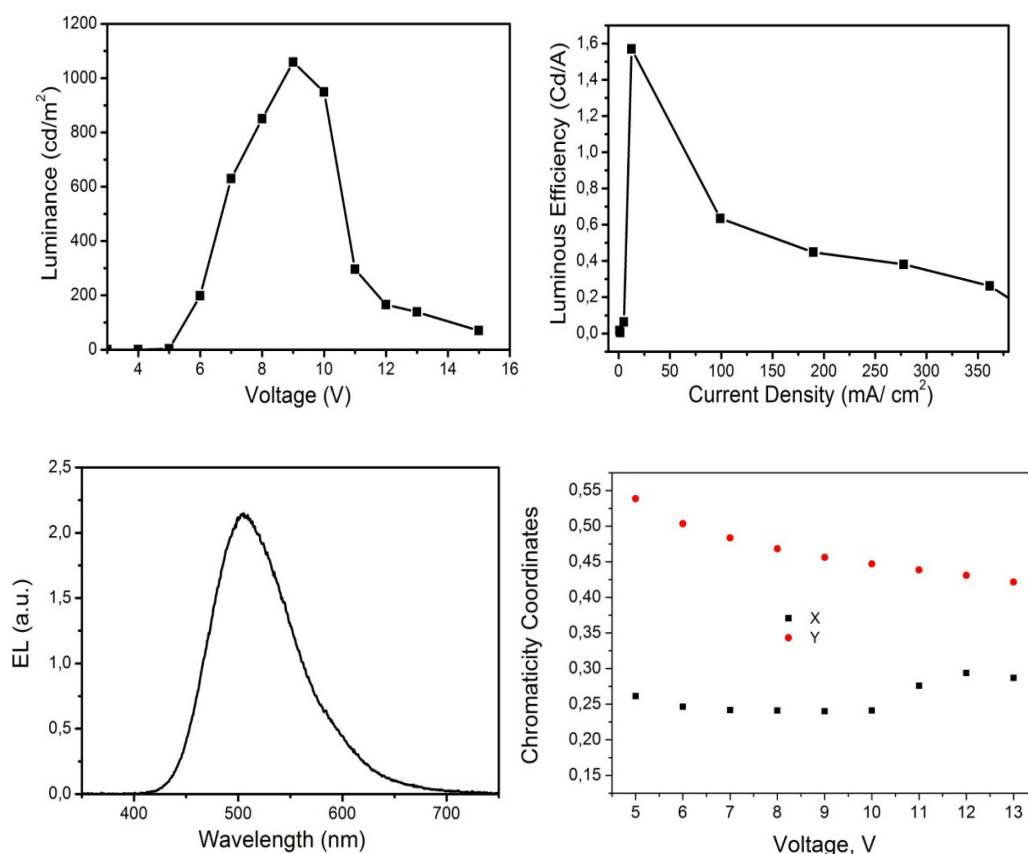


Figure 68. (Top-left) Luminance-voltage, (top-right) luminous efficiency, (bottom left) electroluminescence and (bottom right) chromaticity coordinate curves of OLED device 4 using TTBCPE as a light emitting layer

Although the maximum luminance value was greater than TTBCPE, TDCPE has lower luminance efficiency values. The reason is that the device consumed much energy to achieve the desired luminance so the efficiency values decreased. The OLED device 5 gave external quantum efficiency 0.3. The external quantum efficiency was much lower than the Device 3. The CIE coordinates of the Device 5. made by TDCPE as an emitter at a 1000 cd m^{-2} were calculated as 0.24, 0.44 for x and y respectively. The device 5 emitted light green color with a wavelength at 508 nm.

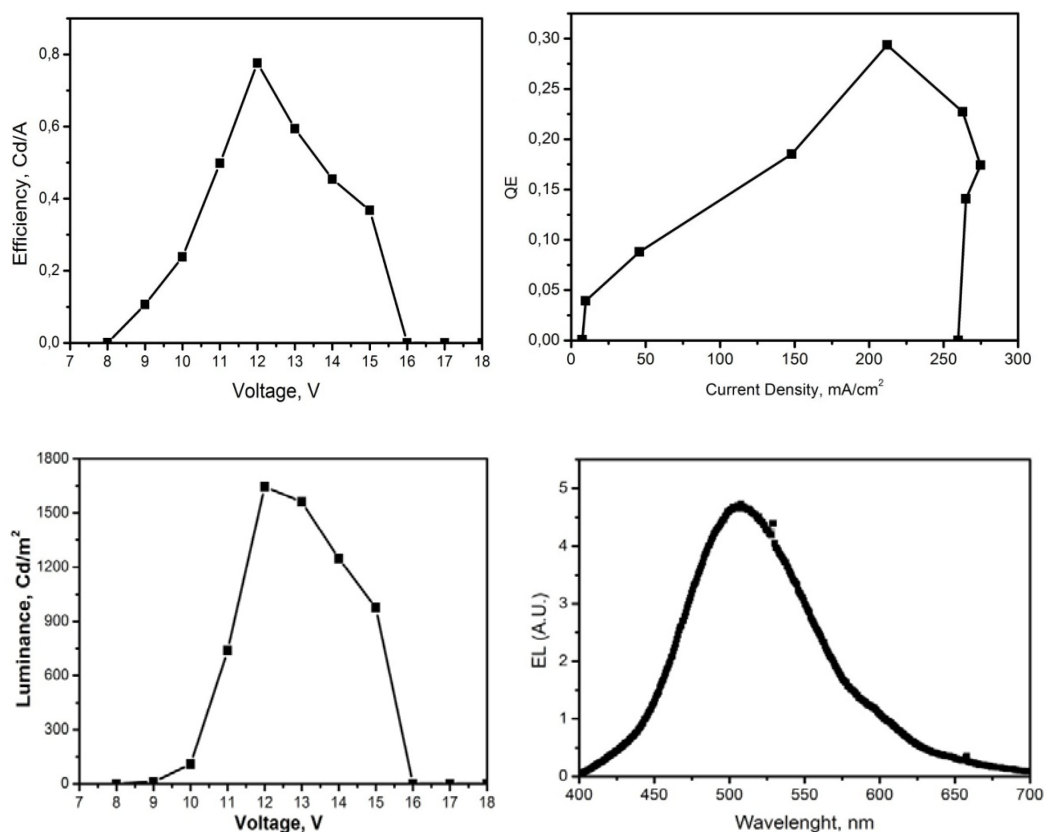


Figure 69. (Top-left) Luminous efficiency, (top-right) EQE – current density, (bottom left) Luminance-voltage and (bottom right) electroluminescence curves of OLED device 5 using TDCPE as a light emitting layer

In an OLED device the emitting material characteristic determine the performance of the OLED device even all the pre-analysis results were almost same each other, the two molecules can give two different performance results as in TIPE and TDCPE did.

The OLED performance of the pyrrole derivative of TPE, TPPE, was investigated by using the optimized device configuration. Even though any dopant molecule were not used, the fabricated OLED performed successfully. The turn on voltage of the device 6 was 7 V and the maximum luminance value was 555 cd m⁻². Although there was a big decrease in maximum luminance value comparing with the device 3, the maximum luminous is 2.1 cd A⁻¹.

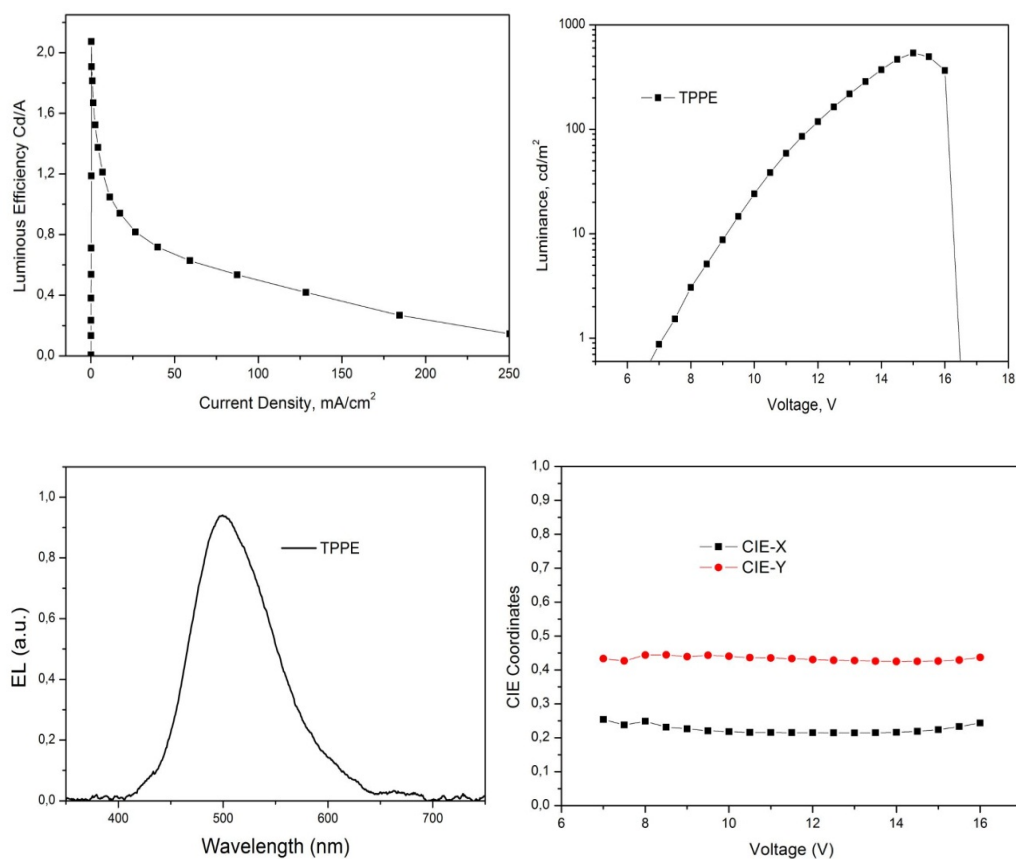


Figure 70. (Top-left) Luminous efficiency, (top-right) Luminance-voltage, (bottom left) electroluminescence and (bottom right) chromaticity coordinate curves of OLED device 6 using TPPE as a light emitting layer

The reason of this decrease was same as TDCPE case. Furthermore the OLED device made by TPPE as an emitter gave external quantum efficiencies 0.8. The CIE coordinates at a 1000 cd m⁻² were calculated as 0.22, 0.44 for x and y respectively (Figure 70). The device efficiencies were relatively high comparing with the maximum luminance value. The reason of this fact can also be explain probably due to that the device 6 had better electron transfer but these electron transfers were not steady and dropped rapidly as the current densities increases. The OLED device made by TPPE as an emitter was shown in Figure 71. The device emitted a bright turquoise color with a value of 499 nm.



Figure 71. OLED device 6 using TPPE as an emitter

The device 7 is made by TIMPE used as light emitting layer. The device 7 exhibited the poorest brightness and efficiency values. It gave a maximum luminance value was 190 cd m^{-2} and maximum luminous was 1.0 cd A^{-1} . Furthermore turn-on voltage of the corresponding device was 10 V which is the highest among the others.

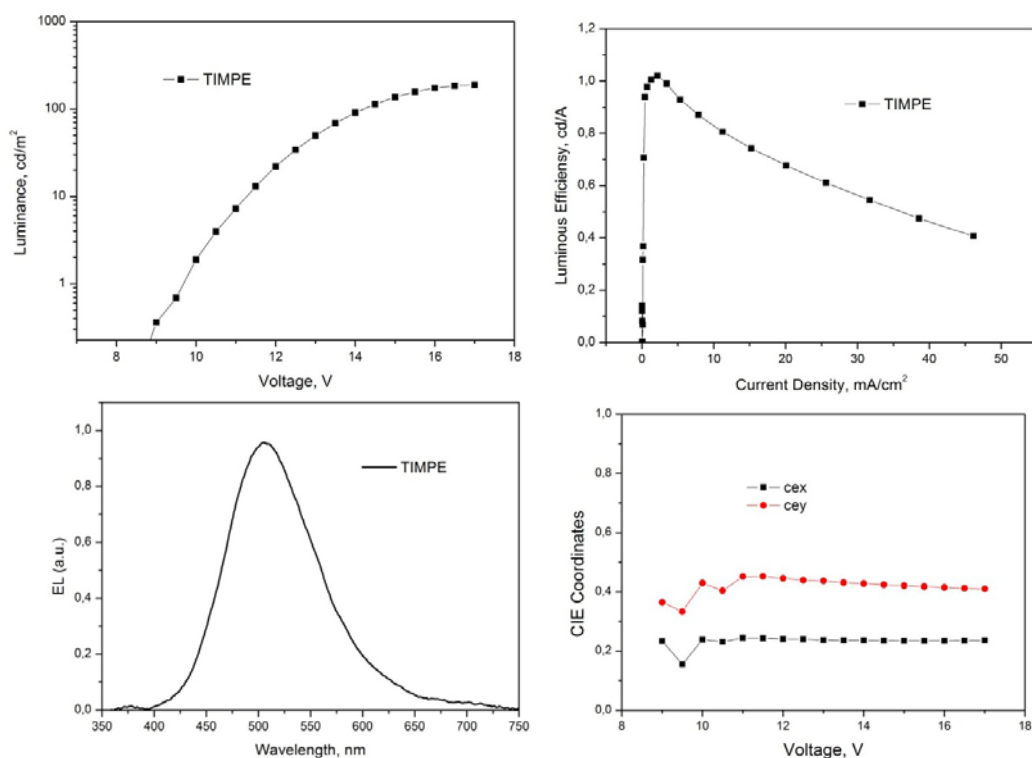


Figure 72. (Top-left) Luminance-voltage, (top-right) luminous efficiency, (bottom left) electroluminescence and (bottom right) chromaticity coordinate curves of OLED device 7 using TIMPE as a light emitting layer

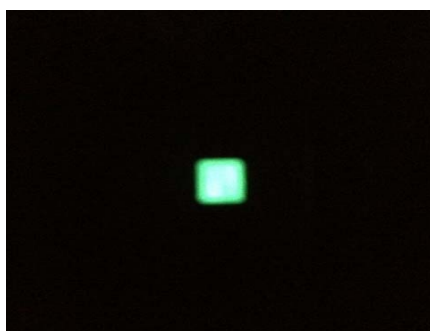


Figure 73. OLED device using TIMPE as an emitter

This could be due to an insufficient electron transfer to the emitter from the electrodes. Moreover, the photo of the OLED device made by TIMPE as a light emitting layer was given in Figure 73. It had external quantum efficiencies 0.4. The CIE coordinates at a 1000 cd m^{-2} were calculated as 0.24, 0.43 for x and y respectively. The device 8 emitted a light green color with a value of 507 nm.

The 8th OLED device was made by TPyPE using as an emitting layer. Figure 74 shows the results of OLED device characterizations. Like all the other device architectures no dopant materials were used and fabricated OLED device performed successfully. The turn on voltage was higher than device 3 with a value of 7.0 V. The maximum luminance value was 2600 cd m^{-2} that is the second highest value among the synthesized luminogens. The luminance efficiency was 2.2 cd A^{-1} . Although the luminance and efficiency values were good, device 8 gave an external quantum efficiency value of 0.8. The external quantum efficiency was much lower than the Device 3. The CIE coordinates of the device 8 made by TPyPE as an emitter at a 1000 cd m^{-2} were calculated as 0.20, 0.38 for x and y respectively. The device 8 had two emission peaks at 488 and 500 nm.

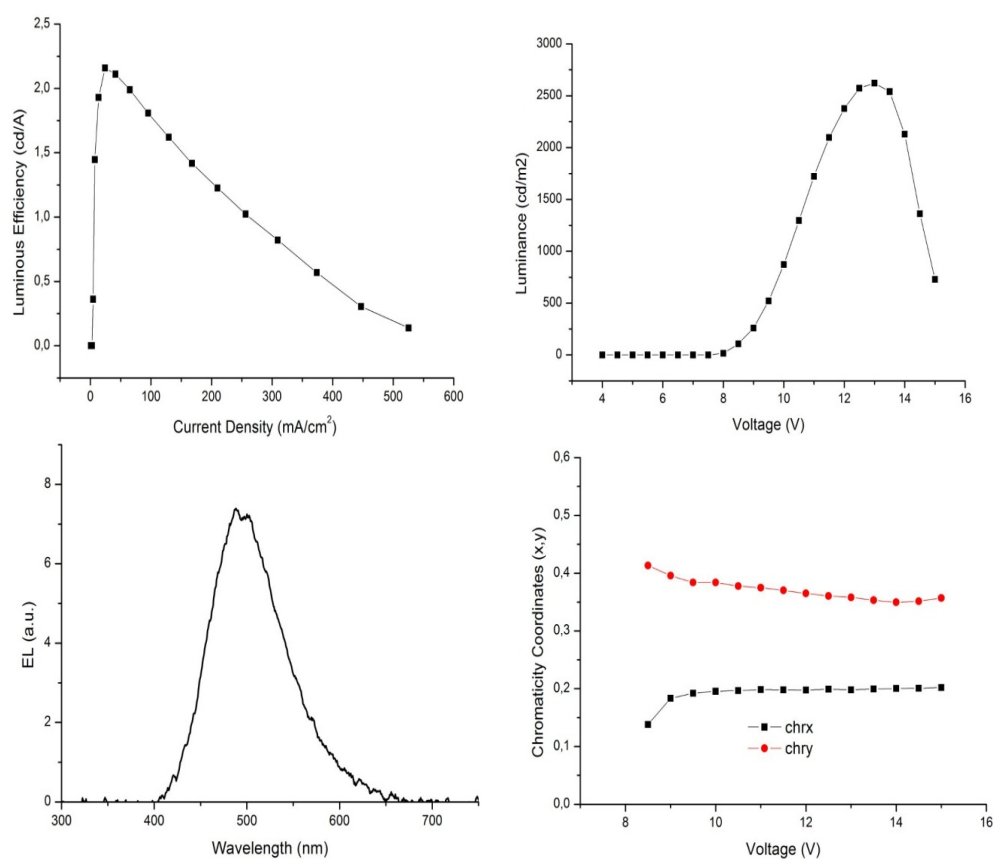


Figure 74 (Top-left) Luminous efficiency, (top-right) Luminance-voltage, (bottom left) Electroluminescence and (bottom right) Chromaticity coordinate curves of OLED device 8 using TPyPE as a light emitting layer

After that, the device 9 was made by using TBIMPE as a light emitting layer. Figure 75 shows the device performance results. As can be seen in Figure 75, the luminance efficiency and external quantum efficiency of TBIMPE reached to 3.6 cd/A and 1.5%, respectively at 2 mA/cm². Comparing with TPyPE values on the other hand, both LE and EQE of TBIMPE versus current density dropped rapidly compared to those of TPyPE. In other words, at high current densities TPyPE serves higher efficiencies. For example, at 25 mA/cm² the LE values of TBIMPE and TPyPE are 1.5 and 2.2 cd/A, respectively. The CIE coordinates of the device 9 made by TBIMPE as a light emitting layer with no dopant molecule at a 1000 cd m⁻² were calculated as 0.24, 0.41 for x and y respectively. The device 9 had one

emission peak at 488 nm and a small shoulder at 516 nm. Figure 76 shows the OLED device using TBIMPE as a light emitting layer.

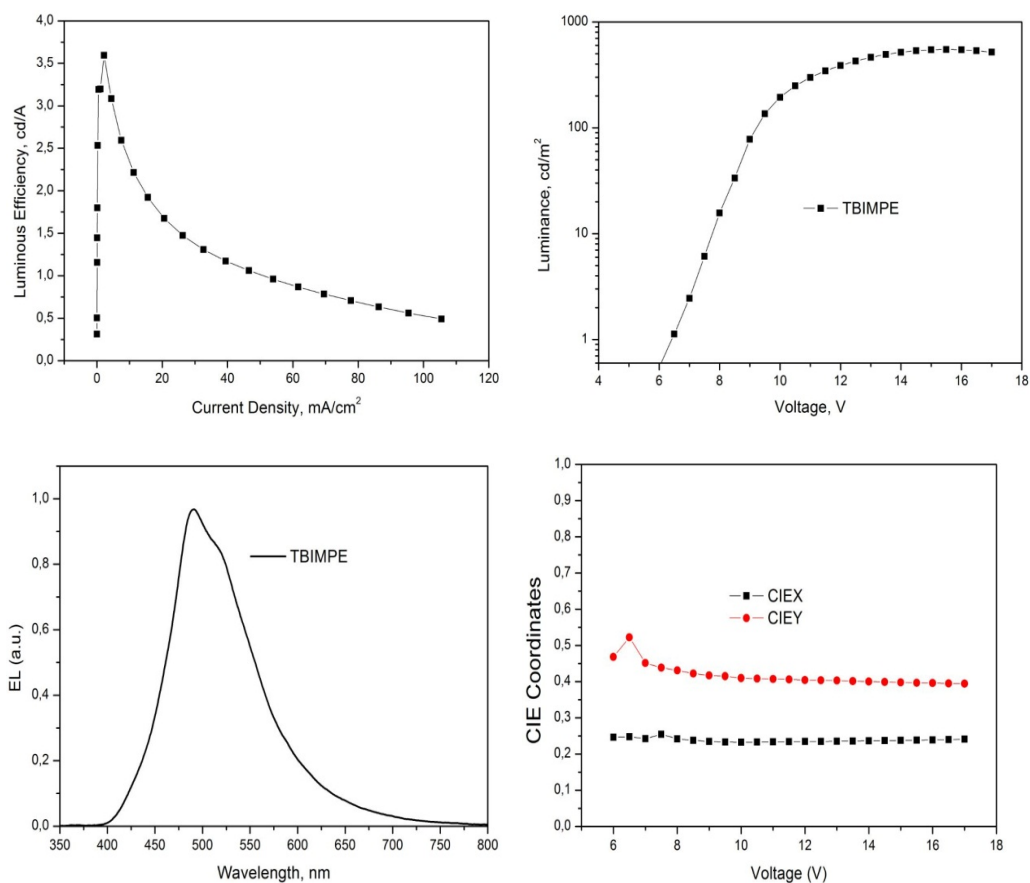


Figure 75. (Top-left) Luminous efficiency, (top-right) Luminance-voltage, (bottom left) Electroluminescence and (bottom right) Chromaticity coordinate curves of OLED device 9 using TBIMPE as a light emitting layer



Figure 76. OLED device using TBIMPE as an emitter

Device 10 was made by T5MIPE as a light emitting layer and hole and electron transport layers were used as same as device 3. T5MIPE has a structural analogy with TIPE so the methoxy group on the fifth position would determine the difference in device performances between two molecules. Figure 77 shows the results of the characterization of device 10. T5MIPE did not exhibit good results like TIPE did. The turn on voltage was same a TIPE with a value of 5V. The maximum luminance value was 700 cd m⁻² and the luminance efficiency was 0.2 cd A⁻¹ which were much lower than device 3. So, electron donating groups on the indole substituted TPE molecule had destructive effect on the device performances. The device 10 had an emission peak at around 493 nm having a blue shift compared with the device 3.

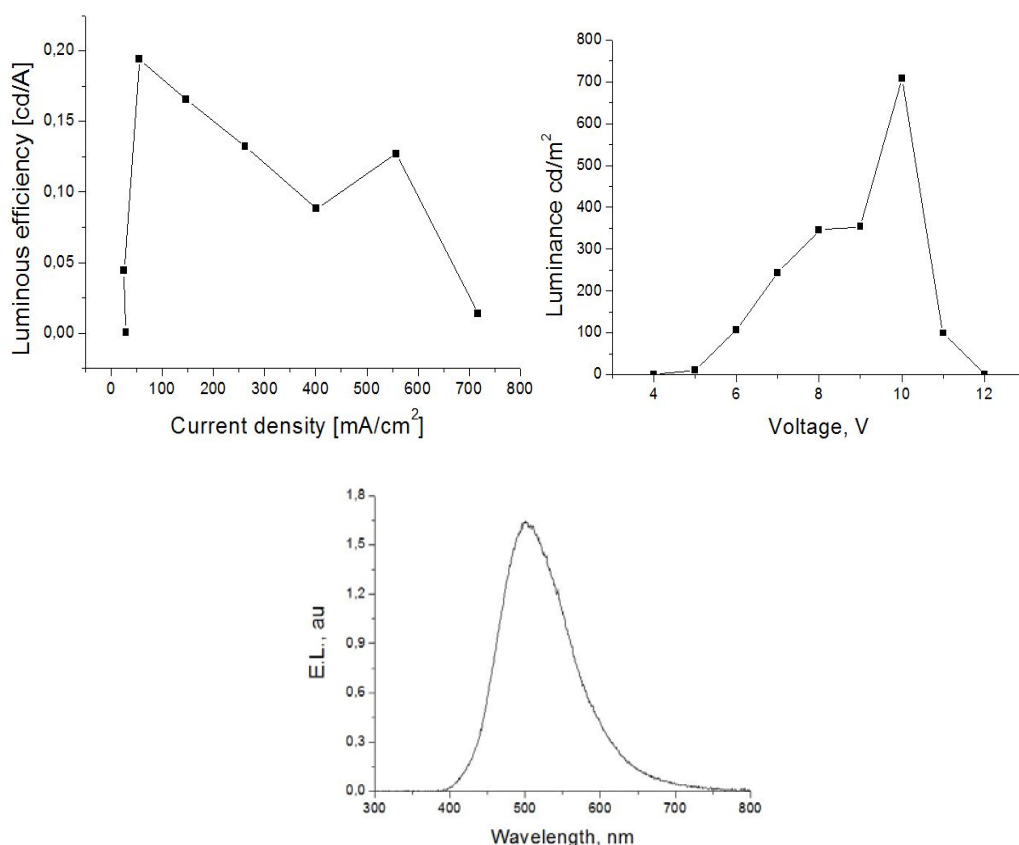


Figure 77. (Top-left) Luminous efficiency, (top-right) Luminance-voltage, (bottom left) Electroluminescence curves of OLED device 10 using T5MIPE as a light emitting layer

After all the device experiments related with the device layout 3, shown in Figure 64, we decided to add an additional electron transport layer to investigate whether this additional level could increase the device performances. 1,3,5-tris(N-phenylbenzimidazol-2-yl)benzene (TPBI) were chosen as an additional electron transport layer. TPBI has a high HOMO level so it can act also as a hole blocking layer. The device layout was shown in Figure 79. TIPE and its structural analog T5MIPE were used as a light emitting layer and the results were shown in Figure 78 and 80. According to the results using TPBI as an additional layer has constructive effect both for TIPE and T5MIPE.

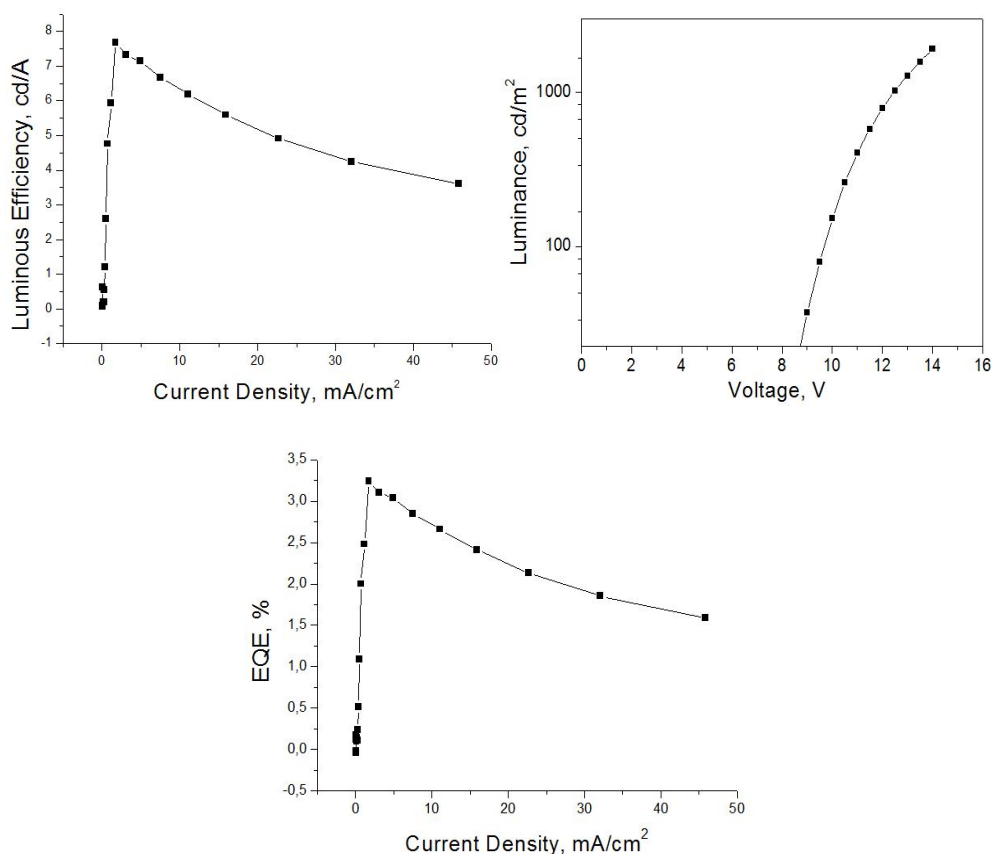


Figure 78. (Top-left) Luminous efficiency, (top-right) Luminance-voltage, (bottom) External quantum efficiency results of device 11 using TIPE as a light emitting layer

Figure 78 shows the performance results of device 11. Luminous efficiency value increased to 7.7 cd A^{-1} and external quantum efficiency enhanced to 3.2% which are quite satisfactory results for an OLED device using fluorescence small organic molecule as a light emitting layer. On the other hand the turn on voltage (9V), and the maximum luminance (2000 cd m^{-2}) values were not as most favorable as that of device 3. As mentioned before the device efficiencies were increased probably due to a better electron transfer but they were not steady and dropped very rapidly as the current densities increases.

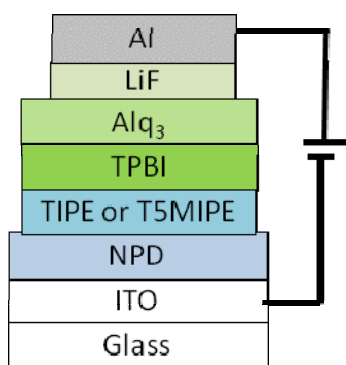


Figure 79. Device Layout 4

Figure 79 illustrated the performance results of device 12. Again a drastic increase was achieved by using TPBI and Alq₃ as a bi-layer electron transport layer. The luminous efficiency were boosted over 20 fold and reached a value of 4.7 cd A^{-1} . Moreover external quantum efficiency were increased by 10 fold and reached a value of 1,89%. Even though the luminance was increased to 1440 cd m^{-2} the increase rate is not as same as luminance efficiency and EQE values.

Finally, all the device performances were tabulated on the Table 9. According to the results the best OLED device was performed by using TIPE as an emitter and TPBI/ALq₃ as an electron transport layer.

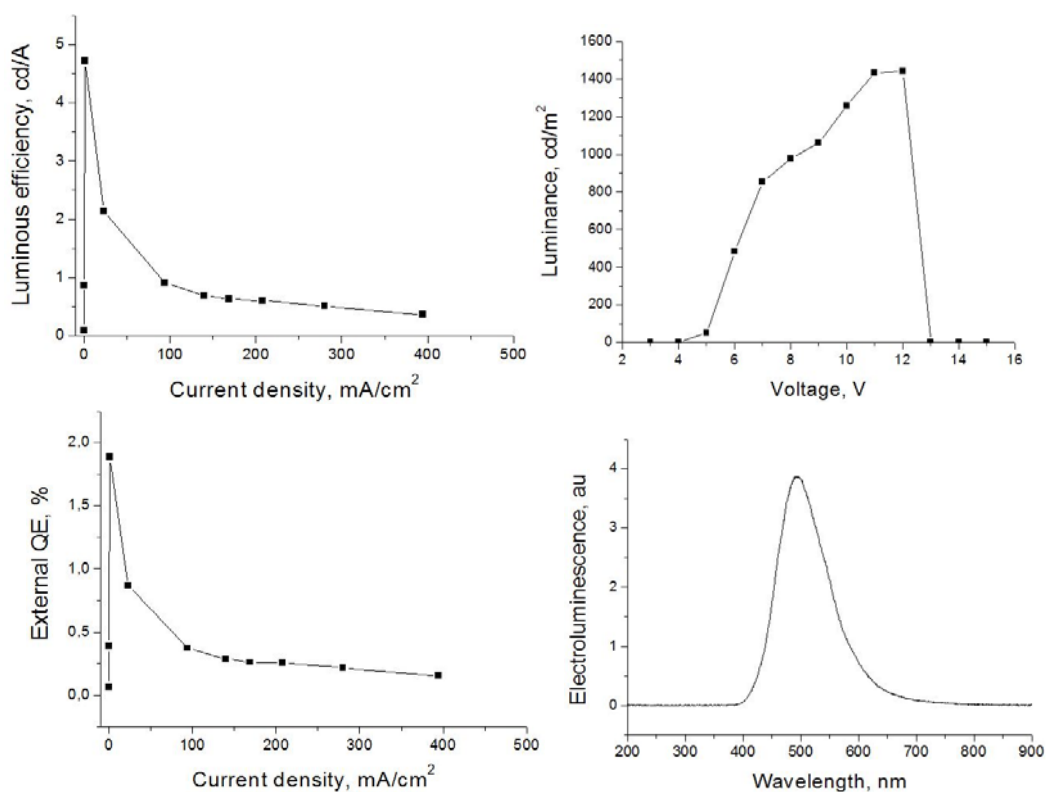


Figure 80. (Top-left) Luminous efficiency, (top-right) Luminance-voltage, (bottom left) External quantum efficiency, (bottom right) Electroluminescence curves of device 12 using T5MIPE as a light emitting layer

The performance differences between the devices 3 -11 and 10-12 showed that even though the chemistry ie. the organic molecules, are important for the high quality device performances, the device architectures are also a key factor that could enhance the device performance drastically. Moreover, OLED is a multidisciplinary technology, therefore to effectuate a high performance device, chemists, physicists and electronic engineers must work together.

Table 9. All the OLED device characterization data of the synthesized luminogens

Device No	Emitter	V _{ON} (V) ^a	L (cd m ⁻²) ^b	LE (cd A ⁻¹) ^b	EQE (%) ^b	λ _{EL} (nm) ^c
3	TIPE	5	18000	5.2	2.0	500
4	TTBCPE	5	1050	1.6	0.6	505
5	TDCPE	9	1650	0.8	0.3	508
6	TPPE	7	555	2.1	0.8	499
7	TIMPE	10	192	1.0	0.4	507
8	TPyPE	7	2627	2.2	0.8	488, 500
9	TBIMPE	6	554	3.6	1.5	490, 516 ^d
10	T5MIPE	5	700	0.2	0.2	493
11	TIPE	9	2000	7.7	3.2	500
12	T5MIPE	5	1440	4.7	1.9	500

^aTurn-on voltage at 1 cd/m², ^bMaximum values, ^cMaximum emission peak, ^dShoulder.

CHAPTER 3

EXPERIMENTAL

3.1. Materials and Methods

In this study, the structure elucidation of the compounds was done with the instruments as written.

All reactions were performed under inert atmosphere unless otherwise mentioned. All commercial reagents were used without further purification unless otherwise noted. Tetrahydrofuran was dried over metallic sodium together with benzophenone under an argon atmosphere and immediately used. All chemicals and reagents were purchased from Aldrich and Alfa Aesar and used as received.

The ^1H NMR and ^{13}C NMR spectra were recorded in CDCl_3 , DMSO and CH_2Cl_2 on a Bruker Spectrospin Avance 500 MHz spectroscopy. Chemical shifts were given in ppm downfield from tetramethylsilane. Apparent splittings were given in all cases. Infrared spectra were measured on a Perkin Elmer Instruments, One Spectrophotometer. UV-Vis spectra were measured on a Shimadzu UV-1650 PC Spectrophotometer. PL spectra were recorded on a Horiba Jobinyvon, Fluorolog. High resolution mass spectra were recorded by Bruker Daltonics MicroToF II mass spectrometer using Tunemix as an internal standard and enhanced quadratic correlation were done. Thermogravimetric analyses were carried on a Perkin Elmer Thermogravimetric Analyzer Pyris 1 TGA under nitrogen at a heating rate of $10\text{ }^\circ\text{C min}^{-1}$. Thermal transitions were studied with differential scanning calorimetry using a Perkin Elmer, Jade DSC under nitrogen at a heating rate of $10\text{ }^\circ\text{C min}^{-1}$. Cyclic voltammetry curves were taken on a Gamry Instrument 600. All the measurements were performed at room temperature using a three electrode configuration in CH_2Cl_2 with $0.1\text{ M Bu}_4\text{NPF}_6$ as supporting electrolyte. The

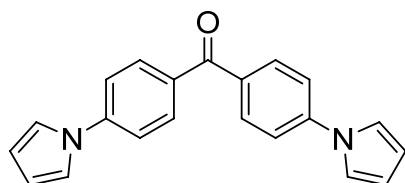
working and reference electrodes were platinum and Ag/AgCl, respectively. The reference electrode was verified using ferrocene as recommended by IUPAC. Flash column chromatography was employed using thick-walled glass columns with a flash grade silica-gel (Merck Silica Gel 60, particle size: 0.040-0.063 mm, 230-400 mesh ASTM). Reactions were monitored by thin layer chromatography using pre-coated silica gel plates (Merck Silica Gel PF-254), visualized with UV-light, KMnO₄ solution as appropriate. The relative portions of solvents are in volume to volume ratio used in column chromatography as eluent.

N,N'-Di-[(1-naphthyl)-N,N'-diphenyl]-1,1'-biphenyl)-4,4'-diamine (NPD, sublimed grade 99%) and Tris-(8-hydroxyquinoline)aluminum (Alq₃, sublimed grade, 99.995%) were acquired from Sigma Aldrich. 2,2',2''-(1,3,5-benzinetriyl)-tris(1-phenyl-1-H-benzimidazole) (TPBi, Sublimed, >99%) was purchased from Lumtec. PEDOT:PSS was purchased from Heraeus Clevios GmbH. The ITO coated glass substrates (ITO thickness 150nm, 15 ohms/sq) were determined from Visiontek Systems. The substrates were firstly etched in aqua-regia solution (3:1:3) (HCl:HNO₃:H₂O) for 2 minutes, and then cleaned consecutively in ultrasonic baths containing de-ionized water, acetone, isopropyl alcohol. Finally the substrates were dried in N₂ flow. The electroluminescence (EL) characteristics of the OLEDs were detected utilizing a Hamamatsu-Brightness Light Distribution Measurement System-C9920-11. The layer thicknesses were measured using a stylus profiler (KLA Tencor P6).

3.2. General Procedure for C-N coupling reactions

Bis(4-fluorophenyl) methanone (**24**) (9.17 mmol) and N-heterocyclic compound (**25-32**) (27.50 mmol) were dissolved in DMSO (40 mL). Cesium carbonate (36.68 mmol) was added to the solution with stirring. The suspension mixture was stirred at 70 °C for 15 h. The mixture was cooled to room temperature, and poured into ice-water (100 mL) and filtered. The crude product was purified by column chromatography on silica, eluting with dichloromethane-n-hexane (1 : 3, v/v).

3.2.1. Synthesis of bis(4-(1H-pyrrol-1-yl)phenyl)methanone (33)



85% chemical yield, as a pale white powder.

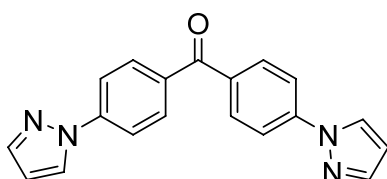
$C_{21}H_{16}N_2O$

mp: 270 °C

MS (ESI-TOF): m/z (M+H)⁺ calcd 313.13, found 313.15

¹H NMR (500 MHz, DMSO): δ ppm 7.85 (d, A part of the AB system J_{AB} =8.7 Hz, 4H), 7.82 (d, B part of the AB system J_{AB} =8.7 Hz, 4H), 7.55 (t, J =2.0 Hz, 4H), 6.35 (t, J =2.0 Hz, 4H).

3.2.2. Synthesis of bis(4-(1H-pyrazol-1-yl)phenyl)methanone (34)



80% chemical yield, as a white powder.

$C_{19}H_{14}N_4O$

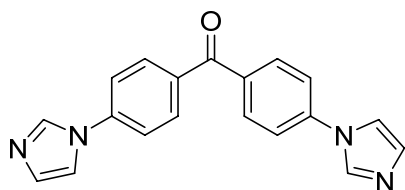
mp: 239 °C

MS (ESI-TOF): m/z (M+H)⁺ calcd 315.12, found 315.14

¹H NMR (500 MHz, DMSO): δ ppm 8.68 (d, J =2.3 Hz, 2H), 8.07 (d, A part of the AB system J_{AB} =8.6 Hz, 4H), 7.92 (d, B part of the AB system J_{AB} =8.6 Hz, 4H), 7.86 (s, 2H), 6.64 (t, J =1.6 Hz, 2H).

¹³C NMR (125 MHz, DMSO): δ ppm 194.0, 143.0, 142.5, 134.8, 131.9, 128.8, 118.4, 109.2.

3.2.3. Synthesis of bis(4-(1H-imidazol-1-yl)phenyl)methanone (35)



75% chemical yield, as a pale green powder.

$C_{19}H_{14}N_4O$

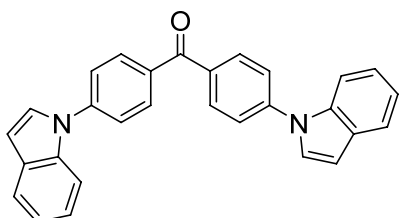
mp: 192 °C

MS (ESI-TOF): m/z (M+H)⁺ calcd 315.12, found 315.12

¹H NMR (500 MHz, CDCl₃): δ ppm 7.99 (t, $J=1.1$ Hz, 2H), 7.97 (d, A part of the AB system $J_{AB}=8.7$ Hz, 4H), 7.56 (d, B part of the AB system $J_{AB}=8.7$ Hz, 4H), 7.40 (t, $J=1.4$ Hz, 2H), 7.27 (t, $J=1.1$ Hz, 2H).

¹³C NMR (125 MHz, CDCl₃): δ ppm 193.7, 140.5, 135.9, 135.4, 132.0, 131.2, 120.7, 117.8.

3.2.4. Synthesis of bis(4-(1H-indol-1-yl)phenyl)methanone (36)



75% chemical yield, as a pale green powder.

$C_{29}H_{20}N_2O$

mp: 198 °C

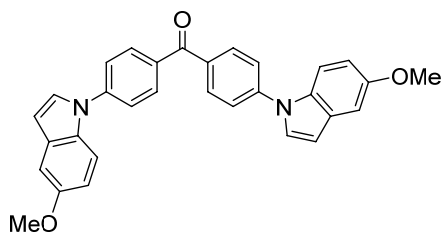
MS (ESI-TOF): m/z (M+H)⁺ calcd 413.17, found 413.16

¹H NMR (500 MHz, CDCl₃): δ ppm 8.03 (d, A part of the AB system $J_{AB}=8.5$ Hz, 4H), 7.70 (t, $J=6.9$ Hz, 4H), 7.67 (d, B part of the AB system $J_{AB}=8.5$ Hz, 4H), 7.41 (d, $J=3.3$ Hz, 2H), 7.28 (t, $J=8.0$ Hz, 2H), 7.22 (t, $J=8.0$ Hz, 2H), 6.76 (d, $J=3.3$ Hz, 2H).

¹³C NMR (125 MHz, CDCl₃): δ ppm 194.3, 143.5, 135.5, 134.9, 131.8, 129.9,

127.4, 123.3, 123.0, 121.5, 121.1, 110.6, 105.1.

3.2.5. Synthesis of bis(4-(5-methoxy-1H-indol-1-yl)phenyl)methanone (37)



85% chemical yield, as a brown powder

$C_{31}H_{24}N_2O_3$

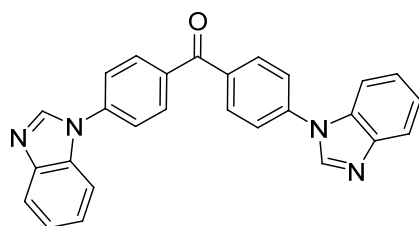
mp: 196 °C

MS (ESI-TOF): m/z (M+H)⁺ calcd 473.55, found 473.21

¹H NMR (500 MHz, CD₂Cl₂): δ ppm 8.01 (d, A part of the AB system J_{AB} =8.6 Hz, 4H), 7.67 (d, B part of the AB system J_{AB} =8.6 Hz, 4H), 7.62 (d, J =8.9 Hz, 2H), 7.44 (d, J =3.3 Hz, 2H), 7.16 (d, J =2.4 Hz, 2H), 6.92 (dd, J =8.9, 2.5 Hz, 2H), 6.68 (d, J =2.8 Hz, 2H), 3.86 (s, 6H).

¹³C NMR (125 MHz, CD₂Cl₂): δ ppm 194.3, 155.4, 143.8, 135.1, 132.1, 131.0, 130.9, 128.3, 123.1, 113.0, 111.8, 105.0, 103.3, 56.0.

3.2.6. Synthesis of bis(4-(1H-benzo[d]imidazol-1-yl)phenyl)methanone (38)



75% chemical yield, as a white powder.

$C_{27}H_{18}N_4O$

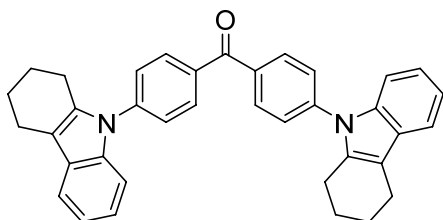
mp: 217 °C

MS (ESI-TOF): m/z (M+H)⁺ calcd 415.16, found 415.16

¹H NMR (500 MHz, CDCl₃): δ ppm 8.23 (s, 2H), 8.11 (d, A part of the AB system J_{AB} =8.5 Hz, 4H), 7.93 (dd, J =6.4, 2.1 Hz, 2H), 7.74 (d, B part of the AB system J_{AB} =8.5 Hz, 4H), 7.67 (dd, J =8.7, 1.9 Hz, 2H), 7.42 – 7.39 (m, 4H).

^{13}C NMR (125 MHz, CDCl_3): δ ppm 193.8, 144.3, 141.9, 140.1, 136.3, 133.1, 132.1, 124.3, 123.5, 123.4, 121.0, 110.5.

3.2.7. Synthesis of bis(4-(3,4-dihydro-1H-carbazol-9(2H)-yl)phenyl) methanone (**39**)



The crude product was washed with ethyl acetate 3 times (3x100 mL) to afford **39** as a pale yellow powder with an 80% chemical yield.

$\text{C}_{37}\text{H}_{32}\text{N}_2\text{O}$

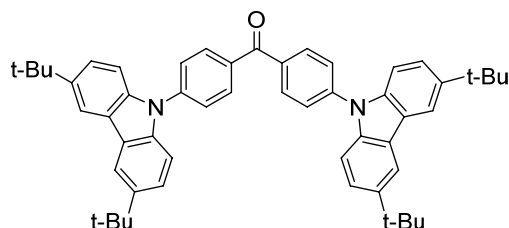
mp: 211 °C

MS (ESI-TOF): m/z ($\text{M}+\text{H}$)⁺ calcd 521.26, found 521.27

^1H NMR (500 MHz, CDCl_3): δ ppm 8.04 (d, $J=8.0$ Hz, 4H), 7.55 (d, $J=8.3$ Hz, 6H), 7.38 - 7.36 (m, 2H), 7.18 - 7.15 (m, 4H), 2.81 (bs, 4H), 2.70 (bs, 4H), 1.93 (bs, 8H).

^{13}C NMR (125 MHz, CDCl_3): δ ppm 194.7, 142.0, 136.7, 135.4, 131.3, 128.3, 126.4, 121.9, 120.3, 118.1, 112.5, 109.9, 23.6, 23.5, 23.0, 21.1 (1 signal is overlapping).

3.2.8. Synthesis of bis(4-(3,6-di-tert-butyl-9H-carbazol-9-yl)phenyl) methanone (40)



80% chemical yield, as a pale green powder
 $C_{53}H_{56}N_2O$
mp: 346 °C

MS (ESI-TOF): m/z (M)⁺ calcd 736.44, found 736.46

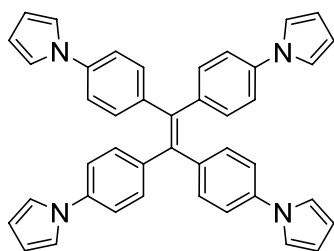
¹H NMR (500 MHz, CDCl₃): δ ppm 8.15 (d, *J*=9.6 Hz, 8H), 7.78 (d, *J*=8.1 Hz, 4H), 7.50 (bs, 8H), 1.47 (s, 36H).

¹³C NMR (125 MHz, CDCl₃): δ ppm 193.5, 143.7, 141.4, 137.6, 134.3, 130.8, 124.8, 122.9, 122.9, 115.4, 108.3, 33.8, 30.9.

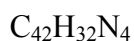
3.3. General procedure McMurry coupling reactions

Under an Ar atmosphere, a three-necked flask equipped with a magnetic stirrer was charged with zinc powder (24.25 mmol) and 30 mL freshly distilled THF. The mixture was cooled to -20 °C, and TiCl₄ (12.12 mmol) was slowly added by a syringe with the temperature kept under 0 °C. The suspending mixture was warmed to room temperature and stirred for 0.5 h, then heated at reflux for 2 h. The mixture was cooled to 0 °C, charged with pyridine (6.06 mmol) and stirred for 10 min. Compound (33-40) (4.85 mmol) in 25 mL THF was added slowly. After addition, the reaction mixture was heated at reflux until the carbonyl compound was consumed. The reaction was quenched with 10% K₂CO₃ aqueous solution and taken up with CH₂Cl₂. The organic layer was collected and dried over Na₂SO₄ and evaporation of the solvent afforded the desired product. The crude material was purified by chromatography eluting with dichloromethane–n-hexane (1 : 3, v/v)

3.3.1. Synthesis of 1,1,2,2-Tetrakis(4-(1H-pyrrol-1-yl)phenyl)ethane (41)



75% chemical yield, as a white powder.



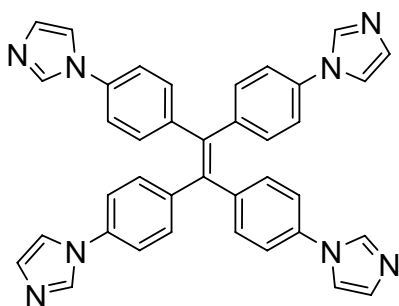
FTIR: 3433, 3027, 1606, 1519, 1328, 726.

HRMS (ESI-TOF): m/z (M+H)⁺ calcd 593.2705, found 593.2684.

¹H NMR (500 MHz, CDCl₃): δ ppm 7.18 (d, A part of the AB system J_{AB} =8.6 Hz, 8H), 7.12 (d, B part of the AB system J_{AB} =8.6 Hz, 8H), 7.05 (t, J =2.1 Hz, 8H), 6.31 (t, J =2.1 Hz, 8H).

¹³C NMR (125 MHz, CDCl₃): δ ppm 140.5, 139.5, 139.1, 132.6, 119.5, 119.0, 110.6.

3.3.2. Synthesis of 1,1,2,2-Tetrakis(4-(1H-pyrazol-1-yl)phenyl)ethane (42)



75% chemical yield, as a white powder.



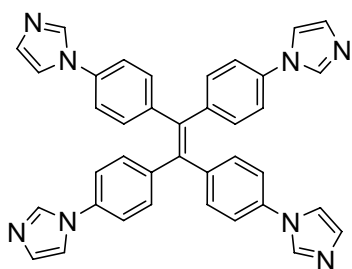
FTIR: 3410, 3107, 1605, 1520, 1396, 758.

HRMS (ESI-TOF): m/z (M+H)⁺ calcd 597.2515, found 597.2663.

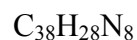
¹H NMR (500 MHz, CDCl₃): δ ppm 7.88 (d, *J*=2.5 Hz, 4H), 7.69 (d, *J*=1.7 Hz, 4H), 7.50 (d, A part of the AB system *J*_{AB}=8.6 Hz, 8H), 7.17 (d, B part of the AB system *J*_{AB}=8.6 Hz, 8H), 6.44 (t, *J*=2.1 Hz, 4H).

¹³C-NMR (125 MHz, CDCl₃): δ ppm 141.3, 141.2, 139.8, 138.7, 132.5, 126.7, 118.6, 107.7.

3.3.3. Synthesis of 1,1,2,2-Tetrakis(4-(1H-imidazol-1-yl)phenyl)ethane (43)



As an off white powder with a chemical yield 65%.



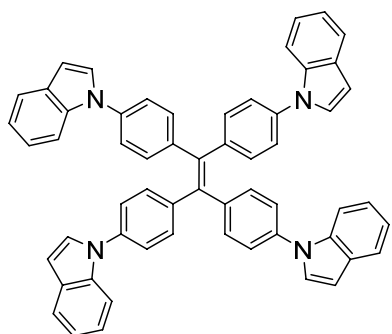
FTIR: 3367, 3111, 1606, 1520, 1304, 1056, 808.

HRMS (ESI-TOF): *m/z* (M+H)⁺ calcd 597.2515, found 597.2497.

¹H NMR (500 MHz, CDCl₃): δ ppm 7.85 (bs, 4H), 7.26 (t, *J*=1.3 Hz, 4H), 7.24 (d, A part of the AB system *J*_{AB}=8.7 Hz, 8H), 7.21 (d, B part of the AB system *J*_{AB}=8.7 Hz, 8H), 7.19 (bs, 4H).

¹³C NMR (125 MHz, CDCl₃): δ ppm 141.7, 139.8, 136.1, 135.3, 132.8, 130.7, 120.8, 117.8.

3.3.4. Synthesis of 1,1,2,2-Tetrakis(4-(1H-indol-1-yl)phenyl)ethane (44)



As an off white powder with a chemical yield 80%.



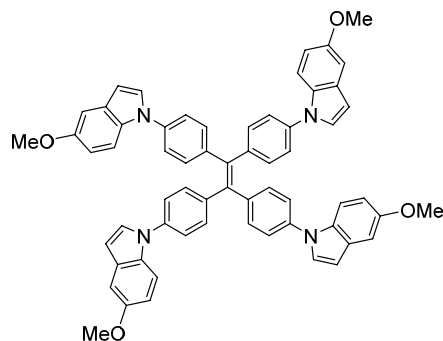
FTIR: 3334, 2924, 1602, 1333.

HRMS (ESI-TOF): m/z (M+H)⁺ calcd 793.3331, found 793.3331.

¹H NMR (500 MHz, CDCl₃): δ ppm 7.68 (d, $J=7.9$ Hz, 4H), 7.56 (d, $J=7.9$ Hz, 4H), 7.37 (d, A part of the AB system $J_{AB}=8.4$ Hz, 8H), 7.31 (d, B part of the AB system $J_{AB}=8.4$ Hz, 8H), 7.33 (d, $J=3.2$ Hz, 4H), (7.22 - 7.15 (m, 8H), 6.68 (d, $J=3.2$ Hz, 4H).

¹³C NMR (125 MHz, CDCl₃): δ ppm 141.1, 140.2, 138.5, 135.7, 132.6, 129.5, 127.7, 123.5, 122.5, 121.2, 120.5, 110.5, 103.9.

3.3.5. Synthesis of 1,1,2,2-Tetrakis(4-(5-methoxy-1H-indol-1-yl)phenyl)ethane (45)



As a white powder with a chemical yield 85%.



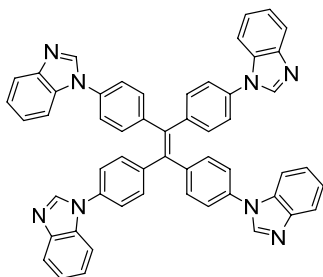
FTIR: 3434, 2829, 1604, 1513, 1258, 797.

HRMS (ESI-TOF): m/z (M+H)⁺ calcd 913.3754, found 913.3749.

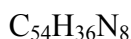
¹H NMR (500 MHz, CDCl₃): δ ppm 7.38 (d, $J=8.9$ Hz, 4H), 7.27 (d, A part of the AB system $J_{AB}=8.6$ Hz, 8H), 7.25 (d, $J=3.1$ Hz, 4H), 7.23 (d, B part of the AB system $J_{AB}=8.6$ Hz, 8H), 7.05 (d, $J=2.4$ Hz, 4H), 6.78 (dd, $J=8.9, 2.4$ Hz, 4H), 6.52 (d, $J=3.1$ Hz, 4H), 3.79 (s, 12H)

¹³C NMR (125 MHz, CDCl₃): δ ppm 154.6, 141.0, 140.2, 138.6, 132.7, 130.9, 130.1, 128.1, 123.1, 112.5, 111.3, 103.6, 102.9, 55.9.

3.3.6. Synthesis of 1,1,2,2-Tetrakis(4-(1H-benzo[d]imidazol-1-yl)phenyl)ethane (46)



As an off white powder with a chemical yield 65%.



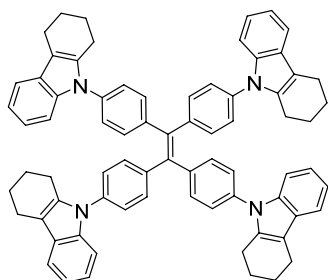
FTIR: 3409, 3063, 1604, 1513, 1293, 740.

HRMS (ESI-TOF): m/z (M+H)⁺ calcd 797.3141, found 797.3160.

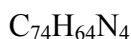
¹H NMR (500 MHz, CDCl₃): δ ppm 8.14 (s, 4H), 7.88 (dd, *J*=6.9, 1.4 Hz, 4H), 7.54 (dd, *J*=6.8, 1.4 Hz, 4H), 7.45 (dd, A part of the AB system *J*=8.6 and 2.0 Hz, 8H), 7.41 (dd, B part of the AB system *J*=8.6 and 2.0 Hz, 8H), 7.37 - 7.31 (m, 8H).

¹³C NMR (125 MHz, CDCl₃): δ ppm 144.2, 142.2, 142.0, 140.4, 135.5, 133.4, 133.01, 123.9, 123.5, 123.1, 120.9, 110.3.

3.3.7. Synthesis of 1,1,2,2-Tetrakis(4-(3,4-dihydro-1H-carbazol-9(2H)-yl)phenyl)ethane (47)



The crude material was purified by flash chromatography eluting with dichloromethane–n-hexane (1 : 1, v/v) as an off white powder with a chemical yield 65%.



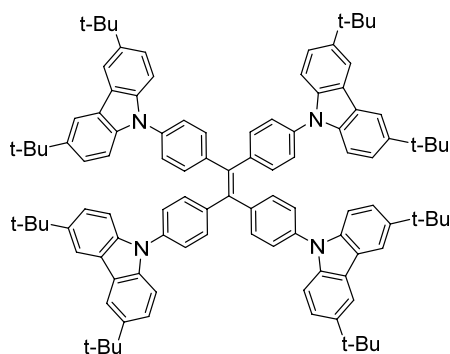
FTIR: 3435, 2926, 1603, 1512, 1458, 1376.

HRMS (ESI-TOF): m/z (M+H)⁺ calcd 1009.5204, found 1009.5167.

¹H NMR (500 MHz, CDCl₃): δ ppm 7.51 (d, *J*=7.5 Hz, 4H), 7.31 (d, A part of the AB system *J*_{AB}=8.4 Hz, 8H), 7.22 (d, B part of the AB system *J*_{AB}=8.4 Hz, 8H), 7.21 (d, *J*=6.3 Hz, 4H), 7.13 - 7.07 (m, 8H), 2.79 (t, *J*=5.3 Hz, 8H), 2.59 (t, *J*=5.3 Hz, 8H), 1.90 – 1.86 (m, 16H).

¹³C NMR (125 MHz, CDCl₃): δ ppm 141.7, 140.8, 137.0, 136.7, 135.6, 132.5, 127.8, 126.5, 121.4, 119.7, 117.8, 111.2, 109.7, 23.5, 23.3, 23.1, 21.1.

3.3.8. Synthesis of 1,1,2,2-Tetrakis(4-(3,6-di-tert-butyl-9H-carbazol-9-yl)phenyl)ethane (48)



As an off green powder with a chemical yield 65%.



FTIR: 3434, 2960, 2864, 1604, 1363.

HRMS (ESI-TOF): m/z (M+H)⁺ calcd 1441.7965, found 1441.8969.

¹H NMR (500 MHz, CDCl₃): δ ppm 8.14 (bs, 8H), 7.51– 7.47 (m, 16H), 7.40(bs, 16H), 1.45 (s, 72H).

¹³C NMR (125 MHz, CDCl₃): δ ppm 142.9, 141.6, 140.9, 139.0, 136.9, 132.8, 125.9, 123.7, 123.5, 116.2, 109.3, 34.7, 32.02.

3.4. Preparation of aggregates

In order to produce the aggregates first the synthesized luminogens were dissolved in THF to prepare a stock solution with 0.1 mM concentration. Then from this stock solution 1 mL was taken to another 10 mL flask and prepared 10 μ M solutions by adding appropriate amount of water and/or THF. The prepared samples were proceed to ultrasound treatment in order to have complete solubility and homogeneity and used immediately after preparation.

CHAPTER 4

CONCLUSION

In this work, a series of new luminogenic molecules having excellent thermal, electrochemical, optical and aggregation induced emission properties were synthesized. The target compound syntheses were performed practically in two steps without any expensive boronic acids or Pd metal catalysts. The reaction conditions applied were mild and environmentally friendly compared with ordinary coupling reactions.

The compounds emitted in the range of 496 – 525 nm gave color ranging from turquoise to light green. They had excellent thermal characteristic up to 516 °C degradation temperature and exhibited exceptional AIE properties with an increase up to 200-fold.

Non-doped OLED devices showed turquoise and light green color and exhibited maximum brightness up to 18000 cd m⁻², a maximum current efficiencies up to 7.2 cd A⁻¹, low turn-on voltages between 5.0 – 10.0 V and with external quantum efficiencies up to 3.2. Playing with the architecture of the OLED device the performances could be enhanced to upper values. Additionally, our modular synthetic methodology could permit to anchor various electron donor or withdrawing units on the TPE and especially indole moiety. Consequently, much efficient OLED devices could be made.

REFERENCES

1. Solid-State Lighting Research and Development (Multi-Year Program Plan FY'09 -FY'15), U.S. Department of Energy, **2009**.
2. CRT monitors, <http://www.pctechguide.com/crt-monitors>, last visited on December 2013
3. Keefe, T. J. "The Nature of Light" **2007**.
4. Johnson J. *Chem. Eng. News* **2007**, 85, 46.
5. <http://energy.gov/eere/energybasics/articles/lighting-basics>, last visited on December 2013.
6. EU Commission Regulation (EC) No 244/2009 of 18 March 2009: Ecodesign requirements for non-directional household lamps.
7. Tonzani S. *Nature* **2009**, 459, 312.
8. Miyata S.; Sakuratani Y.; Tao X. T. *Optical Materials* **2002**, 21, 99.
9. Naesaenen R.; Karlsson J.; Ojanpaeae H. *Displays* **2001**, 22, 107.
10. Wong M. "Flat panels drive old TVs from market" *USA Today*, **2006**.
11. Boeuf, J. P. *J. Phys. D: Appl. Phys* **2003**, 36, R5.
12. Tuilo, A. H. *C&EN*, **2001**, 19, 49.
13. Forrest, S. R. *Org. Electr.* **2003**, 4, 45.
14. Rohatgi, K. K. *Fundamentals of photochemistry* **1980**, New age international (P) limited, New Delhi, India.
15. Skoog, F.; Holler, J.; Nieman, T. A. *Principles of Instrumental Analysis* 5th ed, **1997**, Thomson Brooks/Cole.

16. Oxtoby, D. W. *Annu. Rev. Phys. Chem.* **1981**, *32*, 77.
17. Lakowicz, J. R. *Principles of Fluorescence Spectroscopy* **2007**, Springer.
18. Round, H. J. *Electron World* **1907**, *19*, 309.
19. Holonyak, N.; Bevacqua, S. F. Jr. *Appl. Phys. Lett.* **1962**, *1*, 82.
20. Perry, T. S. *IEEE Spectrum* **2003**, *40*, 11.
21. Bernanose, A.; Comte, M.; Vouaux, P. *J. Chim. Phys.* **1953**, *50*, 64.
22. Bernanose, A. *J. Chim. Phys.* **1955**, *52*, 396.
23. Kallmann, H.; Pope, M. *Nature* **1960**, *186*, 31.
24. Pope, M.; Kallmann, H. P.; Magnante, P. *J. Chem. Phys.* **1963**, *38*, 2042.
25. Helfrich, W.; Schneider, W. G. *Phys. Rev. Lett.* **1965**, *14*, 229.
26. Partridge, R. H. Radiation Sources, U.S. Patent 3,995,299, **1976**.
27. Dresner, J. *RCA Rev.* **1969**, *30*, 322.
28. Williams, D. F.; Schadt, M. *J. Chem. Phys.* **1970**, *53*, 3480.
29. Vincett, P. S., Barlow, W. A.; Hann, R. A. Roberts, G. G. *Thin Solid Films* **1982**, *94*, 171.
30. Tang, C. W.; VanSlyke, S. A. *Appl. Phys. Lett.* **1987**, *51*, 913.
31. Burroughes, J. H.; Bradley, D. D. C.; Brown, A. R.; Marks, R. N.; Mackay, K.; Friend, R. H.; Burns, P. L.; Holmes, A. B. *Nature* **1990**, *347*, 539.
32. Baldo, M. A.; O'Brien, D. F.; You, Y.; Shoustikov, A.; Sibley, S.; Thompson, M. E.; Forrest, S. R. *Nature* **1998**, *395*, 151.
33. Adachi, C.; Baldo, M. A.; Thompson, M. E.; Forrest, S. R.; *J. Appl. Phys.* **2001**, *90*, 5048.
34. Allen, K. J. *Proc. IEEE* **2005**, *93*, 1394.

35. Tang, C. W.; Vanslyke, S. A.; Chen, C. H.; *J. Appl. Phys.* **1989**, *65*, 3610.
36. Friend, R. H.; Gymer, R. W.; Holmes, A. B.; Burroughes, J. H.; Marks, R. N.; Taliani, C.; Bradley, D. D. C.; Dos Santos, D. A.; Brédas, J. L.; Logdlund, M.; Salaneck, W. R. *Nature* **1999**, *397*, 121.
37. Dimitrakopoulos, C. D.; Malenfant, P. R. L. *Adv. Mater.* **2002**, *2*, 99.
38. Singh, T. B.; Sariciftci, N. S. *Annu. Rev. Mater. Res.* **2006**, *36*, 199.
39. Peumans, P.; Yakimov, A.; Forrest, S. R. *J. Appl. Phys.* **2003**, *7*, 3693.
40. Forrest, S. R. *Nature* **2004**, *428*, 911.
41. Newman, C. R.; Frisbie, C. D.; da Silva, D. A.; Bredas, J. L.; Ewbank, P. C.; Mann, K. R. *Chem. Mater.* **2004**, *23*, 4436.
42. The 2000 Nobel Prize for Chemistry, Retrieved November 2013 from <http://www.nobel.se/chemistry/laureates/2000/public.html>.
43. Shirakawa, H. *Angew. Chem. Int. Ed.* **2001**, *40*, 2574.
44. MacDiarmid, A. G. *Angew. Chem. Int. Ed.* **2001**, *40*, 2581.
45. Heeger, A. J. *Angew. Chem. Int. Ed.* **2001**, *40*, 2591.
46. Brütting, W. *Physics of Organic Semiconductors*, Wiley-VCH Verlag, Weinheim **2005**.
47. Kelley, T. W.; Baude, P. F.; Gerlach, C.; Ender, D. E.; Muires, D.; Haase, M. A. D.; Vogel, E.; Theiss, S. D. *Chem. Mater.* **2004**, *16*, 4413.
48. Shaw, J. M.; Seidler, P. F. *IBM J. Res. & Dev.* **2001**, *1*, 3
49. Forrest, S. R.; Thompson, M. E. *Chem. Rev.* **2007**, *107*, 923.
50. Berggren, M.; Nilsson, D.; Robinson, N. D. *Nature Materials* **2007**, *6*, 3.
51. Klauk, H. *Organic Electronics: Materials, Manufacturing and Applications* **2006**, Wiley

52. Kafafi, Z. H. Organic light-emitting materials and devices **1997**, 314, SPIE Proceeding series.
53. Bässler, H. *Phys. Stat. Sol. (B)* **1981**, 107, 9.
54. Bässler, H. *Phys. Stat. Sol. (B)* **1993**, 175, 15.
55. Schmechel, R.; von Seggern, H. *Phys. Stat. Sol. (A)* **2004**, 201, 1215.
56. Godlewski, J.; Obarowska, M. *Opto-Electron. Rev.* **2007**, 15, 179.
57. Bardsley, J. N. *IEEE J. Sel. Top. Quantum Electron.* **2004**, 10, 3.
58. <http://www.udcoled.com/default.asp?contentID=604>, last visited on December 2013.
59. Sugiyama, K.; Ishii, H.; Ouchi, Y.; Seki, K. *J. App. Phys.* **2000**, 87, 295.
60. Burrows, P. E.; Bulovic, V.; Forrest, S. R.; Sapochak, L. S.; McCarty, D. M.; Thompson, M. E. *Appl. Phys. Lett.* **1994**, 65, 2922.
61. Pattison, L. Solid State Lighting Services, Inc. DOE Market Introduction Workshop **2011**, Seattle, WA.
62. Van Slyke, S. A.; Chen, C. H.; Tang, C. W. *Appl. Phys. Lett.* **1996**, 69, 2160.
63. Nagamoto, T.; Maruta, Y.; Omoto, O. *Thin Solid Films* **1990**, 192, 17.
64. Elliott, C. M.; Bloom, C. J. "New OLED Cathode Materials with Tailored Low Work Function" **2008**, Patent number: 7,414,359.
65. Niu, L.; Guan, Y. *Phys. Status Solidi A* **2010**, 207, 993.
66. Peyghambarian, N.; Norwood, R. A. *Opt. Photonics News* **2005**, 16, 28.
67. Adachi, C.; Nagai, K.; Tamoto, N. *Appl. Phys. Lett.* **1995**, 66, 2679.
68. Shirota, Y.; Okumoto K. *Proc. SPIE* **2001**, 4105, 158.
69. Zhi-lin, Z.; Xue-yin, J.; Shao-hong, X.; Nagatomo, T.; Omoto, O. *Chinese Phys. Lett.* **1997**, 14, 302.

70. Kulkarni, A. P.; Tonzola, C. J.; Babel, A.; Jenekhe, S. A. *Chem. Mater.* **2004**, *16*, 4556.
71. Chen, C. H.; Shi, J. *Coord. Chem. Rev.* **1998**, *171*, 161.
72. Kido, J.; Ohtaki, C.; Hongawa, K.; Okuyama, K.; Nagai, K. *Jpn. J. Appl. Phys.* **1993**, *32*, L917.
73. Bettenhausen, J.; Greczmiel, M.; Jandke, M.; Strohriegl, P. *Synth. Metals* **1997**, *91*, 223.
74. Salleh, M. M.; Aziz, T. H. T.; Sepeai, S.; Yahaya, M. *MIPA* **2007**, *17*, 9.
75. Chwang, A. B.; Rothman, M. A.; Mao, S. Y.; Hewitt, R. H.; Weaver, M. S.; Silvernail, J. A.; Rajan, K.; Hack, M.; Brown, J. J.; Chu, X.; Moro, L.; Krajewski, T.; Rutherford, N. *Appl. Phys. Lett.* **2003**, *83*, 413.
76. Bröms, P.; Birgersson, J.; Johansson, N.; Lögdlund, M.; Salaneck, W.; *Synth. Metals* **1995**, *74*, 179.
77. Tsujimura, T. *OLED Displays Fundamentals and Applications* **2012**, John Wiley & Sons, Inc.
78. Mueller, C. D.; Falcou, A.; Reckefuss, N.; Rojahn, M.; Wiederhirn, V.; Rudati, P.; Frohne, H.; Nuyken, O.; Becker, H.; Meerholz, K. *Nature* **2003**, *421*, 829.
79. Shinar J. ed., *Organic Light-Emitting Devices: A Survey* **2003**, Springer.
80. Gather, M. C.; Köhnen, A.; Meerholz, K. *Adv. Mater.* **2011**, *23*, 233.
81. Dakin, J. P.; Brown, R. G. W. *Handbook of Optoelectronics* **2006**, Taylor and Francis.
82. Zardareh, S. Z.; Boroumand, F. A. *World Academy of Science, Engineering and Technology* **2009**, *38*, 278.
83. Forrest, S. R.; Bradley, D. D. C.; Thompson, M. E. *Adv. Mater.* **2003**, *15*, 1043.
84. Duggal, A. R.; Shiang, J. J.; Heller, C. M.; Foust, D. F. *Appl. Phys. Lett.* **2002**, *80*, 3470.

85. Komoda, T.; Ide, N.; Kido, J. *Light Vis. Environ.* **2008**, *32*, 75.
86. D'Andrade, B. W.; Forrest, S. R. *Adv. Mater.* **2004**, *16*, 1585.
87. Forrest, S. R. *Nature* **2004**, *428*, 911.
88. Schubert, E. F.; Kim, J. K. *Science* **2005**, *308*, 1274.
89. Huber, G.; Kränkel, C.; Petermann, K. *J. Opt. Soc. of Am. B: Optical Physics* **2010**, *27*, B93.
90. Zissis, G.; Kitsinelis, S. *J. Phys. D: App. Phys.* **2009**, *42*, 1.
91. Kang, B.; Ceder, G. *Nature* **2009**, *458*, 190.
92. Norby, T. *Solid State Ionics* **1999**, *125*, 1.
93. Grätzel, M. *Nature* **2001**, *414*, 338.
94. Ulbricht, C.; Beyer, B.; Friebe, C.; Winter, A. U. S. Schubert, *Adv. Mater.* **2009**, *21*, 4418.
95. Kamtekar, K. T.; Monkman, A. P.; Bryce, M. R. *Adv. Mater.* **2010**, *22*, 572.
96. Ulrich, G.; Ziessel, R.; Harriman, A. *Angew. Chem. Inter. Ed.* **2008**, *47*, 1184.
97. Kirchmeyer, S.; Reuter, K. *J. Mater. Chem.* **2005**, *15*, 2077.
98. Slavík, J. *Fluorescence Microscopy and Fluorescent Probes*, Plenum **1996**, New York.
99. Valeur, B. *Molecular Fluorescence: Principle and Applications* **2002**, Wiley-VCH, Weinheim
100. Geddes, C. D.; Lakopwicz, J. R.; *Advanced Concepts in Fluorescence Sensing* 2005, Springer, Norwell
101. Thompson, R. B.; *Fluorescence Sensors and Biosensors* 2006, CRC, Boca Raton.

102. Tan, W. H.; Wang, K. M.; Drake, T. J. *Curr. Opin. Chem. Biol.* **2004**, *8*, 547.
103. Förster, T.; Kasper, K. *Z. Phys. Chem.* **1954**, *1*, 275.
104. Malkin, J. *Photophysical and Photochemical Properties of Aromatic Compounds* **1992**, CRC, Boca Raton.
105. Birks, J. B. *Photophysics of Aromatic Molecules* **1970**, Wiley, London.
106. Hong, Y.; Lam, J. W. Y.; Tang, B. Z. *Chem. Commun.* **2009**, 4332.
107. Wang, J.; Zhao, Y.; Dou, Y. C.; Sun, H.; Xu, P.; Ye, K.; Zhang, J.; Jiang, S.; Li, F.; Wang, Y. *J. Phys. Chem. B* **2007**, *111*, 50.
108. Wu, C. W.; Tsai, C. M.; Lin, H. C. *Macromolecules* **2006**, *39*, 4298.
109. Luo, J.; Xie, Z.; Lam, J. W. Y.; Cheng, L.; Chen, H.; Qiu, C.; Kwok, H. S.; Zhan, X.; Liu, Y.; Zhu, D.; Tang, B. Z. *Chem. Commun.* **2001**, 1740.
110. Tang, B. Z.; Zhan, X.; Yu, G.; Lee, P. P. S.; Liu, Y.; Zhu, D. *J. Mater. Chem.* **2001**, *11*, 2974.
111. Li, K.; Qin, W.; Ding, D.; Tomczak, N.; Geng, J.; Liu, R.; Liu, J.; Zhang, X.; Liu, H.; Liu, B.; Tang, B. Z. *Scientific Reports* **2012**, *3*, 1.
112. Liu, Y.; Tao, X.; Wang, F.; Dang, X.; Zou, D.; Ren, Y.; Jiang, M.; *J. Phys. Chem. C* **2008**, *112*, 3975.
113. Qian, G.; Dai, B.; Luo, M.; Yu, D.; Zhan, J.; Zhang, Z.; Dongge, M.; Wang, Z. Y. *Chem. of Mater.* **2008**, *20*, 6208.
114. Li, H.; Zhang, X.; Chi, Z.; Xu, B.; Zhou, W.; Liu, S.; Zhang, Y.; Xu, J. *Org. Lett.* **2011**, *4*, 556.
115. Wang, M.; Gu, X.; Zhang, G.; Zhang, D.; Zhu, D. *Anal. Chem.* **2009**, *11*, 4444.
116. Tang, B. Z.; Qin, A. *Aggregation-Induced Emission: Applications* **2013**, Wiley.

117. Tseng, N. W.; Liu, J.; Ng, J. C. Y.; Lam, J. W. Y.; Sung, H. H. Y.; Williams, I. D.; Tang, B. Z. *Chem. Sci.* **2012**, *3*, 49.
118. Shustova, N. B.; Ong, Ta-C.; Cozzolino, A. F.; Michaelis, V. K.; Griffin, R. G.; Dinca, M. *J. Am. Chem. Soc.* **2012**, *134*, 15061.
119. Chen, J.; Law, C. C. W.; Lam, J. W. Y.; Dong, Y.; Lo, S. M. F.; Williams, I. D.; Zhu, D.; Tang, B. Z. *Chem. Mater.* **2003**, *15*, 1535.
120. Rathore, R.; Lindeman, S. V.; Kumar, A. S.; Kochi, J. K. *J. Am. Chem. Soc.* **1998**, *24*, 6012.
121. Hong, Y.; Lam, J. W. Y.; Tang, B. Z. *Chem. Soc. Rev.* **2011**, *40*, 5361.
122. de Boissieu, *Bull. Soc. Chim.* **1888**, *49*, 691.
123. Zhao, Z.; Chan, Y. K. C.; Chen, S. Deng, C.; Lam, J. W. Y.; Jim, C. K. W.; Hong, Y.; Lu, P.; Chang, Z.; Chen, X.; Lu, P.; Kwok, H. S.; Qiu H.; Tang, B. Z. *J. Mater. Chem.* **2012**, *22*, 4527.
124. Hu, R.; Maldonado, J. L.; Rodriguez M.; Deng, C.; Jim, C. K. W.; Lam, J. W. Y.; Yuen, M. M. F.; Ortiz, G. R.; Tang, B. Z. *J. Mater. Chem.* **2012**, *22*, 232.
125. Wang, W.; Lin, T.; Wang, M.; Liu, T.-X.; Ren, L.; Chen, D.; Huang, S. *J. Phys. Chem. B* **2010**, *114*, 5983.
126. Okuma, K.; Kojima, K.; Oyama, K.; Kubo, K.; Shioji, K. *Eur. J. Org. Chem.* **2004**, 820
127. Okuma, K.; Koda, G.; Okumura, S.; Ohno, A. *Chem. Lett.* **1996**, 609.
128. Okuma, K.; Kojima, K.; Ohta, H. *Phosphorus, Sulfur, Silicon Relat. Elem.* **1993**, *80*, 259.
129. McMurry, J. E.; Fleming, M. P. *Chem. Rev.* **1989**, *89*, 1513.
130. Schultz, A.; Diele, S.; Laschat, S.; Nimitz, M. *Adv. Funct. Mater.* **2001**, *11*, 441.
131. Duan, X. F.; Zeng, J.; Lu, J. W.; Zhang, Z. B. *Synthesis*, **2007**, *5*, 713.

132. Schreivogel, A.; Maurer, J.; Winter, R.; Baro, A.; Laschat, S. *Eur. J. Org. Chem.* **2006**, 3395.
133. Zhao, Z.; Lam, J. W. Y.; Tang, B. Z. *J. Mater. Chem.* **2012**, *22*, 23726.
134. Baglan, M.; Atilgan, S. *Chem. Comm.* **2013**, *46*, 5325.
135. Qin, A.; Lam, J. W. Y.; Tang, B. Z. *Prog. in Poly. Sci.* **2012**, *1*, 182.
136. Shen, X. Y.; Wang, Y. J.; Zhao, E.; Yuan, W. Z.; Liu, Y.; Lu, P.; Qin, A.; Ma, Y.; Sun, J. Z.; Tang, B. Z. *J. Phys. Chem. C* **2013**, *14*, 7334.
137. Wang, J.; Mei, J.; Zhao, E.; Song, Z.; Qin, A.; Sun, J. Z.; B. Z. Tang, *Macromolecules* **2012**, *45*, 7692.
138. Zhao, Z.; Geng, J.; Chang, Z.; Chen, S.; Deng, C.; Jiang, T.; Qin, W.; Lam, J. W. Y.; Kwok, H. S.; Qiu, H.; Liu B.; Tang, B. Z. *J. Mater. Chem.* **2012**, *22*, 11018.
139. Zhao, Z.; Chen, S.; Deng, C.; Lam, J. W. Y.; Chan, C. Y. K.; Lu, P.; Wang, Z.; Hu, B.; Chen, X.; Lu, P.; Kwok, H. S.; Ma, Y.; Qiu, H.; Tang, B. Z. *J. Mater. Chem.* **2011**, *21*, 10949.
140. Zhao, Z.; Deng, C.; Chen, S.; Lam, J. W. Y.; Qin, W.; Lu, P.; Wang, Z.; Kwok, H. S.; Ma, Y.; Qiu, H.; Tang, B. Z. *Chem. Commun.* **2011**, *47*, 8847.
141. Liu, Y.; Chen, S.; Lam, J. W. Y.; Lu, P.; Kwok, R. T. K.; Mahtab, F.; Kwok, H. S.; B. Z. Tang, *Chem. Mater.* **2011**, *23*, 2536.
142. Liu, Y.; Chen, S.; Lam, J. W. Y.; Mahtab, F.; Kwok, H. S.; Tang, B. Z. *J. Mater. Chem.* **2012**, *22*, 5184.
143. Deng, C.; Tang, L.; Qin, A.; Hu, R.; Sun, J. Z.; Tang, B. Z. *J. Am. Chem. Soc.* **2011**, *133*, 660.
144. Liu, L.; Zhang, G.; Xiang, J.; Zhang, D.; Zhu, D.; *Org. Lett.* **2008**, *20*, 4581.
145. Wang, M.; Zhang, G.; Zhang, D.; Zhu, D. B. Z. Tang, *J. Mater. Chem.* **2010**, *20*, 1858.
146. Yuan, W. Z.; Gong, Y.; Chen, S.; Shen, X. Y.; Lam, J. W. Y.; Lu, P.; Lu, Y.; Wang, Z.; Hu, R.; Xie, N.; Kwok, H. S.; Zhang, Y.; Sun, J. Z.; Tang, B. Z. *Chem. Mater.* **2012**, *24*, 1518.

147. Shi, H.; Kwok, R. T. K.; Liu, J.; Xing, B.; Tang, B. Z.; Liu, B. *J. Am. Chem. Soc.* **2012**, *134*, 17972.
148. Yang, X.; Shen, B.; Jiang, Y.; Zhao, Z.; Wang, C.; Ma, C.; Yang, B.; Lin, Q. *J. Mater. Chem. A* **2013**, *1*, 1201.
149. Miyaura, N.; Suzuki, A. *Chem. Rev.* **1995**, *95*, 2457.
150. Chincilla, C.; Nájera, C. *Chem. Rev.* **2007**, *107*, 874.
151. The price comparison was done according to Sigma – Aldrich web results, August **2013**.
152. Li, Z.; Chen, Y.; Lv, X.; Fu, W. F. *New J. Chem.* **2013**, *37*, 3755.
153. Zhang, X.; Liu, M.; Yang, B.; Zhang, X.; Wei, Y. *Colloids and Surfaces B: Biointerfaces* **2013**, *112*, 81.
154. Lee, H.; Park, H. W.; Chang, J. Y. *Macromol. Res.* **2013**, *11*, 1274.
155. Huang, J.; Yang, X.; Wang, J.; Zhong, C.; Wang, L.; Qin, J.; Li, Z. *J. Mater. Chem.*, **2012**, *22*, 2478.
156. Li, H.; Chi, Z.; Xu, B.; Zhang, X.; Li, X.; Liu, S.; Zhang, Y.; Xu, J. *J. Mater. Chem.* **2011**, *11*, 3760.
157. Li, Q.; Yu, S.; Li, Z.; Qin, J. *J. Phys. Org. Chem.* **2009**, *22*, 241.
158. Song, P.; Chen, X.; Xiang, Y. Huang, L.; Zhou, Z.; Wei, R.; Tong, A. *J. Mater. Chem.* **2011**, *21*, 13470.
159. Asselin, A. A.; Humber, T L.G.; Dobson, A.; Komlossy, J. *J. Med. Chem.* **1976**, *19*, 787.
160. Scott, K. R.; Alt, C. J.; Kemp, M.; Hayes, E.; Telang, V. G.; *J. Pharm. Sci.* **1984**, *73*, 1531.
161. Giancaspro, G. I.; Pizzorno, M. T.; Albonico, S. M.; Bindstein, E.; Garofalo, A. R. *Zeichen, Farmaco* **1989**, *44*, 483.

162. Debray, J.; Zeghida, W.; Baldeyrou, B.; Mahieu, C.; Lansiaux, A.; Demeunynck, M. *Bioorg. Med. Chem. Lett.* **2010**, *20*, 4244.
163. Hui, X.; Ling-ling, F. *Eur. J. Med. Chem.* **2011**, *46*, 364.
164. Gopalakrishnan, A.; Shanmugasundaram, A.; Tae, J. Y. *Bioorg. Med. Chem. Lett.* **2010**, *20*, 2242.
165. Galli, C. *Org. Prep. Proced. Int.* **1992**, *24*, 287.
166. Gong, J. R. Wan, L. J.; Lei, S. B.; Bai, C. L.; Zhang, X. H.; Lee, S. T. *J Phys Chem B.* **2005**, *109*, 1675.
167. Kim, S. Y.; Kim, K. Y.; Tak, Y. H.; Lee, J. L. *Appl. Phys. Lett.* **2006**, *89*, 132108.
168. So, F.; Kondakov, D. *Adv. Mater.* **2010**, *22*, 3762.
169. Zhang, X.; Chi, Z.; Xu, B.; Li, H.; Yang, Z.; Li, X.; Liu, S.; Zhang, Y.; Xu, J. *Dyes and Pigments* **2011**, *89*, 56.
170. Mie, G. *Ann. Physik* **1908**, *25*, 429
171. Lechner, M. *J. Serbian Chem. Soc.* **2005**, *70*, 361.
172. Dong, S.; Li, Z.; Qin, J. *J. Phy. Chem. B* **2009**, *113*, 434.
173. Yang, Z.; Chi, Z.; Yu, T.; Zhang, X.; Chen, M.; Xu, B.; Liu, S.; Zhang, Y.; Xu, J. *J. Mater. Chem.* **2009**, *19*, 5541.
174. Ning, Z.; Chen, Z.; Zhang, Q.; Yan, Y.; Qian, S.; Cao, Y.; Tian, H. *Adv. Funct. Mater.* **2007**, *17*, 3799.
175. Zhang, X.; Chi, Z.; Li, H.; Xu, B.; Li, X.; Liu, S.; Zhang, Y.; Xu, J. *J. Mater. Chem.* **2011**, *21*, 1788.

APPENDIX

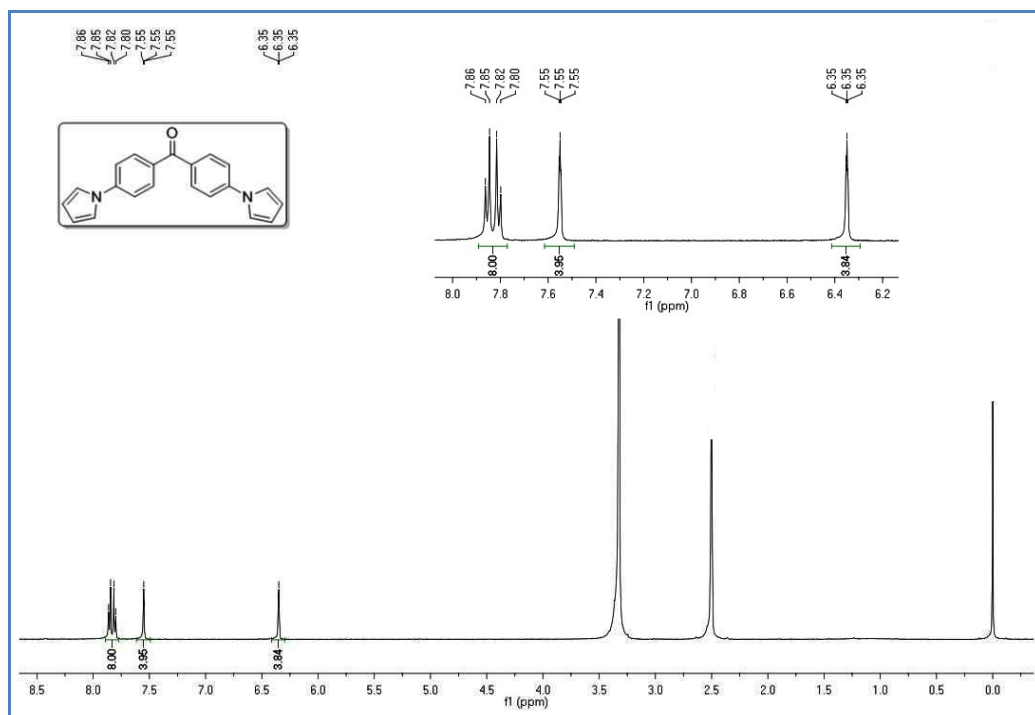


Figure A 1. ^1H NMR spectrum of compound **33**

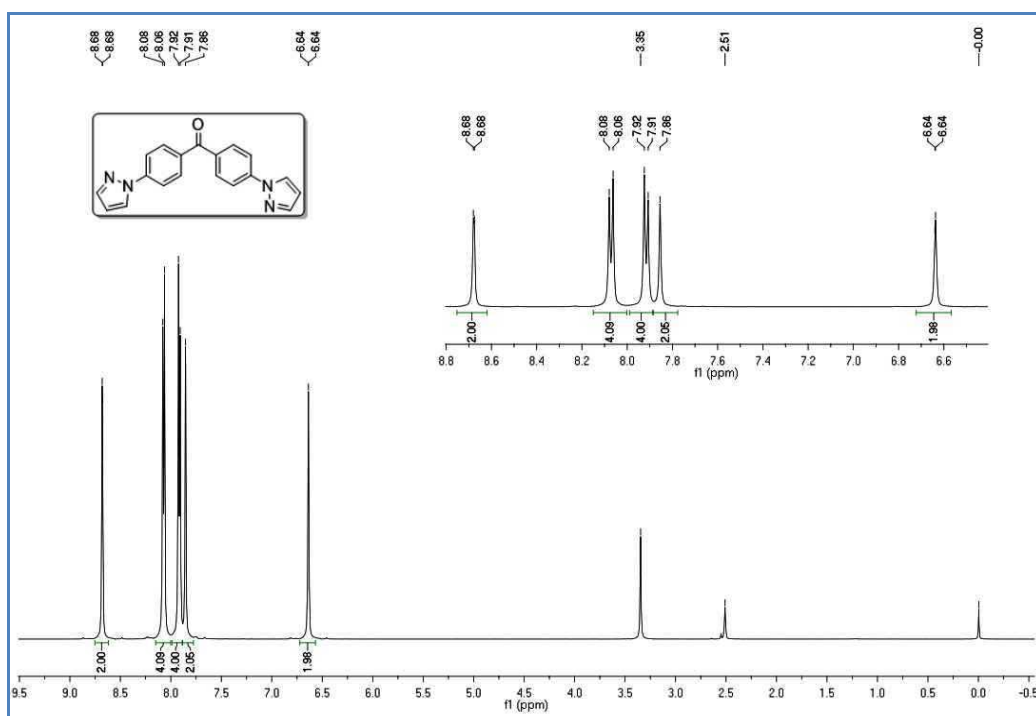


Figure A 2. ¹H NMR spectrum of compound 34

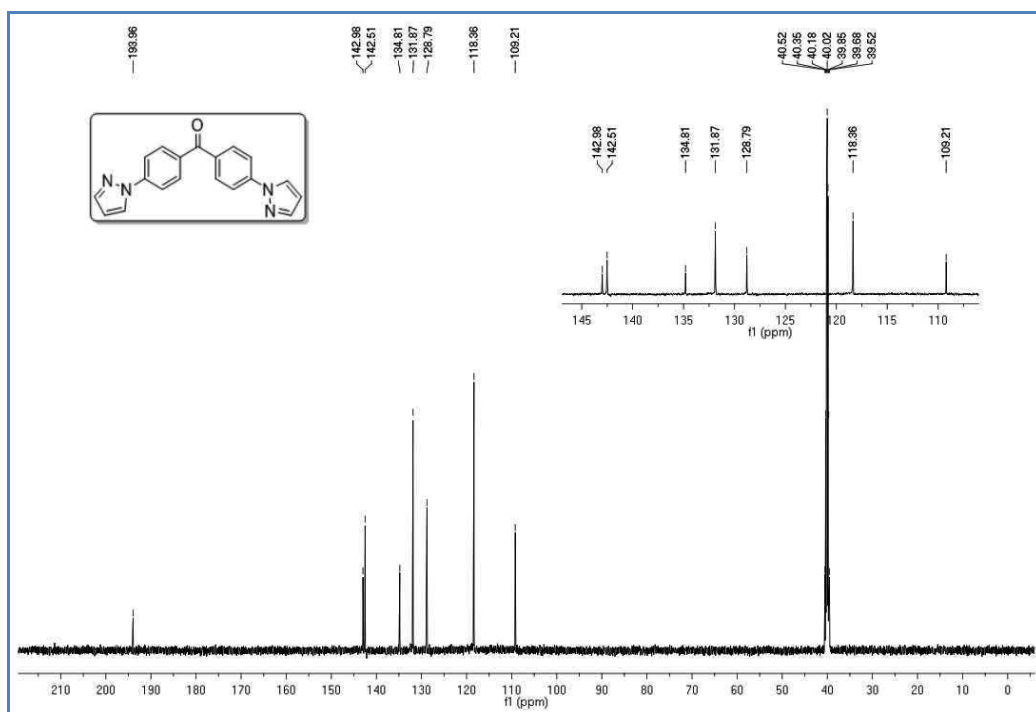


Figure A 3. ¹³C NMR spectrum of compound 34

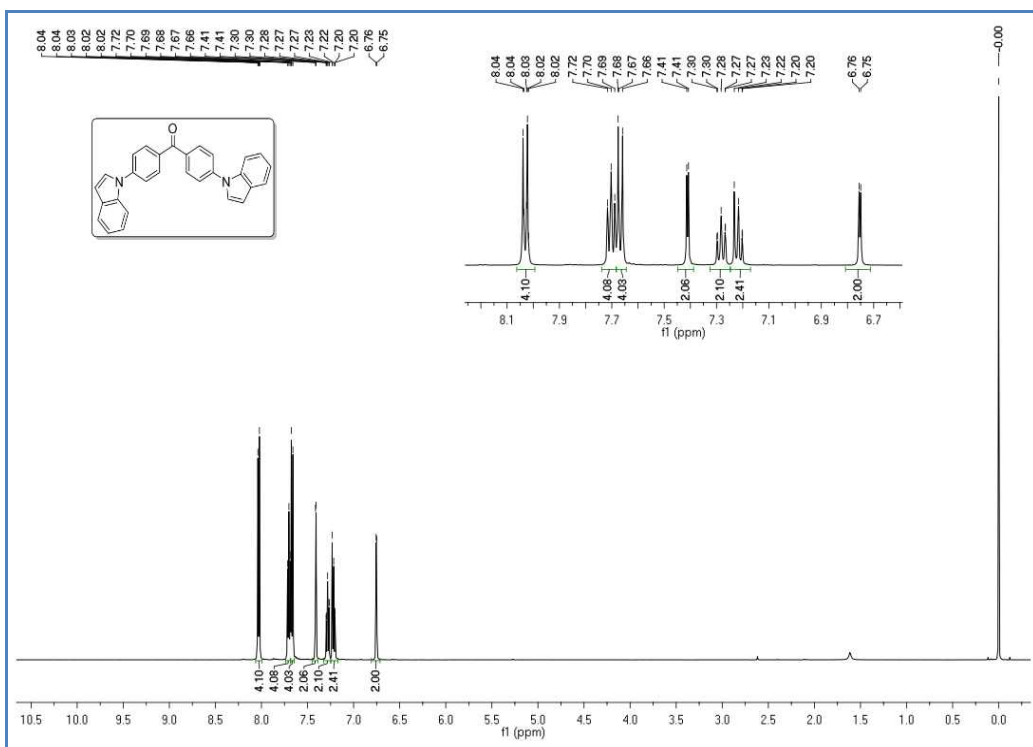


Figure A 6. ¹H NMR spectrum of compound 36

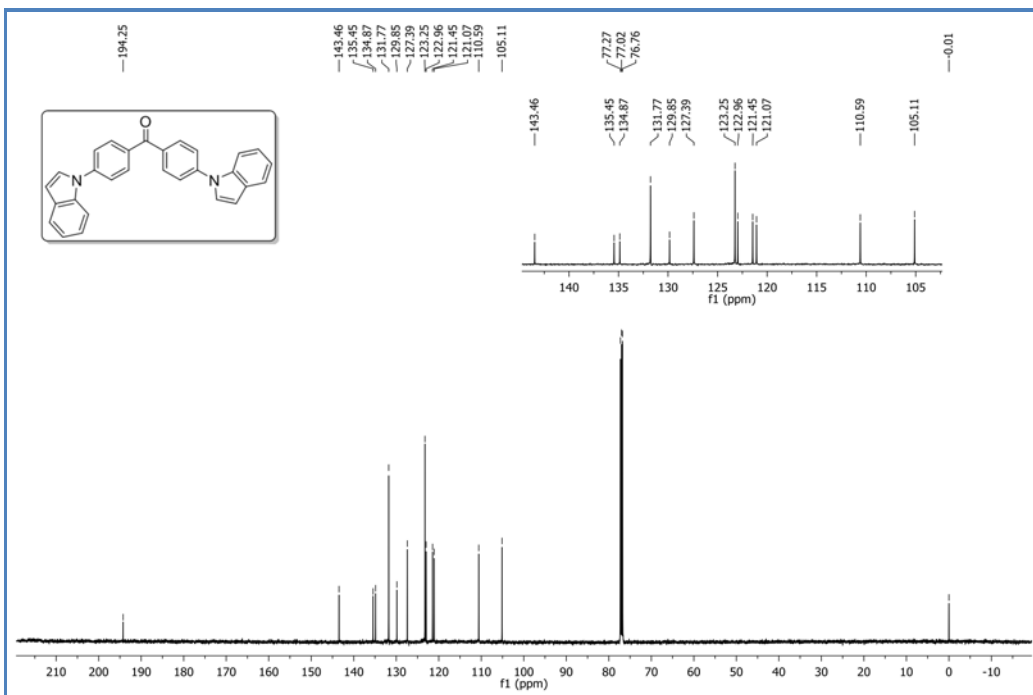


Figure A 7. ¹³C NMR spectrum of compound 36

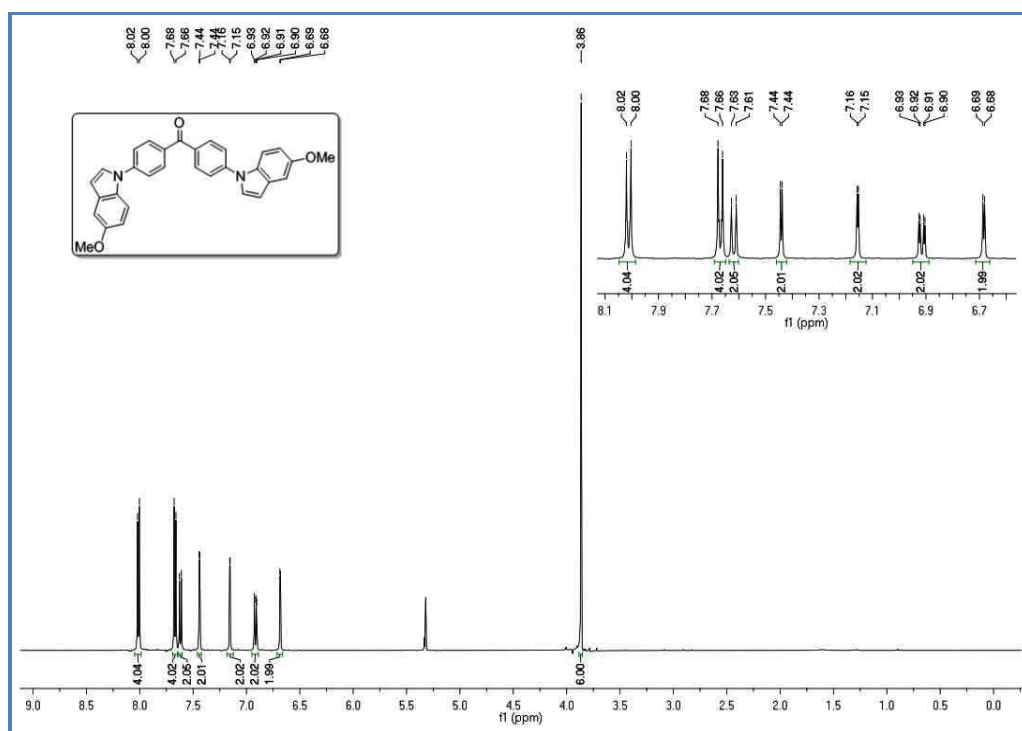


Figure A 8. ^1H NMR spectrum of compound 37

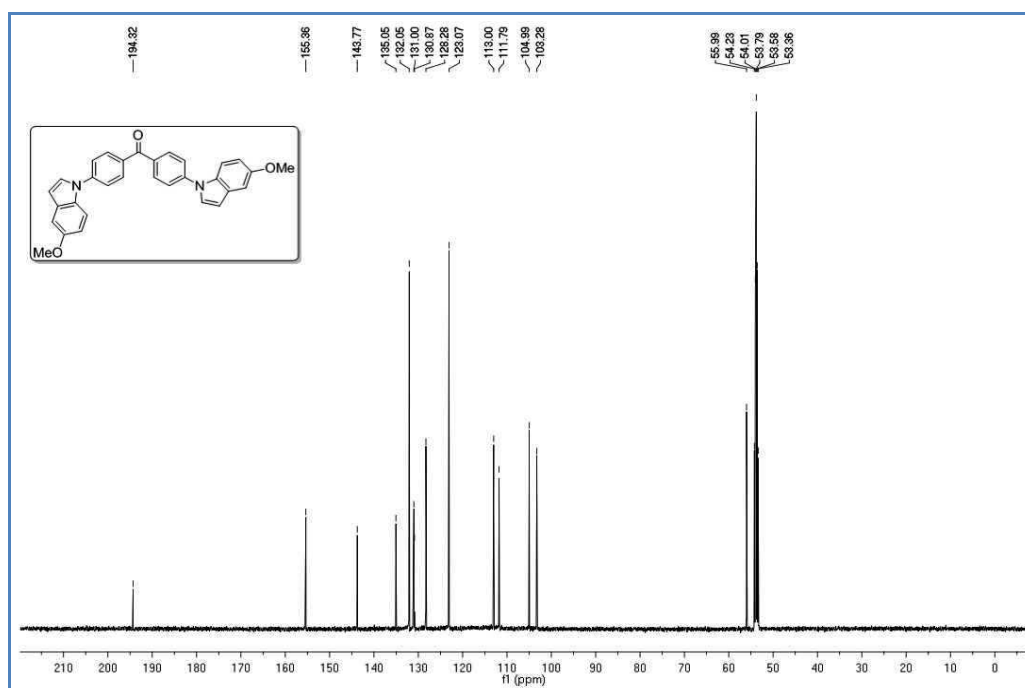


Figure A 9. ^{13}C NMR spectrum of compound 37

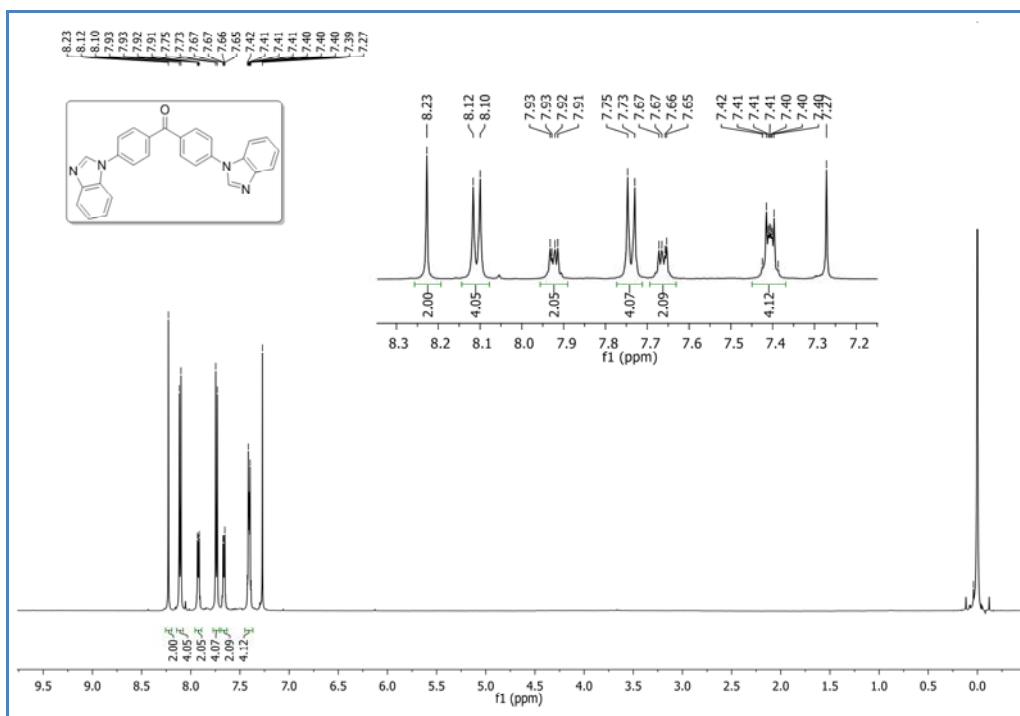


Figure A 10. ¹H NMR spectrum of compound 38

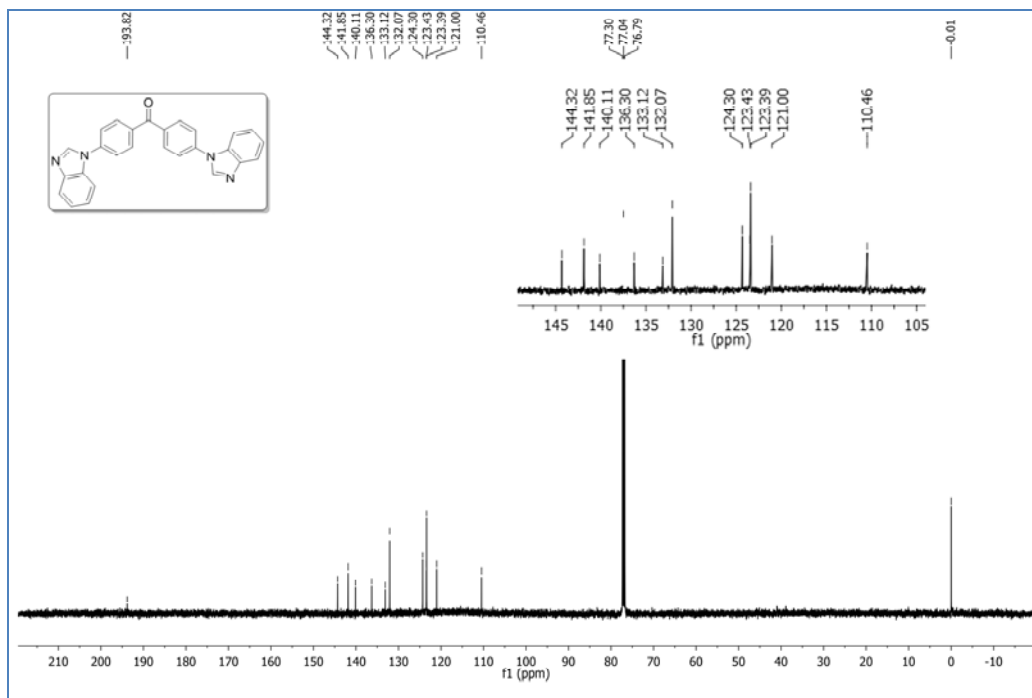


Figure A 11. ¹³C NMR spectrum of compound 38

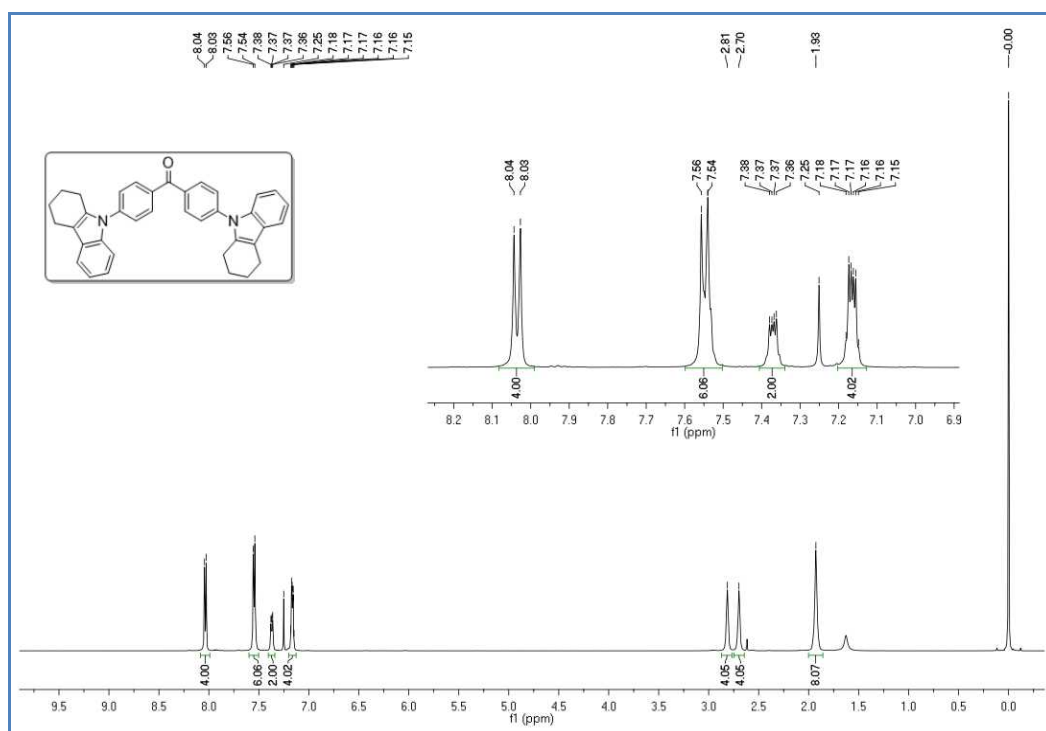


Figure A 12. ¹H NMR spectrum of compound 39

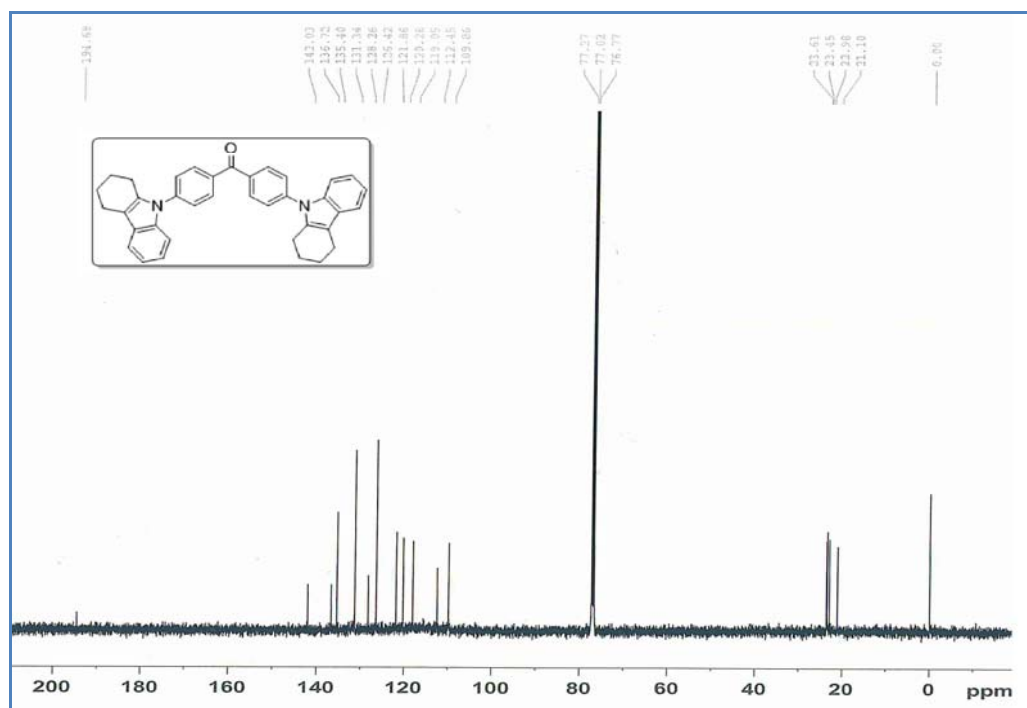


Figure A 13. ¹³C NMR spectrum of compound 39

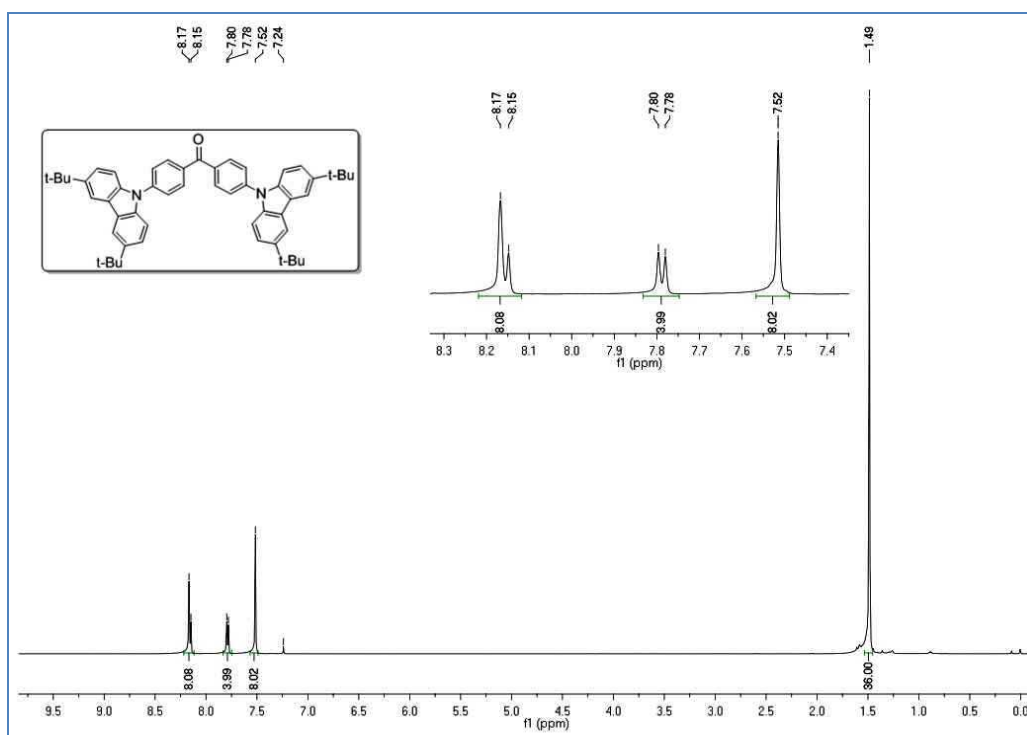


Figure A 14. ^1H NMR spectrum of compound 40

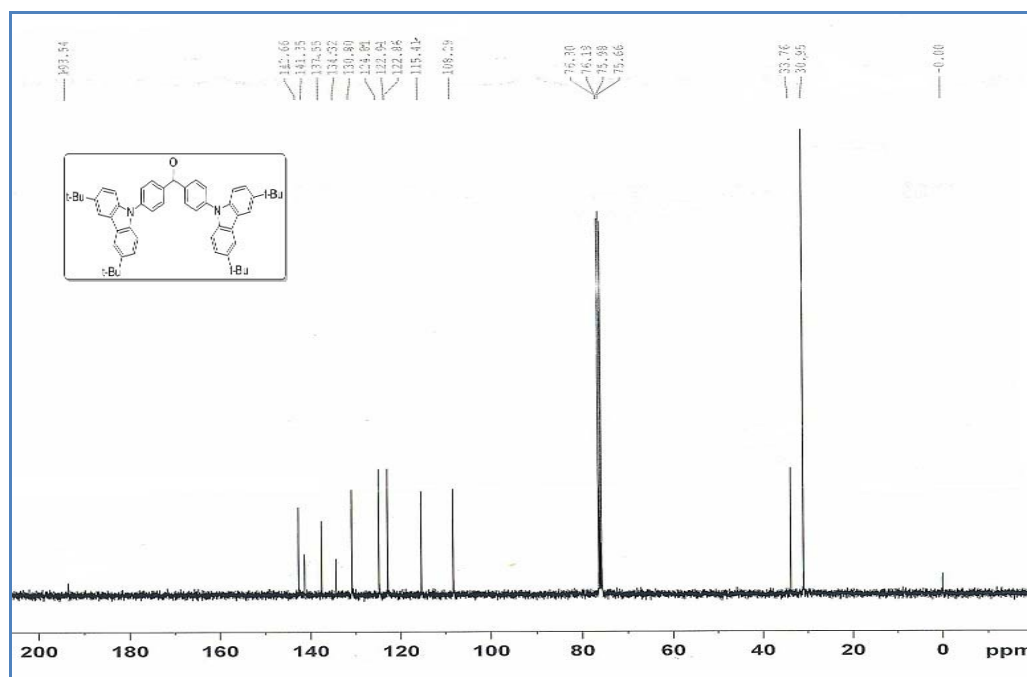


Figure A 15. ^{13}C NMR spectrum of compound 40

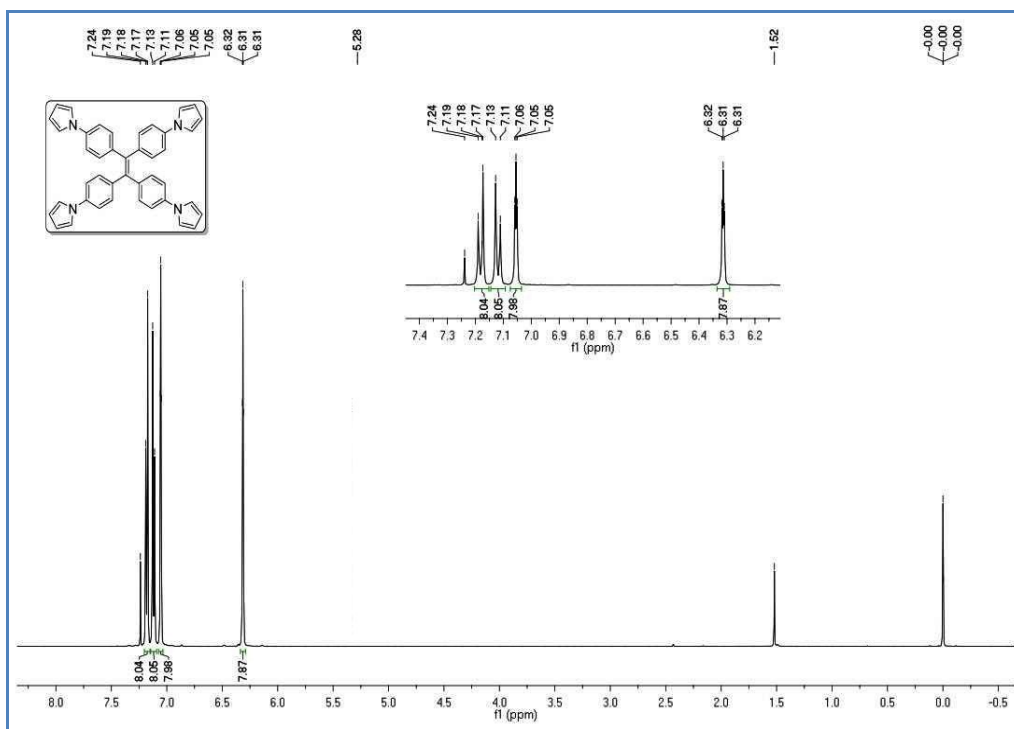


Figure A 16. ^1H NMR spectrum of compound 41

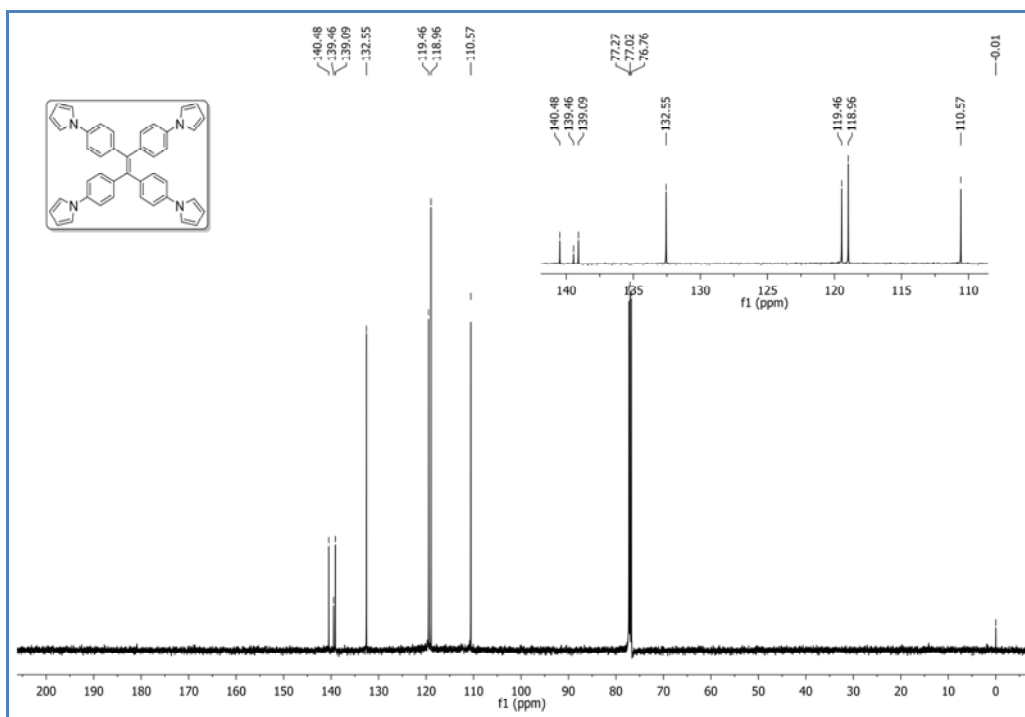


Figure A 17. ^{13}C NMR spectrum of compound 41

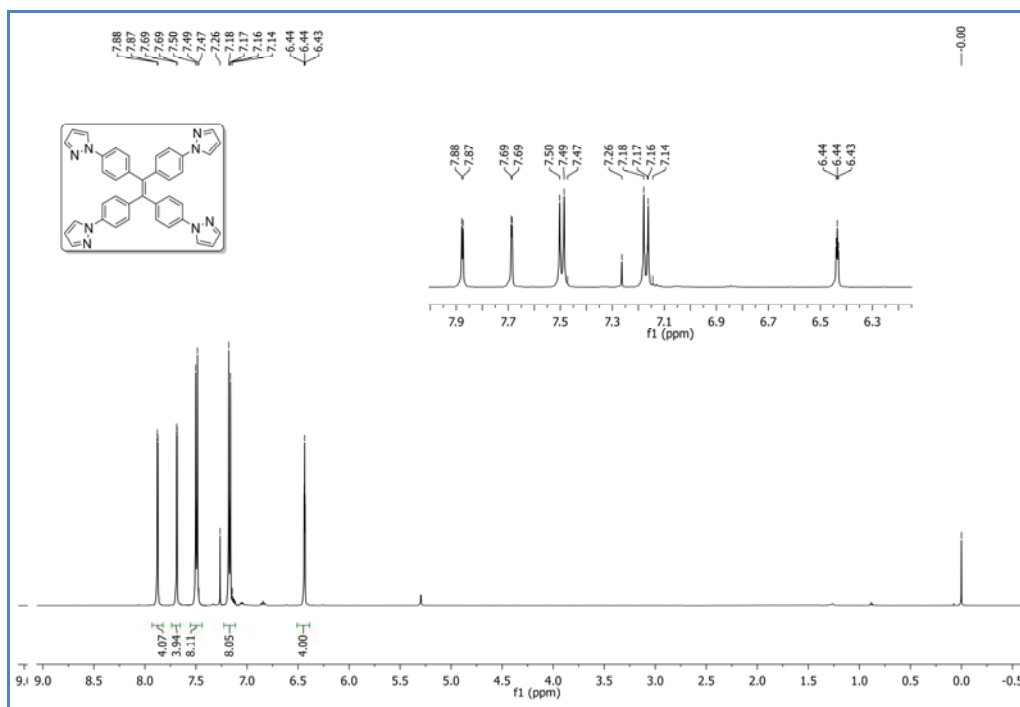


Figure A 18. ^1H NMR spectrum of compound **42**

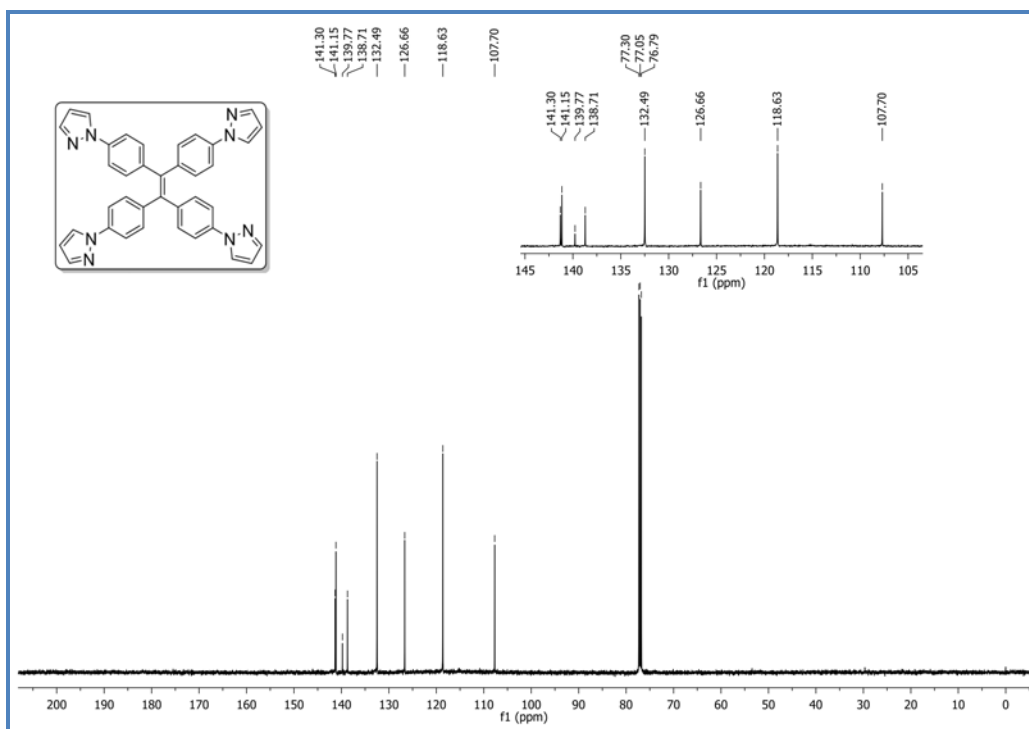


Figure A 19. ^{13}C NMR spectrum of compound **42**

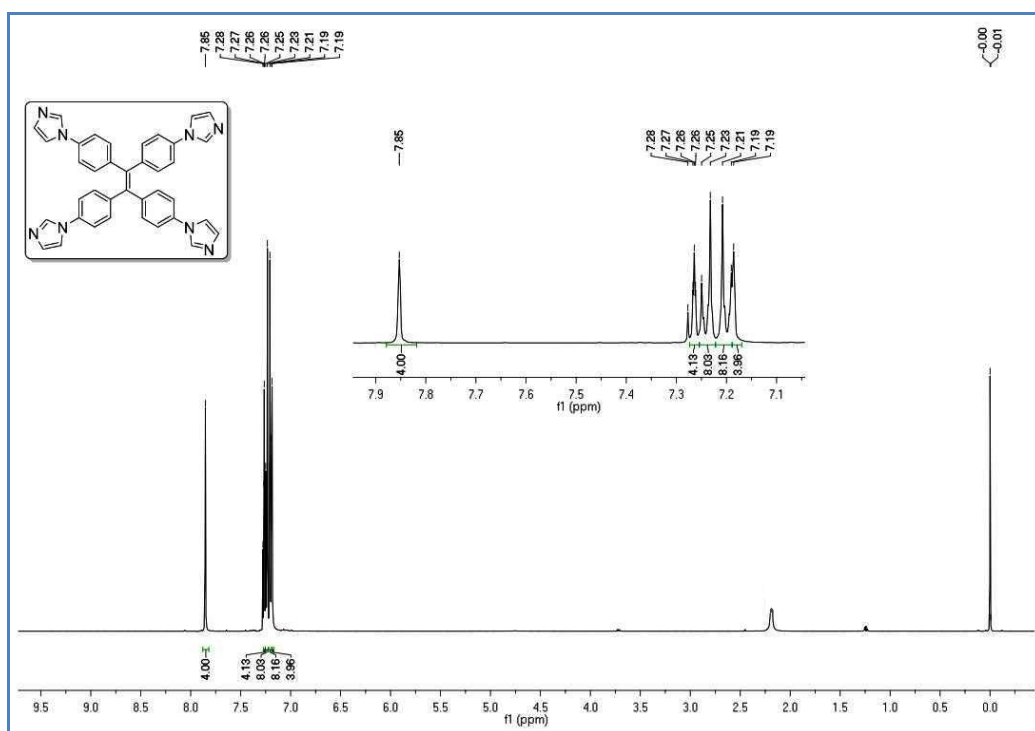


Figure A 20. ^1H NMR spectrum of compound 43

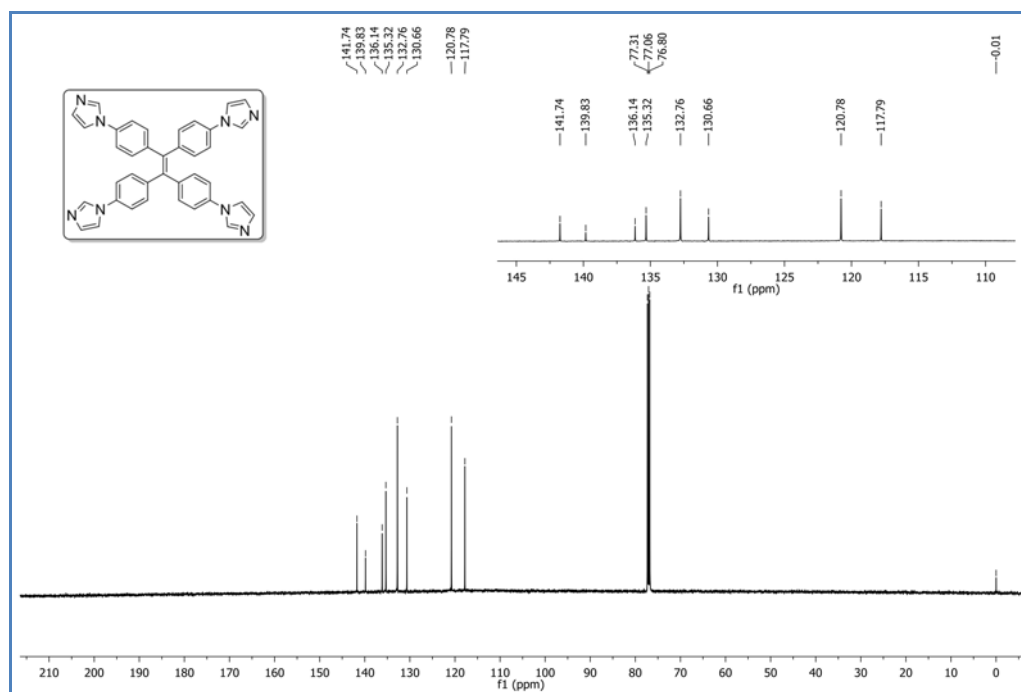


Figure A 21. ^{13}C NMR spectrum of compound 43

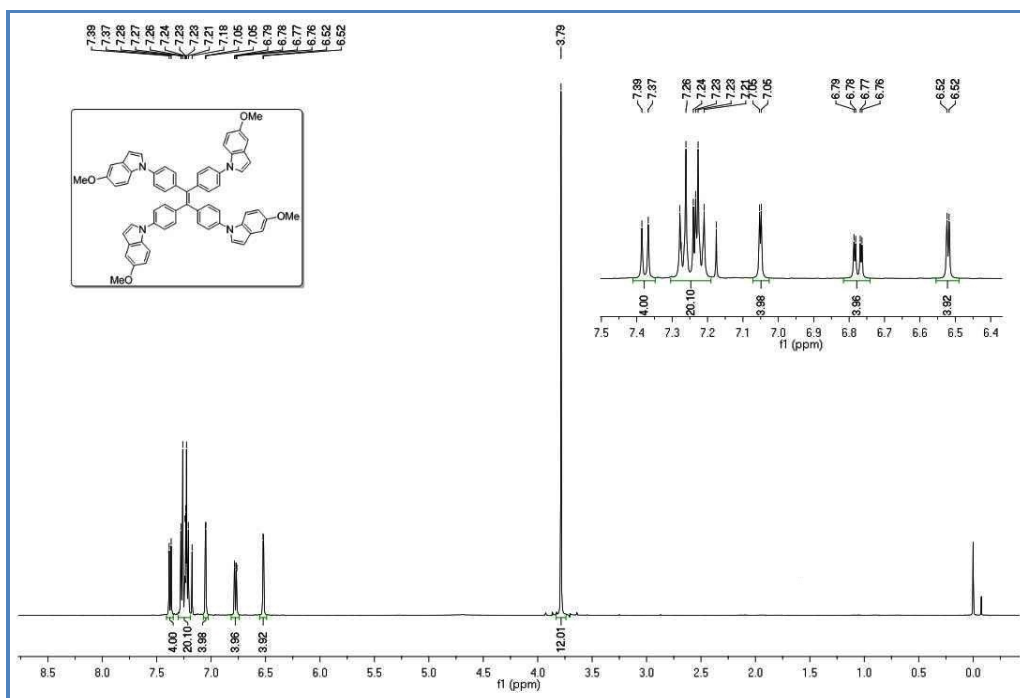


Figure A 24. ¹H NMR spectrum of compound 45

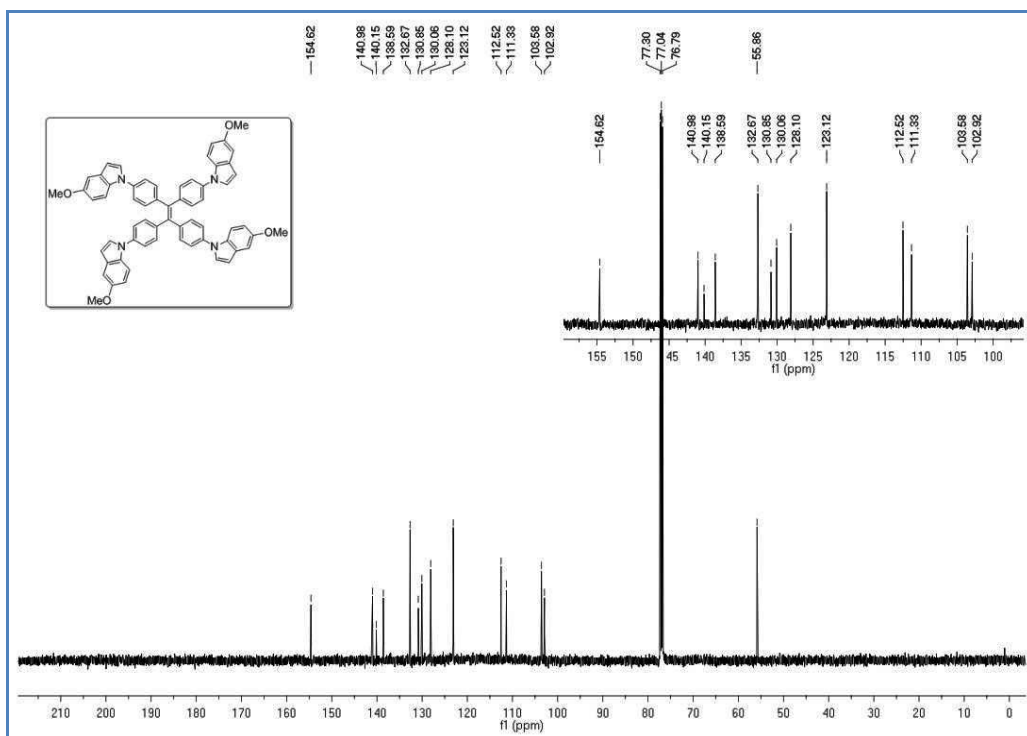


Figure A 25. ¹³C NMR spectrum of compound 45

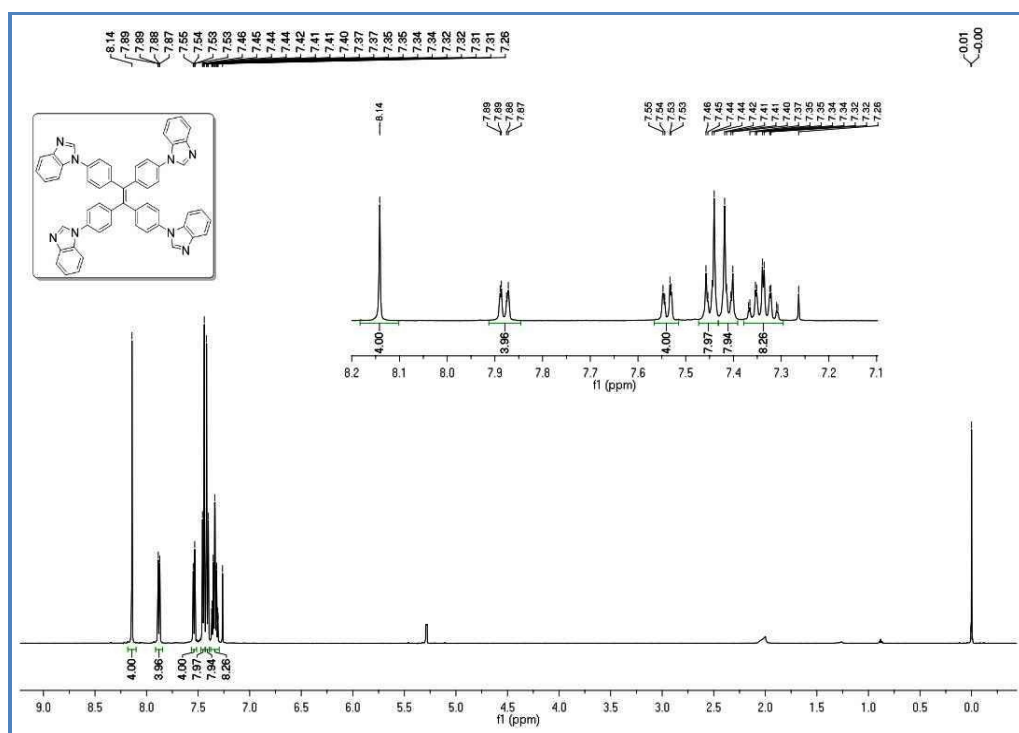


Figure A 26. ¹H NMR spectrum of compound 46

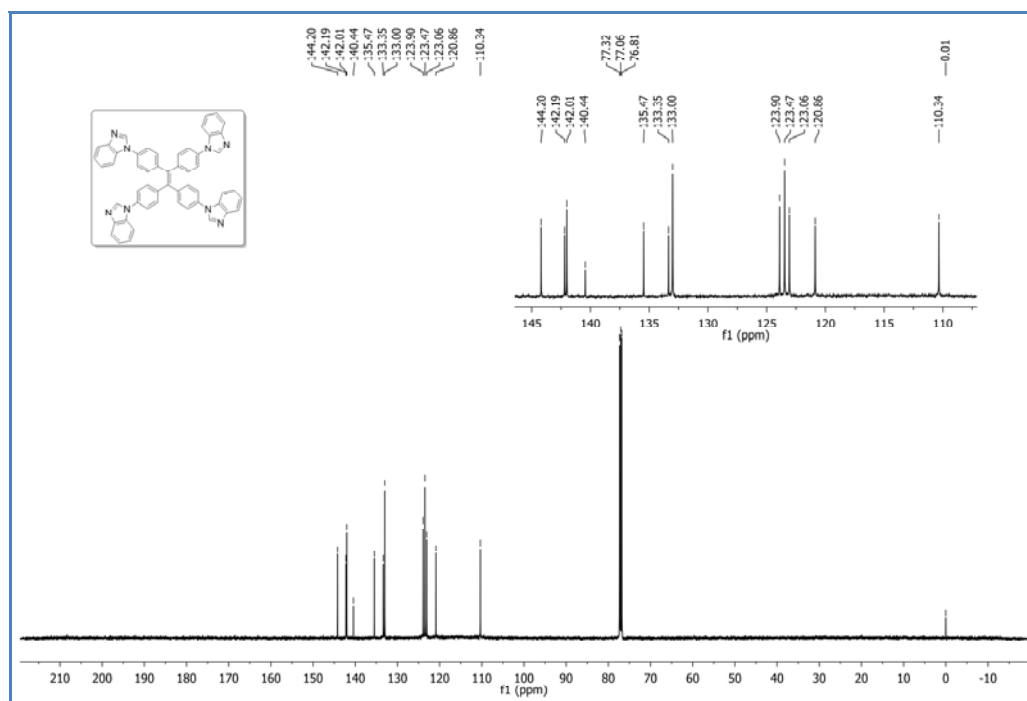


Figure A 27. ¹³C NMR spectrum of compound 46

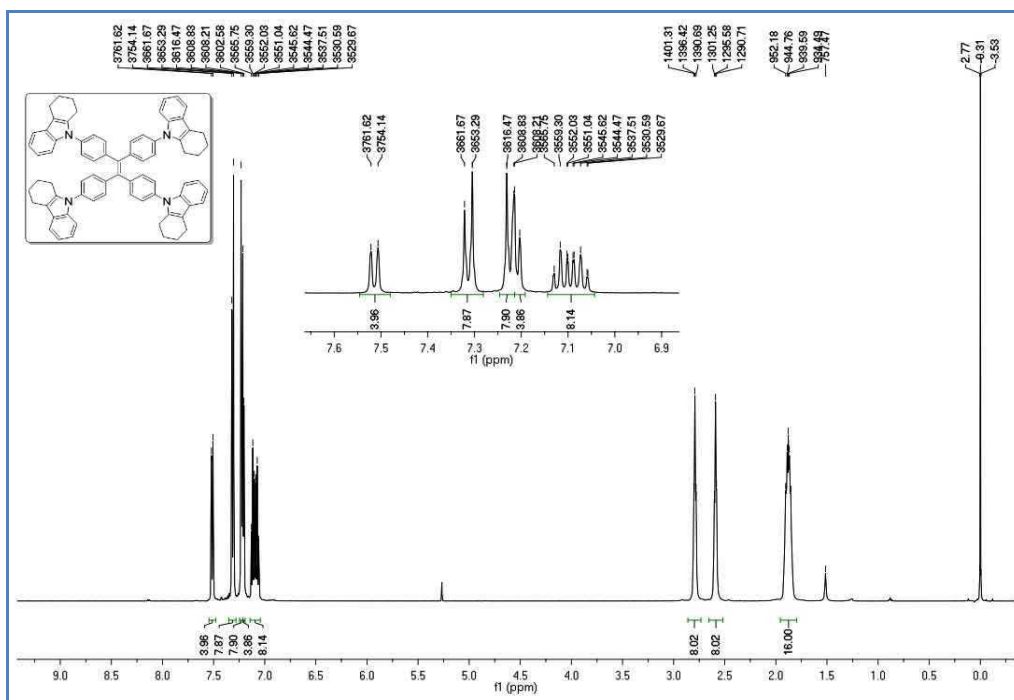


Figure A 28. ^1H NMR spectrum of compound 47

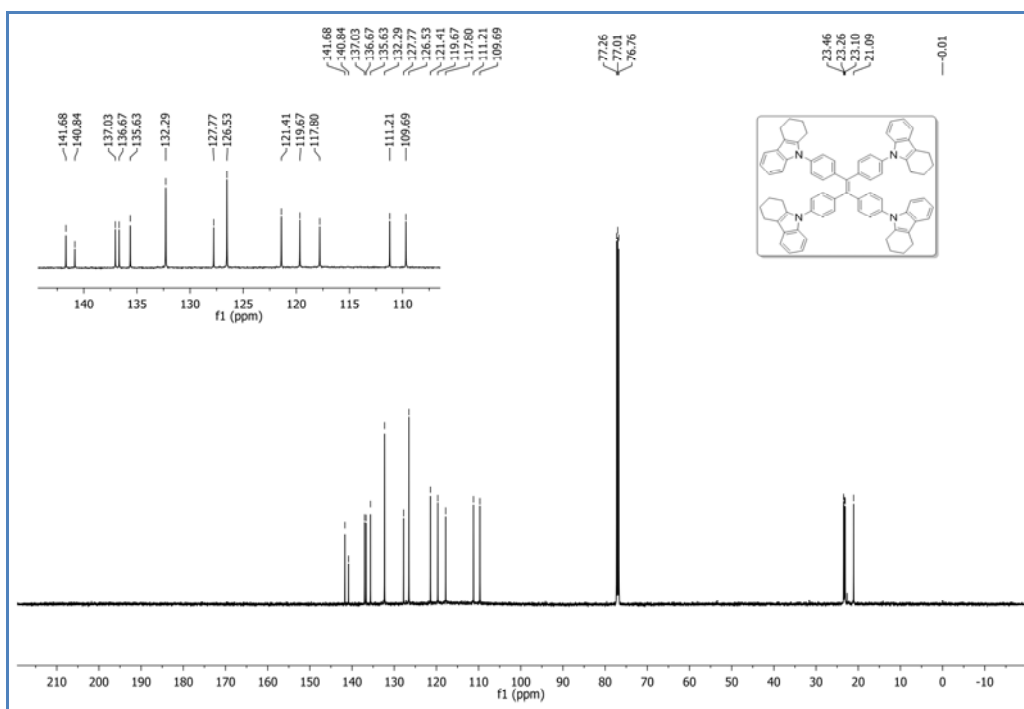


Figure A 29. ^{13}C NMR spectrum of compound 47

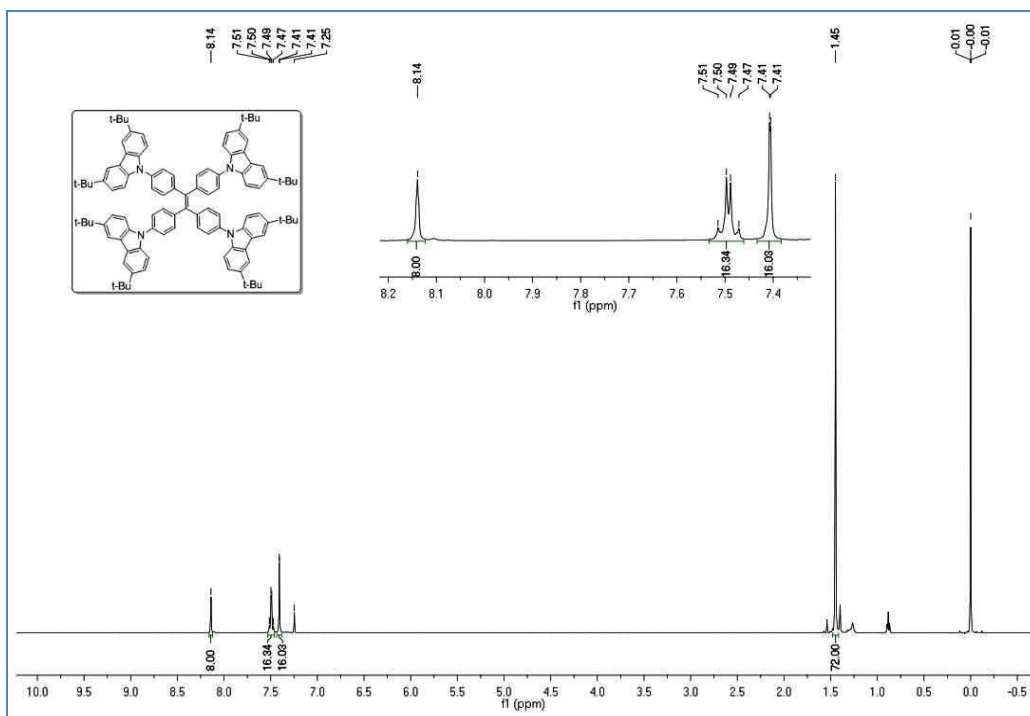


Figure A 30. ^1H NMR spectrum of compound 48

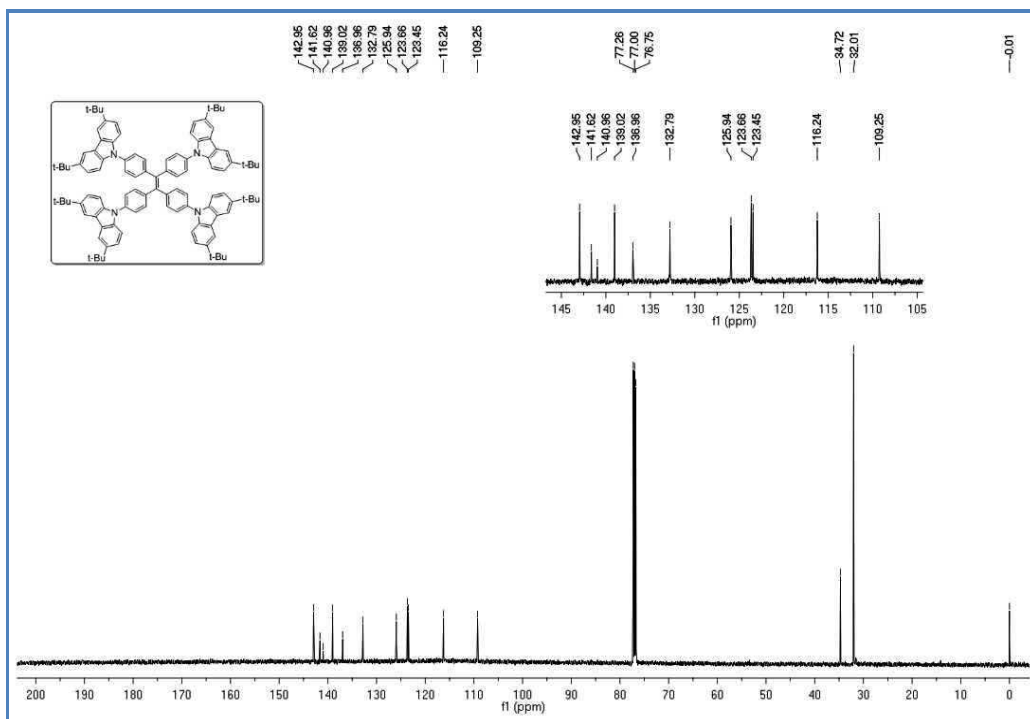


Figure A 31. ^{13}C NMR spectrum of compound 48

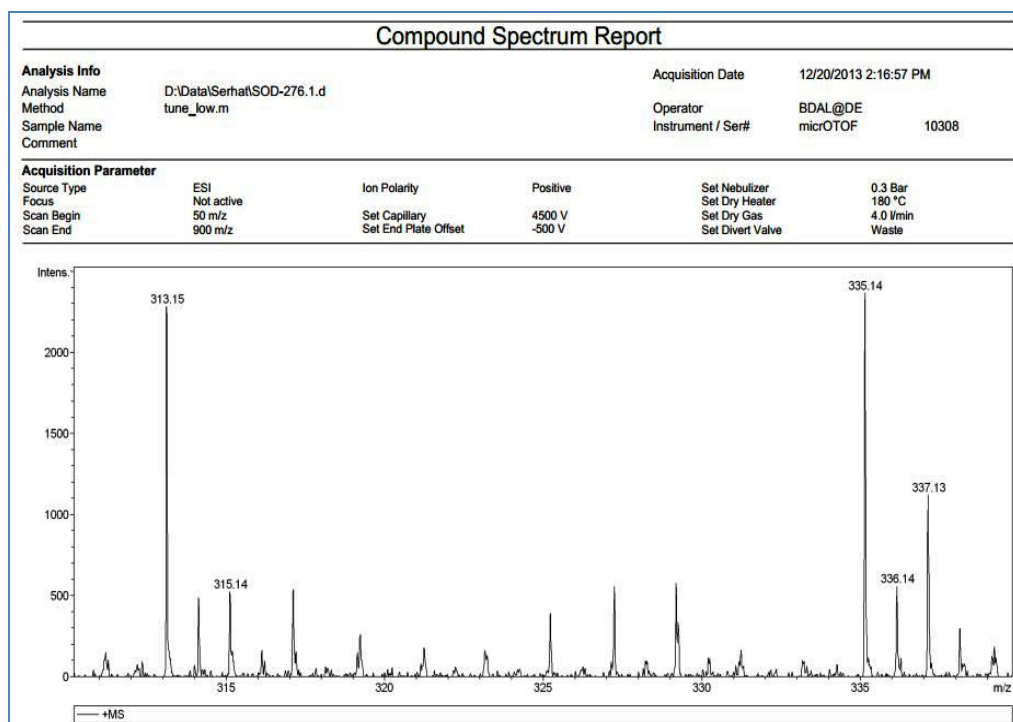


Figure A 32. ESI-TOF spectrum of compound **33**

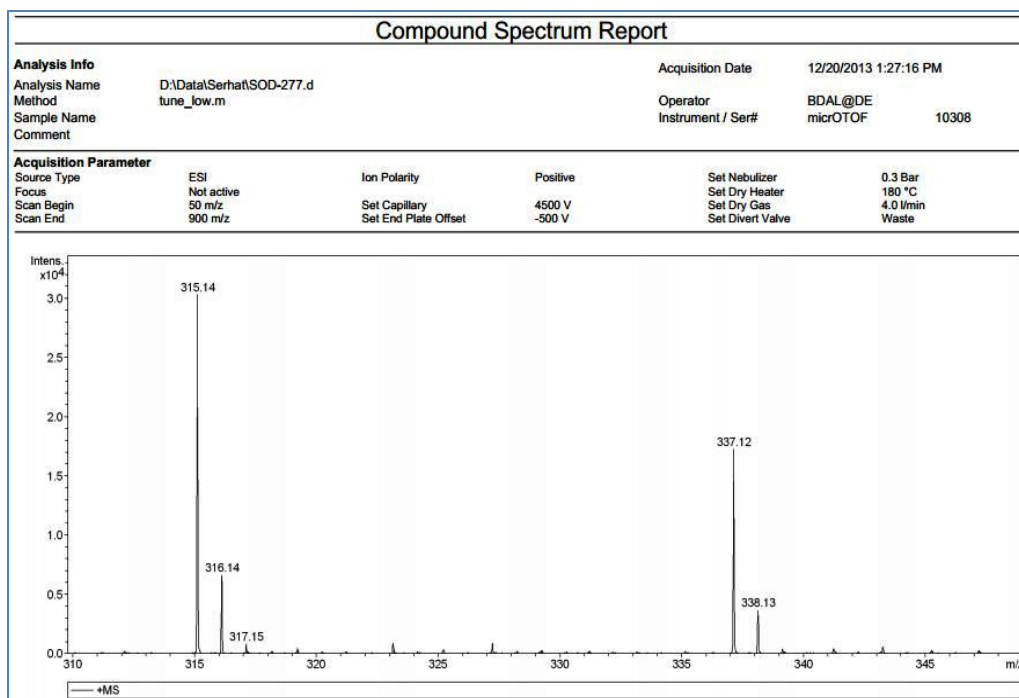


Figure A 33. ESI-TOF spectrum of compound **34**

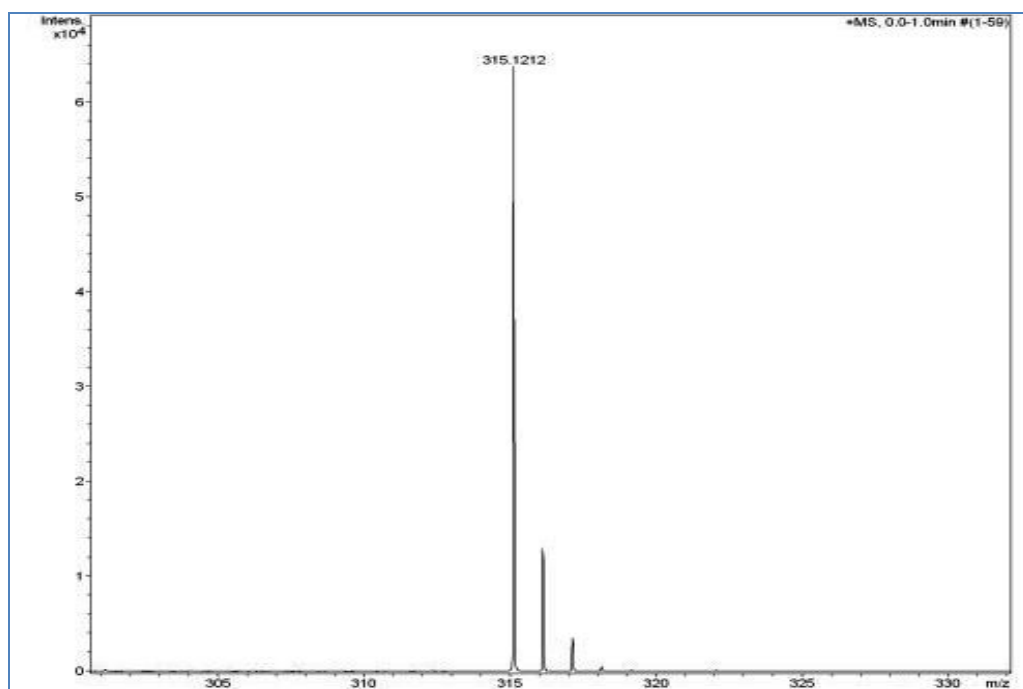


Figure A 34. ESI-TOF spectrum of compound 35

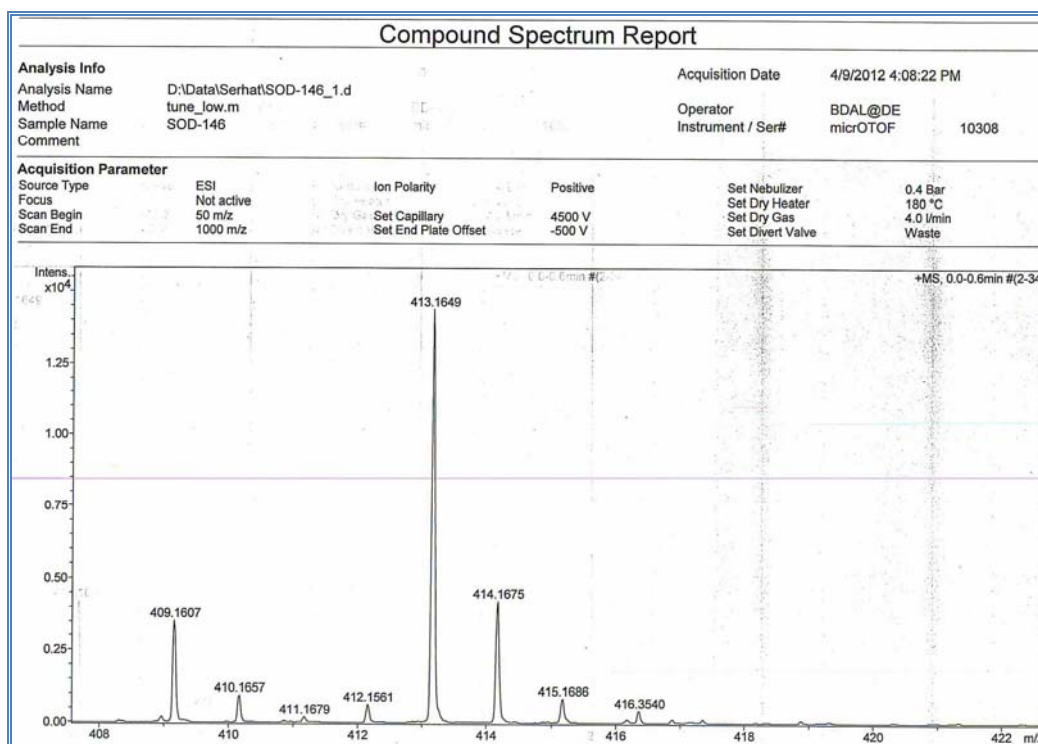


Figure A 35. ESI-TOF spectrum of compound 36

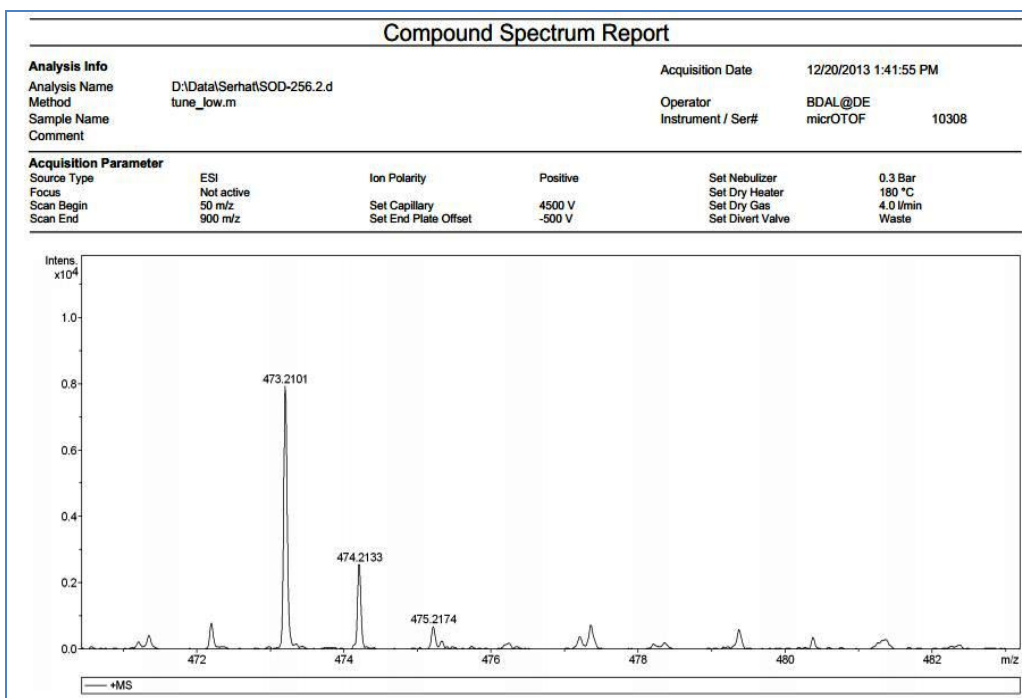


Figure A 36. ESI-TOF spectrum of compound **37**

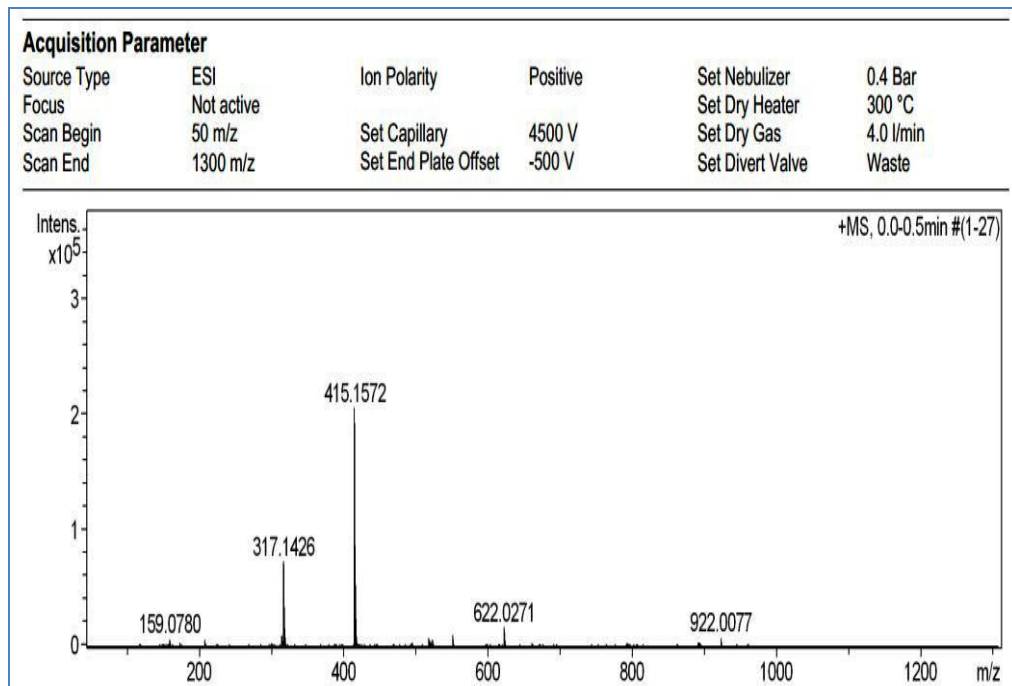


Figure A 37. ESI-TOF spectrum of compound **38**

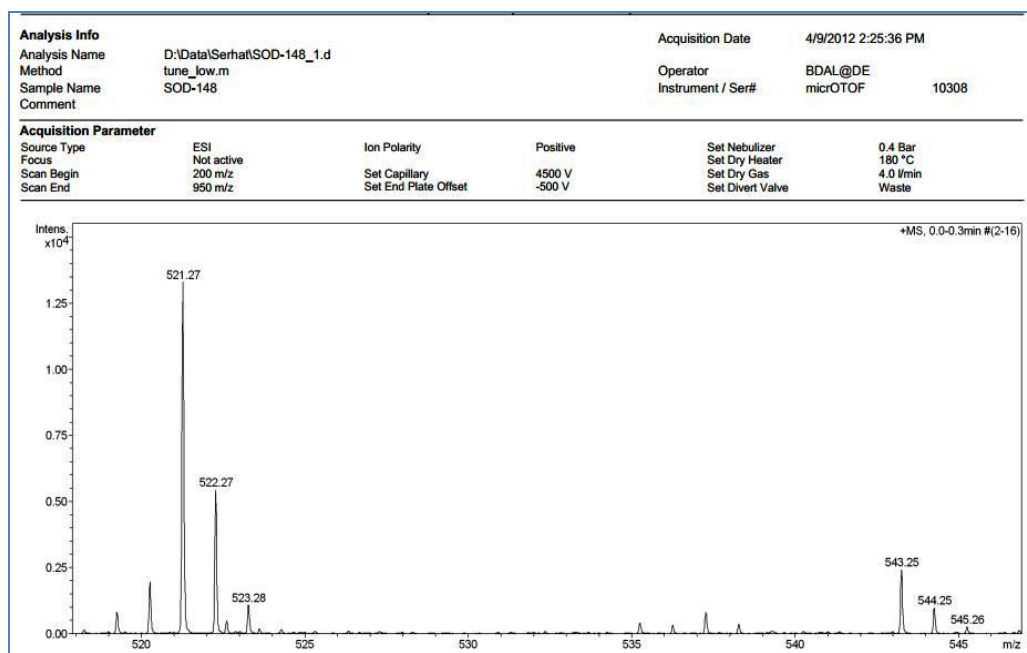


Figure A 38. ESI-TOF spectrum of compound **39**

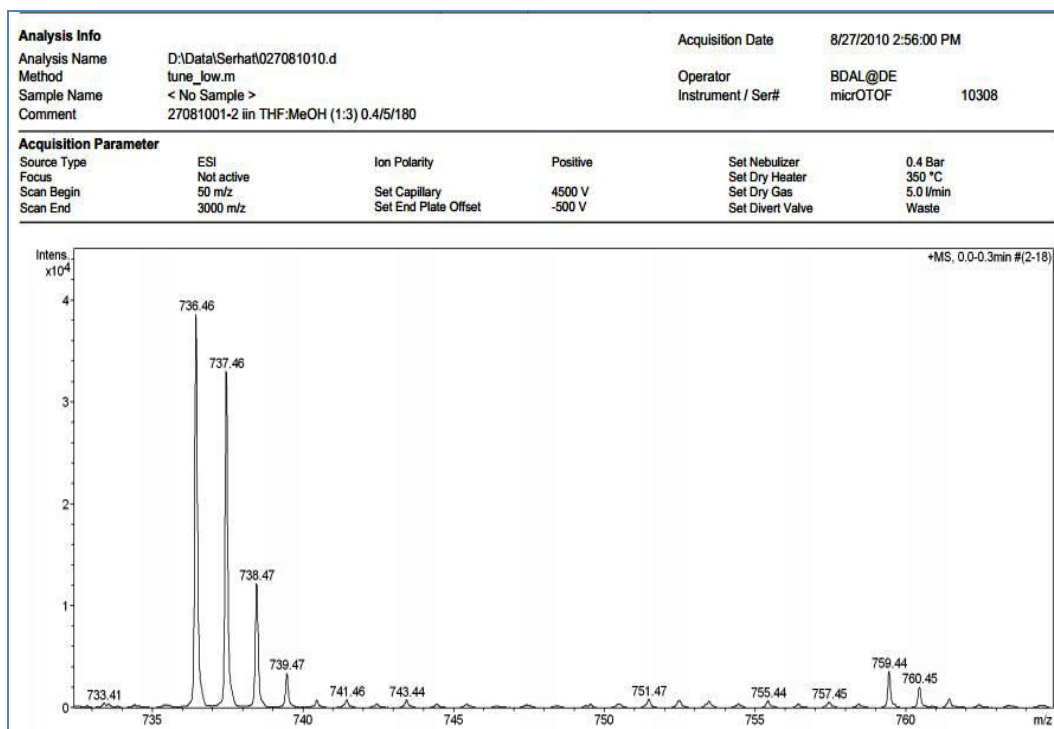


Figure A 39. ESI-TOF spectrum of compound **40**

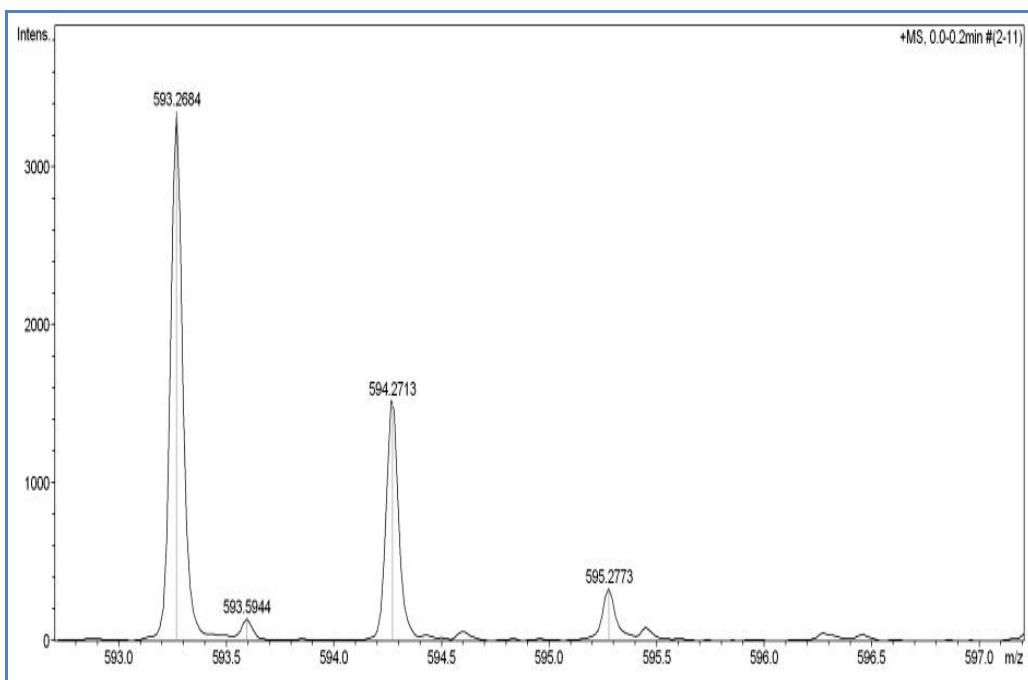


Figure A 40. HRMS spectrum of TPPE (41)

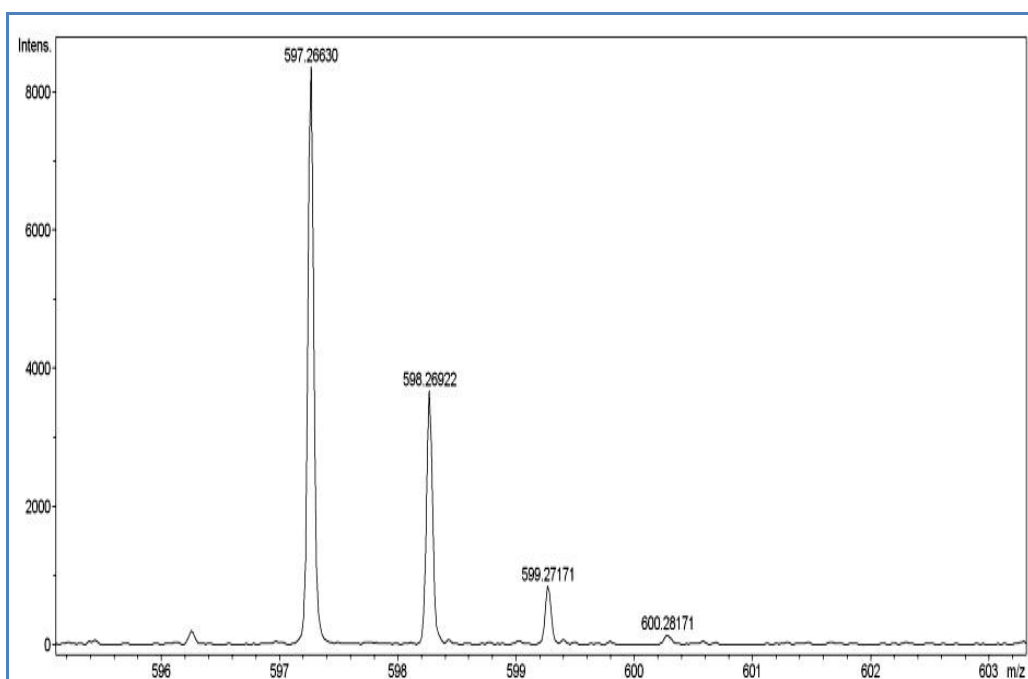


Figure A 41. HRMS spectrum of TPyPE (42)

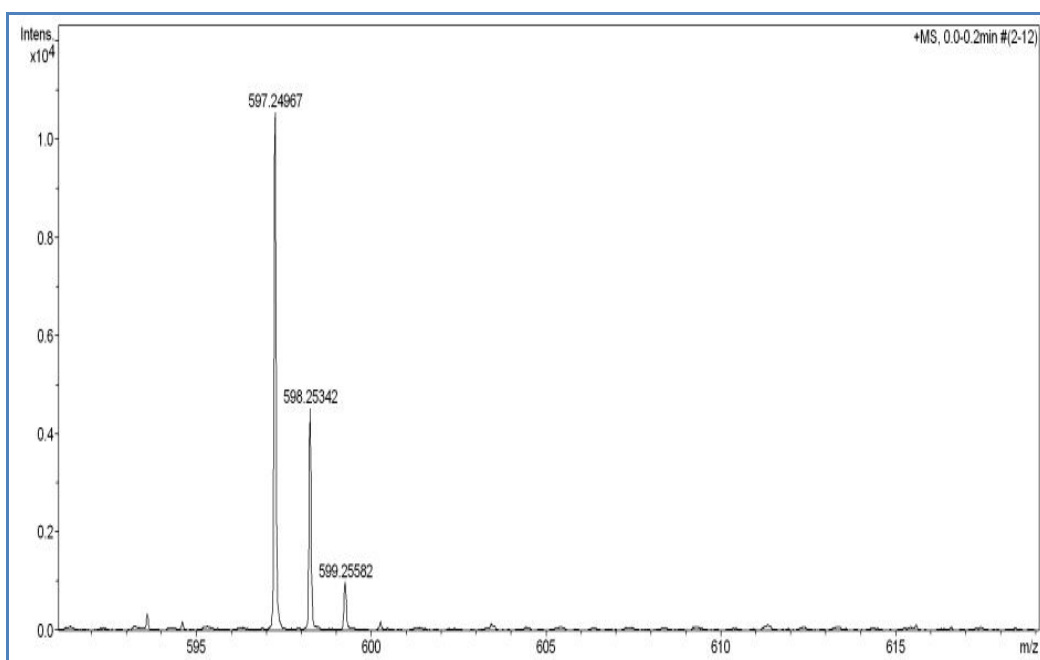


Figure A 42. HRMS spectrum of TIMPE (43)

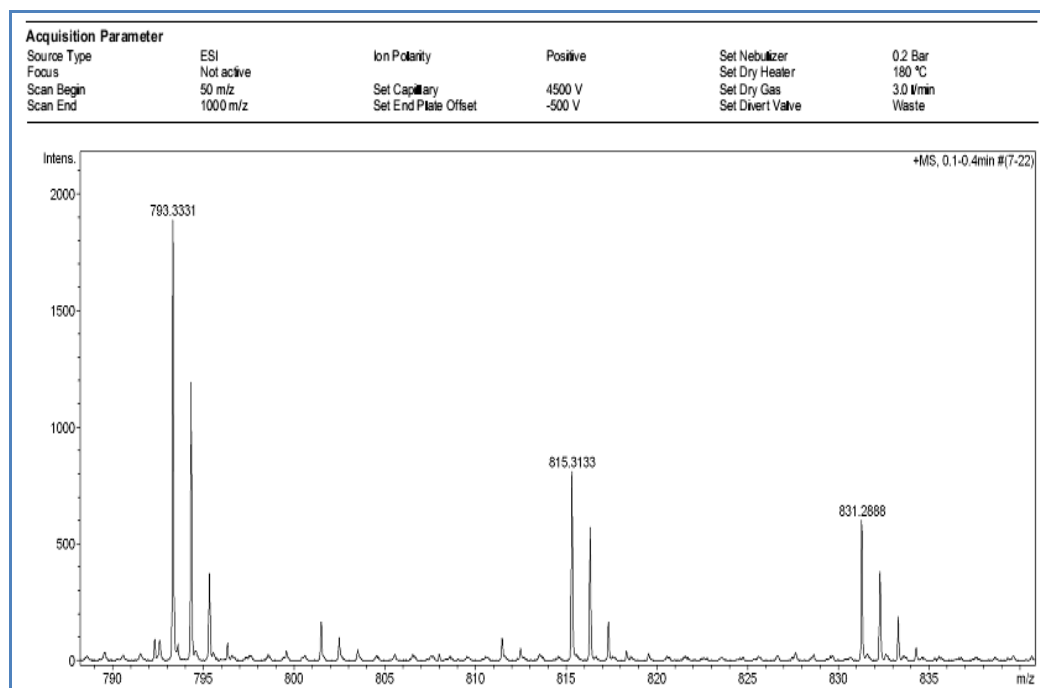


Figure A 43. HRMS spectrum of TIPE (44)

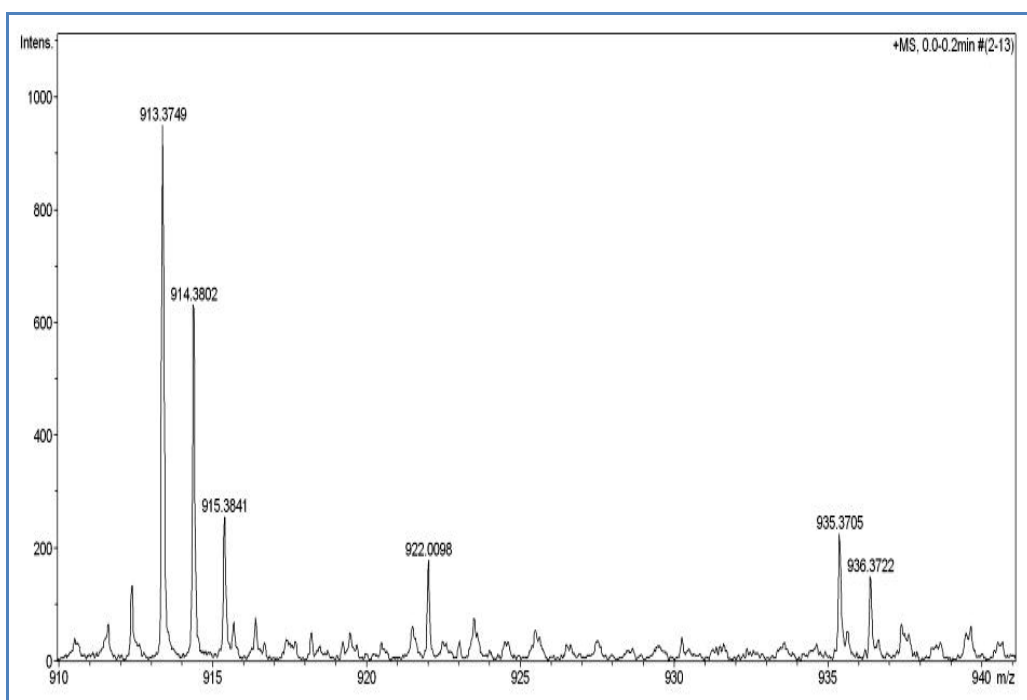


Figure A 44. HRMS spectrum of T5MIPE (45)

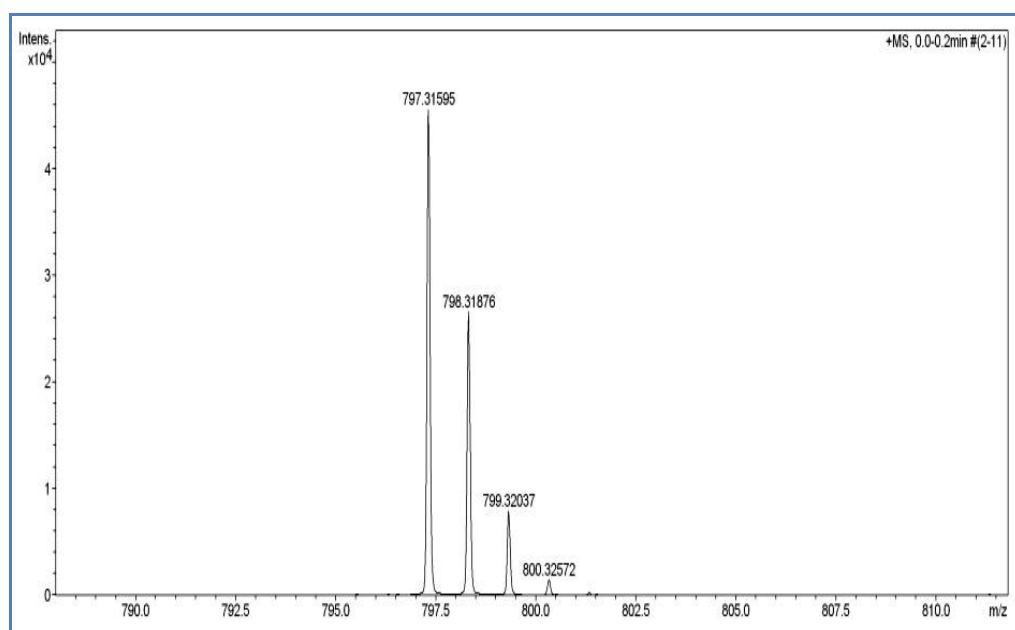


Figure A 45. HRMS spectrum of TBIMPE (46)

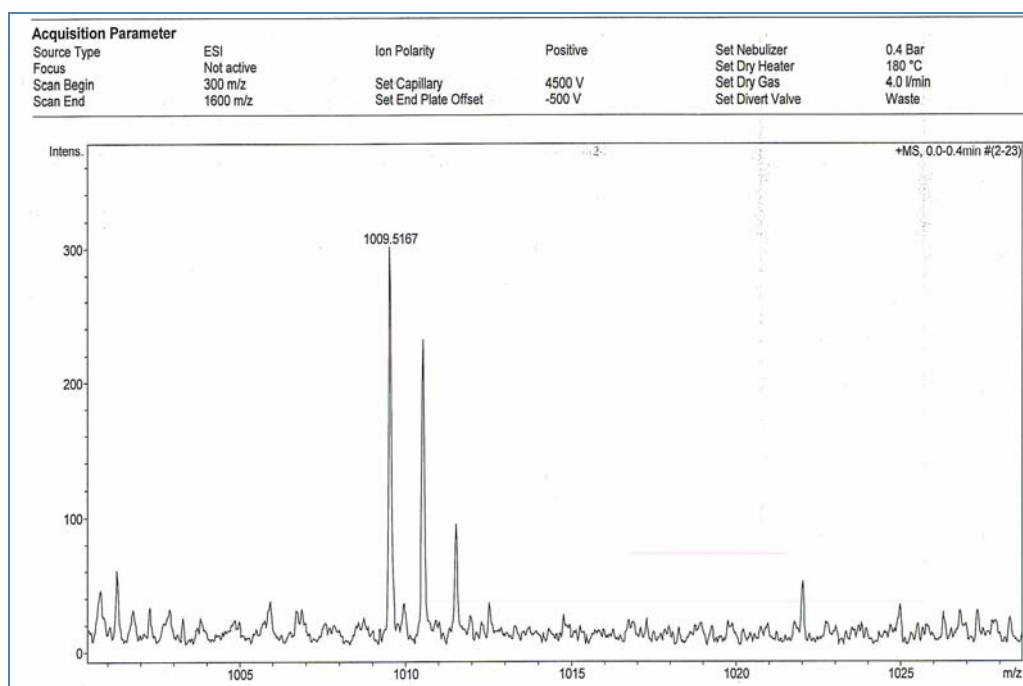


Figure A 46. HRMS spectrum of TDCPE (47)

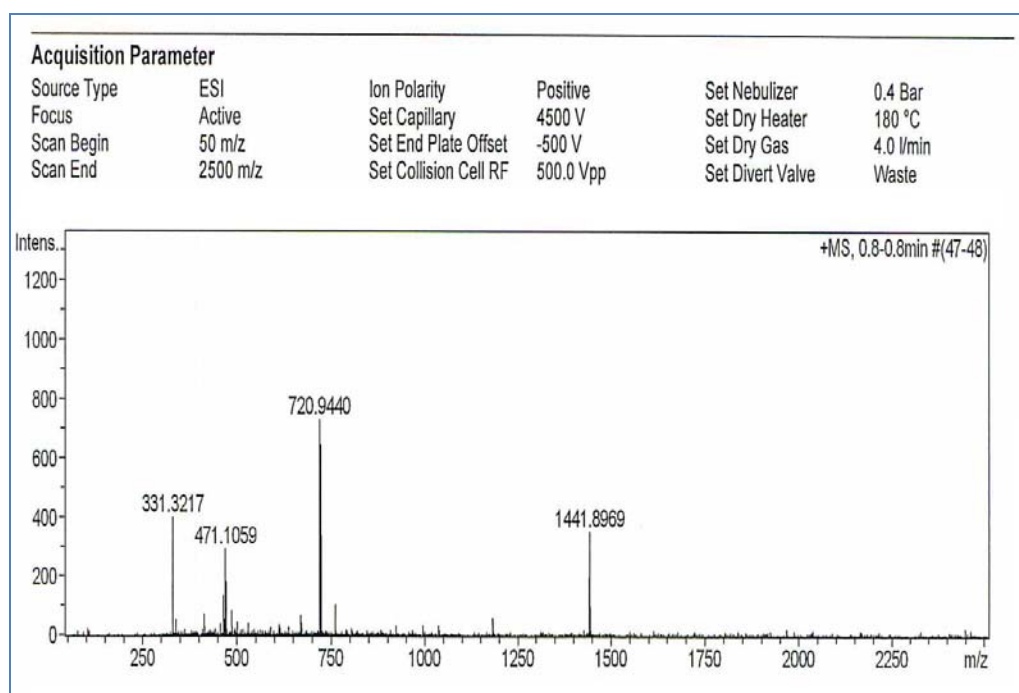


Figure A 47. HRMS spectrum of TTBCPE (48)

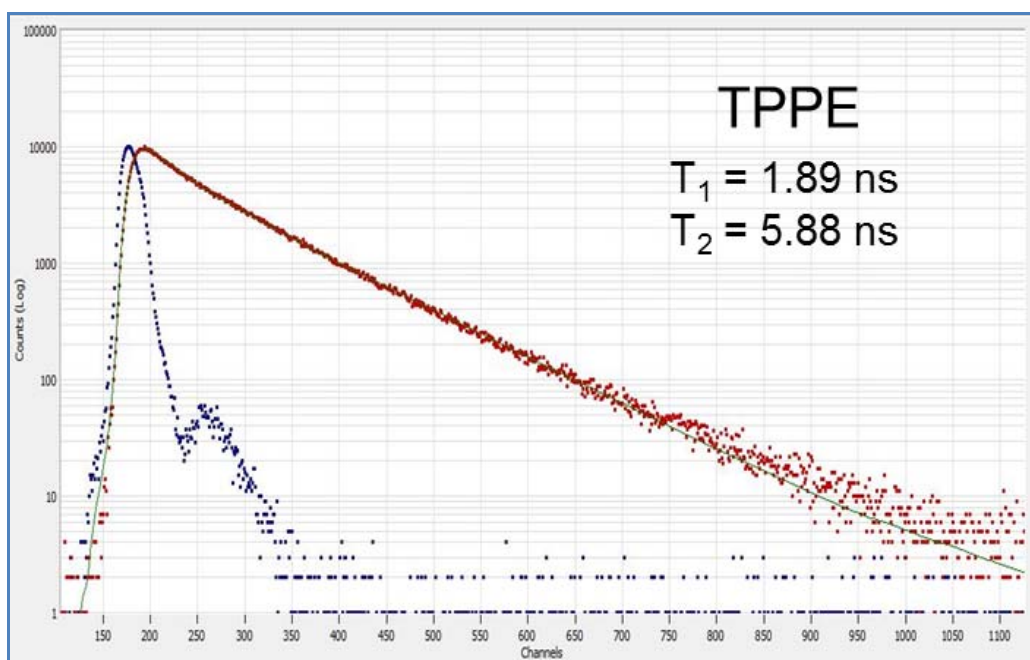


Figure A 48. Fluorescence decay curve of TPPE (41)

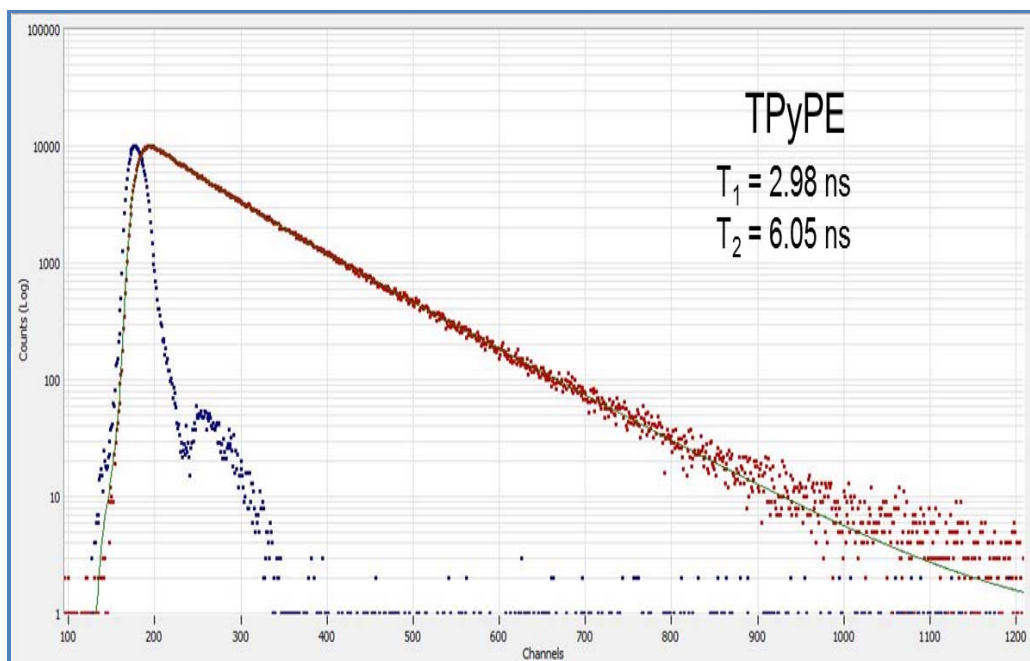


Figure A 49. Fluorescence decay curve of TPyPE (42)

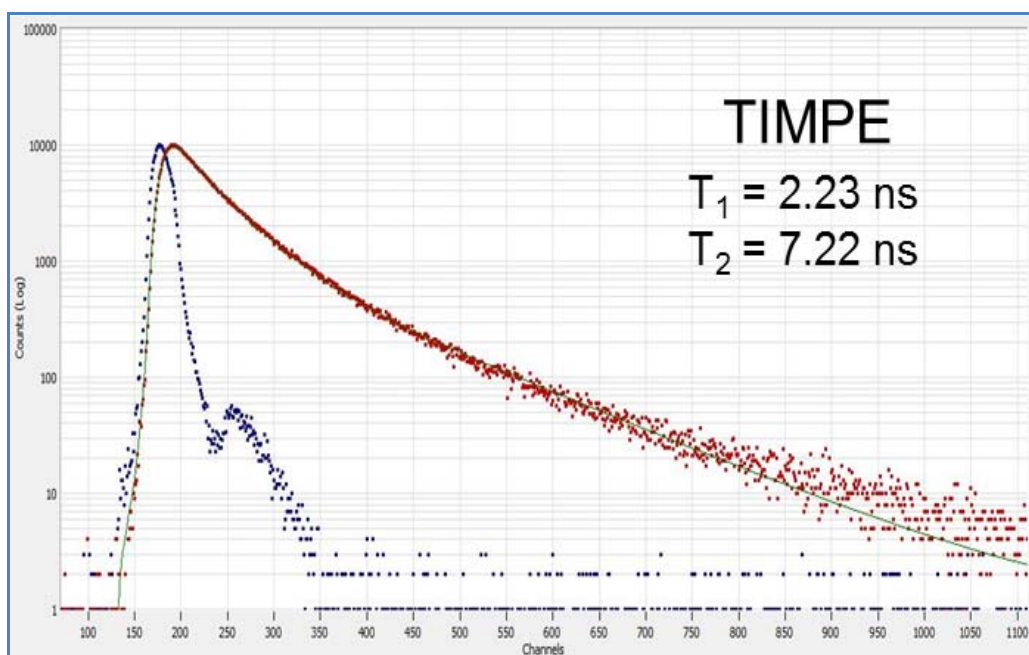


Figure A 50. Fluorescence decay curve of TIMPE (43)

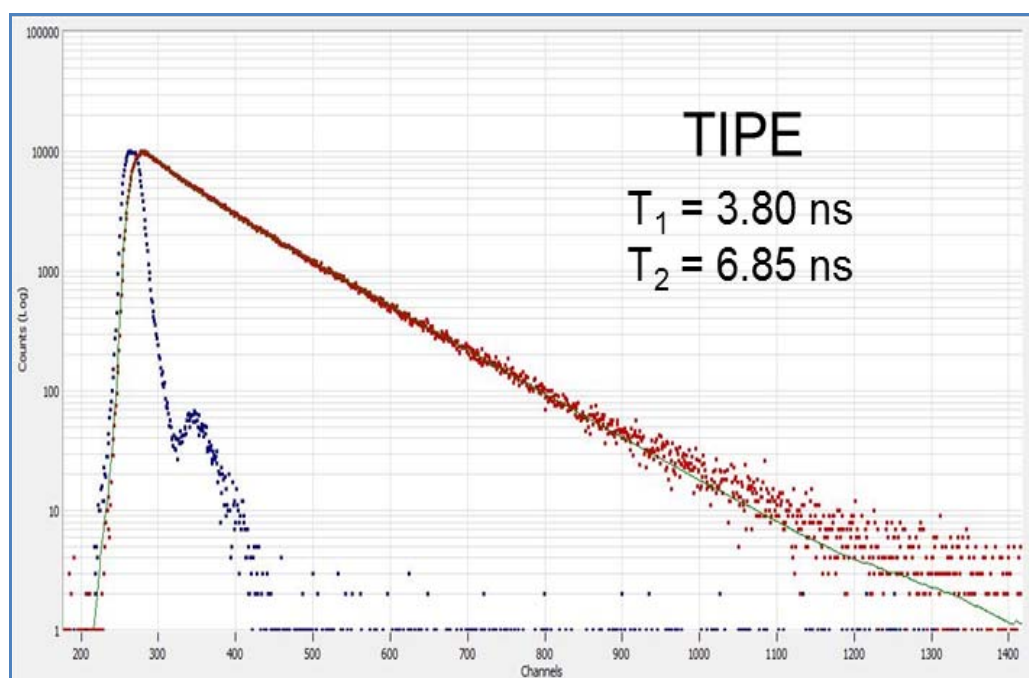


Figure A 51. Fluorescence decay curve of TIPE (44)

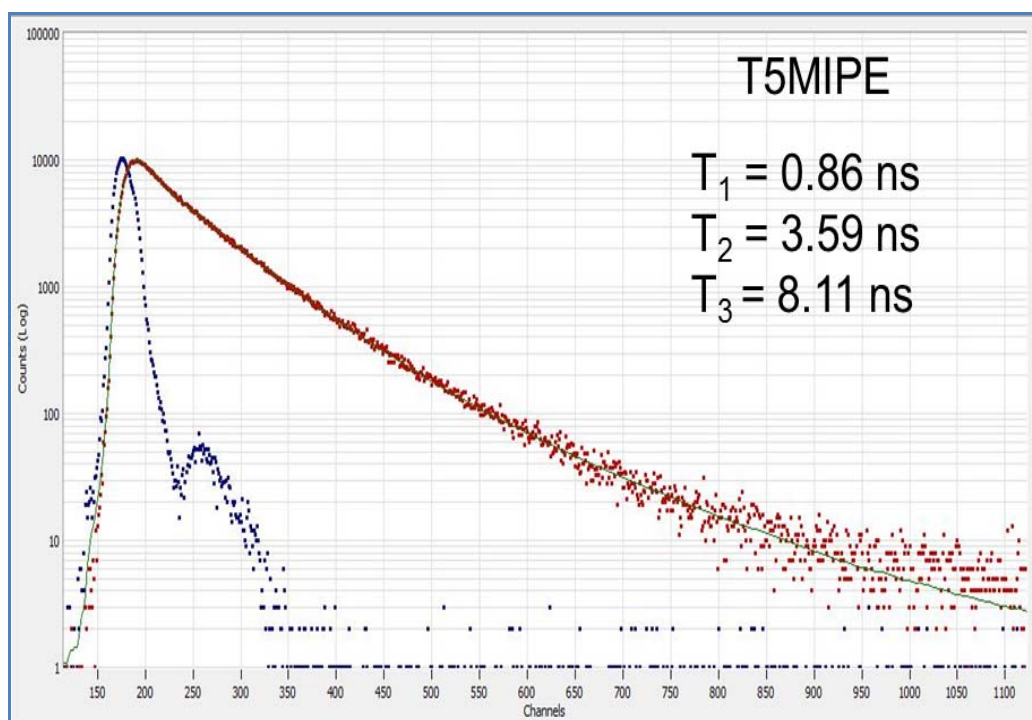


Figure A 52. Fluorescence decay curve of T5MIPE (45)

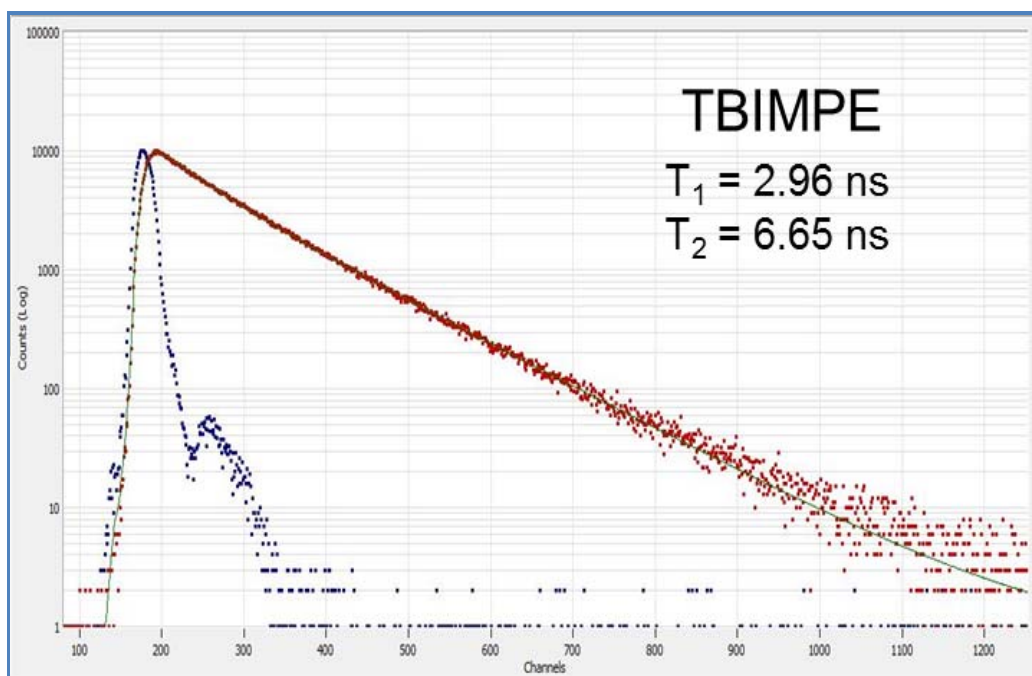


Figure A 53. Fluorescence decay curve of TBIMPE (46)

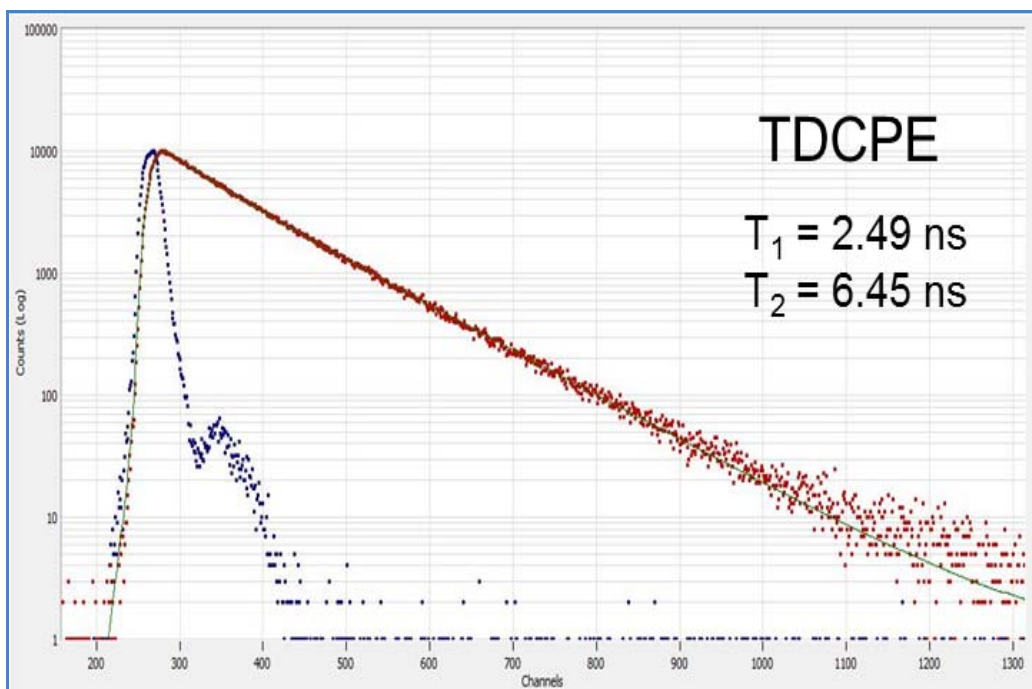


Figure A 54. Fluorescence decay curve of TDCPE (47)

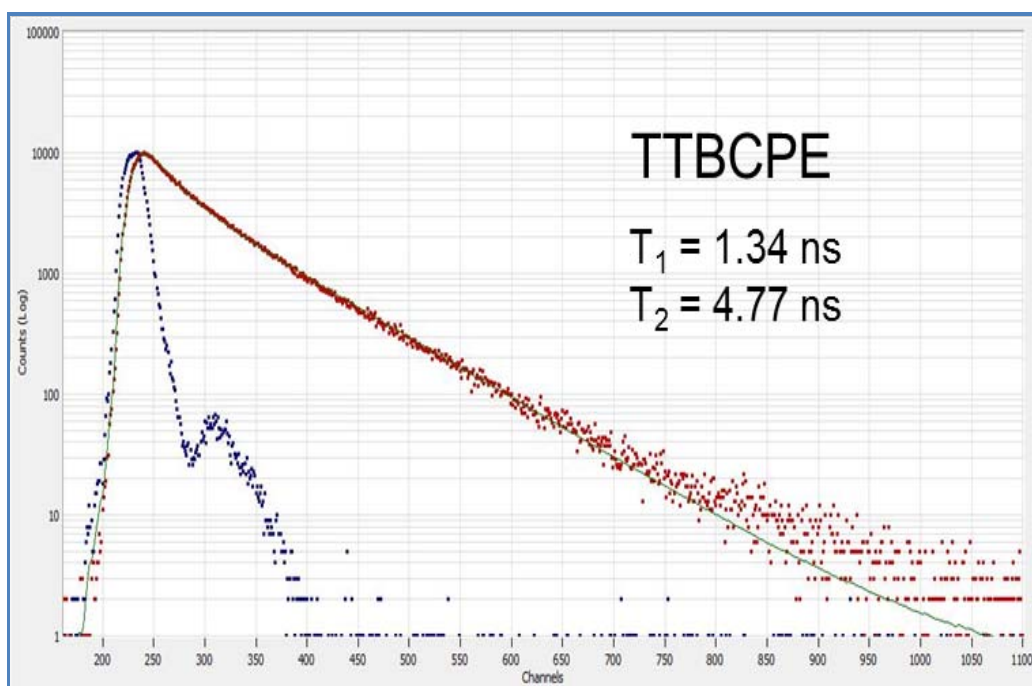


Figure A 55. Fluorescence decay curve of TTBCPE (48)

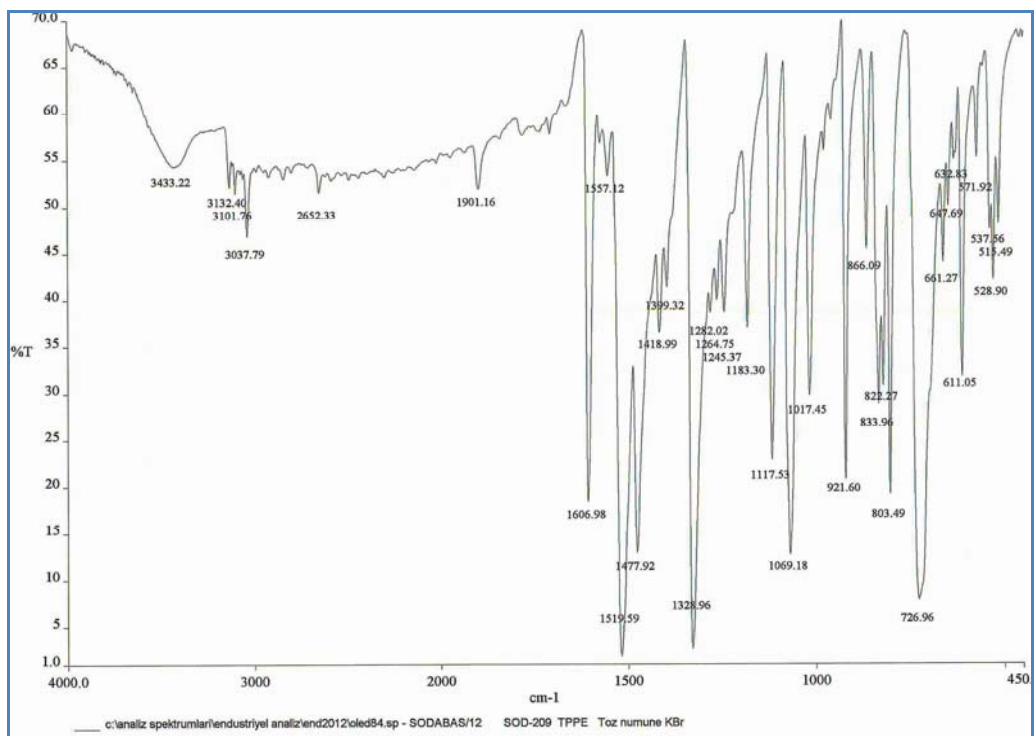


Figure A 56. FTIR spectrum of TPPE (41)

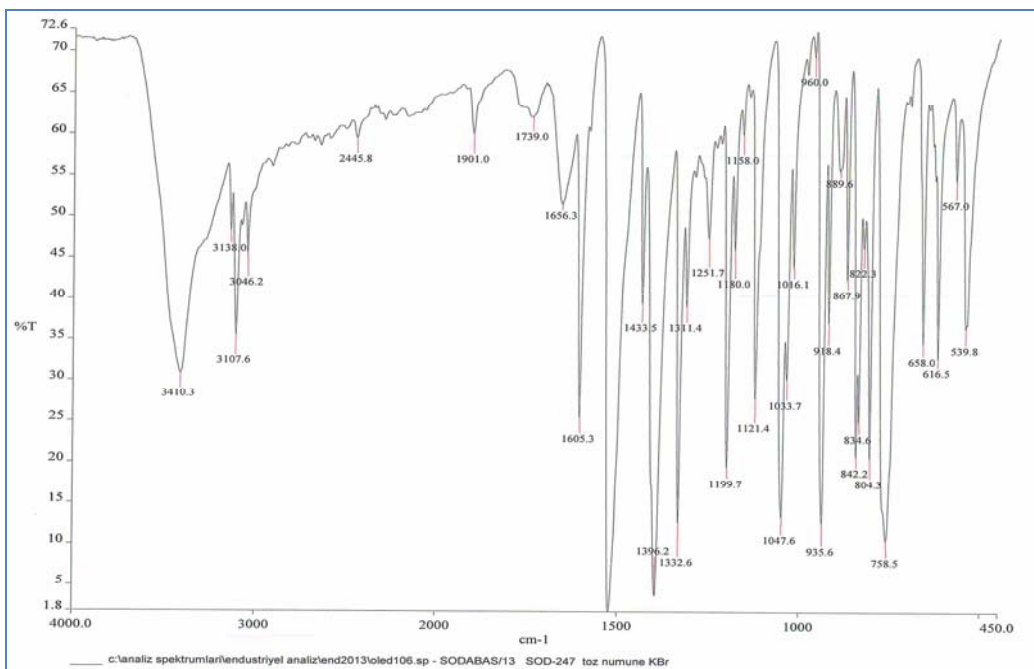


Figure A 57. FTIR spectrum of TPyPE (42)

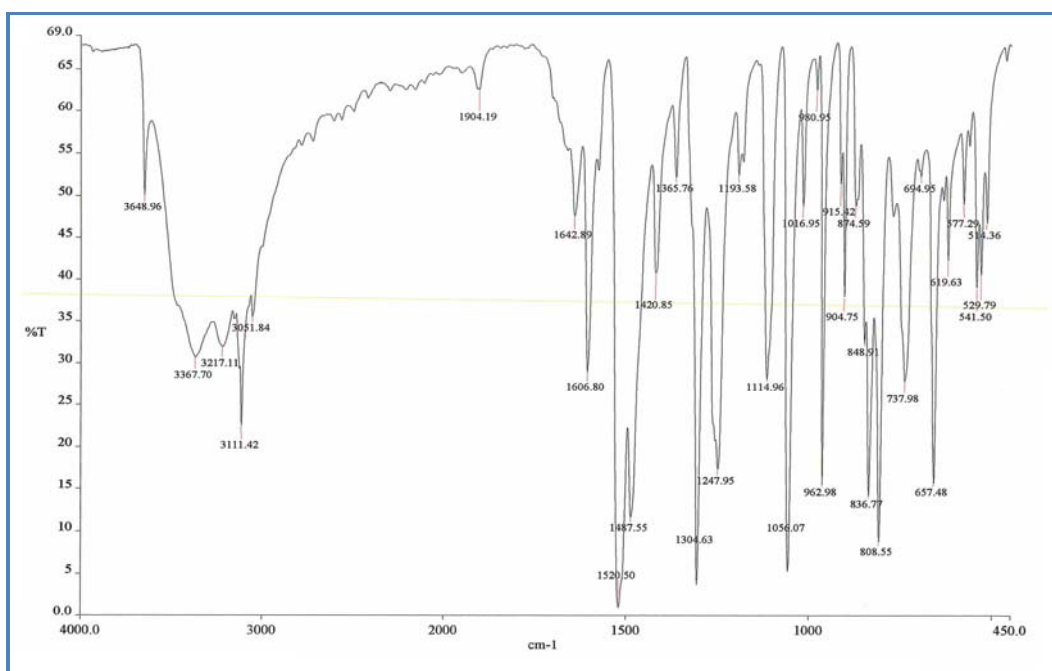


Figure A 58. FTIR spectrum of TIMPE (43)

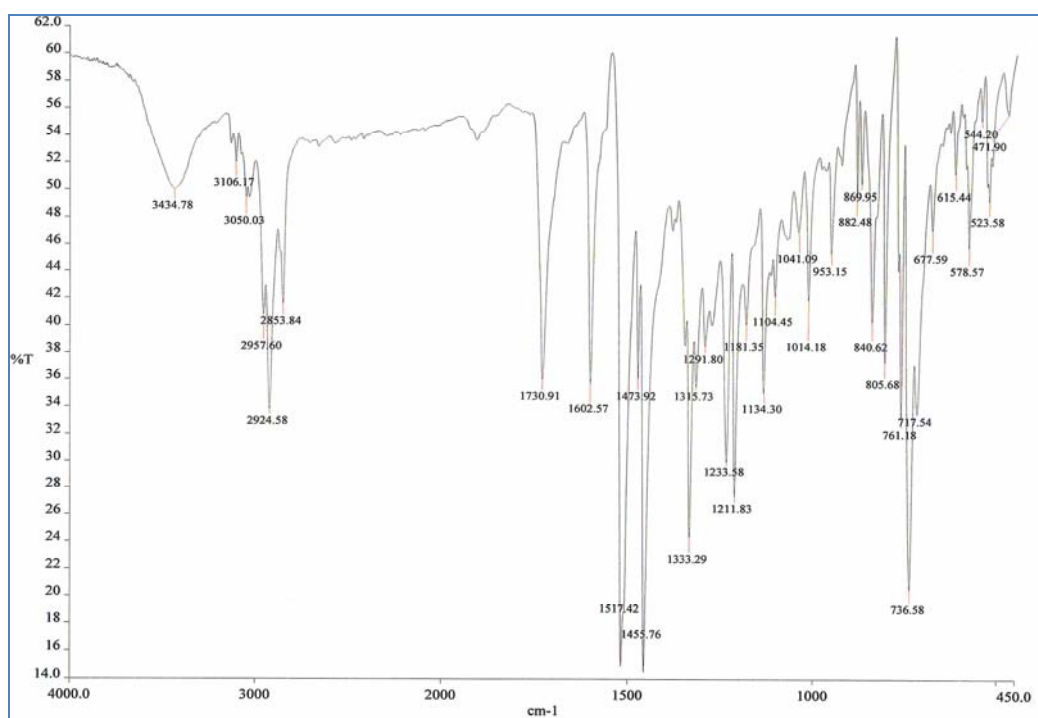


Figure A 59. FTIR spectrum of TIPE (44)

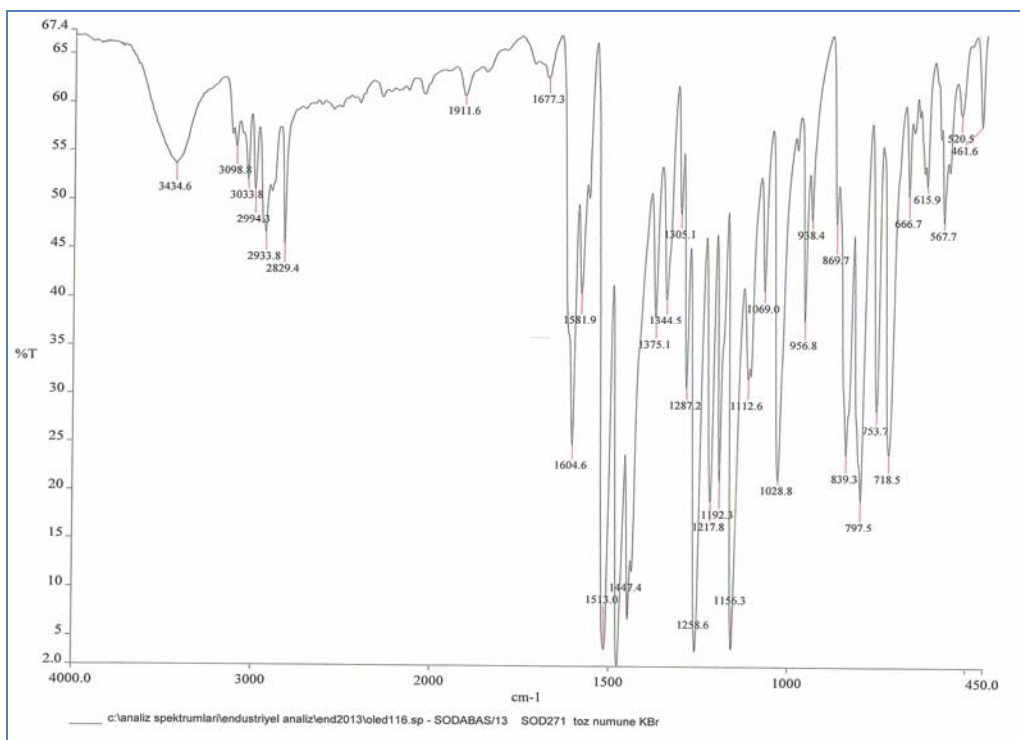


Figure A 60. FTIR spectrum of T5MIPE (45)

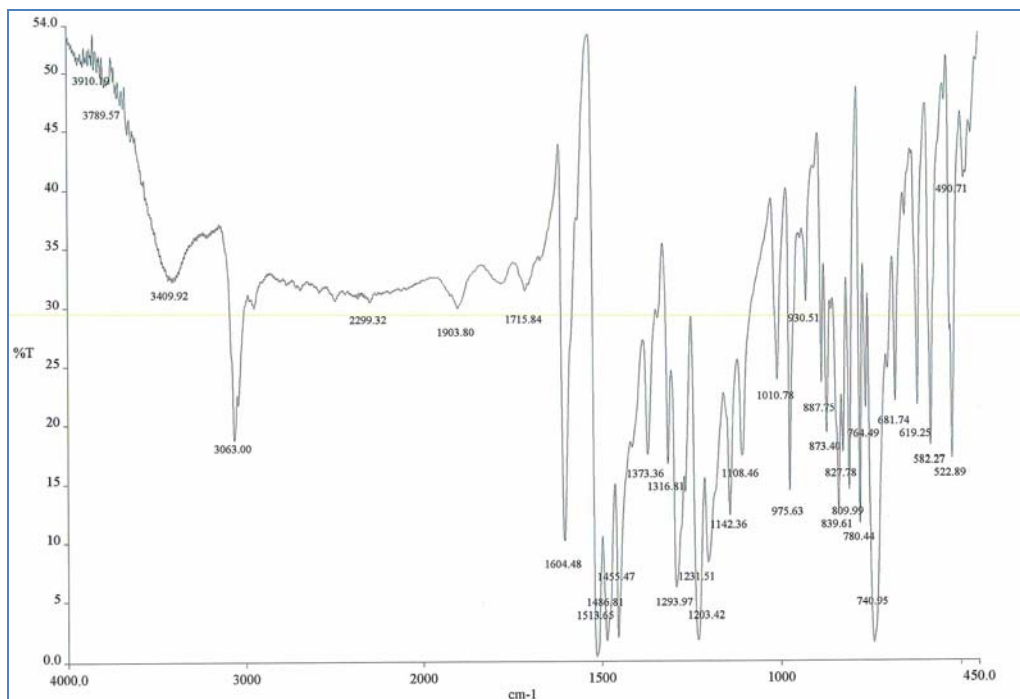


Figure A 61. FTIR spectrum of TBIMPE (46)

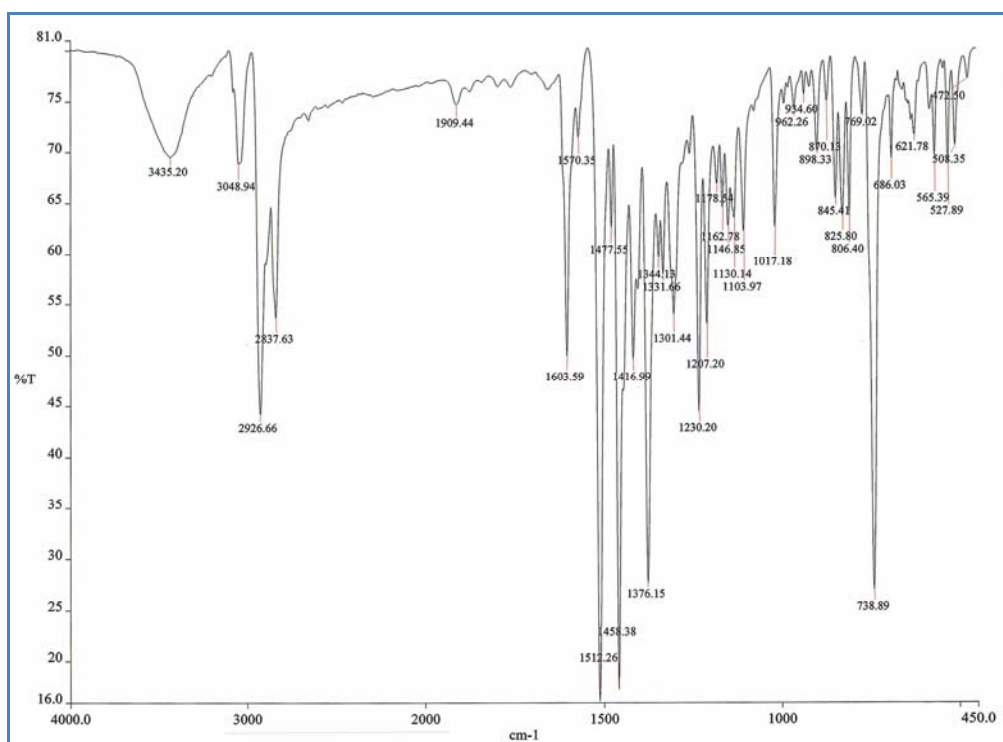


Figure A 62. FTIR spectrum of TDCPE (47)

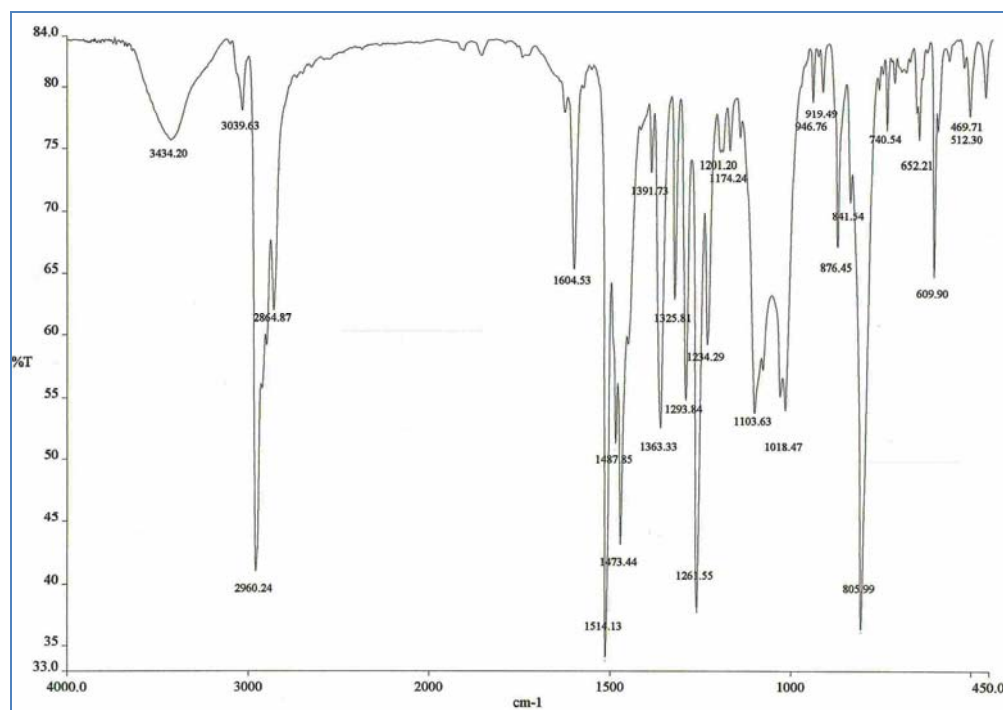


Figure A 63. FTIR spectrum of TTBCPE (48)

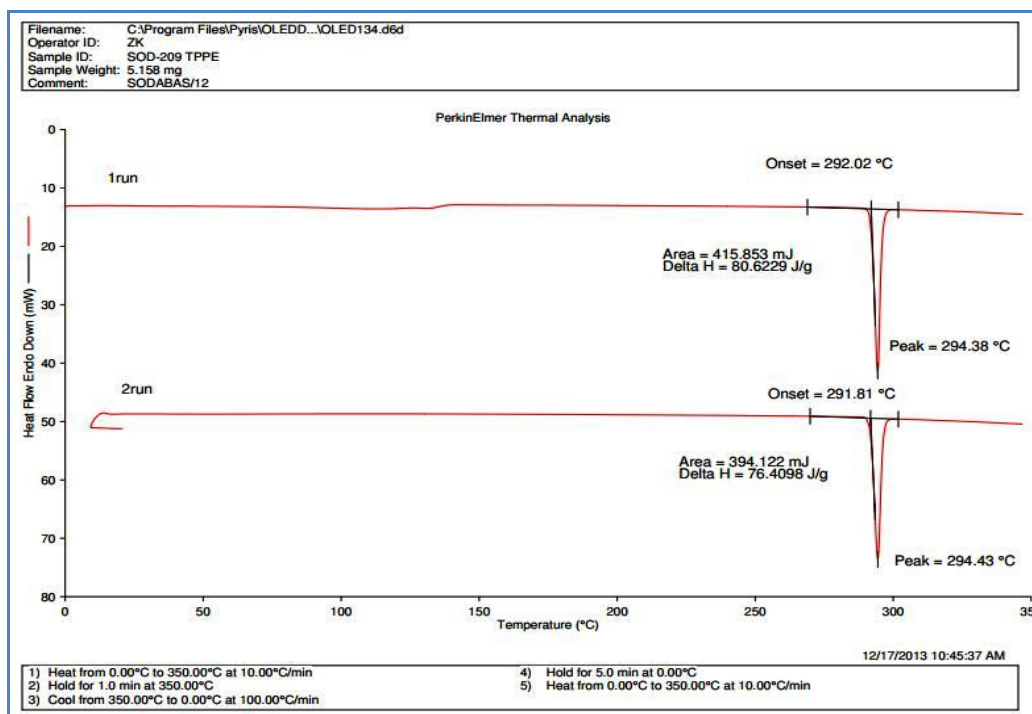


Figure A 64. DSC Thermogram of TPPE (41)

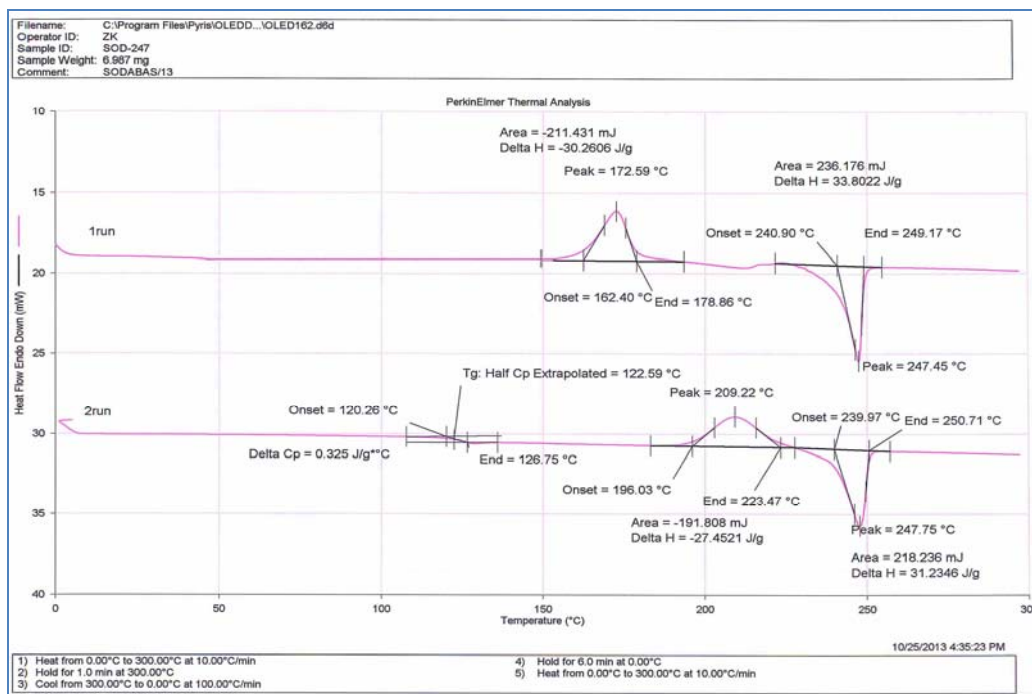


Figure A 65. DSC Thermogram of TPyPE (42)

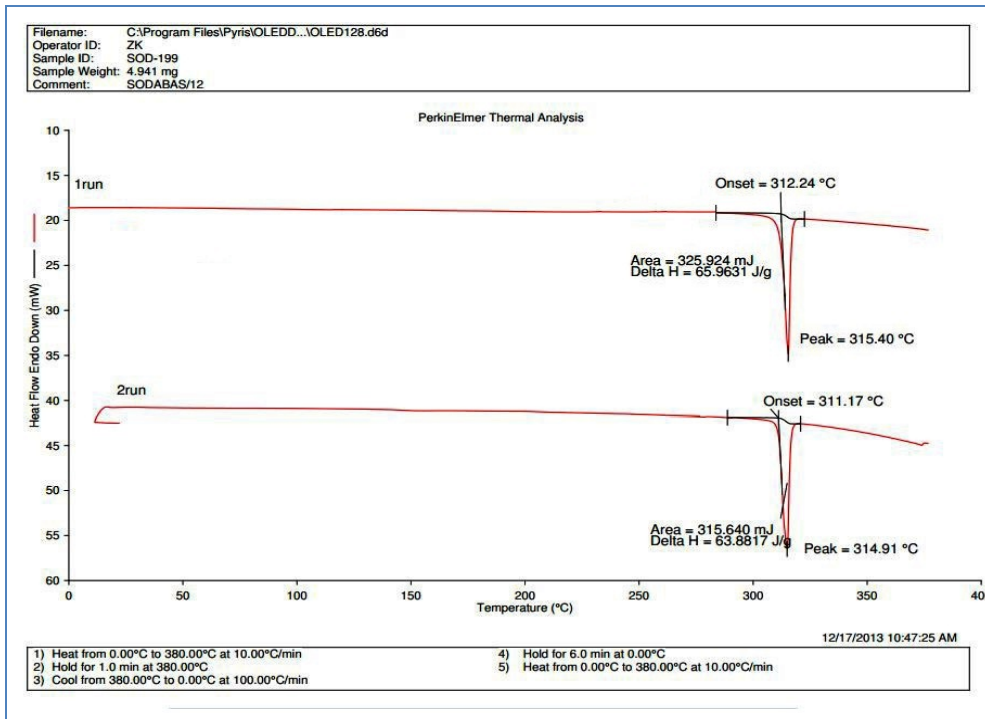


Figure A 66. DSC Thermogram of TIMPE (43)

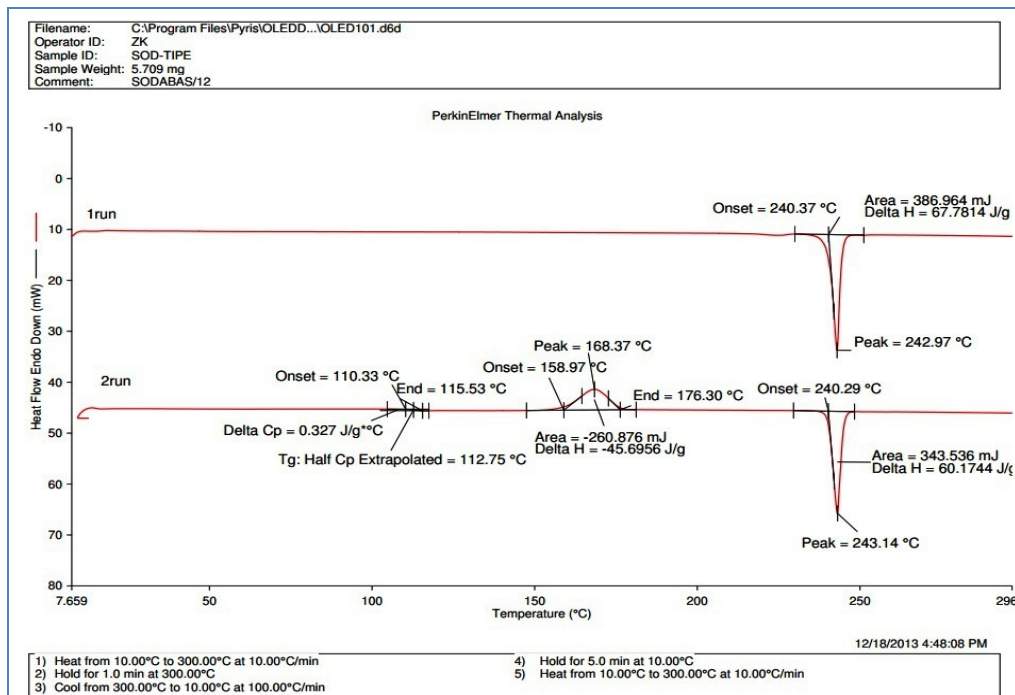


Figure A 67. DSC Thermogram of TIPE (44)

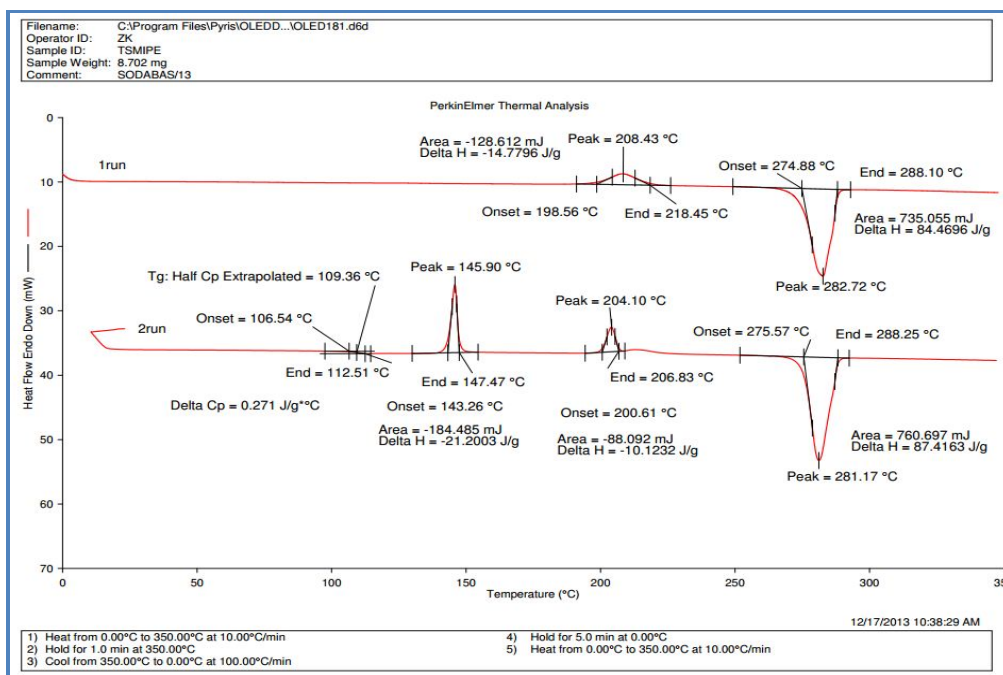


Figure A 68. DSC Thermogram of TSMIPE (45)

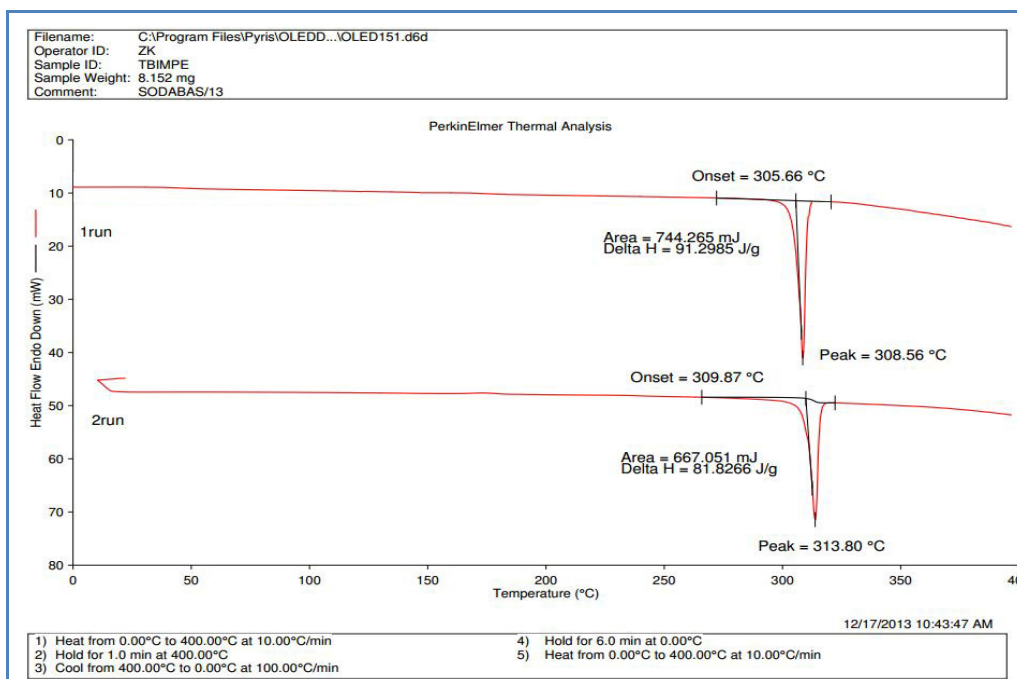


Figure A 69. DSC Thermogram of TBIMPE (46)

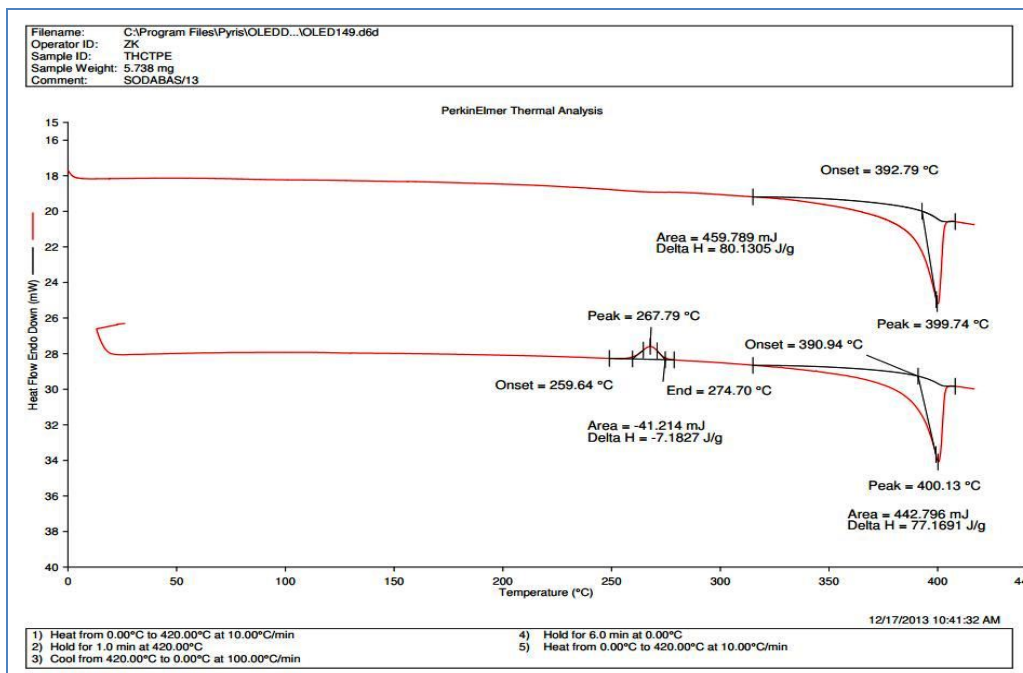


Figure A 70. DSC Thermogram of TDCPE (47)

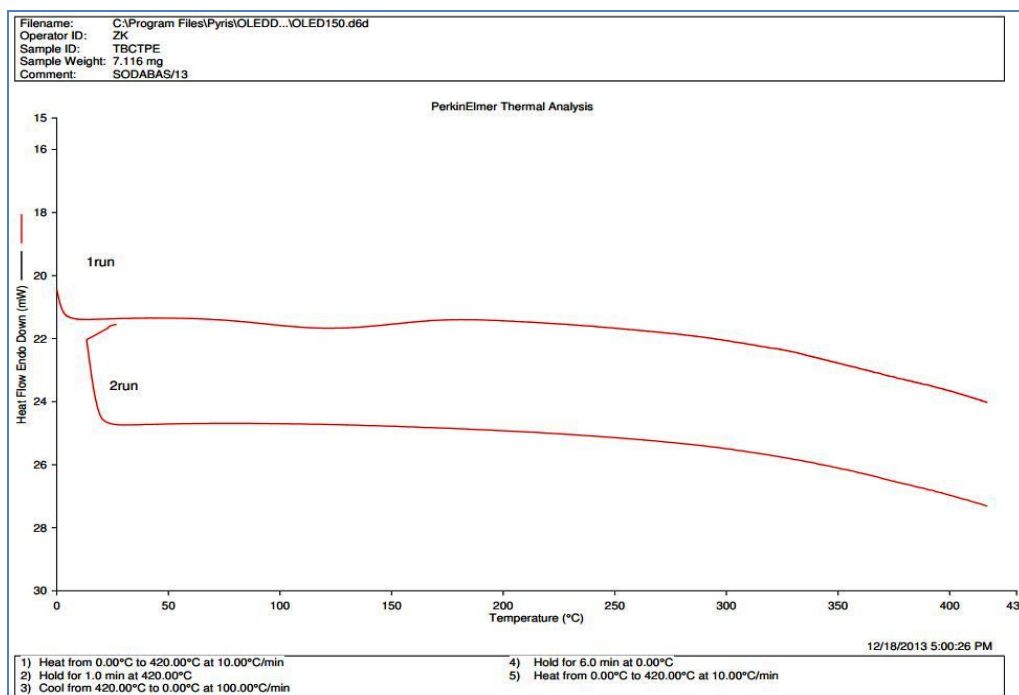


Figure A 71. DSC Thermogram of TTBCPE (48)

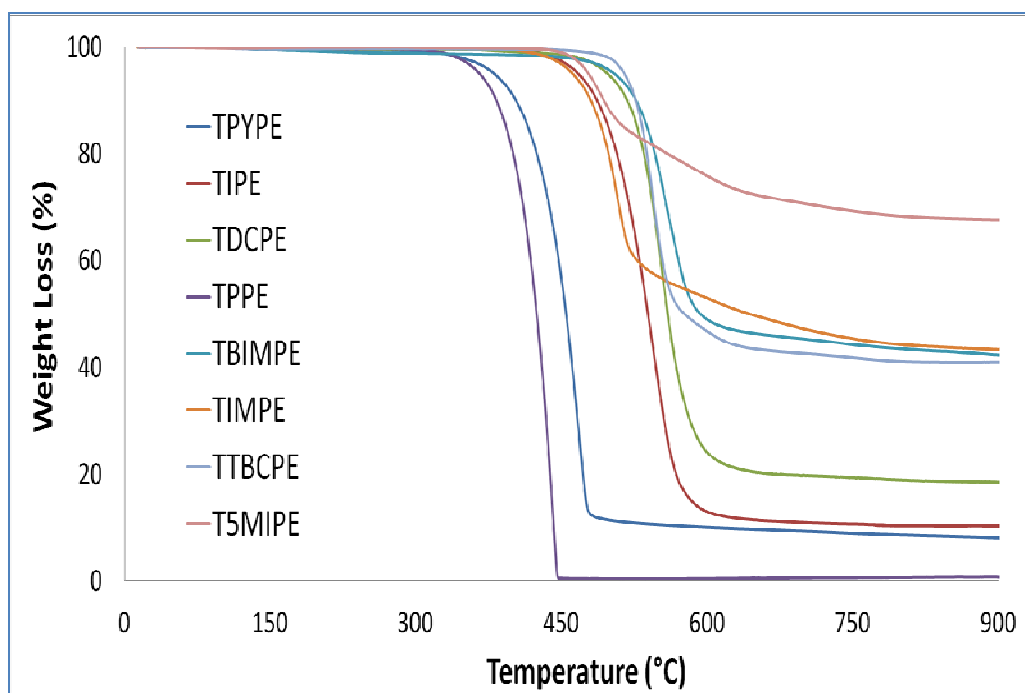


Figure A 72. TGA thermograms of the synthesized luminogens (41-48)

CURRICULUM VITAE

PERSONAL INFORMATION

Surname, Name: Odabaş, Serhat

Nationality: Turkish (TC)

Date and Place of Birth: 1 Mai 1982 , Ankara

Marital Status: Married

Phone: +90 535 503 38 29

email: serhat.odabas@tubitak.gov.tr

EDUCATION

Ph.D.: Middle East Technical University, Faculty of Arts and Sciences,

Department of Chemistry 09.2007 – 01.2014

Thesis: Synthesis and Luminescence Properties of Tetraphenylethene-Based Small Molecules Used In Organic Light Emitting Diodes

Supervisor: Prof. Dr. Cihangir TANYELİ

M.Sc.: Middle East Technical University, Faculty of Arts and Sciences,

Department of Chemistry, 09.2005 – 06.2007

Thesis: Asymmetric synthesis of N-Aryl substituted chiral 1,4-amino alcohol derivatives and applications in various asymmetric transformation reactions

Supervisor: Prof. Dr. Cihangir TANYELİ

B.Sc.: Middle East Technical University, Faculty of Arts and Sciences,

Department of Chemistry, 09.2000 – 06.2005

WORK EXPERIENCE

TÜBİTAK-MAM KE February 2008- Present

Researcher

FOREIGN LANGUAGES

English, German (Elementary)

PUBLICATIONS

1. Odabas, S.; Tekin, E.; Turksoy, F. Tanyeli, C. J. Mater. Chem C 2013, 42, 7081.
2. Tanyeli, C.; Odabas, S.; Erdem, M.; Cakir, E.; Keskin, E. Tetrahedron: Asymmetry 2013, 18, 2349.

Conference Papers

1. S. Odabas, F. Türksoy, C. Tanyeli Synthesis and Oled Applications of Tetraphenylethene-Based Compounds: Having Excellent Aggregation Induced Emission Properties 44th IUPAC World Chemistry Congress, August 2013
2. S. Odabaş, F. Türksoy, C. Tanyeli, Aggregation Induced Emission and Luminescence Properties of Novel Tetraphenylethylene-Based Emitter with Indole Side Groups, 7th Nanoscience and Nanotechnology Conference – July 2011, Istanbul, Türkiye.
3. S. Odabaş, F. Türksoy, C. Tanyeli, Synthesis and Luminescence Properties of Tetraphenylethene-Based Emitter with Carbazole Side Groups 6th Nanoscience and Nanotechnology Conference, Poster, June 2010, İzmir, Türkiye
4. S. Odabas, E. Keskin, C. Tanyeli, Asymmetric Synthesis Of Novel Chiral N-Aryl Substituted 1,4-Amino Alcohols, International Conference on Organic Chemistry, June 2007, Erzurum, Türkiye